Equilibrium Speciation of Select Lanthanides in the Presence of Acidic Ligands in Homo- and Heterogeneous Solutions

T Robinson

August 2011

Pacific Northwest
NATIONAL LABORATORY

Proudly Operated by **Battelle** *Since 1965*

DISCLAIMER

This report was prepared as an account of work sponsored by an agency of the United States Government. Neither the United States Government nor any agency thereof, nor Battelle Memorial Institute, nor any of their employees, makes **any warranty, express or implied, or assumes any legal liability or responsibility for the accuracy, completeness, or usefulness of any information, apparatus, product, or process disclosed, or represents that its use would not infringe privately owned rights**. Reference herein to any specific commercial product, process, or service by trade name, trademark, manufacturer, or otherwise does not necessarily constitute or imply its endorsement, recommendation, or favoring by the United States Government or any agency thereof, or Battelle Memorial Institute. The views and opinions of authors expressed herein do not necessarily state or reflect those of the United States Government or any agency thereof.

This document was printed on recycled paper.
(9/2003)

EQUILIBRIUM SPECIATION OF SELECT LANTHANIDES IN THE PRESENCE OF ACIDIC

LIGANDS IN HOMO- AND HETEROGENEOUS SOLUTIONS

By

Troy Robinson

Bachelor of Science
Brigham Young University
2005

A dissertation submitted in partial fulfillment of
the requirements for the

Doctor of Philosophy in Radiochemistry
Department of Chemistry
College of Science

Graduate College
University of Nevada, Las Vegas
August 2011

We recommend the dissertation prepared under our supervision by

Troy Robinson

entitled

Equilibrium Speciation of Select Lanthanides in the Presence of Acidic Ligands in Homo- and Heterogeneous Solutions

be accepted in partial fulfillment of the requirements for the degree of

Doctorate of Philosophy in Radiochemistry
Department of Chemistry

Ken Czerwinski, Committee Chair

Sam Bryan, Committee Member

Patricia Paviet-Hartman, Committee Member

Tatiana Leviskaia, Committee Member

Ralf Sudowe, Graduate College Representative

Ronald Smith, Ph. D., Vice President for Research and Graduate Studies
and Dean of the Graduate College

August 2011

ABSTRACT

Equilibrium Speciation of Select Lanthanides in the Presence of Acidic Ligands in Homo- and Heterogeneous Solutions

by

Troy Robinson

Dr. Kenneth R. Czerwinski, Examination Committee Chair
Professor of Chemistry
Chair of the Department of Radiochemistry
University of Nevada, Las Vegas

This dissertation explores lanthanide speciation in liquid solution systems related to separation schemes involving the acidic ligands: bis(2-ethylhexyl) phosphoric acid (HDEHP), lactate, and 8-hydroxyquinoline. Equilibrium speciation of neodymium (Nd^{3+}), sodium (Na^+), HDEHP, water, and lactate in the TALSPEAK liquid-liquid extraction system was explored under varied Nd^{3+} loading of HDEHP in the organic phase and through extraction from aqueous HCl and lactate media. System speciation was probed through vapor pressure osmometry, visible and Fourier Transform Infrared (FTIR) spectroscopy, ^{22}Na and ^{13}C labeled lactate radiotracer distribution measurements, Karl Fischer titrations, and equilibrium pH measurements. Distribution of Nd^{3+}, Na^+, lactate, and equilibrium pH were modeled using the SXLSQI software to obtain $\log K_{Nd}$ and $\log K_{Na}$ extraction constants under selected conditions. Results showed that high Nd^{3+} loading of the HDEHP led to Nd^{3+} speciation that departs from the ion exchange mechanism and includes formation of highly aggregated, polynuclear $[NdLactate(DEHP)_2]_x$; (with x > 1). By substituting lanthanum (La^{3+}) for Nd^{3+} in this system, NMR scoping experiments using ^{23}Na, ^{31}P nuclei and ^{13}C labeled lactate were performed. Results indicated that this technique is sensitive to changes in system speciation, and that further experiments are warranted. In a homogeneous system representing the TALSPEAK aqueous phase, Lactate protonation behavior at various temperatures was characterized using a combination of

potentiometric titration and modeling with the Hyperquad computer program. The temperature

dependent deprotonation behavior of lactate showed little change with temperature at 2.0 M

NaCl ionic strength.

Cloud point extraction is a non-traditional separation technique that starts with a

homogeneous phase that becomes heterogeneous by the micellization of surfactants through

the increase of temperature. To better understand the behavior of europium (Eu^{3+}) and 8-

hydroxyquinoline under cloud point extraction conditions, potentiometric and

spectrophotometric titrations coupled with modeling with Hyperquad and SQUAD computer

programs were performed to assess europium (Eu^{3+}) and 8-hydroxyquinoline speciation.

Experiments in both water and a 1wt% Triton X-114/water mixed solvent were compared to

understand the effect of Triton X-114 on the system speciation. Results indicated that increased

solvation of 8-hydroxyquinoline by the mixed solvent lead to more stable complexes involving 8-

hydroxyquinoline than in water, whereas competition between hydroxide and Triton X-114 for

Eu^{3+} led to lower stability hydrolysis complexes in the mixed solvent than in water.

Lanthanide speciation is challenging due to the trivalent oxidation state that leads to

multiple ligand complexes, including some mixed complexes. The complexity of the system

demands well-designed and precise experiments that capture the nuances of the chemistry. This

work increased the understanding of lanthanide speciation in the explored systems, but more

work is required to produce a comprehensive understanding of the speciation involved.

ACKNOWLEDGEMENTS

TABLE OF CONTENTS

CHAPTER 1

INTRODUCTION

1.1   Motivation for Research

The "Trivalent Actinide Lanthanide Separation by Phosphorus reagent Extraction from

Aqueous Komplexes" (TALSPEAK) process[1] has been demonstrated to successfully separate

trivalent actinides from the lanthanides on the laboratory scale.[2] Despite this success, there are

aspects of the fundamental chemistry that are not completely understood. In a recent review of

the process, Nilsson and Nash[3] have shown that modeling the TALSPEAK system leads to

predictions that are not observed in the experimental data. The authors suggest that the

differences may be caused by the formation of aqueous mixed complexes that are not included

in the model or that the thermodynamic parameters are significantly changed at pH > 3.6 due to

the increase in ionic strength and free lactate concentration. Leggett et al.[4] studied mixed

complexes in the TALSPEAK aqueous phase and reported that they form in such small quantities

that they can't account for the previously noted modeling inconsistencies.

Prior to implementing the TALSPEAK process on the industrial scale it is necessary for the

fundamental chemistry to be understood so the process can be satisfactorily modeled.

Otherwise, a premature application may lead to unsatisfactory separation results, process

delays or failures. This work was undertaken to increase understanding of the TALSPEAK process

that will lead to accurate modeling of the process in the future. This work studied the extraction

of Nd^{3+} over a range of loading regimes, characterized the speciation of Nd^{3+} in the organic

phase, and modeled the extraction behavior where aqueous thermodynamic parameters are

available. For conditions where aqueous thermodynamic data is not available, the speciation will

still be characterized so that when this data is made available, the system can be accurately

modeled

Due to the narrow operating envelope required by the TALSPEAK system, other separation systems may prove to be more convenient for the trivalent lanthanide/trivalent actinide separation. Recent work with cloud point extraction has shown that lanthanum was selectively removed from gadolinium using 8-hydroxyquinoline.[5-7] This same separation system is under exploration as a possible candidate for trivalent lanthanide/trivalent actinide separation. The cloud point extraction technique was developed as an alternative to liquid-liquid extraction that enables the extraction of metal ion complexes.[8-9] This work explores the complexation behavior of 8-hydroxyquinoline with europium in the cloud point medium of Triton X-114/H_2O and also the H_2O system behavior for comparison at 0°C.

1.2   Background

1.2.1   Partitioning and Transmutation

The fundamental premise of partitioning and transmutation (P&T) is separating long-lived radioisotopes from irradiated nuclear fuel and re-irradiating to convert them to shorter-lived or stable radioisotopes. In irradiated nuclear fuel, with a few exceptions, fission products are short-lived isotopes and transuranium elements are longer lived. Past simulation of dose from irradiated nuclear fuel shows that between 1,000 and 10,000 years after irradiation, the major contributors are plutonium and the minor actinides (neptunium, americium and curium).[10] Thus, plutonium and the minor actinides are prime targets of P&T research.

Due to the focus on recovery of plutonium for nuclear weapons purposes during the cold war, its chemistry and separation is well understood.[11] Neptunium separation has been a more recent achievement,[12-13] but it appears to be feasible within current nuclear reprocessing facilities. Americium and curium represent a more difficult problem in P&T research. During nuclear fuel irradiation, these trivalent actinides and the lighter lanthanides, La^{3+} through Gd^{3+}, are introduced into the fuel through neutron activation and fission respectively. When the fuel

is dissolved in acidic solution these actinides and lanthanides all exist as trivalent ions with no other easily accessible or stable oxidation states available. In addition, these trivalent ions are also very similar in size.[14] Due to the similar charge density and affinity to complexing agents between the trivalent actinides and the lanthanides, the separation has been described as "…the most challenging aspect of advanced nuclear fuel partitioning schemes."[15] It is necessary to separate the trivalent actinides from the trivalent lanthanides in a P&T scheme because the neutron absorption cross-section of the lanthanides.[15] Because the lanthanides have such large cross-sections (Table 1.1), they would act as a neutron poison and hinder the utility of a nuclear fuel containing these elements.

Table 1.1- Thermal neutron capture cross section[16] (barns) of the fission product lanthanides. Isotopes with fission yields of zero were omitted. Values in bold font are for isotopes with $T_{1/2} >$ 20 years that are more likely to be present after the post-irradiation cooling period.

Element (1st mass)	La (139)	Ce (140)	Pr (141)	Nd (143)	Pm (147)	Sm (147)	Eu (151)	Gd (155)
1st mass+0	**9.0**	**0.58**	**11.4***	**330**	182*	**57**	**~9200***	**61,000**
+1	2.7	29		**3.6**		**3**		**2**
+2		**0.97**	90	**45**	140	**40,000**	350	**255,000**
+3		6		**1.4**		**103**	1,400	**2.4**
+4		1.0		400	200	15,100	3,900	
+5				**2.5**		**210**		**1**
+6						400		20,000
+7				**1.0**		**7**		

*These values were listed as a sum of two or more cross-sections (i.e. x+x+…), but are listed here as the single value of the sum of the separately listed values.

1.2.2   Partitioning Schemes Overview

Partitioning schemes are developed both to target species in the nuclear fuel and to achieve various purposes. These purposes include the reduction of overall bulk or mass, limitation of

dose, recycling of fissile and fertile fuel materials, or the transmutation of long-lived radiotoxic constituents. For purposes of the discussion in this section, irradiated nuclear fuel will be assumed to be 30 MWd/kg M burnup fuel with 10 year decay period and a 2.9% initial ^{235}U enrichment with elemental constituent breakdown obtained from ORIGEN2[17] simulation shown in the appendix of Guenther *et al*.[18] The major constituents of irradiated fuel are ranked by their bulk (mass) and activity in Table 1.2 and Table 1.3. The data is shown grouped in an elemental rather than isotopic break-down because partitioning schemes discussed in this work target elements.

In the PUREX reprocessing scheme[11, 19] the fertile and fissile isotopes of uranium and plutonium are targeted for reuse in nuclear power reactors, or for production of nuclear weapons. Because the PUREX process effectively removes the uranium from the remaining irradiated fuel constituents and uranium makes up the vast bulk of irradiated fuel (98.4 wt%, see Table 1.2) the PUREX process in its original or modified form is used as a head-end process for subsequent nuclear separations. Different modifications of PUREX enable the co-recovery of neptunium,[12] or prevent the creation of separated plutonium as in the COEX, and UREX + NPEX[2] processes (see Figure 1.1). An alternative to the PUREX process was developed using completely incinerable extractants, specifically N,N-dialkylamide type extractants, that recovered uranium and plutonium using different conditions and chemistry, but providing a similar separation as PUREX.[20] The use of N,N-dialkylamide for the recovery of uranium and plutonium has been abandoned due to problems with third phase formation causing problems for the separation.[20] Structure of the PUREX process extractant, tributyl phosphate, and the N,N-dialkylamide alternative are shown in Figure 1.2.

A large reduction of radioactive dose from the used fuel materials is a goal that is achieved by targeting cesium and strontium for separation from the irradiated fuel mixture. As shown in

Table 1.3, cesium and strontium and their daughter products barium and yttrium account for

71% of the total activity, but only 0.16% of the mass. Separation schemes using the chlorinated

cobalt dicarbollide (CCD) with Polyethylene Glycol (PEG),[21-22] or calixarene type[23-24] molecules

enable the selective extraction of cesium and strontium. The structures of the molecules used in

cesium and strontium extraction are shown in Figure 1.3. A schematic representation of the

cesium and Strontium extraction is shown in Figure 1.4.

Table 1.2- The top 15 elements in irradiated fuel sorted by mass percent. Category is either Actinides (Act.) or Fission Product (F.P).

Rank	Category	Element	Mass%	Activity%
1	Act.	U	98.43%	0.00%
2	Act.	Pu	0.85%	22.37%
3	F.P.	Nd	0.13%	0.00%
4	F.P.	Cs	0.13%	22.19%
5	F.P.	Ce	0.10%	0.01%
6	F.P.	Tc	0.07%	0.00%
7	F.P.	Zr	0.07%	0.00%
8	Act.	Am	0.06%	0.59%
9	Act.	Np	0.04%	0.00%
10	F.P.	Sr	0.04%	14.77%
11	F.P.	Rb	0.02%	0.00%
12	F.P.	Sm	0.02%	0.09%
13	F.P.	I	0.02%	0.00%
14	Act.	Cm	0.01%	0.33%
15	F.P.	Sn	0.00%	0.00%

Table 1.3- The top 15 elements in irradiated fuel sorted by Percent of total activity. Category is either Actinides (Act.) or Fission Product (F.P.).

Rank	Category	Element	Mass%	Activity%
1	Act.	Pu	0.85%	**22.37%**
2	F.P.	Cs	0.13%	**22.19%**
3	F.P.	Ba	0.00%	**20.23%**
4	F.P.	Y	0.00%	**14.77%**
5	F.P.	Sr	0.04%	**14.77%**
6	F.P.	Pm	0.00%	**1.63%**
7	F.P.	Eu	0.00%	**1.51%**
8	F.P.	Kr	0.00%	**1.09%**
9	Act.	Am	0.06%	**0.59%**
10	Act.	Cm	0.01%	**0.33%**
11	F.P.	Sb	0.00%	**0.16%**
12	F.P.	Sm	0.02%	**0.09%**
13	F.P.	H	0.00%	**0.07%**
14	F.P.	Rh	0.00%	**0.06%**
15	F.P.	Ru	0.00%	**0.06%**
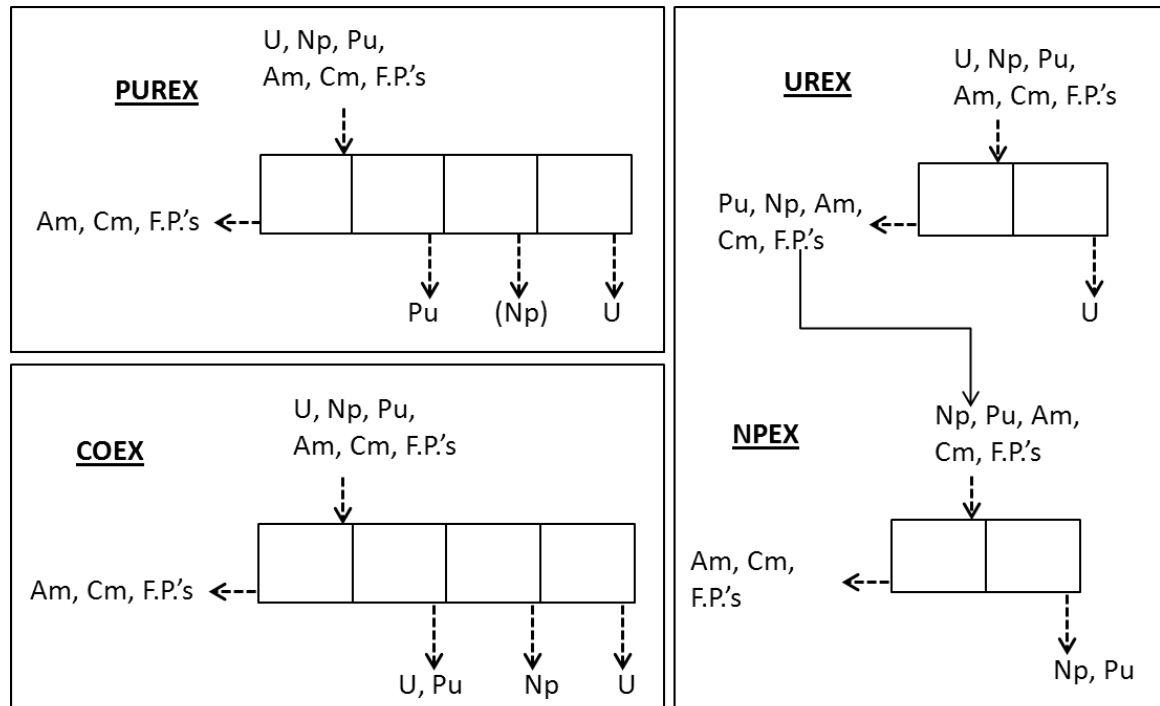
Figure 1.1- A schematic representations showing the basic material flow for the PUREX, COEX, UREX and NPEX processes. The separation of neptunium in the PUREX was not historically performed (see Irish *et al.*[19]), but has been added in more modern applications of this process, and is thus shown in parentheses.
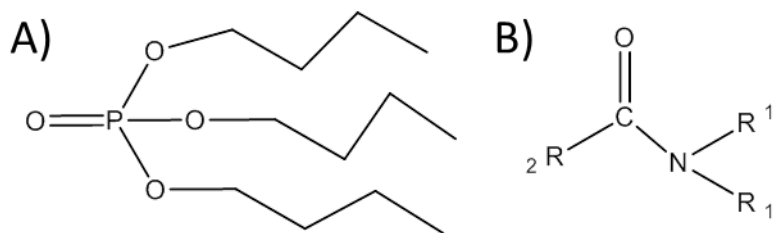
Figure 1.2- Extractants developed for Uranium, Neptunium and Plutonium extraction: A) Tri-n-butyl phosphate; B) N',N' dialkyl amide functional group. The R groups in 'B' are varied between n-alkyl and branched alkyl groups (see Musikas et al.[20]).
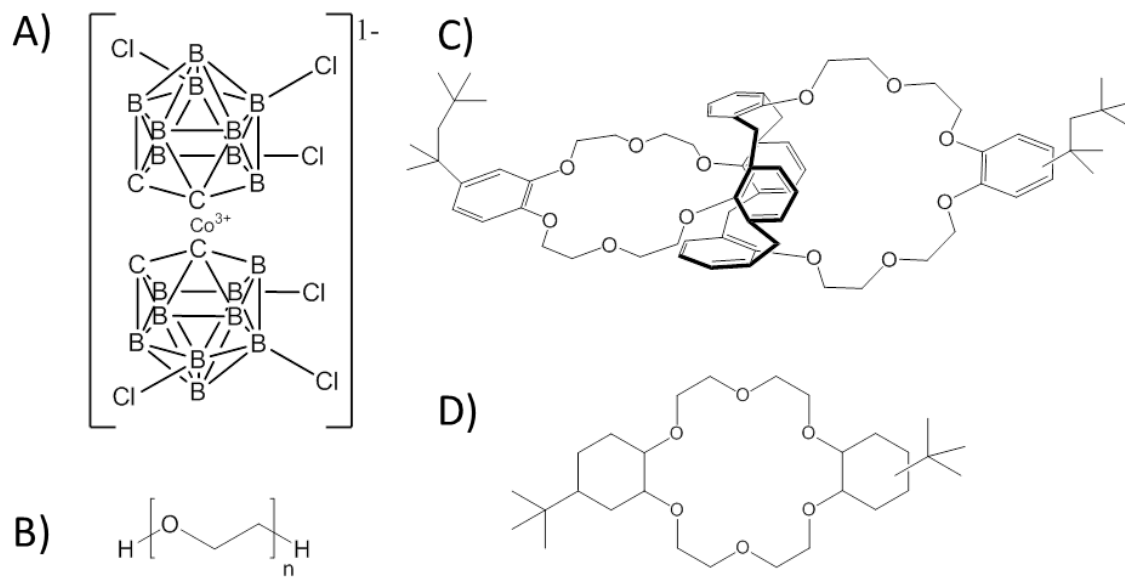
Figure 1.3- Extractants used in cesium and strontium extraction: A) Chlorinated Cobalt Dicarbollide; B) Polyethylene Glycol; C) Calix[4]arene-bis(4-tert-octylbenzo-crown-6); D) bis [4,4'(5')-(tert-butyl)cyclohexano]-18-crown-6.
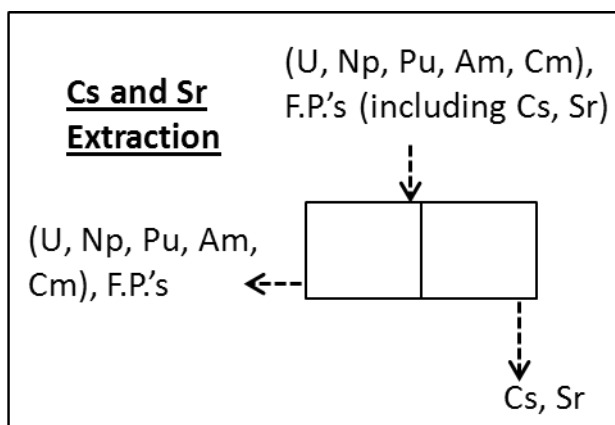
Figure 1.4- A schematic representation of the material flow in the Cs and Sr extraction. These processes have been developed for use with dissolved irradiated fuel or other Cs and Sr bearing wastes. The parentheses enclosing U, Np, Pu, Am, and Cm are to indicate that these processes are effective with or without these elements present.

The transmutation of the long-lived radiotoxic minor actinides is a goal that requires the separation of these elements from the other fission products (see section 1.2.1). Because neptunium extraction is feasible through a modified PUREX process,[12] the separation of americium and curium from the fission product mixture has been developed as a separate process. A preliminary extraction of all trivalent actinides and trivalent lanthanides from the other fission products precedes the separation of the trivalent actinides from the lanthanides.[25] This separation has been performed using the phosphate based ligand octyl (phenyl)-N,N-diisobutylcarbamoyl-methylphosphine oxide (CMPO) in a process named the Transuranic Extraction (TRUEX) process,[25] or bifunctional malonamides in a process named the Diamide Extraction (DIAMEX) process.[20] The structures of these extractants are shown in Figure 1.5. Once the other fission products are removed from the trivalent actinide / trivalent lanthanide mixture, the separation of the trivalent actinides can be achieved. The trivalent actinide / trivalent lanthanide separation was first developed as a fractional precipitation[26] and later using ion exchange.[26] Solvent extraction processes are under continual development for

deployment at the industrial scale in advanced recycling schemes that utilizes thiophosphinic

acid extractants,[27] aromatic nitrogen ligands such as triazines and terpyridines,[28] the

TALSPEAK Process[1] that utilizes a combination of organophosphoric acid and

aminopolycarboxylic acid ligands.
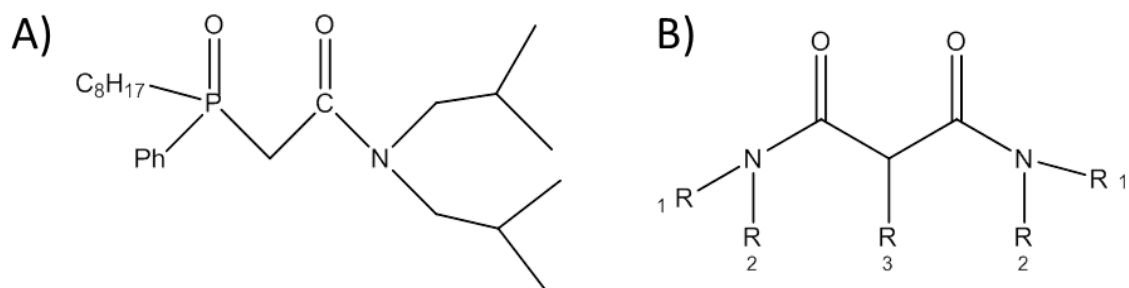
Figure 1.5- Examples of extractants developed for the trivalent actinide/trivalent lanthanide co-extraction: A) octyl (phenyl)-N,N-diisobutylcarbamoyl-methylphosphine oxide; B) generic form of the diamide extractant.
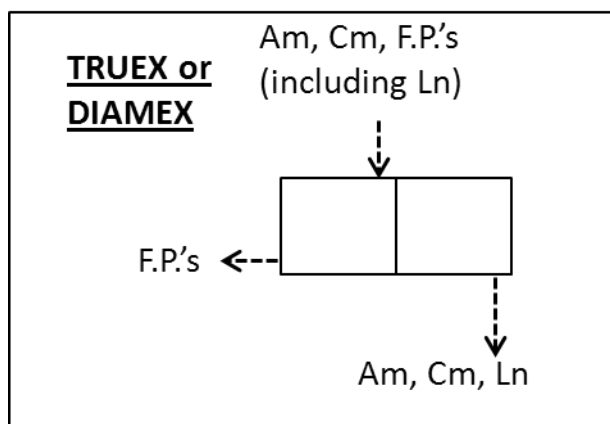
Figure 1.6- A schematic representation of the material flow in the TRUEX or DIAMEX systems.

Extraction processes can be used in sequence in an overall waste partitioning scheme. The UREX+ set of processes was designed and demonstrated at the lab-scale.[29-30] This reported series of extractions consisted of 1) Modified PUREX for uranium only extraction (named 'UREX'), 2) CCD-PEG for cesium and strontium recovery, 3) a 2nd modified PUREX for neptunium and plutonium co-extraction (named 'NPEX'), 4) TRUEX for trivalent actinide / trivalent lanthanide co-extraction, and 5) Cyanex 301 (the trade name for bis(2,4,4-trimethylpentyl)dithiophosphinic acid) for trivalent actinide separation from trivalent lanthanides.

Some efforts have been made to simplify the overall fuel recycling flowsheets into fewer processes by combining processes. The Universal Solvent Extraction (UNEX) process was developed more as a decontamination rather than recycling process that targets the highest activity species for removal from an acidic nuclear waste stream. The UNEX process solvent was a combination of the TRUEX and the CCD/PEG processes that achieved extraction of all actinides, lanthanides and cesium and strontium.[31-32] The TRUSPEAK process[33-34] is currently under development and seeks to combine the TRUEX and TALSPEAK processes to enable extraction of both trivalent actinides and trivalent lanthanides, but achieve the separation through selective stripping.
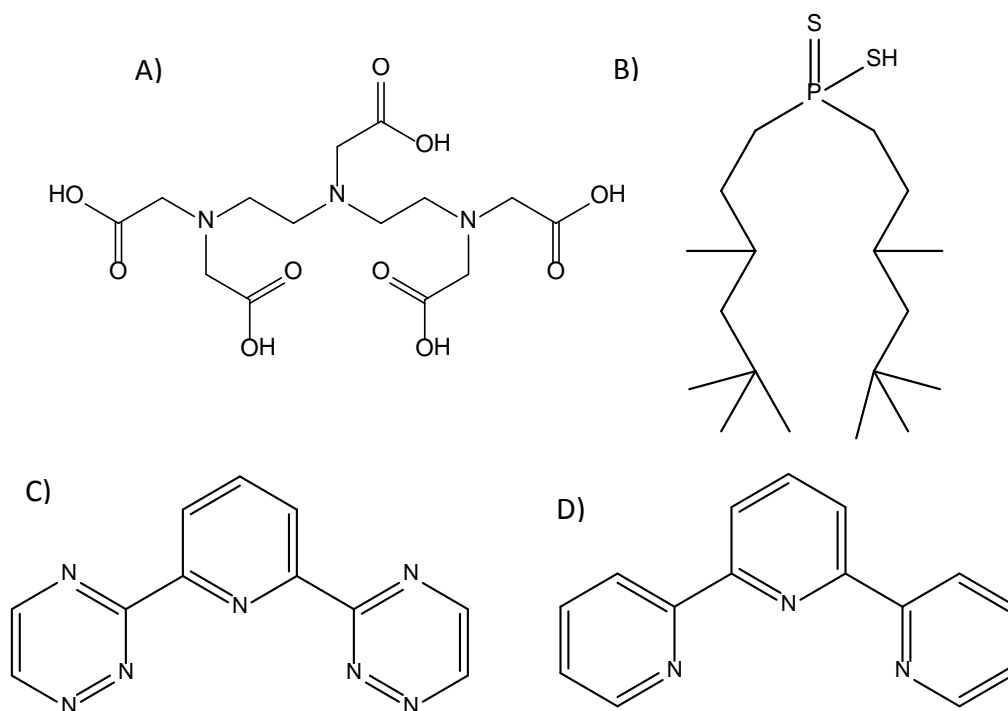
Figure 1.7- Selective complexants developed for the trivalent actinide/trivalent lanthanide separation: A) diethlyenetriaminepentaacetic acid; B) bis(2,4,4-trimethylpentyl)dithiophosphinic acid; C) bis-triazinyl-pyridine; D) terpyridine.
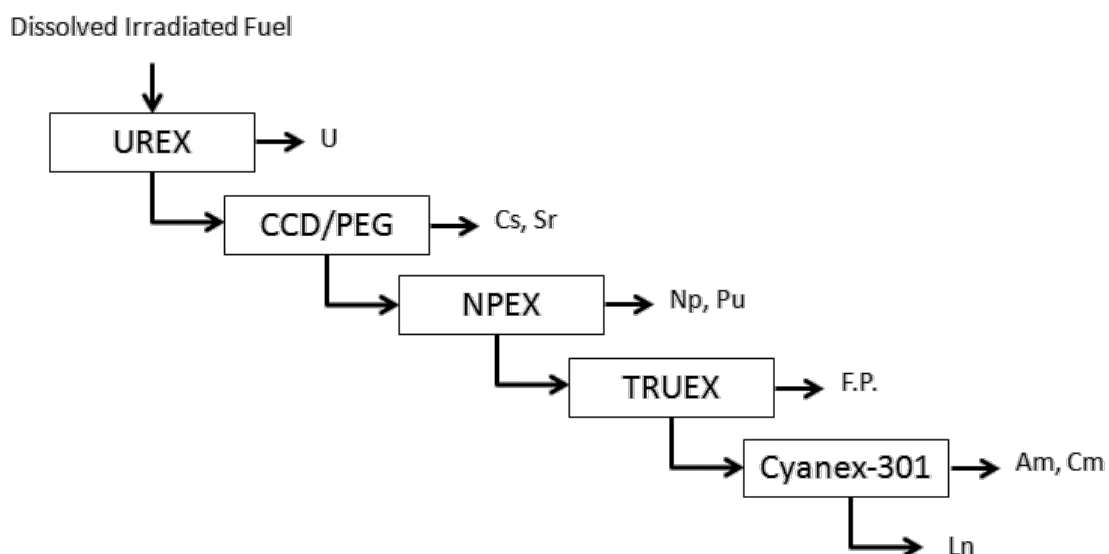
Figure 1.8- A schematic representation of the UREX+ separation scheme.
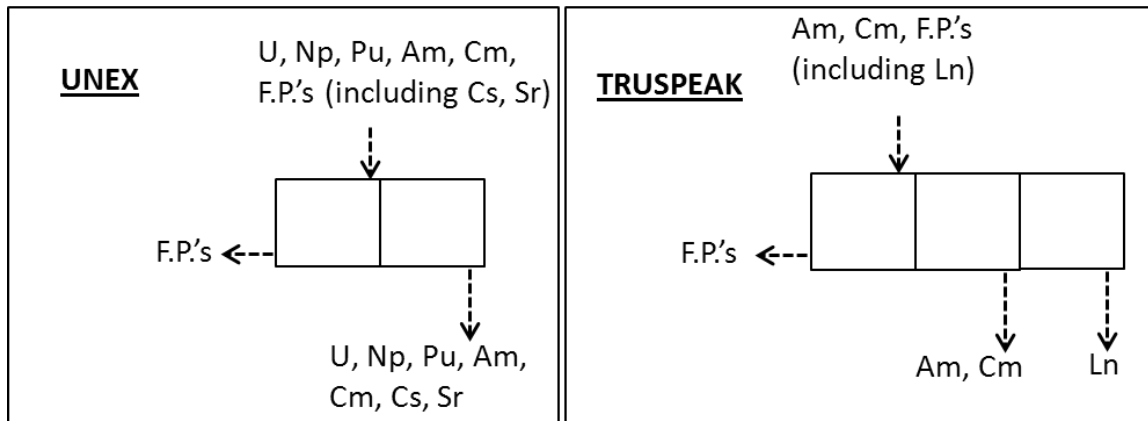
Figure 1.9- A schematic representations showing the basic material flow for the UNEX and TRUSPEAK systems.

1.2.3 Cloud Point Extraction

Cloud point extraction is a method utilizing surfactants (surface active agents) as the phase separating reagents. Cloud point extraction is similar to liquid-liquid extraction because it utilizes two phases with selective distribution of hydrophobic species but it differs in that the system begins as a single phase. The term "Cloud Point" refers to the temperature of transition where the surfactants change from solutes in the bulk phase to self-aggregate micelles.[35] Because temperature is the driving force in non-ionic surfactant micellization, it is believed to be an entropic process[36-37] that can be described by the Gibbs free energy equation shown in equation (1.1).

$$\Delta G_{micelle} = \Delta H_{micelle} - T\Delta S_{micelle} \qquad (1.1)$$

As the temperature is increased the magnitude of the TΔS term in the equation will exceed that of the ΔH term, causing spontaneous micellization where the solution becomes a cloudy, two-phase system. The reaction is reversible if the temperature is decreased.[36]

Cloud point extraction was introduced as an alternative separation technique to solvent extraction[36] by Watanabe and co-workers.[8] Since then most of the work utilizing this technique has been separation and pre-concentration of trace metals,[35, 37-38] and protein isolation.[38-39] Although reviews concerned with cloud point extraction deal mostly with laboratory applications,[35-37, 40] there are some efforts to apply this method to industrial scale waste treatment using the continuous disk rotating contactor.[41-42]

1.2.4 Trivalent Actinide/Lanthanide Separation Principles

Trivalent actinides and lanthanides must be separated by exploiting their chemical and physical differences. The difference in ionic radius is one basis for separating these elements. A separation designed purely on the basis of size will be difficult for the actinide/lanthanide separation because the ionic radius of americium and curium are approximately the same size as promethium and samarium respectively (Table 1.4). Some success has been achieved through ion exchange that leads to the elution of progressively larger trivalent ions.[43] Differences in ionic radius and thus charge density lead to variations in affinity for the ion exchange resin, and complexants in the mobile phase such as a-hydroxy isobutyrate,[43-44] citrate,[43] lactate,[43] or ethylenediaminetetraacetic acid (EDTA).[43, 45-46] The ionic radius differences are small, but when a sufficiently large column is used, a successful separation is achieved.

The "Hard-Soft Acid-Base" character of the actinides and lanthanides is another difference that can be exploited to achieve separation. The Hard-Soft Acid Base theory[47] suggests that certain electron pair acceptor acids will form stronger complexes with certain electron pair donor bases when the acid-base pair share either Hard or Soft character. Hard or Soft character is determined by the polarizability of the acid or base and the degree of covalency in the resulting complex's bond. Soft acid/ base complexes have polarizable valence electrons and form bonds with higher covalent character than hard acid/base complexes.[47]

13

Table 1.4- Ionic radius of Trivalent lanthanide and actinide ions.[48]

Lanthanides		Actinides	
(M^{+3})	Ionic Radius (pm)	(M^{+3})	Ionic Radius (pm)
La	103.2	Ac	112
Ce	101	Th	
Pr	99	Pa	
Nd	98.3	U	102.5
Pm	97	Np	101
Sm	95.8	Pu	100
Eu	94.7	Am	97.5
Gd	93.8	Cm	96
Tb	92.3	Bk	96
Dy	91.2	Cf	95
Ho	90.1	Es	
Er	89	Fm	
Tm	88	Md	
Yb	86.8	No	
Lu	86.1	Lr	

* Coordination number is 6 for all ions in table.

The actinides and lanthanides are in general hard acids,[47, 49] but the actinides show a small but significant preference for soft donor ligands.[48, 50] Relativistic calculations predict that the valence d- and f- orbitals extend further for actinides than lanthanides.[49] Electron spin resonance (ESR) experiments with iso-electronic uranium and neodymium fluoride compounds show some interaction between the fluorine nuclei and the electron spin of the uranium ion, while the neodymium showed no similar interaction.[51] Both the relativistic calculations and the ESR experiments support the hypothesis of increased covalency in actinide bonding. In a review by Nash,[48] the comparison of the enthalpy of complexation for Am^{3+}, Cm^{3+} and Eu^{3+} with aminocarboxylate ligands showed no clear difference between actinides and lanthanides, thus indicated no clear increased covalency in the actinide complexes. Choppin[49] points out that, although a large difference was not manifest, a small difference that resulted in a correlation of 1.08 when the stability constants of Am vs. Nd were plotted, indicating there may be a slightly

14

more covalent bonding for Am than for Nd. Choppin[49] also mentions data from optical, Mössbauer, and nuclear magnetic resonance spectroscopy that led him to conclude concerning f-element covalent bonding:

> "In summary, the data are consistent with ionicity as the predominant character of lanthanide and actinide bonding. However, there is compelling evidence for some small amount of covalency, which is stronger in the actinide bonds. The argument for this extra covalency involving the f orbitals does not seem to have strong experimental support, and more likely, the s orbitals play the major role in the covalency of the bonding f-element cations."

So, although bonds through f orbitals were not implicated in increased covalent character of actinide bonding, data from a variety of techniques supports a slightly increased covalent character of actinide bonds over the analogous lanthanide bonds. This slightly increased covalent character of actinide bonds appears to be the fundamental reason behind the effectiveness of soft donor ligands to selectively complex actinides over lanthanides and is the basis for much of the ligand design theory and practice in trivalent actinide / trivalent lanthanide separations.

1.3   Summary of Dissertation

This work explores various principles and phenomena related to the trivalent lanthanide / trivalent actinide separation. This chapter established the motivation for this research and presented background information introducing the subject area that will be explored later in this work. Chapter 2 discusses the characterization of the organic phase of the TALSPEAK solvent extraction system under variable loading conditions. Chapter 3 discusses a study of the temperature dependent behavior of lactate, which is used in the TALSPEAK solvent extraction system as a major component of the aqueous phase. Chapter 4 discusses a study of the complexation constants between europium and 8-hydroxyquinoline, a ligand that is being evaluated for selectivity in the trivalent lanthanide/trivalent actinide separations.

CHAPTER 2

TALSPEAK ORGANIC PHASE SPECIATION UNDER VARIABLE LOADING

CONDITIONS: HCl AND LACTATE AQUEOUS MEDIUM STUDIES

2.1   Introduction

The Trivalent Actinide-Lanthanide Separation by Phosphorus reagent Extraction from

Aqueous Komplexes (TALSPEAK) Process[1] has been demonstrated to work on various scales.[2]

Under carefully controlled conditions this process achieves one of the most difficult separations

that are encountered in nuclear separations: that of trivalent actinides (An^{3+}) from trivalent

lanthanides (Ln^{3+}). This separation is a necessary part of a partitioning and transmutation

scheme that involves the recycle of all transuranium elements in irradiated nuclear fuel. The

TALSPEAK is a well-studied process that is nearing the level of understanding required for

successful industrial application, but this process still lacks a comprehensive extraction model

that will account for the system behavior at all conditions.[52]

Lactate plays a vital role in the TALSPEAK system. It acts as an aqueous phase buffer that

prevents the pH from leaving the narrow operating window required for this challenging

separation. As will be discussed in this chapter, lactate also affects the system speciation in

various ways, including: co-extraction with M^{3+} and causing the formation of highly aggregated

species. Understanding the ionization behavior of lactate under various temperatures is vital to

creating a complete model of the TALSPEAK system. Lactate is the major constituent (1 M)[53] of

the aqueous phase of the TALSPEAK system. The dissociation of lactic acid will significantly

change the ionic strength of the aqueous phase, resulting in large activity coefficient changes.

Measuring the acid/base behavior of lactate is therefore an important step to establishing a

complete TALSPEAK model.

For the chemical reaction in equation (2.1), the general form for the chemical equilibrium constants[54] is shown in equation (2.2)

$$aA + bB \xleftrightarrow{K} cC + dD \tag{2.1}$$
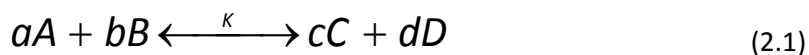
$$K = \frac{\mathcal{A}_C^c \mathcal{A}_D^d}{\mathcal{A}_A^a \mathcal{A}_B^b} = \frac{[C]^c \gamma_C^c [D]^d \gamma_D^d}{[A]^a \gamma_A^a [B]^b \gamma_B^b} \tag{2.2}$$

where $\mathcal{A}$ is the activity, the quantities shown in square brackets are the molar concentrations, and γ is the activity coefficient. Analytical chemistry techniques provide a measure of the bracketed quantities in the equilibrium expression. The activity coefficients are more difficult to measure and correlate. Because activity coefficients depend on ionic strength, performing experiments at constant ionic strength is a way to keep the activity coefficients constant and lump them in with the equilibrium constant as shown in equation (2.3).

$$K \frac{\gamma_A^a \gamma_B^b}{\gamma_C^c \gamma_D^d} = \frac{[C]^c [D]^d}{[A]^a [B]^b} = K_{cond} \tag{2.3}$$

This new expression shows the value known as the conditional equilibrium constant. In this work the chemical equilibrium constants presented as either equilibrium constants as shown in equation (2.2) or conditional chemical equilibrium constants as shown in equation (2.3).

The ionization equation and derivation of pK_a for lactic acid is:

$$HA \xleftrightarrow{K_a} H^+ + A^- \tag{2.4}$$

$$K_a = \frac{[H^+][A^-]}{[HA]} \tag{2.5}$$

$$pK_a = -\log_{10}(K_a) \tag{2.6}$$

The current IUPAC recommended values of the pK_a of lactic acid are listed in Table 2.1.

Table 2.1- IUPAC recommended values for the conditional pK_a of Lactic Acid.[55]

Ionic Strength (medium unspecified)	Temp (°C)	pK_a of Lactic Acid
0 M	25	3.86
1.0 M	25	3.64
2.0 M	25	3.80

From the literature, it appears the medium most used was $NaClO_4$.[55] The data

recommended by the IUPAC for the lactic acid pK_a in NaCl medium are shown in Table 2.2.

Table 2.2- IUPAC recommended data for the conditional pK_a of Lactic acid in NaCl media.[55]

Ionic Strength (NaCl)	Temp (°C)	pK_a of Lactic Acid
0 M	25	3.86
0.15 M	25	3.51
0.15 M	37	3.70
0.5 M	25	3.50
0.6 M	25	3.572

The selection of 25°C for laboratory experiments is a convenient choice, but may not be

relevant to industrial applications. Because TALSPEAK is being evaluated and prepared for

industrial scale application, a wider temperature range will be necessary. For this purpose

extending the current published data record with lactic acid pK_a values for the temperature

range of 25-65°C is desirable.

Research on a simplified TALSPEAK process has shown the mechanism of extraction of Ln^{3+}

by bis(2-ethylhexyl) phosphoric acid (HA). By excluding lactate (Lac) and

diethyltriaminepentaacetic acid (DTPA) from the aqueous phase Peppard *et al.*[56] showed that

lanthanides are extracted from HCl or HNO_3 by HA according to the mechanism shown in equation (2.7).

$$Ln^{+3} + n\overline{(HA)_2} \leftrightarrow 3H^+ + \overline{LnA_3(HA)_{2n-3}}$$ (2.7)
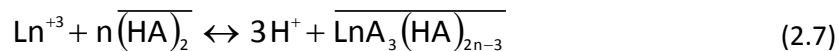
Various values for the HA dimer stoichiometric coefficient (n) have been reported. Peppard *et al.*[56] concluded that n = 3 when extracting tracer quantities into an aromatic diluent. Lundqvist *et al.*[57] later showed that n=2.5 or 3 depending on the diluent. For aromatic diluents and aliphatic diluents with very low $[HA]_{org}$ ($10^{-4.5}$–$10^{-3.5}$ M HA) n = 3, however, n = 2.5 for aliphatic diluents where the $[HA]_{org}$ is greater. Other authors[58-59] have expressed n as a function of the number of deprotonated HA complexed to the metal (d), the number of protonated HA complexed to the metal (p), and the degree of polymerization of HA in the diluent (s) as shown in equation (2.8).

$$n = \frac{d + p}{s}$$ (2.8)

This formulation does not explicitly assume that HA is strictly a dimer as other authors have. Dubuquoy *et al.*[58] first proposed this formulation for n and suggested that s for HA was 2 below $[HA]_{org} < 0.3$ M but was 3 at where $[HA]_{org} > 0.3$ M. In contrast, Thomas and Burkhart[59] note that other research by various authors has shown that s is not strictly 2 or 3 at any given time, but that partial trimerization of HA occurs over a range of $[HA]_{org}$ (0.1–1 M HA) and increases with increasing $[HA]_{org}$.

Mel'nik *et al.*[60] reported that there are conditions where the HA-Ln^{3+} extraction behavior deviates from that shown in equation (2.7). When performing extractions with weighable quantities of Ln^{3+}, log-slope analysis consistently produced 2.7 ± 0.1 instead of the previous published 3.[56] Mel'nik *et al.* reasoned that when sufficient quantities of Ln^{3+} salts are present,

aqueous complexes between Ln^{3+} and the counter ions can be extracted by ion-pair extraction by the mechanism shown in equation (2.9).

$$LnB_b^{3-b} + n\overline{(HA)_2} \leftrightarrow (3-b)H^+ + \overline{LnB_bA_{3-b}(HA)_{2n-(3-b)}}$$ (2.9)
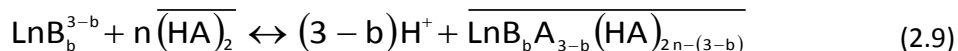
This behavior occurs under two types of conditions: 1) where pH drives Ln^{3+} extraction beyond the ideal HA extraction stoichiometry in equation (2.1)[53] and 2) where high concentrations of acid counter ion (B) exist to shift the extracted species to $LnB_3(HA)_3$. This second behavior was observed at HCl concentrations greater than 5 M HCl for Y^{3+},[61] and at HNO_3 concentrations greater 5–7 M HNO_3 for La^{3+} through Lu^{3+} respectively.[62-63]

The Na^+ distribution data in the literature shows that it is transferred to the organic phase of non-polar diluents when HA is converted to NaA by the mechanism[57] shown in equation (2.10) with n = 2.

$$Na^+ + n\overline{(HA)_2} \leftrightarrow H^+ + \overline{NaA(HA)_{2n-1}}$$ (2.10)
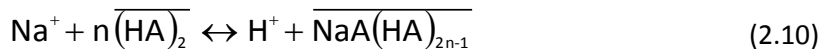
If more than 25% of the HA is converted to NaA, the HA dimers are destroyed and NaA aggregates, forming a third phase.[57]

Average aggregation increases with the extraction of Ln^{3+} ions.[64] This is a result of the speciation [equation (2.1)] that has two to three HA dimers complexing the Ln^{3+} metal center. High loading conditions can cause problems in the TALSPEAK process if they lead to loss of extractant solubility. Under extremely high trivalent metal loading conditions, insoluble gels will form as an interphase between the organic and aqueous phases resulting in loss of system flow properties.[65-66] The formation of a gel interphase can occur under equilibrium conditions, or temporarily under high mass transfer conditions.[65] A detailed physical description of the process through which interphase species form is in Kizim *et al.*[67] Previous work on the

formation of gel interphase indicate that this behavior is dependent on HA concentration, aqueous acidity, and aqueous metal concentration.[66] Targeted synthesis to understand other high aggregation species has produced the following compounds: $LnA(NO_3HA)_2$,[68] $LnA_2(ClHA)$,[68] $Ln(A)_3$,[69-70] and $Ln(Acetate)_b(A)_{2-b}$.[71] Additional tests on the species $Ln(A)_3$ and $Ln(Acetate)_b(A)_{2-b}$ showed that they were insoluble in excess diluent (octane[15] and decane[16]), but are solvated by the addition of excess HA.[71-72] Neutralization of HA by NaOH in the absence of Ln^{3+} can also lead to extreme aggregation of HA[73] and formation of a gel-like third phase.[74] This extractant loss can be prevented by adding strong electrolytes such as NaCl, $NaNO_3$, or Na_2SO_4 to the aqueous phase[73-74] or organic phase modifiers.[75-76] Blake *et al.*[75] tested 63 possible candidates and showed that a variety of primary alcohols with 8-13 carbons, tributyl phosphate, dibutly butyl phosphonate, butyl dibutyl phosphonate, and tributyl phosphine oxide were among the most promising organic phase modifiers.

Visible spectroscopic studies of the complexes formed under TALSPEAK conditions increase the understanding of their structures. Jensen *et al.*[64] showed hypersensitive bands in the Nd^{3+} spectrum that were indicative of rearrangement of ligands surrounding the Nd^{+3} metal center. The change occurring as suggested by Jensen *et al.* was from $Nd(AHA)_3$ or NdA_3 to $Nd_2(A)_6$ that occurred with increasing metal loading. Comparison of the visible spectra of various Nd^{3+} complexes has shown that the coordination chemistry surrounding the Nd^{3+} metal center leads to a recognizable spectral profile. In systems where organophosphorus ligand dimers complex Nd^{3+} [Cyanex 272[77], HA in $Ln(AHA)_3$] the Nd^{3+} absorbance spectrum shows bands at 570, 577, 585, 590 and 605 nm.[64, 78] In systems where organophosphorus ligand monomers complex Nd^{3+} (Cyanex-302,Cyanex-301[77]; HA in LnA_3) the Nd^{3+} absorbance spectrum shows a band at 585 nm with a shoulder at 577 nm.[64, 69] The interpretation of these references indicates that the

presence of the 570 nm band indicates the presence of dimerized HA in the coordination sphere of Nd^{3+}.

Studies of the IR spectrum of HA complexed with Ln^{3+} or Na^+ have shown spectral changes indicative of metal complexation. The IR spectrum of HA[79-80] and its Na^+,[79-81] and Ln^{3+} [68, 70-71] complexes has been presented in detail in various sources. The IR spectral features of highest interest is the asymmetric stretching of the P=O and P-O bonds that show bands at 1230 and 1035 cm^{-1} respectively. When HA is complexed with metals, the 1230 cm^{-1} band will shift depending on the metal involved in complexation (Na^+= 1220, Ln^{3+} = 1200 cm^{-1}). [68, 81] Literature also has shown that large aggregate Ln^{3+}:HA complexes contain –O–P–O– bridging bands that appear at 1090 or 1100 cm^{-1}.[68, 71] IR absorbance bands in Ln^{3+}:HA complexes appearing in the 1500-1700 region have been given various assignments. A vibration band at 1620 cm^{-1} in $LaA(NO_3)_2 \cdot 2H_2O$ complex was assigned to H_2O bending. A vibration band in $LnAcetateA_2$ complex involving Ho^{3+}, Er^{3+}, Yb^{3+} and Lu^{3+} at 1575–1590 cm^{-1} was assigned to the acetate-Ln^{3+} complex vibrations in bridging acetate molecules.[71]

The presence of water in non-polar diluent phases is predominantly bound in organic complexes. However, past work with HA has shown that water is absent from the inner coordination sphere of the Ln^{3+}:HA extracted species.[82-83] Thus, it is expected that little water will be found in the organic phase unless there exists complexes between HA and non-Ln^{3+} species in solution. Non-Ln^{3+} complexes that may contain water are the HA dimer, and NaA, which has been shown to contain water in various studies.[73, 81, 84]

Past research has focused on isolated aspects of the chemistry, at times connecting a few related phenomena, but rarely providing a comprehensive characterization of the organic phases. The conditions studied also tend to focus on either low or high loading so that speciation is predictable and uniform. Published research has demonstrated formation of high-

order aggregates of $(LnA_3)_x$ [69, 72] or $(LnBA_2)_x$ [71] at high organic phase loading, but the gap in understanding of the dynamic change from the high to low HA aggregation and speciation change due to transition from high to moderate and low loading conditions still exists. The investigation reported herein enhances the knowledge of the HA speciation that exists over the dynamic range of high to low loading in the organic phase. In this investigation the organic phase was initially characterized by measuring the distribution of Nd^{3+}, Na^+, H_2O and H^+. Additional characterization included vapor pressure osmometry to assess the HA aggregation, and visible and IR absorbance spectroscopy to probe the coordination environment of Nd^{3+} and HA respectively. This work is designed to develop organic phase characterization methods that will be used in future studies of the TALSPEAK system.

2.2   Experimental

2.2.1   Materials

Bis(2-ethylhexyl) phosphoric acid (HA or HA) (97%) was obtained from sigma-Aldrich and was diluted using 2,2,4-trimethylpentane (99%) (isooctane) obtained from Lancaster Synthesis, Inc. to make solutions ranging from 0–1 M. HA was not purified, however, all solutions were washed once with deionized water prior to use. Bibenzyl (99%) was obtained from Aldrich and recrystallized twice from methanol prior to dissolution in isooctane. Water used in preparing solutions was at least 15 MΩ-cm. $NdCl_3 \cdot 6H_2O$ (99.9% metals basis), concentrated DL-lactic acid (85%+), 50 wt% NaOH, NaCl, were obtained from Aldrich and used as received. The concentrated lactic acid was diluted with DI water, boiled for 24 hours to eliminate polymerization, and then standardized by potentiometric titration prior to use. For the radiotracer distribution measurements of lactate and sodium, ^{14}C labeled sodium lactate, and [22]Na stocks were obtained from Perkin Elmer. For the NMR experiments, ^{13}C labeled lactate (carbonyl C label) and d18-isooctane (98 atom%) were obtained from Sigma-Aldrich. Isooctane

was used as the diluent in these studies because n-dodecane that is typically used in the

TALSPEAK process did not have a vapor pressure high enough for the vapor pressure osmometer

used in this study.

2.2.2 Vapor Presssure Osmometry of Aqueous Lactate

A series of varied lactic acid concentrations (0.1–1.9 mol/L) dissolved in DI water was also

prepared for the vapor pressure osmometry (VPO) experiments. Measurements by VPO were

performed on a Wescor Vapro 5520 vapor pressure osmometer. The instrument operates at

ambient temperature, 21.9 ± 0.2°C for these experiments. The instrument was calibrated and

operated according to the manufacturer's recommended instructions.[85]

2.2.3 Quantification of the pK_a of Lactate

Lactic acid in the titration solution was 0.15 mol/L in 1.925 mol/L NaCl. The pcH (described

later in this section) titration solution was 0.1 M HCl in 1.9 M NaCl. The titrant for these

experiments was 1 M NaOH in 1 M NaCl. The NaOH solution was made using boiled >15 MΩ cm

de-ionized (DI) water and stored in an Ascarite vented bottle to prevent CO_2 absorption.

The automatic potentiometric titrations were performed using a Metrohm TIAMO auto-

titration system that was running the TIAMO version 1.2 software. Titration curves were

obtained using the static titration function measuring mV with the fixed volume additions of 50

μL. The initial solution volume for each titration was 30 mL. Ionic strength was maintained at

$I_{total, mol/L}$ = 2.0 M. Temperature was held constant by an aluminum heating block that was

controlled by a J-Kem Model 150T Temperature controller that was self-tuned at start-up every

day. Stirring was provided by a stir-plate on which the heating block was placed. Titrations were

performed in Teflon beakers manufactured for use with the heating block. Temperature and pH

measurements were recorded simultaneously and automatically by a combination

pH/temperature electrode that was connected to the TIAMO system.

Initial experiments were performed using pH 4, 7 and 10 buffers to calibrate the pH electrode prior to each potentiometric titration. This method of pH calibration proved to be insufficiently precise and the titration curves obtained did not yield satisfactory results. A second, more robust method of pH calibration proved to offer much better results. This method is known as the pcH method. In the pcH method adapted from the Gran Plot method,[86-88] the actual concentration of $\underline{H}^+$ (cH) is correlated with the potentiometer's response in mV. The conversion of mV to the concentration of H^+ is more convenient, because the conditional equilibrium constant is not a function of hydrogen ion activity, but rather the concentration of H^+ [see equation (2.3)]. In the pcH method, the potentiometer's response in mV is measured against an entire titration of a strong acid of known concentration. Because the strong acid is completely ionized, the cH can be calculated from the original solution concentration and the volume of titrant added using equations (2.11)[88] and (2.12)[88].

$$\left[H^+\right] = \frac{VH - vB}{V + v} = \frac{VH(v_e - v)}{v_e(V + v)} = \frac{B(v_e - v)}{V + v} \tag{2.11}$$

$$\left[H^+\right] = \frac{K_w}{\left[OH^-\right]} = \frac{K_w(V + v)}{B(v - v_e)} \tag{2.12}$$

where H is the H^+ concentration in the initial acid solution, V is the initial volume of acid, v is the volume of titrant added, v_e is the equivalence point volume, B is the concentration of base in the titrant, and K_w is the dissociation constant of water. Equation (2.11)[88] is used for the titration points before the equivalence point and equation (2.12)[88] is used for titration points after the equivalence point. A linear regression of the mV response of the potentiometer and the -Log(cH) (i.e. pcH) can be obtained and used on mV data from titrations of weak acids to obtain pcH curves. This method can be applied to various temperatures and ionic strengths as long as a new mV vs. pcH correlation is obtained for each new experimental condition (ionic

strength and temperature). Plotting the results in a Van't Hoff curve require changing the base

of the logarithmic pK_a, which is in base 10.

2.2.4   Liquid-Liquid Distribution Measurements Methodology

To assess effect of the extractant loading on the distribution of the aqueous phase

components and speciation of the organic phase, HA concentration was varied from 0–1 M in all

extraction systems. For each extraction system, the aqueous phase composition was held

constant. For the HCl medium experiments, the initial aqueous pH was adjusted to about either

1 or 4 using HCl. For the lactate medium experiments, the pH of the lactic acid solutions was

adjusted by adding NaOH. Aqueous concentration of Nd^{3+} was 0, 30, or 60 mM. Aqueous phase

ionic strength was held constant at 1.2 M using NaCl as a supporting electrolyte. The initial

aqueous phase concentrations are shown in Table 2.3 and Table 2.4. The initial aqueous phase

concentrations were calculated based on the mass of 50wt% NaOH, $NdCl_3 \cdot 6\ H_2O$ or NaCl salt, or

volume of standardized lactic acid or HCl solution added to these solutions.

Table 2.3- Aqueous phase solution concentrations for the HCl medium experiments.

	pH 1+0 mM Nd+HCl	pH 1+30 mM Nd+HCl	pH 4+0 mM Nd+HCl	pH 4+30 mM Nd+HCl
$pH_{initial}$	0.93	0.94	4.05	4.31
$[Nd^{3+}]$ / M	0	0.03	0	0.03
$[Na^+]$ / M	1.134	0.884	1.172	1.000
$[Cl^-]$ / M	1.219	1.059	1.172	1.090
I_{Calc} / M	1.20	1.19	1.20	1.20

To control the ionic strength of the aqueous phase, the aqueous phase compositions were

modeled prior to mixing the solution using the Debye–Hückel approximation of the activity of

the lactate and hydrogen ions in solution[89] and the complexation constants for the Nd:lactate complexes.[90] Complexation constants used are shown in Table 2.5.

Table 2.4- Aqueous phase solution concentrations for the lactate medium experiments.

	pH 1+0 mM Nd+Lac	pH 1+30 mM Nd+Lac	pH 4+0 mM Nd+Lac	pH 4+30 mM Nd+Lac	pH 4+60 mM Nd+Lac
$pH_{initial}$	1.10	1.03	4.21	4.13	4.04
$[Nd^{3+}]$ / M	0	0.03	0	0.03	0.06
Lactate / M	1	1	1	1	1
$[Na^+]$ / M	0.76	0.67	1.26	1.03	1.03
$[Cl^-]$ / M	0.83	0.83	1.26	1.22	1.21
I_{calc} / M	1.20	1.18	1.21	1.10	1.17

Table 2.5- Constants used to model ionic strength of aqueous phase for phase contacts.

Nd:Lactate	Nd:Lactate Log(β)	Condition	H:Lactate Log(β)	Condition
1:1	2.45[90];	21°C, 2.0 M, NaClO$_4$	3.86[89]	25°C, NaCl, 0 M
1:2	4.39[90]			
1:3	5.44[90]			
1:4	5.82[91]	20°C, 1.0 M, NaClO$_4$		

In the text, each extraction system is referenced by initial aqueous pH, Nd^{3+} concentration, and aqueous medium (HCl or Lac). Multiple systems are referenced by referring to more than one of the system variables enclosed in parentheses. An example is pH 4 + (0, 30) mM Nd would refer to both pH 4 + 0 mM Nd and pH 4 + 30 mM Nd. All samples were shaken overnight (15+ hours) at 20 ± 2°C. The organic and aqueous phase volumes were equal for phase contacts except in the [22]Na and ^{14}C tracer tests where the addition of tracer spike increased the aqueous

volume to 5% greater than the organic phase. Control distribution experiments were conducted for each analyte using isooctane diluent without HA. Multiple measurements were performed for each experiment.

2.2.5   Equilibrium pH Measurement

The pH was measured for all pre- and post-contact aqueous phase samples using a Radiometer TIMS900 Auto-titration Manager in pH measurement mode with an Orion ROSS Ultra Semi-micro pH probe. The pH probe was calibrated before use using pH 4 and 7 buffers from Fisher Scientific. Measurement error is 0.01 pH units.

2.2.6 Nd^{3+} Extraction

The Nd^{3+} distribution into an organic phase was quantified using the visible spectra obtained from the aqueous phase assuming the 100% mass balance is sustained. For the HCl system the molar absorptivity was quantified for each system using a calibration curve with $[Nd^{3+}]_{aq}$ from 0-40 mM at both pH 1 and 4. The molar absorptivity observed for 574.94 nm was 6.77 ± 0.02 for the pH 1 + 30 mM Nd + HCl and 6.88 ± 0.03 L mol^{-1} cm^{-1} for the pH 4 + 30 mM Nd + HCl system (see all absorptivities for pH 1 and 4 systems in Table 2.6). Only the 574 nm band was utilized for quantifying the aqueous Nd^{3+} concentration in the HCl systems. An example of the Nd^{3+} absorbance bands observed in the aqueous phase is shown in the upper spectrum of Figure 2.9.

Other molar absorptivities published for 574.94 nm are 6.93 (in ClO_4^- media)[92], and estimated from a figure at 6.74 (in Cl^- media).[93] The concentration of neodymium in the aqueous post-contact phase was determined using the average of the observed absorptivies of Nd^{3+} at 574 nm in HCl media. This aqueous concentration was used in the mass balance to calculate equilibrium organic Nd^{3+} concentration. A conservative 2% error is assumed for all Nd^{3+} concentrations based on the 1.1% standard deviation that was observed in the average of the two molar absorptivities of Nd^{3+} in the HCl systems.

Table 2.6- Molar absorptivities observed for Nd^{3+} in the aqueous phase.

Wavelength (nm)	pH 1 + 30 mM Nd + HCl		pH 4 + 30 mM Nd + HCl	
	ε (L mol^{-1} cm^{-1})	R^2	ε (L mol^{-1} cm^{-1})	R^2
512.18	1.71 ± 0.02	0.9986	1.66 ± 0.02	0.9985
521.28	3.92 ± 0.02	0.9996	3.96 ± 0.02	0.9995
574.94	6.77 ± 0.02	0.9999	6.88 ± 0.03	0.9996
731.66	3.78 ± 0.03	0.9993	3.81 ± 0.02	0.9995
740.32	6.50 ± 0.04	0.9993	6.60 ± 0.03	0.9997
794.19	10.59 ± 0.05	0.9997	10.78 ± 0.04	0.9998
801.37	6.14 ± 0.04	0.9994	6.24 ± 0.03	0.9997
865.68	3.72 ± 0.03	0.9988	3.79 ± 0.02	0.9996

The presence of lactate in the aqueous phase lead to the formation of Nd^{3+}:Lactate complexes for the pH 4 systems, changing the absorbance spectra. Thus, pH 4 system Nd^{3+} concentration was measured from the observed molar absorptivity of the pre-contact aqueous solution of known concentration using the aqueous phase absorbance at 797.94 nm. The pH 1 + 30 mN Nd + Lac system displayed similar absorbance to the pH 1 + 30 mM Nd + HCl system, so same method used for the HCl systems was used. A summary of the absorptivities used for the Nd systems is shown in Table 2.7.

Table 2.7- Summary of the molar absorptivity data, and calibration techniques used in the quantification of Nd^{3+} in the aqueous phase solutions.

Systems	pH (1, 4) + 30 mM Nd + HCl pH 1 + 30 mM Nd + HCl	pH 4 + (30, 60) mM Nd + Lac
Calibration Data Set	0–40 mM Nd calibration curve	30, 60 mM Nd pre-contact aqueous sample (single point)
Wavelength (nm)	574.94	797.94
Molar Absorptivity Used (L mol^{-1} cm^{-1})	6.82 ± 0.08	10.5 ± 0.2

The calculation of the theoretical loading was performed under the assumption that extracted Nd^{3+} exists as $NdA_3(HA)$ in the organic phase under low loading conditions and n = 2 in equation (2.1). This assumption is consistent with the aggregation data presented herein. The equation defining theoretical loading is shown in equation (2.13)

$$Loading_{theoretical} = \frac{[Nd]_{org}}{[HA]_{org}/2n}$$ (2.13)

where 2n is the ratio of HA-to-Nd^{3+} in the organic phase when equation (2.7) is the mechanism that describes Nd^{3+} extraction.

2.2.7 $^{22}Na^+$ Tracer Extraction

For $^{22}Na^+$ experiments, equal volumes (0.4 mL) of organic and aqueous solutions were aliquoted into cryogenic centrifuge tubes. A spike of 20 μL of a $^{22}Na^+$ tracer was added to each two phase sample. These samples were contacted as described in section 2.2.4. Following the contacts, 200 μL of each phase were transferred to separate test-tubes for counting. Gamma counting was performed using a Perkin Elmer Cobra II Auto-Gamma. The distribution ratios for were measured by calculating the ratio of $^{22}Na^+$ back-ground subtracted activity in the organic vs. aqueous phase. The equation used for the calculation of distribution ratios is shown in equation (2.14)

$$D_{Na} = \frac{[Na^+]_{org}}{[Na^+]_{aq}} = \frac{CPM_{org}}{CPM_{aq}}$$ (2.14)

where CPM is counts per minute. The concentration of sodium in each phase was then calculated from the distribution ratio through an iterative calculation that guessed what fraction of the total sodium was in each phase that resulted in a distribution equal to that observed. The recovery of $^{22}Na^+$ was confirmed by comparison with the mass balance samples. The detection limit for these experiments for $[Na^+]_{org}$ was 0.6–6 mM depending on the background count

rates. Because these samples were counted using an automated counting instrument, and due

to the penetrating nature of gamma radiation there was an elevated background for systems

with higher organic Na^+ concentrations. The HCl and lactate systems were counted separate

from each other, which contributed to high detection limits for the lactate systems than the HCl

systems. Empty counting vials were counted interspersed with the samples to correct the count-

rates for the added background in the high count rate systems, but the increased background

led to a detection limit that varied by system. A table showing the detection limits for the Na^+

extraction experiments is shown in Table 2.8.

Table 2.8- The detection limits for the Na^+ extraction experiments by system.

System	$[Na]_{org}$ / M
pH 1 + 0 mM Nd + HCl	0.0013
pH 1 + 30 mM Nd + HCl	0.0009
pH 4 + 0 mM Nd + HCl	0.0006
pH 4 + 30 mM Nd + HCl	0.001
pH 1 + 0 mM Nd + Lac	0.003
pH 1 + 30 mM Nd + Lac	0.003
pH 4 + 0 mM Nd + Lac	0.006
pH 4 + 30 mM Nd + Lac	0.0016
pH 4 + 60 mM Nd + Lac	0.004

2.2.8 H_2O Distribution (Karl Fischer Titration)

Water content in the organic phase was measured using a Photovolt Aquatest 2010

Coulometric Moisture Analyzer. The instrument function was verified at the start of each set of

samples by titrating samples of 2 μL of DI H_2O. After instrument sensitivity was verified using

water test samples, organic phase samples (0.1–2 mL) were introduced into the titration vessel

using manual pipettes by opening the vessel briefly. Sample sizes were varied to keep the

measurement signal below 2000 μg H_2O per sample.

2.2.9   [14]C labeled Lactate Distribution

For ^{14}C lactate experiments, 0.4 mL of both the organic and aqueous phase were measured

into polypropylene cryogenic vials. A spike of 30 μL of the sodium lactate tracer was then added

to the two phase sample to achieve a ^{14}C activity of 60 μCi, which were contacted as previously

described in section 2.2.4. Liquid scintillation counting was performed using a Packard Tricarb

2550 TR/AB. [14]C labeled lactate distribution ratios (D_{Lac} = $[Lac]_{org}/[Lac]_{aq}$ = CPM_{org}/CPM_{aq}, where

CPM is counts per minute) were measured by taking the ratio of ^{14}C activity in the organic vs.

aqueous phase (both corrected for background CPM) and used to calculate equilibrium organic

[14]C labeled lactate concentration. Mass balance calculations were performed to ensure

measured count rates accounted for the total activity added. Separate mass balance samples

were prepared for each extraction system using spiked aliquots of 0.4 mL aqueous phase from

each system studied. These spiked aliquots were sampled using the same technique as the

batch contact samples.

2.2.10 Solvent extraction data treatment

Based on literature evidence[57] and our vapor pressure osmometry (VPO) results described

herein, the adopted mechanism of Nd^{3+} and Na^+ extraction can be described by equations (2.7)

and (2.10) with n=2 and 1, respectively. Equilibrium constants corresponding to the equations

(2.7) and (2.10) were obtained using solvent extraction modeling program SXLSQI.[94] Equilibrium

values of the $[Nd]_{org}$ and aqueous pH were used as input values to the program. Based on the

VPO results, the HA aggregation number of 2 was applied in the SXLSQI modeling. Under the

conditions of the applied HA concentration >0.025 M, the concentration of monomeric HA

species was assumed to be negligible based on the literature $LogK_{dimer}$ = 4.59 for HA in the

isooctane diluent.[95] For the Nd^{3+} or Na^+ extraction, the single organic-phase product species were included in the computer model: $Nd(A)_3(HA)_2$ or $Na(A)(HA)$, respectively. For both, Nd^{3+} and Na^+ extraction systems, two parameters were refined in the fit, namely the corresponding log$K$ value and the solubility parameter of the product species. Non-ideality effects were taken into account by using Pitzer[96] parameters for aqueous ions, the Hildebrand-Scott treatment for non-ionic effects in the organic phase,[97] and the Debye–Hückel treatment for electrostatic effects in the organic phase.[98] All constants are corrected to infinite dilution. The solubility parameters and molar volumes of the HA extractant and isooctane diluent were estimated from group contributions. In the SXLSQI modeling, experimental precision for each data point was determined to be ± 6% as estimated from a combination of replicate determinations, volumetric error, and counting precision.

2.2.11 Visible Spectroscopy

For the aqueous phase, the visible absorbance spectrum of each solution was recorded using an Oceanoptics USB2000 spectrophotometer (500–880 nm) with a tungsten light source and a 2.1 Optical Density glass filter. The data were collected using 1 cm pathlength PMMA cuvettes. The spectra recorded were averages of 50 scans of 15 milliseconds each with the boxcar averaging feature disabled. Resolution for the scans was 0.35 nm.

For the organic phase, the same spectrophotometer and light source were employed except the 2.9 optical density glass filter was used. The data were collected using 1 cm pathlength quartz cuvettes. The spectra recorded were averages of 60 scans of 60 milliseconds each with the boxcar averaging feature disabled. Resolution for the scans was 0.35 nm.

2.2.12 Fourier Transform Infrared Spectroscopy

A sample of the organic phase was taken following the phase contacts and analyzed using a Thermo Scientific Nicolet 6700 series spectrometer. Each solution spectrum was collected in

absorbance mode and was an average of 64 scans collected at a resolution of 2 cm^{-1} over the range of 650–4000 cm^{-1}. The instrument was continuously purged with dry air to prevent any water from ambient air to interfere with the absorbance spectrum. The spectra of the solvent absorbance bands were subtracted from the sample spectra normalized (divided) by the HA concentration prior to analysis [calculation shown in equation (2.6)].

$$Abs_{Norm} = \frac{Abs_{sample} - Abs_{solvent} \, X_{solvent}}{[HA]_{sample}}$$

(2.15)

where Abs_{Norm} is normalized, solvent subtracted resultant spectrum; Abs_{sample} is original absorbance spectrum of sample; $Abs_{solvent}$ is absorbance spectrum of pure solvent; $X_{solvent}$ is mole fraction of solution sample; $[HA]_{sample}$ is the molar concentration of HA in the sample.

2.2.13 Vapor Pressure Osmometry

Organic phase samples were analyzed using a Wescor Vapro 5520 and was operated at room temperature. The instrument was calibrated at the start of each sample series using the manufacturer provided calibration standards: 100, 290, 1000 mmol NaCl /kg of water. Bibenzyl dissolved in isooctane was used as a non-aggregating standard. The average aggregation for HA was calculated using the ratio of the slopes from the instrument response for the bibenzyl standards divided by the slope of the sample of interest [see Figure 2.1 for an example of instrument response curves, and equations (2.16) and (2.17)]. Each experimental datum in this work was taken as average of 3 replicate measurements. For samples whose instrument response curve displayed non-linear regions, a 3-point slope was used to obtain an approximation of the average aggregation at the central point.

$$Slope = \frac{\Delta(VPO\_Signal)}{\Delta(molality_{Sample})}$$

(2.16)

34

$$N_{agg,average} = \frac{Slope_{Bibenzyl\_standard}}{Slope_{sample}} \tag{2.17}$$
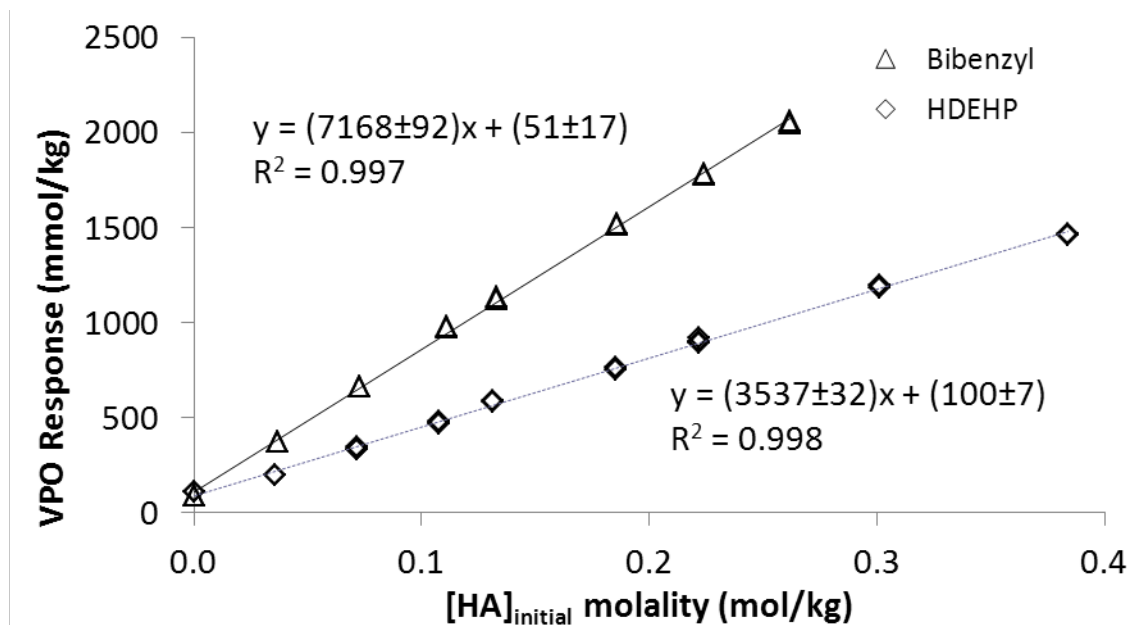
Figure 2.1- An example of the instrument response curve obtained from the bibenzyl standard and unwashed HA solutions.

2.2.14 Vapor Pressure Osmometry Data Treatment

The aggregation of HA was modeled based on the extraction of Nd^{3+} in the organic phase. The expression for the average aggregation number of species containing "A" within the solution is the summation of all products of the "A" containing species with an aggregation value Z_i, and a species fraction value X_i. In this simple system it is assumed two species exist: the extracted Nd^{3+} species containing an unspecified number of "A" ions (NdA_z), and the HA dimer which gives the expression shown below in equation (2.18)

$$N_{agg,Average} = \sum Z_i X_i = Z_2 X_2 + Z_{NdA_z} X_{NdA_z} \tag{2.18}$$

The fraction of the total HA involved in the extracted Nd^{3+} complex (X_{NdAz}) is

$$X_{NdA_z} = \frac{Z_{NdAz}[Nd]_{org}}{[HA]_{total}} \tag{2.19}$$

The remaining fraction of the HA that resides in the dimeric form is equal to

$$X_2 = 1 - X_{NdA_z} \tag{2.20}$$

Since the Z_2 is known to be 2, that can substituted into the equation. By combining equations (2.18), (2.19), and (2.20), equation (2.21) is then obtained:

$$N_{agg, Average} = 2\left(1 - \frac{Z_{NdAz}[Nd]_{org}}{[HA]_{total}}\right) + Z_{NdAz}\left(\frac{Z_{NdAz}[Nd]_{org}}{[HA]_{total}}\right) \tag{2.21}$$

which by inspection is a quadratic equation. By solving for Z_{NdAz}, equation (2.22) is obtained:

$$Z_{NdA_z} = \frac{2[Nd]_{org} \pm \sqrt{(-2[Nd]_{org})^2 - 4[Nd]_{org}\{(2 - N_{agg,Average})[HA]_{total}\}}}{2[Nd]_{org}} \tag{2.22}$$

and was then used to calculate explicitly the value for Z_{NdAz} for each measured VPO data point.

2.2.15 Nuclear Magnetic Resonance Spectroscopy

Due to the paramagnetic shielding effects intrinsic in most lanthanides (including Nd^{3+}), solutions for NMR study were made with the same conditions, except lanthanum was used as the trivalent metal. Lanthanum lacks the unpaired f-electrons that all other lanthanides except lutetium possess, and thus will not shield the sample's NMR signal. Under the assumption that La^{3+} extraction behavior should mimic that of Nd^{3+}, aqueous phase samples were prepared with 20 mol% ^{13}C labeled lactate with the sample composition shown in Table 2.9. The organic phase for these experiments was the same as that used for the regular contact experiments except 20% of the isooctane diluent was deuterated.

The assumption that La^{3+} extraction behavior mimics Nd^{3+} behavior was confirmed by performing batch contact experiments under the same conditions as Nd^{3+}, but with La^{3+}. Extraction behavior of La^{3+} in these batch contact experiments was verified through characterization of the HA aggregation behavior by VPO. The results and discussion of these batch contact experiment are presented in section 2.5.5.

Table 2.9- Aqueous solutions used for the NMR scoping experiments.

	pH 4 + 60 mM La + Lac	pH 4 + 30 mM La + Lac
$pH_{initial}$	4.00	4.10
$[La^{+3}]$ / M	0.060	0.030
$[Lac]_{total}$ / M	1.00	1.00
^{13}C [Lac] / M	0.20	0.20
$[Na^+]$ / M	1.06	1.14
$[Cl^-]$ / M	0.69	0.68
I_{calc} / M	1.19	1.19
$[HA]_{org}$ / M	0.125	1.0

The NMR samples were run using a 300 MHz Oxford magnet with a Techmag computer console. The temperature of the samples was regulated at 15°C. Deuterated isooctane was used as the locking solvent for all scans. The IUPAC recommended NMR standards[99] were used for the ^{23}Na and ^{31}P experiments (0.1 NaCl in D_2O, and 85% H_3PO_4, respectively). For the ^{13}C experiments the signal was taken in reference to the deuterated isooctane peaks. The NMR frequency used was 75.480, 79.395, and 121.502 MHz for ^{13}C, ^{23}Na and ^{31}P respectively.

2.3   Results and Discussion: Lactate pK$_a$ Measurement

2.3.1   Vapor Pressure Osmometry of Aqueous Lactic Acid

Prior to measuring the pK$_a$ of lactic acid, it was necessary to verify that lactic acid does not form dimers or larger aggregates in solution. The degree of aggregation was measured by standard VPO technique as described below. If lactic acid was found to dimerize in the aqueous solution there would be other competing reactions in addition to the reaction shown in equation (2.4) and this would complicate the analysis of the data.
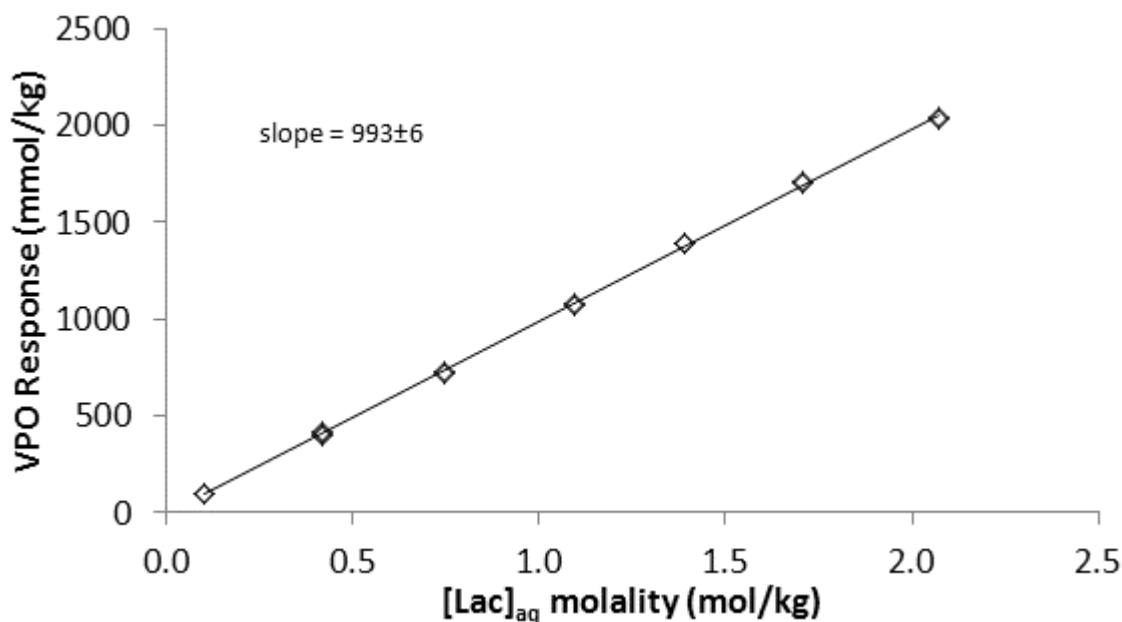
Figure 2.2- VPO Instrument response data from the aqueous lactate samples.

The VPO instrument was calibrated with aqueous NaCl solutions, which also serve as the non-aggregating standard for the aqueous lactic acid in this experiment. The slope from NaCl calibration (non-aggregating aqueous standard) is 1000. The instrument response data obtained

for aqueous lactate is shown in Figure 2.2. Using equation (2.17) to calculate lactate

aggregation, the aggregation number for lactic acid in DI water was 0.993 ± 0.006. This result

indicates that lactic acid remains monomeric, and thus the simple equilibrium reaction shown in

equation (2.4) will be sufficient for our analysis.

2.3.2 The pK$_a$ of Lactic acid at 25–65°C

The titration results gave pK$_a$ values with a linear trend when plotted vs 1/T(K). Results are

shown in Figure 2.3. According to the Van't Hoff equation[100] [see equation (2.23)], there exists

a linear relationship between the natural log of the equilibrium constant and the inverse of the

temperature.

$$\frac{d(\ln K)}{d(1/T)} = -\frac{\Delta H^o}{R} \qquad (2.23)$$
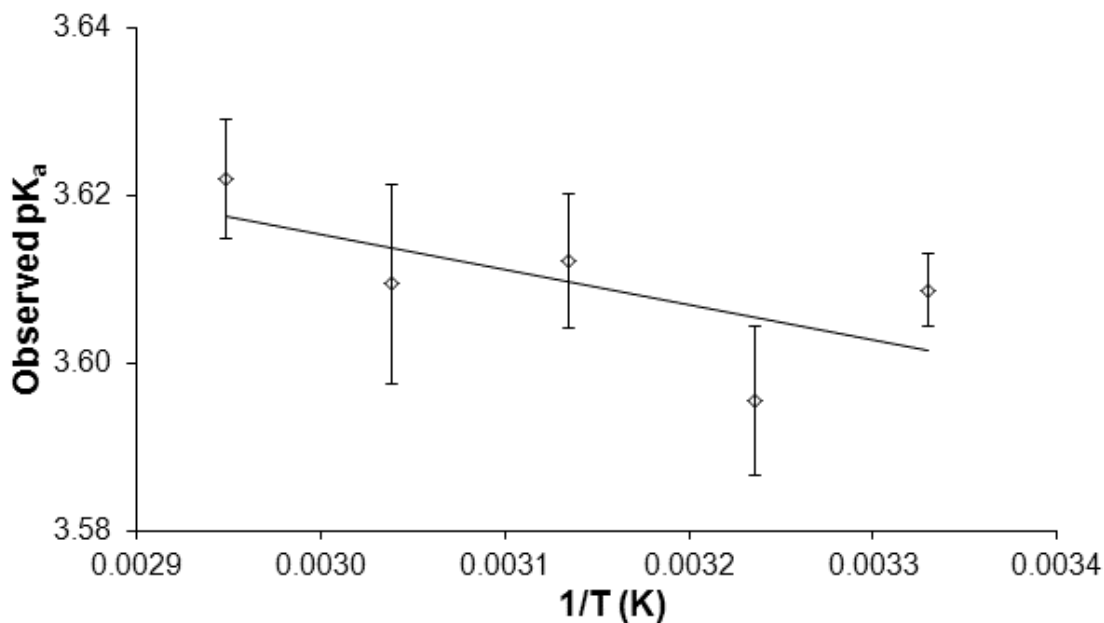
Figure 2.3- The conditional equilibrium constants obtained from the potentiometric titrations of lactic acid at 25–65°C at ionic strength of 2.0 M NaCl.

Therefore, if a series of equilibrium constants at various temperatures are obtained, they can be plotted as ln(K) vs 1/T and the data will fall on a line whose slope is equal to -ΔH°/R. The symbol ΔH° signifies the standard enthalpy of the reaction. The Van't Hoff plot of the data obtained in the potentiometric titrations of Lactic acid are shown in Figure 2.4. Using the slope from Figure 2.4 and the Van't Hoff Equation, the standard enthalpy for this reaction was calculated with the result shown in Table 2.10.
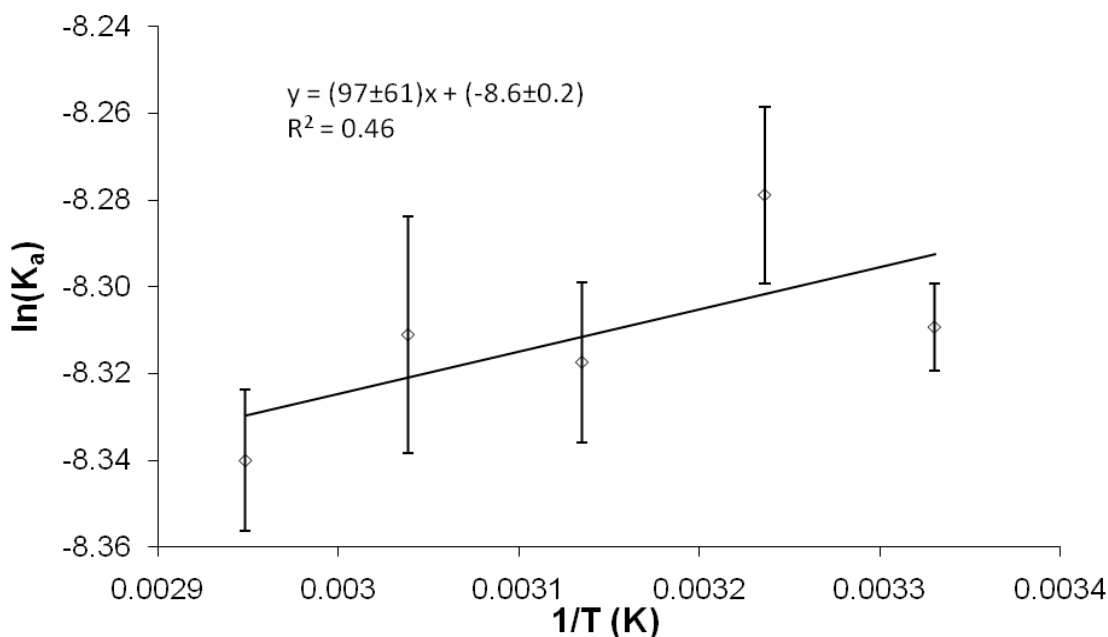
Figure 2.4- Van't Hoff plot of the acid dissociation constant results for lactic acid titrations at 25–65°C at ionic strength of 2.0 M NaCl.

The values for the conditional pK_a of lactic acid are lower than the IUPAC recommended data for I=2.0 M and 25°C. The 3.80 recommended by IUPAC vs. the 3.6 ± 0.1 measured in our experiment shows a small but significant difference. The standard enthalpy of reaction

calculated for lactate deprotonation indicates that temperature has a small effect on the pK_a at I

= 2.0 M NaCl.

This result is consistent with published data measured for poly-carboxylic acids by De

Stefano *et al.*[101] In De Stefano *et al.*'s work, the measured enthalpy of the first protonation of

malonic, propanetricarboxylic, citric, and butanetetracarboxylic acids show that with increasing

ionic strength the enthalpy of protonation decreases.[102] De Stefano *et al.* reports that for

malonic, propanetricarboxylic, and citric acids the reaction enthalpy changes from positive to

negative enthalpy near I = 2.0 M NaCl. Thus, our result showing an enthalpy near zero (-0.8 ± 0.1

kJ/mol) at 2.0 M NaCl for the lactic acid is consistent with the behavior of other carboxylic acids

of similar molecular weights and functionalities. While the data point at 2.0 M NaCl is

consistent, the trend in the deprotonation enthalpy for lactic acid needs to be measured over a

range of ionic strengths before it can be compared to the literature data.

Table 2.10- Standard enthalpy of reaction obtained for lactic acid potentiometric titrations at
25–65°C at ionic strength of 2.0 M NaCl.

I (mol/L)	$\Delta H°$ (KJ/mol)
2.0 M (NaCl)	-0.8 ± 0.1

2.4   Results and Discussion: HCl Aqueous Media

2.4.1   HA Aggregation Results

HA exists predominantly in dimeric form in non-polar diluents,[103] however, the aggregation

will change upon complexation with a metal. Experiments performed on both unwashed and

washed HA in isooctane showed that HA was present exclusively in its dimeric form (N_{agg} = 2.03

± 0.03, 2.02 ± 0.03, respectively). The pH (1, 4) + 0 mM Nd + HCl systems also showed an

average aggregation number of 2.03 ± 0.03 and 1.99 ± 0.03. The aggregation increased in the pH

(1, 4) + 30 mM Nd + HCl systems with values of 2.45 ± 0.04 and 2.54 ± 0.04 respectively. The

increase in aggregation for these systems is a result of the extraction mechanism shown in

equation (2.7) that indicates that for every Nd^{3+} extracted there are two to three dimerized HA

per metal center. There was a small portion of the pH 4 + 30 mM Nd + HCl system at the lowest

$[HA]_{org}$ (0.025–0.05 M) that showed a non-linearity in the instrument response curve (see Figure

2.5) that was consistent with the formation of large aggregation seen in other systems with

similar aggregation present (see Figure 2.14). Because of the data indicating high aggregation

formation was only two to three data points, the best result that can be calculated is a lower

bound of the average aggregation in this region. The lower bound of the average aggregation

was approximated using a 3-point slope of the instrument response data centered on the 0.025

M HA data point showed an elevated aggregation of 4.0 ± 0.5. This aggregation was not

unexpected due to the high loading of the organic phase at these low $[HA]_{org}$. This result is

consistent with the formation of $(NdA_3)_x$ for a small fraction of the total extracted Nd^{3+} that was

observed in the FTIR data.

When the aggregation results were modeled according to the method described in section

2.2.14, the Z_{NdAz} was calculated (Z_{NdAz} = 2n). The calculation averaging both pH (1, 4) + 30 mM

Nd + HCl systems showed that the observed Z_{NdAz} is 4.0 ± 0.4. This value is lower than n = 2.5 (or

Z_{NdAz} = 5) reported in the literature for aliphatic diluents[57] under low loading of HA and

indicates a 4:1 stoichiometry for HA:Nd^{3+} complex under moderately high extractant loading.

The lower stoichiometry observed through the aggregation modeling indicates that there are

only 4 HA molecules per Nd^{3+} in the organic phase. This can indicate that 3 deprotonated and 1

protonated HA molecules are present, or that 2 deprotonated and 2 protonated HA molecules

are present with a co-extracted Cl⁻ to counterbalance the charge. It is impossible to judge

between these possibilities at this time, however, future plans for this research include

quantification of the Cl⁻ distribution in this system that could resolve this question.
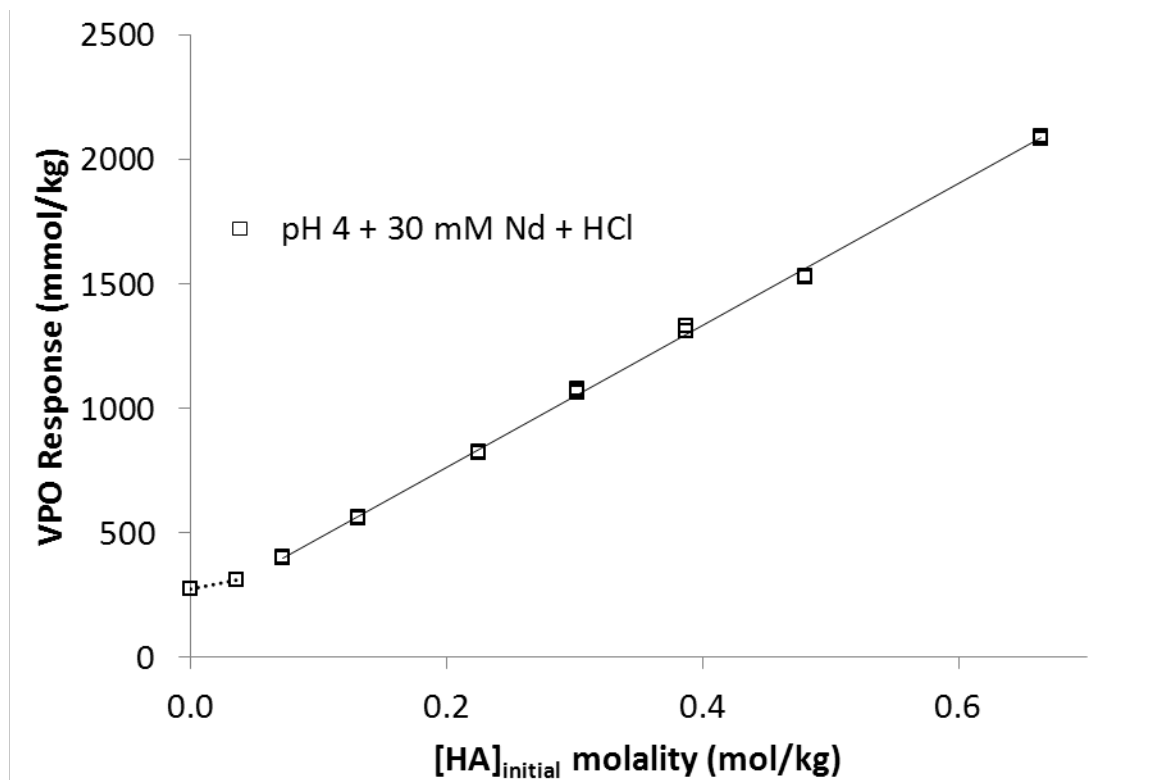
Figure 2.5- Instrument response curve for the pH 4 + 0 mM Nd + HCl system. At low $[HA]_{initial}$ there is a small portion of the data that shows a different slope, indicating increased aggregation.

2.4.2   Liquid-Liquid Distribution Measurements

Overall results for the liquid-liquid distribution measurements are shown in Table 2.11 and

will be discussed in the upcoming sections.

2.4.2.1 Nd^{3+} Distribution Results

Figure 2.6 shows the effect of initial HA concentration on the organic equilibrium Nd^{3+}

concentration. At initial pH of 1, Nd^{3+} extraction gradually increased with increasing HA

concentration. As observed from the data in Table 2.11, there is a concurrent decrease in the pH

from the initial pre-contact to equilibrium post-contact values supports the ion exchange

extraction mechanism as described by equation (2.7). Increase of initial aqueous pH from 1 to 4

facilitated HA ionization and thus Nd^{3+} extraction. For the pH 4 + 30 mM Nd + HCl system, the

concurrent aqueous pH change upon phase equilibration was significant and also consistent

with the equation (2.7) (pH = 4.31 and 0.94 for pre- and post-equilibration, respectively in the 1

M HA isooctane solution. See Table 2.12).
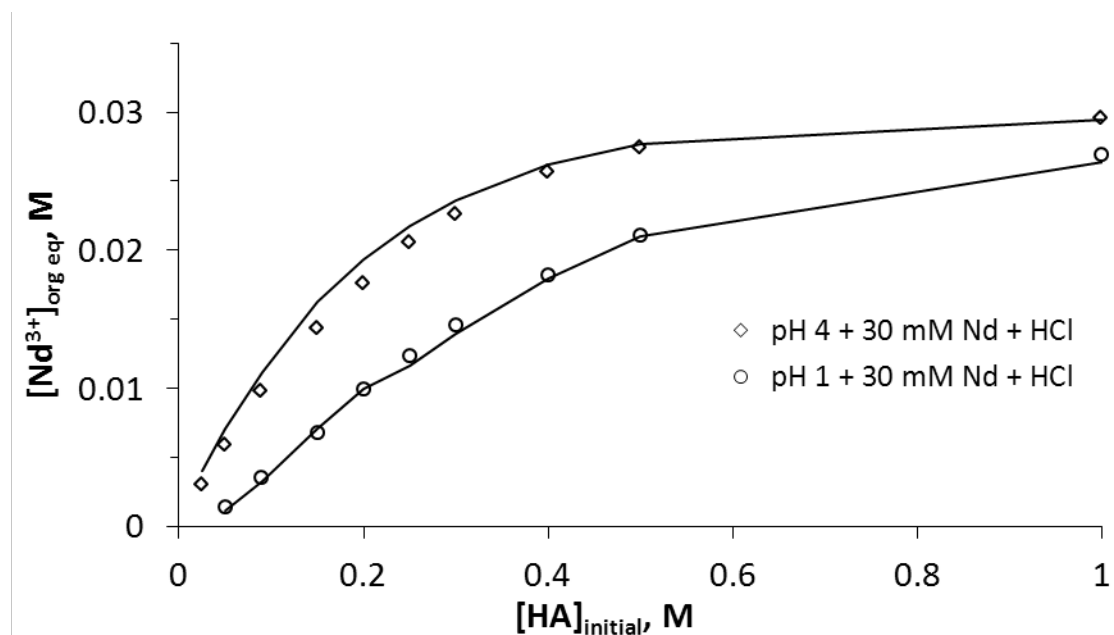
Figure 2.6- Calculated by SXLSQI (line) and observed (symbols) organic Nd^{3+} concentration as a function of initial HA molarity.

Table 2.11- Equilibrium pH, $[Na^+]_{org}$, and $[Nd^{3+}]_{org}$ results for the pH 1 + (0, 30) mM Nd + HCl systems. Estimated error for these values is: $pH_{eq} \pm 0.01$, $[Nd^{3+}]_{org} \pm 2\%$.

| [HA] | pH 1 + 0 mM Nd + HCl | | pH 1 + 30 mM Nd + HCl | | |
	pH_{eq}	$[Na]_{org,eq}$ / M	pH_{eq}	$[Na]_{org,eq}$ / M	$[Nd]_{org,eq}$ / M
0	0.93		0.94		
0.05	0.93		0.92		0.0014
0.09	0.93		0.89		0.0035
0.15	0.93		0.86		0.0068
0.2	0.93		0.83		0.0099
0.25	0.93	BD	0.80	BD	0.0123
0.3	0.93		0.78		0.0146
0.4	0.93		0.75		0.0182
0.5	0.93		0.73		0.0211
1	0.92		0.63		0.0269

BD = Below detection

Table 2.12- Equilibrium pH, $[Na^+]_{org}$, and $[Nd^{3+}]_{org}$ results for the pH 4 + (0, 30) mM Nd + HCl systems. Estimated error for these values is: $pH_{eq} \pm 0.01$, $[Nd^{3+}]_{org} \pm 2\%$.

| [HA] | pH 4 + 0 mM Nd + HCl | | pH 4 + 30 mM Nd + HCl | | |
	pH_{eq}	$[Na]_{org,eq}$ / M	pH_{eq}	$[Na]_{org,eq}$ / M	$[Nd]_{org,eq}$ / M
0	4.08	BD	4.31		
0.025			1.91		0.0031
0.05	3.17	0.0005 ± 0.0002	1.63		0.0059
0.09	2.85	0.0008 ± 0.0003	1.41		0.0098
0.15	2.65	0.0014 ± 0.0004	1.25		0.0144
0.2	2.53	0.0020 ± 0.0005	1.16	BD	0.0176
0.25	2.43	0.0025 ± 0.0006	1.10		0.0206
0.3	2.37	0.0031 ± 0.0006	1.06		0.0226
0.4	2.27	0.0044 ± 0.0007	1.01		0.0257
0.5	2.19	0.0056 ± 0.0009	0.98		0.0275
1	1.95	0.011 ± 0.001	0.94		0.0296

BD = Below detection

The logarithmic value of the equilibrium constant K_{Nd} corresponding to equation (2.7) were

determined using SXLSQI model by fitting the Nd^{3+} distribution results collected for the pH (1, 4)

+ 30 mM Nd + HCl systems simultaneously. The composition of the product species

$Nd(A)_3(HA)_{(org)}$ was deduced using the average aggregation numbers (VPO data), total HA and

Nd^{3+} concentrations in the equilibrium organic phases for these two extraction systems. Based

upon the assumption that in these systems HA exists in two forms: 1) a free dimer and 2) within

a Nd complex, the analysis of these data indicated that the latter contained 4 (4.0 ± 0.4)

extractant molecules. The equilibrium constant or $\log K_{Nd}$ obtained for these systems was –0.14

± 0.06.

2.4.2.2   Na$^{\pm}$ Distribution Results

No Na^+ extraction was observed in the pH 1 + (0, 30) mM Nd + HCl system or in the pH 4 +

30 mM Nd + HCl system (see Table 2.11). In the pH 4 + 0 mM Nd system, Na^+ extraction was

observed with approximately 1% of the HA converted to NaA. Log-slope analysis of the

extraction mechanism (shown in Figure 2.7) shows a slope dependence of 0.99 ± 0.02 (R^2 =

0.997) indicating 1:1 stoichiometry between Na^+ and HA (see data in Table 2.12). The extraction

of Na^+ in the pH 4 + 0 mM Nd + HCl system was modeled by the SXLSQI program as described in

section 2.2.10. The modeling results showed an equilibrium constant or Log K_{Na} of –0.989 ±

0.009 for the reaction shown in equation (2.10) where n = 1.

2.4.2.3   H$_2$O Distribution Results

When contacted with water there is no measurable water extracted by pure isooctane.

However, when HA is dissolved in isooctane, it does extract water upon contact. Karl Fischer

titrations results are shown in Table 2.13. When the data obtained for the other systems [pH (1,

4) + (0, 30) mM Nd + HCl] is compared with that of the washed solvent it is notable that the

organic phase water concentration observed under all systems is equal to that of the washed

solvent within experimental error. This indicates that Nd^{3+} and Na^+ are extracted as dehydrated

ions into the organic phase. Other lanthanides have also been shown to extract by HA as

dehydrated ions.[82-83] Past studies with Na^+ extraction have shown that little water is extracted

with Na^+ until the percent conversion of HA to NaA is above 10%.[73] In these experiments the

conversion of HA to NaA did not exceed more than 2% (see results for pH 4 + 0 mM Nd + HCl

system in Table 2.11). A log-slope comparison of the washed solvent and the pH 4 + 0 mM Nd +

HCl system is shown in Figure 2.8 shows matching slopes that is consistent with slight excess

water extraction with Na^+.
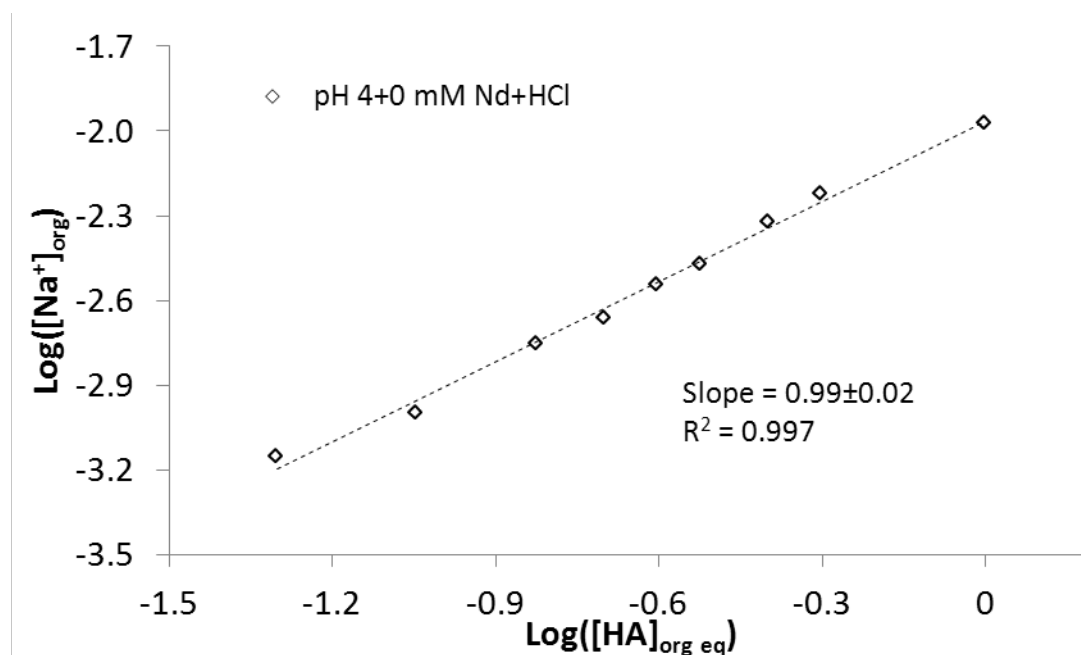
Figure 2.7- Log-slope analysis of Na^+ Extraction in the pH 4 + 0 mM Nd + HCl system.

Table 2.13- Organic phase water concentration for the pH (1,4) + (0, 30) mM Nd + HCl systems.

[HA]$_{org}$ / M	Washed Solvent [H$_2$O]$_{org}$ / M	pH 1 + HCl		pH 4 + HCl	
		0 mM Nd [H$_2$O]$_{org}$ / M	30 mM Nd [H$_2$O]$_{org}$ / M	0 mM Nd [H$_2$O]$_{org}$ / M	30 mM Nd [H$_2$O]$_{org}$ / M
0	0.000 ± 0.003	0.005 ± 0.003	0.003 ± 0.003	0.002 ± 0.003	0.004 ± 0.003
0.05	0.003 ± 0.003	0.005 ± 0.003	0.005 ± 0.003	0.003 ± 0.003	0.004 ± 0.003
0.09	0.007 ± 0.003	0.007 ± 0.003	0.006 ± 0.003	0.004 ± 0.003	0.007 ± 0.003
0.15	0.010 ± 0.003	0.010 ± 0.003	0.012 ± 0.003	0.010 ± 0.003	0.009 ± 0.003
0.2	0.015 ± 0.003	0.017 ± 0.003	0.017 ± 0.003	0.017 ± 0.003	0.014 ± 0.003
0.25	0.023 ± 0.003	0.022 ± 0.003	0.020 ± 0.003	0.021 ± 0.003	0.020 ± 0.003
0.3	0.029 ± 0.005	0.035 ± 0.006	0.027 ± 0.005	0.037 ± 0.006	0.025 ± 0.006
0.4	0.053 ± 0.007	0.051 ± 0.008	0.046 ± 0.007	0.057 ± 0.008	0.049 ± 0.006
0.5	0.07 ± 0.01	0.08 ± 0.01	0.07 ± 0.01	0.08 ± 0.01	0.07 ± 0.01
1	0.21 ± 0.03	0.20 ± 0.04	0.20 ± 0.03	0.28 ± 0.04	0.17 ± 0.02
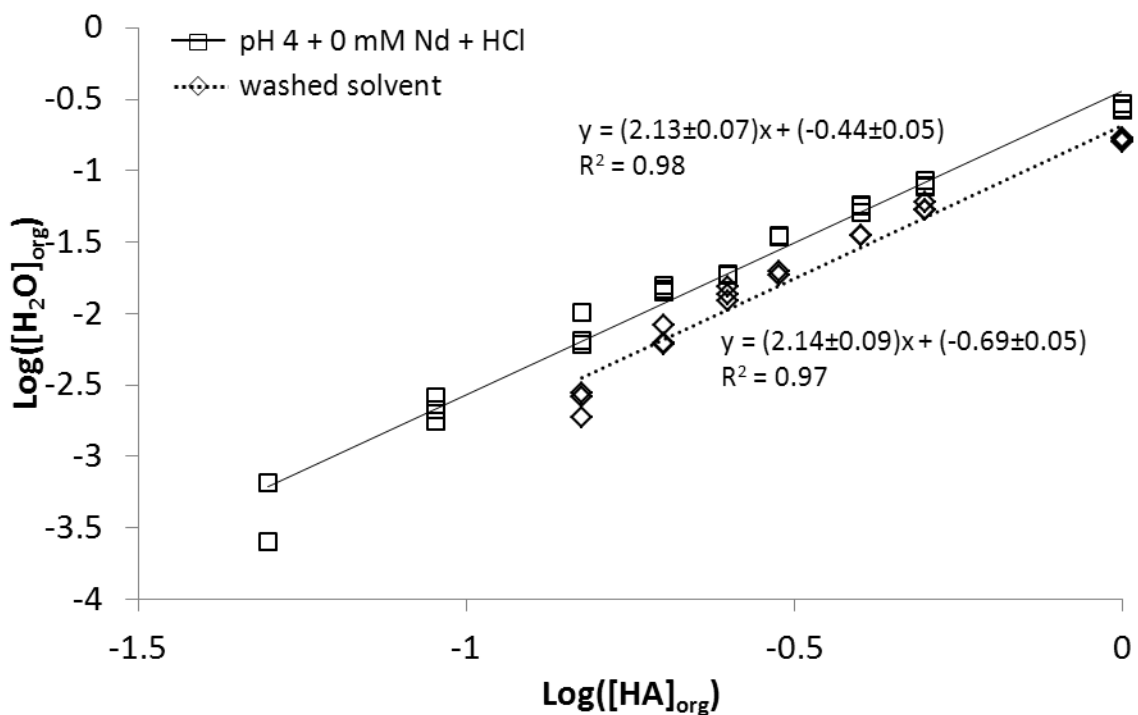
Figure 2.8- Log-slope analysis of water in the washed solvent and the pH 4 + 0 mM Nd + HCl system. The matching slopes indicate that no water was co-extracted with Na$^+$ in the pH 4 + 0 mM Nd + HCl system.

2.4.3   Visible Spectroscopy

2.4.3.1   Aqueous Phase

The molar absorptivity observed for the aqueous phase showed numerous absorbance bands for the Nd^{3+} ion in systems studied. In the observed window (500–881 nm) the absorbance bands with an extinction coefficient at least 1.0 L mol^{-1} cm^{-1} are 511, 521, 575, 732, 740, 794, 801 and 865 nm (See trace "pH 4 + 30 mM Nd = HCl (Aq)" in Figure 2.9). These bands are also listed in Table 2.14. The spectrum shown is representative of pH (1,4) + 30 mM Nd + HCl systems and was not changed between pH 1 and pH 4 systems. A comparison of the organic phase (containing HA) and aqueous phase Nd^{3+} spectra for pH 4 + 30 mM Nd + HCl are shown in Figure 2.9.
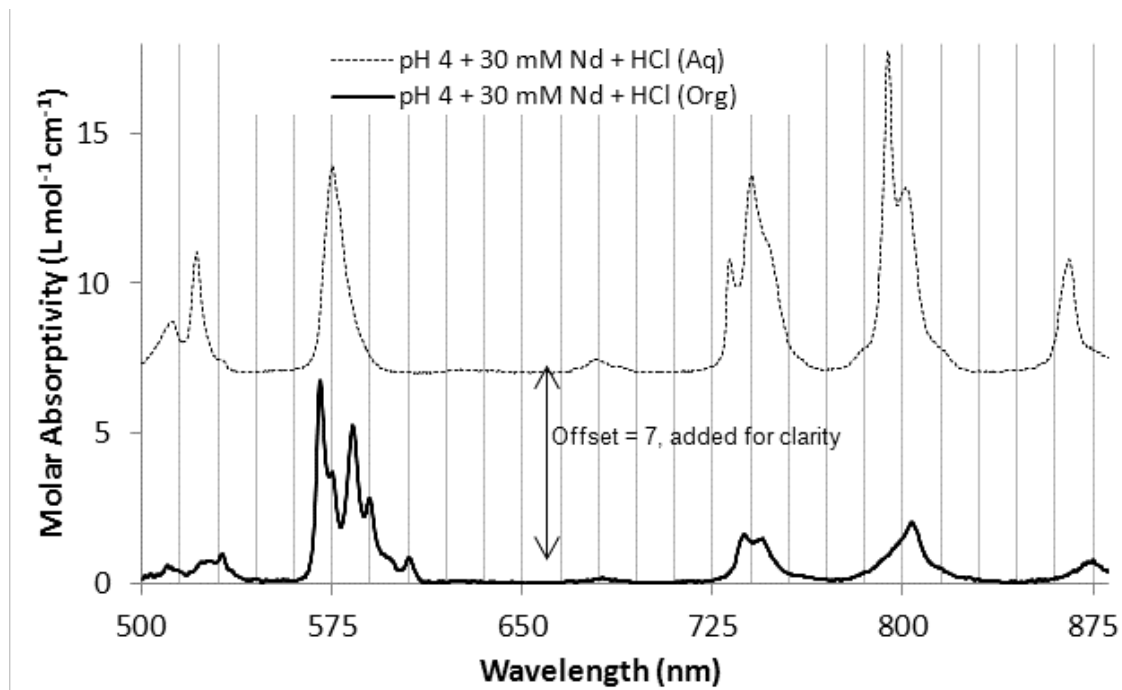
Figure 2.9- A comparison of the absorbance spectra of the Nd^{3+} ion in the aqueous and organic phases. The HA concentration for the organic solution shown is 0.2 M.

Table 2.14- Prominent bands of the molar absorptivity of Nd^{3+} in the aqueous and organic phase of the HCl systems. Bands that found in the shoulder of other bands without a prominent maximum are shown in parentheses.

HCl System Aqueous Phase (nm)	HCl System Organic Phase (nm)
511	512
521	524
	571
575	575
	583
	588
	604
732	
740	738
(745)	745
794	(794)
801	802
865	874

2.4.3.2 Organic Phase

The absorbance bands in the organic phase show band shifts and band splits due to different speciation (See Figure 2.9). The 511 and 521 nm aqueous absorbance bands were essentially unchanged in position, but are lower in intensity, appearing at 512 and 524 nm in the organic absorbance spectrum respectively. The 575 nm aqueous band appears to have split into 5 different bands at 571, 575, 583, 588, and 604 nm. The 732 nm aqueous band appears to disappear in the organic phase. The 740 nm band plus its shoulder (~745 nm) in the aqueous spectrum appear to have resolved into bands at 738 and 745 nm in the organic absorbance spectrum, remaining relatively unchanged. The 794 nm aqueous band appears to decrease in organic phase spectrum until it is lost in the shoulder of the 802 nm, which is unchanged from

50

the aqueous to the organic phase spectrum. Finally, the 865 nm aqueous band shifted to an 874

nm organic band.

Hypersensitive bands in the Nd^{3+} organic phase visible spectrum changes with shifts in the

Nd^{3+} speciation. The molar absorptivity spectra (see Figure 2.10 Plots A and B) demonstrate that

many of the bands show some little change, but the 570 nm band has the largest absorbance

change in the $^4I_{9/2} \rightarrow {}^4G_{5/2}, {}^2G_{7/2}$ electronic transition.[104]

The absence of the shift of the position of the spectral bands with HA concentration

indicates the presence of a single Nd^{3+} complex species, namely $NdA_3(HA)$ in the organic phase.

The modulation of the molar absorptivity value that is especially pronounced for the 571 nm

band can be attributed to the change of organic solvent properties with increased HA

concentration. It has been demonstrated that the organic spectrum of Nd^{3+} provides

information about Nd^{3+}-HA speciation.[64] In this past cited work, the changes in the absorbance

spectrum are associated with a speciation shift of Nd^{3+}-HA from the NdA_3 or $NdA_3(HA)_2$ that

form at low loading, to $Nd_2(A)_6$ that forms at high loading. The data presented here shows that

the change observed in the 570 nm band did not correlate with the organic phase Nd^{3+} loading

at pH 1, but it did at pH 4 (see Figure 2.11). The molar absorptivity decreases with increasing

$[HA]_{org}$ for both pH (1, 4) + 30 mM Nd + HCl systems. The data are consistent with the conclusion

that the change in the 570 nm band appears to show rearrangement of ligands in the

coordination sphere of Nd^{3+}, but the changes in the 570 nm band correlate to the overall $[HA]_{org}$

and not to theoretical Nd^{3+} loading.
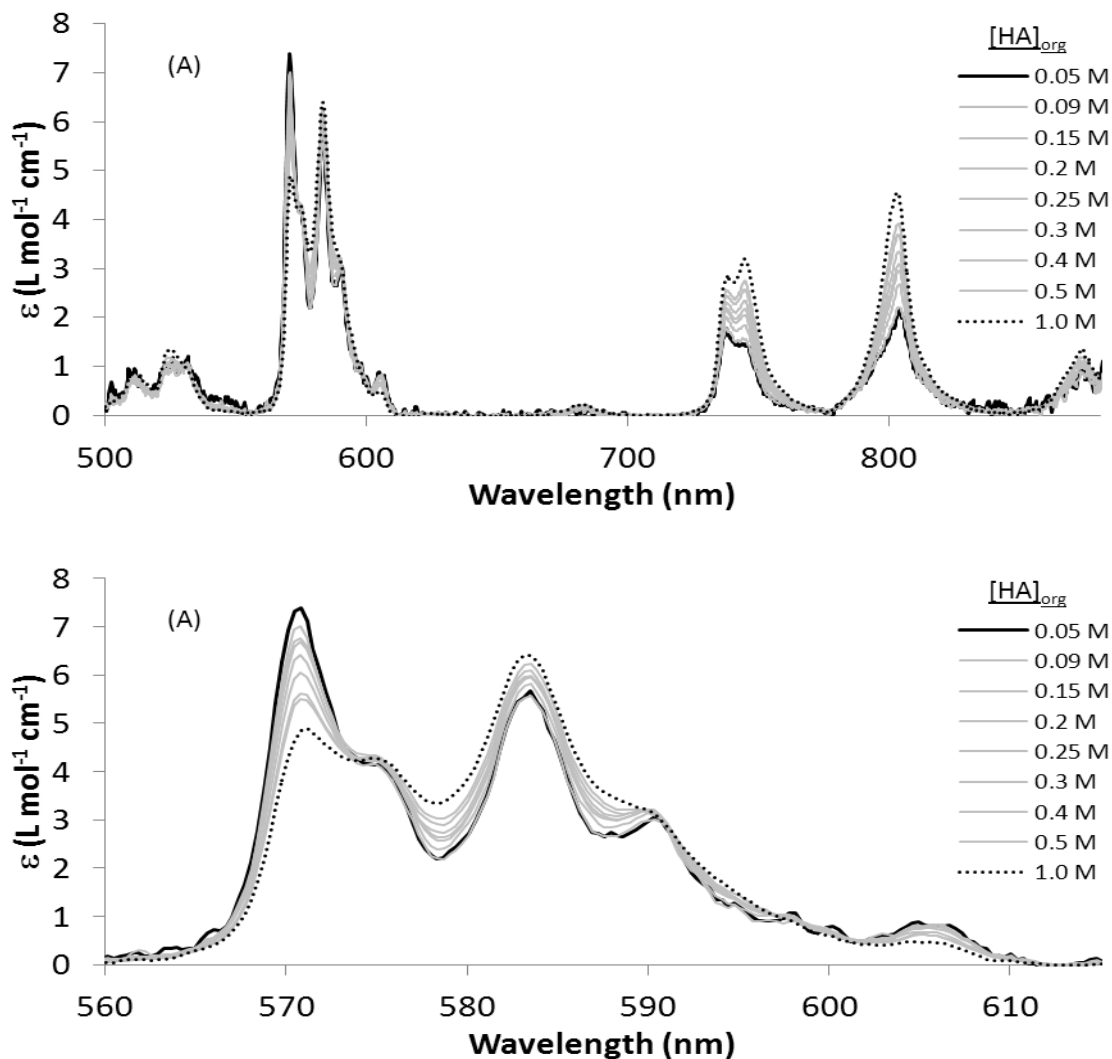
Figure 2.10- Organic phase molar absorptivity from the pH 4 + 30 mM Nd + HCl system. Plot (B) shows a more detailed view of Plot (A) from 560–615 nm.

The spectral profile of the Nd^{3+} in the organic phase did offer some information regarding the coordination sphere surrounding the metal center. For the multiple band spectral profile with peaks at 570, 575, 583, 588, and 604 nm in the 560–620 nm window, the Nd^{3+} complex present in our systems showed the greatest similarity with and is practically identical to, the spectra observed for $Nd(AHA)_3$ complex for both Nd-Cyanex272 and Nd-HA previously published.[64] The spectra published for NdA_3 complex is different with only one absorbance

band at 585 nm and a shoulder band at 577 nm.[64, 69] The shape of the spectrum in the 560–620 nm window is consistent with the low Nd^{3+} loading regime where dimeric HA surround the Nd^{3+} center.
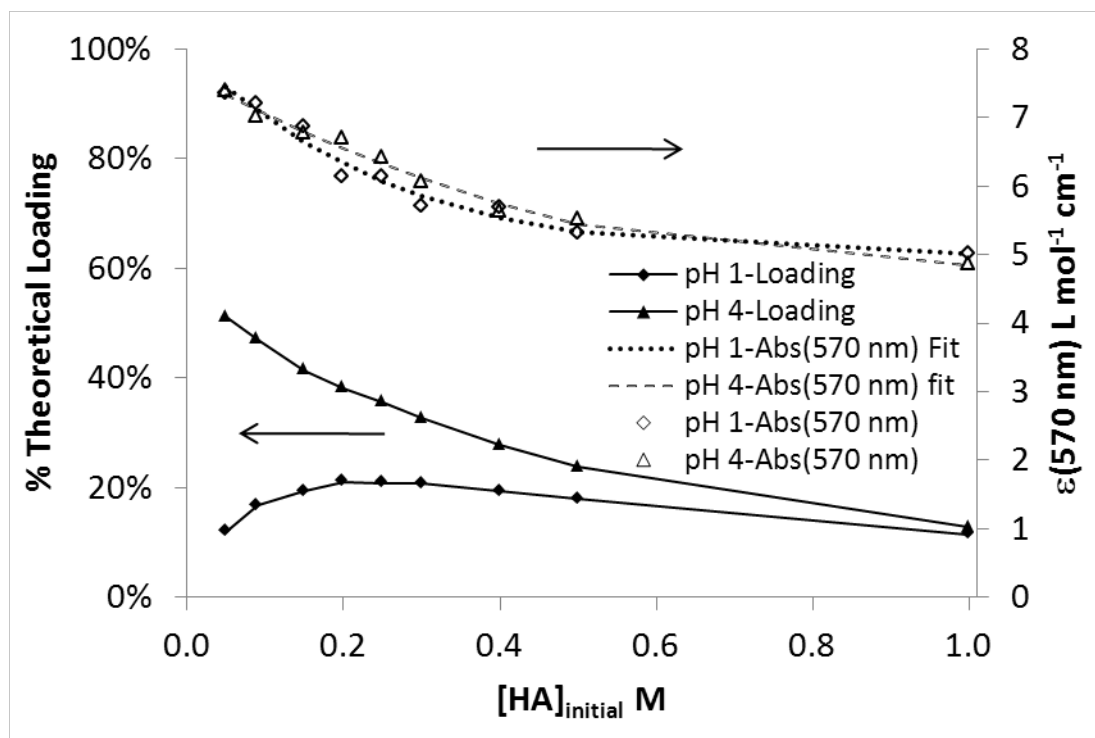
Figure 2.11- Trend in the 570 nm absorbance band as a function of $[HA]_{initial}$ from the pH (1,4) + 30 mM Nd + HCl systems. Also included in this plot is the percent theoretical loading of the solvent based on the assumption of HA dimer stoichiometric coefficient (n) of 2.

2.4.4 Fourier Transform Infrared Spectroscopy of the Organic Phase

In all systems, the two peaks of highest interest for the presented study are the 1230 and 1035 cm^{-1} associated with P=O and P–O stretching, respectively.[105] The complexation of Nd^{3+} by HA leads to a withdrawal of electron density in the P=O bond resulting in the decrease of the stretching mode frequency. This is supported by the shift in the 1230 band to 1200 cm^{-1} in pH (1,

4) + 30 mM Nd+ HCl systems where Nd^{+3} extraction occurs (see Figure 2.12). Na^+ extraction in

the pH 4 + 0 M Nd + HCl system was too small to change the FTIR spectrum. Formation of highly

aggregated $(NdA_3)_x$ species leads to bridging -O-P-O- groups as evident from the appearance of

the weak 1097 cm^{-1} band[71] for pH 4 + 30 mM Nd + HCl systems at low $[HA]_{org}$ ($[HA]_{org}$ = 0.05 M

is shown in Figure 2.12 as the dotted spectrum).
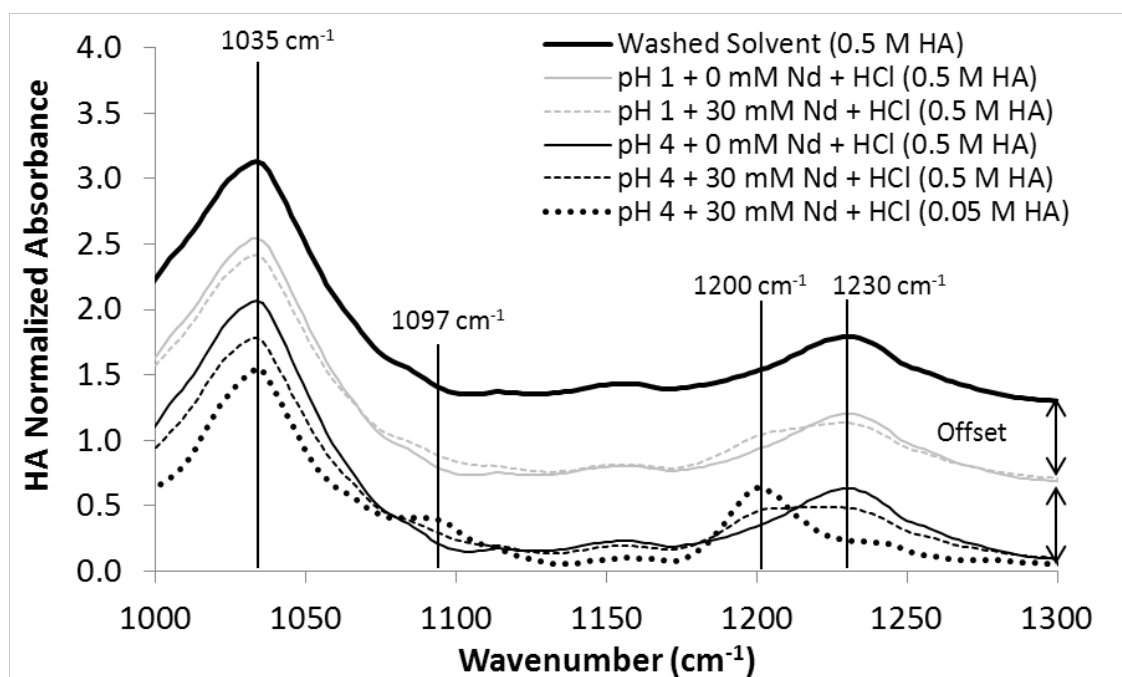
Figure 2.12- Infrared spectra normalized by $[HA]_{org}$. The isooctane peaks have been removed from the spectrum.

2.5   Results and Discussion: Lactate Aqueous Media

2.5.1   HA aggregation

In the washed solvent, an HA aggregation number of 2.02 ± 0.03 was observed. The same

aggregation number was also observed for the pH 1 + 0 mM Nd + Lac system (1.97 ± 0.03).

Average HA aggregation was observed to increase when Nd^{3+} extraction was significant, which

occurred in the pH 1 + 30 mM Nd + Lac system (2.37 ± 0.04). This increase in average

aggregation was due to the formation of $NdA_3(HA)$. The HA aggregation model described in

section 2.2.14 was applied to the pH 1 + 30 mM Nd + Lac system and revealed a Z_{NdAz} of 4.2 ±

0.3. This value is in agreement with the results obtained for pH (1, 4) + 30 mM Nd + HCl systems

(4.0 ± 0.4). In the pH 4 + 0 mM Nd + Lac system a significant increase in the aggregation number

was observed (N_{agg} = 3.82 ± 0.05). The distribution measurements for this system showed that

significant Na^+ and Lac were extracted with 2.7 ± 0.4 times the $[Na^+]_{org}$ as $[Lac]_{org}$. The

aggregation for this system was modelled using the equations described in section 2.2.14, but it

was modified as follows. Species present were $(HA)_2$, NaA(HA), and $NaLac(HA)_{ZNaLac(HA)z}$. Species

aggregation was 2 for both $(HA)_2$ and NaA(HA). The adapted model for the NaLac species was

derived similar to the Nd-HA system described in equations (2.18) – (2.22). The model for the

Na-Lactate-HA system is formulated using the organic phase species: NaA, $NaLac(HA)_2$, and

$(HA)_2$ and is derived in equations (2.24) – (2.27) where ($N_{agg,\ average}$) is the average HA

aggregation number, (Z_i) is the species HA aggregation number, (X_i) is the species fraction, and

bracketed terms are the concentration of species in molarity. The modelling results agreed with

the experimental data within error.

$$N_{agg,Average} = \sum Z_i X_i = Z_2 X_2 + Z_{NaA} X_{NaA} + Z_{NaLac(HA)_z} X_{NaLac(HA)_z} \qquad (2.24)$$

$$X_{NaA} = \frac{Z_{NaA}\left([Na]_{org} - [Lac]_{org}\right)}{[HA]_{total}}$$

(2.25)

$$X_{NaLac(HA)_z} = \frac{Z_{NaLac(HA)_z}[Lac]_{org}}{[HA]_{total}}$$

(2.26)

$$X_2 = 1 - X_{NdA_z} - X_{NaLac(HA)_z}$$

(2.27)

Aggregation modelling results showed that the $Z_{NaLac(HA)z}$ was 5.1 ± 0.3 for this system.

In the pH 4 + (30, 60) mM Nd + Lac systems the aggregation varied as a function of both HA and total Nd^{3+} (see Figure 2.13). The average aggregation (N_{agg}) was measured as high as 100 ± 40 at low $[HA]_{org}$ (~0.01 M) in the pH 4 + 60 mM Nd + Lac system, and dropped systematically to a value of $N_{agg} \approx 3$ at high HA (>0.2 M) (see Figure 2.13). The maximum average aggregation in the pH 4 + 30 mM Nd + Lac system also occurred at the lowest $[HA]_{org}$ but was only 20 ± 4. The instrument response curve is shown with the aggregation data as a demonstration (see Figure 2.14). As $[HA]_{org}$ was increased in these systems, the aggregation number decreased until a constant value of (2.75 ± 0.04, 2.82 ± 0.06 respectively) was attained. The initially high aggregation numbers results indicate that large aggregates form due to high Nd^{3+} loading. Literature accounts have characterized species including NdA_3[69, 72] and $Nd(Acetate)A_2$[71] that form large aggregates. Similar species were most likely present under the present test conditions.
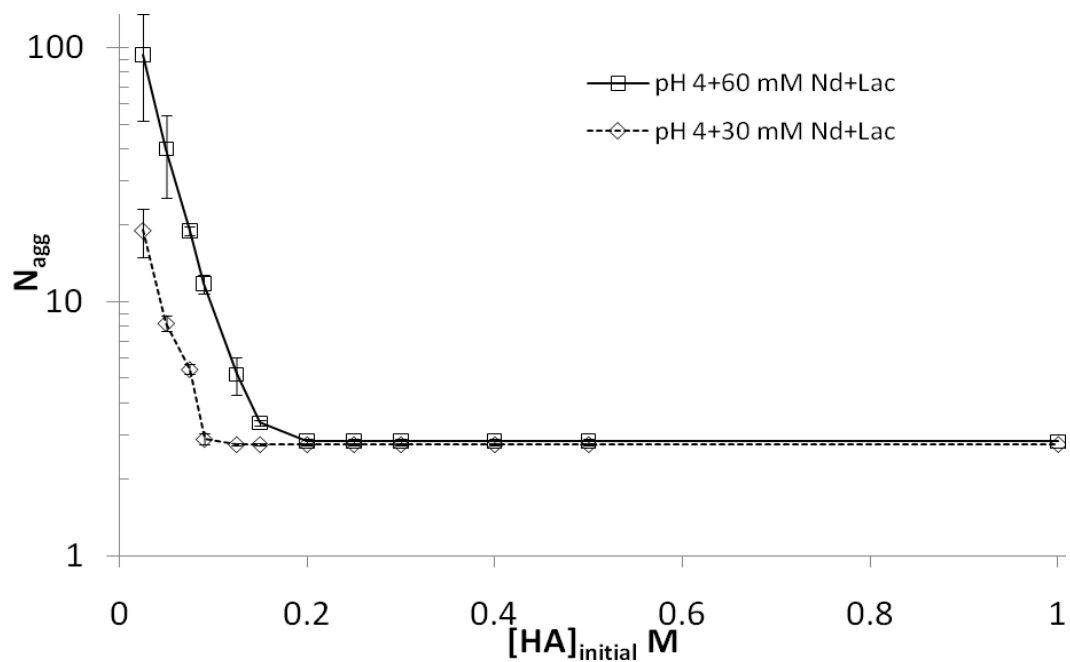
Figure 2.13- Aggregation results for the pH 4 + (30, 60) mM Nd + Lac systems.
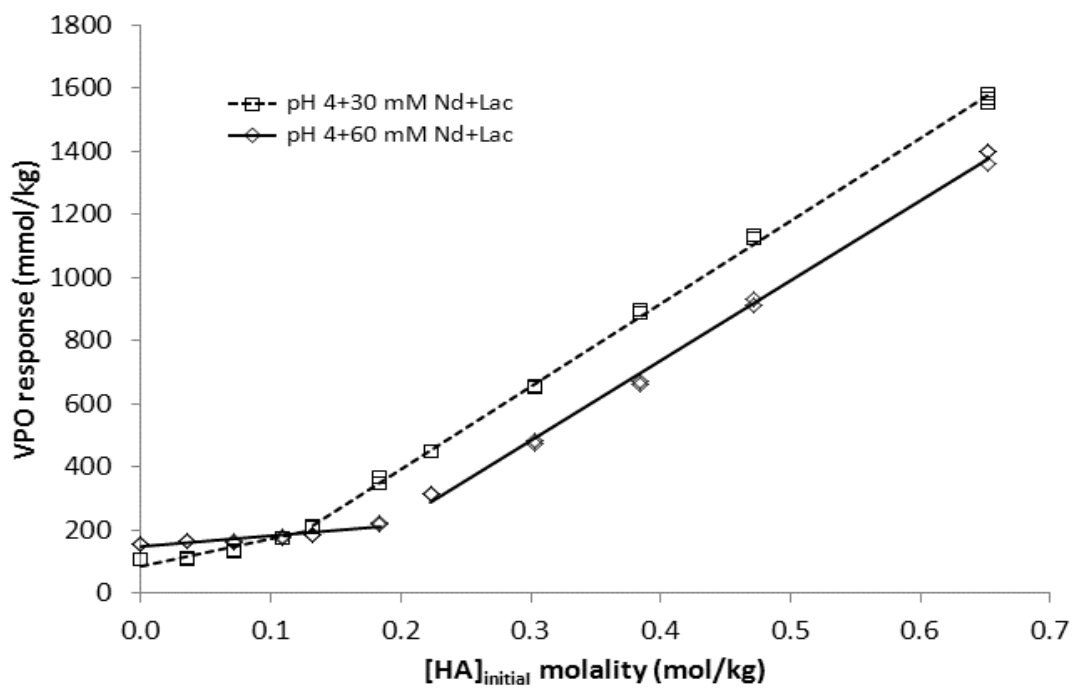
Figure 2.14- Instrument response curve used to calculate the aggregation results for the pH 4 + (30, 60) mM Nd + Lac systems.

2.5.2 Liquid-Liquid Distribution Measurements

Overall results for the extraction measurements are shown in Table 2.15 and Table 2.16 and will be discussed in sections that follow.

2.5.2.1 Nd^{3+} Distribution Results

Nd^{3+} extraction showed significantly different behavior between pH 1 and pH 4. The extraction of Nd^{3+} in the pH 1 + 30 mM Nd + Lac system (see Table 2.15) was very similar to the pH 1 + 30 mM Nd + HCl system (see Table 2.11). At pH 1, the extraction of Nd^{3+} is governed by the ion exchange mechanism shown in equation (2.7). Comparison of the pH data between the pH 1 + 30 mM Nd + (HCl, Lac) systems also showed that pH change was likewise the same within experimental error indicating that no lactate buffering occurred at this low pH (Table 2.11 and Table 2.15). The extraction results from the pH 1 + 30 mM Nd + Lac system were modeled by SXLSQI[94] as described in section 2.2.10 and showed excellent fit with the observed data using only the $(HA)_2$ and $Nd(A)_3(HA)$ species (see Figure 2.15). Use of these species was justified by the vapor pressure aggregation modeling results described in section 2.5.1.

As pH is elevated past the pk_a of lactate ($pK_a = 3.86$[55]) its buffering effects, and the aqueous complexation both impact the extraction of Nd^{3+}. In the pH 4 + (30, 60) mM Nd + Lac systems, the buffering effect of lactate causes the extraction of Nd^{3+} at the saturation level of HA at low $[HA]_{org}$ and quantitative extraction at higher $[HA]_{org}$. The transition concentration of $[HA]_{org}$ between the saturation and the quantitative extraction occurred at twice the aqueous Nd^{3+} concentration (0.0619 ± 0.0009 and 0.123 ± 0.001 M HA for pH 4 + (30, 60) mM Nd + Lac systems respectively; see Figure 2.16). This result is consistent with a neodymium complex containing two deprotonated HA molecules, and one lactate molecule for charge balance as in the $NdX(A)_2$ complex. Results presented later in this work (see section 2.5.2.3) indicate that the

counter ion in the NdX^{2+} salt is lactate. Due to a lack of aqueous phase thermodynamic modeling

parameters required by the SXLSQI software (Pitzer parameters for Nd^{3+} and lactate in lactate

aqueous media), it is not possible at this time to achieve a modeling result for the extraction of

Nd^{3+} in the pH 4 + (30, 60) mM Nd + Lac systems.

Table 2.15- Equilibrium pH, $[Na^+]_{org}$, $[Nd^{3+}]_{org}$, and $[Lac]_{org}$ for the pH 1 + (0, 30) mM Nd + Lac systems. Error for the values shown is: ± 0.01 for pH_{eq}, 2% for $[Nd^{3+}]_{org,eq}$.

[HA]	pH 1 + 0 mM Nd + Lac		pH 1 + 30 mM Nd + Lac			
	pH_{eq}	$[Na]_{org,eq}$	pH_{eq}	$[Na]_{org,eq}$	$[Lac]_{org,eq}$	$[Lac]_{org,eq}$
M		M		M	M	M
0	1.10		4.21	BD	0.0007 ± 0.0004	0.0007 ± 0.0003
0.025	1.10		4.21		0.0013 ± 0.0004	0.0011 ± 0.0003
0.05	1.10		4.20	0.010 ± 0.006	0.0031 ± 0.0004	0.0013 ± 0.0003
0.075	1.09		4.19	0.015 ± 0.007	0.0054 ± 0.0005	0.0014 ± 0.0003
0.09	1.09		4.18	0.021 ± 0.009	0.006 ± 0.001	0.0015 ± 0.0003
0.125	1.10		4.16	0.03 ± 0.01	0.012 ± 0.001	0.0017 ± 0.0003
0.15	1.10	BD	4.16	0.04 ± 0.01	0.015 ± 0.001	0.0019 ± 0.0003
0.2	1.10		4.14	0.06 ± 0.02	0.023 ± 0.002	0.0023 ± 0.0004
0.25	1.09		4.12	0.08 ± 0.02	0.025 ± 0.002	0.0026 ± 0.0004
0.3	1.09		4.08	0.10 ± 0.02	0.039 ± 0.003	0.0029 ± 0.0005
0.4	1.10		4.02	0.13 ± 0.02	0.054 ± 0.004	0.0039 ± 0.0005
0.5	1.10		3.99	0.17 ± 0.03	0.061 ± 0.004	0.0047 ± 0.0005
1	1.09		3.76	0.31 ± 0.04	0.125 ± 0.005	0.0095 ± 0.0009

BD = Below detection

Table 2.16- Equilibrium pH, $[Na^+]_{org}$, $[Nd^{3+}]_{org}$, and $[Lac]_{org}$ for the pH 4 + (0, 30, 60) mM Nd + Lac systems. Error for the values shown is: ± 0.01 for pH_{eq}, 2% for $[Nd^{3+}]_{org,eq}$.

[HA]	pH 4 + 0 mM Nd + Lac			pH 4 + 30 mM Nd + Lac				pH 4 + 60 mM Nd + Lac			
M	pH_{eq}	$[Na]_{org,eq}$ M	$[Lac]_{org,eq}$ M	pH_{eq}	$[Na]_{org,eq}$ M	$[Nd]_{org,eq}$ M	$[Lac]_{org,eq}$ M	pH_{eq}	$[Na]_{org,eq}$ M	$[Nd]_{org,eq}$ M	$[Lac]_{org,eq}$ M
0	4.21	BD	0.0007 ± 0.0004	4.13	BD	0.0000	0.0010 ± 0.0002	4.04	BD	0.0000	0.0007 ± 0.0004
0.025	4.21	BD	0.0013 ± 0.0004	4.12		0.0051	0.013 ± 0.001	4.01		0.0120	0.0140 ± 0.0009
0.05	4.20	0.010 ± 0.006	0.0031 ± 0.0004	4.08		0.0242	0.028 ± 0.002	3.99		0.0246	0.028 ± 0.002
0.075	4.19	0.015 ± 0.007	0.0054 ± 0.0005	4.06		0.0289	0.032 ± 0.003	3.96		0.0361	0.041 ± 0.002
0.09	4.18	0.021 ± 0.009	0.006 ± 0.001	4.06		0.0293	0.029 ± 0.002	3.95		0.0436	0.049 ± 0.002
0.125	4.16	0.03 ± 0.01	0.012 ± 0.001	4.05		0.0296	0.024 ± 0.002	3.92		0.0577	0.062 ± 0.003
0.15	4.16	0.04 ± 0.01	0.015 ± 0.001	4.04	0.002 ± 0.002	0.0297	0.021 ± 0.002	3.91		0.0592	0.0616 ± 0.003
0.2	4.14	0.06 ± 0.02	0.023 ± 0.002	4.03	0.005 ± 0.003	0.0298	0.013 ± 0.001	3.90		0.0596	0.057 ± 0.003
0.25	4.12	0.08 ± 0.02	0.025 ± 0.002	4.02	0.011 ± 0.004	0.0299	0.010 ± 0.001	3.89		0.0597	0.037 ± 0.002
0.3	4.08	0.10 ± 0.02	0.039 ± 0.003	4.00	0.023 ± 0.006	0.0300	0.013 ± 0.001	3.88	0.006 ± 0.004	0.0598	0.038 ± 0.002
0.4	4.02	0.13 ± 0.02	0.054 ± 0.004	3.95	0.051 ± 0.009	0.0300	0.024 ± 0.002	3.86	0.013 ± 0.007	0.0600	0.029 ± 0.002
0.5	3.99	0.17 ± 0.03	0.061 ± 0.004	3.91	0.08 ± 0.01	0.0300	0.037 ± 0.003	3.83	0.03 ± 0.01	0.0600	0.022 ± 0.001
1	3.76	0.31 ± 0.04	0.125 ± 0.005	3.71	0.23 ± 0.02	0.0300	0.104 ± 0.008	3.64	0.16 ± 0.02	0.0600	0.073 ± 0.003

BD = Below detection
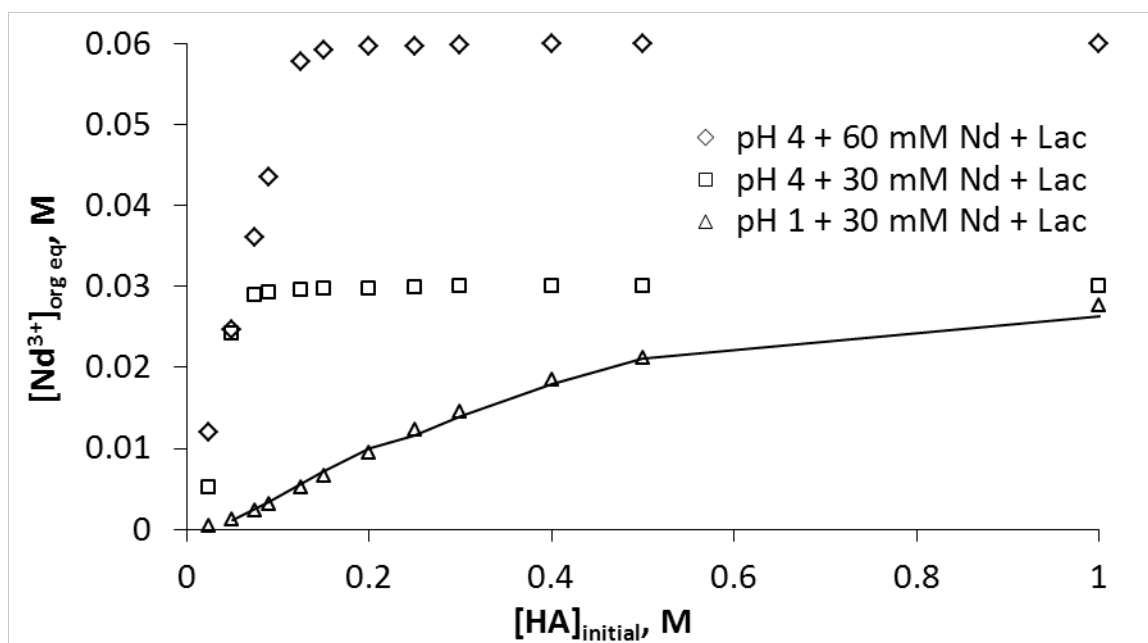
Figure 2.15- Nd^{3+} extraction results. Observed data are depicted as points, SXLSQI modeling results are depicted as the solid curve.
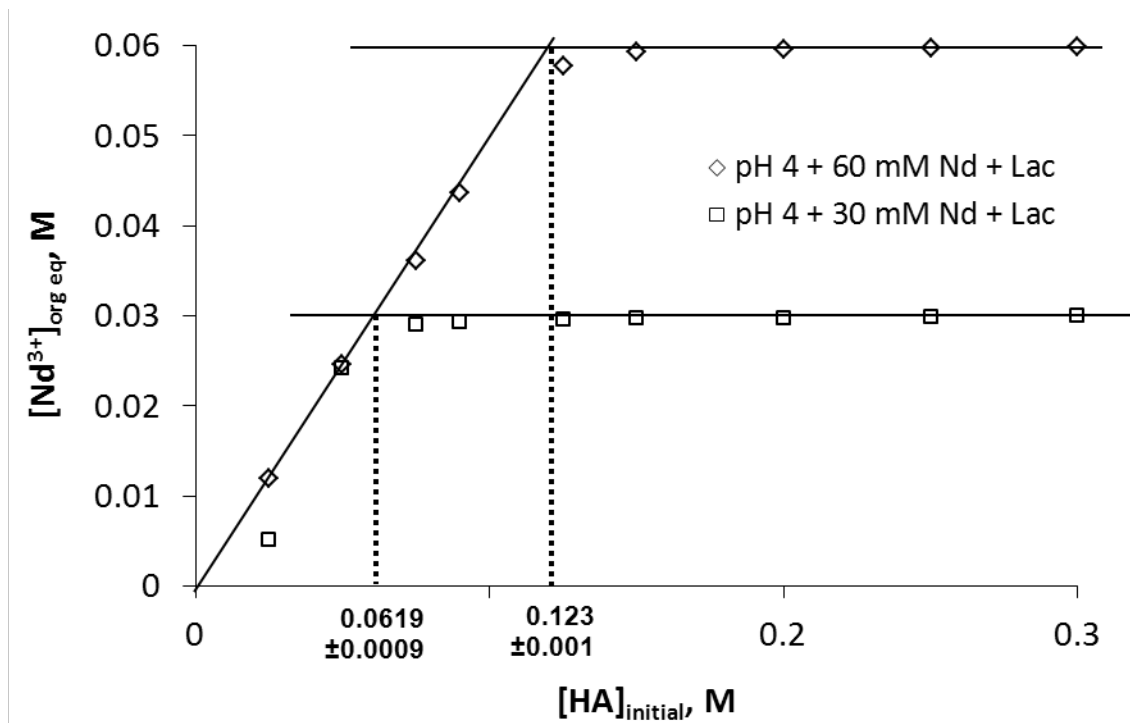
Figure 2.16- The transition between saturation and quantitative extraction supports the 1:2 Nd^{3+}: HA stoichiometry of the NdLacA$_2$ complex.

As pH is elevated past the pk$_a$ of lactate (pK$_a$ = 3.86[55]) its buffering effects, and the aqueous complexation both impact the extraction of Nd^{3+}. In the pH 4 + (30, 60) mM Nd + Lac systems, the buffering effect of lactate causes the extraction of Nd^{3+} at the saturation level of HA at low [HA]$_{org}$ and quantitative extraction at higher [HA]$_{org}$. The transition concentration of [HA]$_{org}$ between the saturation and the quantitative extraction occurred at twice the aqueous Nd^{3+} concentration (0.0619 ± 0.0009 and 0.123 ± 0.001 M HA for pH 4 + (30, 60) mM Nd + Lac systems respectively; see Figure 2.16). This result is consistent with a neodymium complex containing two deprotonated HA molecules, and one lactate molecule for charge balance as in the NdX(A)$_2$ complex. Results presented later in this work (see section 2.5.2.3) indicate that the counter ion in the NdX^{2+} salt is lactate. Due to a lack of aqueous phase thermodynamic modeling parameters required by the SXLSQI software (Pitzer parameters for Nd^{3+} and lactate in lactate aqueous media), it is not possible at this time to achieve a modeling result for the extraction of Nd^{3+} in the pH 4 + (30, 60) mM Nd + Lac systems.

2.5.2.2   Na$^{\pm}$ Distribution Results

Just as with the Nd^{3+} systems, the Na$^+$ extraction data also shows a significantly different behavior between pH 1 and pH 4. Extraction of Na$^+$ was below detection in the pH 1 + (0, 30) mM Nd + Lac systems. A linear increase in Na$^+$ extraction occurred in the pH 4 + 0 mM Nd + Lac system over the range of increasing [HA]$_{org}$. A comparison of the [Na$^+$]$_{org}$ and [Lac]$_{org}$ for this system showed 2.3 ± 0.1 times the [Na$^+$]$_{org}$ as [Lac]$_{org}$ (see Figure 2.20 for a plot of the data), indicating that Na$^+$ is most likely extracted by more than one mechanism and exists as both HA sodium salt (NaA) and NaLac salts within the organic phase. In the HCl system, the NaA species was shown to exists as NaA(HA) in the organic phase because no increase in aggregation was observed under NaA extraction conditions as shown in equation (2.10) (with n = 1). The NaLac salt is therefore extracted by the reaction shown in equation (2.28).

$$NaLac+ n\overline{(HA)_2} \leftrightarrow \overline{NaLac(HA)_{2n}} \tag{2.28}$$
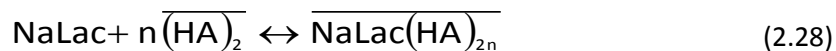
As described in the aggregation modeling section, results give the value for $2n = Z_{NaLacHAz} = 5.1 \pm$ 0.3 (or $n = 2.5 \pm 0.2$). Na^+ extraction was suppressed in pH 4 + (30, 60) mM Nd + Lac systems at low $[HA]_{org}$ but was observed at higher $[HA]_{org}$. The threshold where Na^+ extraction began in these systems was approximately 0.125 M for the pH 4 + 30 mM Nd + Lac system and approximately 0.25 M for the pH 4 + 60 mM + Lac system. This corresponds with the 4:1 ratio of HA to Nd^{3+} in the organic phase. This 4:1 ratio is significant for this system because it is consistent with the formation of the $Nd(A)_3(HA)$ species at lower HA loading. The Na^+ extraction began at greater than 4:1 ratio because there was excess HA available to accommodate Na^+ extraction.

2.5.2.3 Lactate Distribution Results

Lactate was shown to extract in various quantities and species depending on experimental conditions. In the pH 1 + 0 mM Nd + Lac system, weak extraction of lactic acid (HLac) was observed so that organic Lac concentration increased linearly with HA concentration (slope = 0.0086 ± 0.0002, $R^2 = 0.985$). Log-slope analysis of $[Lac]_{org}$ vs. $[HA]_{org}$ shows a slope of approximately 1 (0.93 ± 0.03, $R^2 = 0.994$; results shown in Figure 2.17). VPO results indicated average aggregation of 2 in this system, so the suggested mechanism of the HLac extraction is via solvation by HA dimers [equation (2.29)]

$$HLac+ \overline{(HA)_2} \leftrightarrow \overline{HLac(HA)_2} \tag{2.29}$$
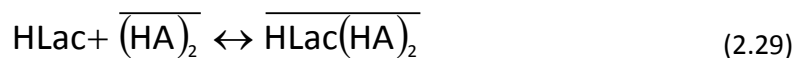
When Nd^{3+} was present in the pH 1 + 30 mM Nd + Lac system, the extraction of Lac was approximately doubled with a linear correlation of $[Lac]_{org}$ with $[HA]_{org}$ (slope = 0.0171 ± 0.0006, $R^2 = 0.994$). The log-slope analysis showed a slope near, but statistically greater than 1 (slope = 1.17 ± 0.03; $R^2 = 0.994$; see Figure 2.17). The slope difference between the pH 1 + (0, 30) mM Nd

+ Lac systems (0.93 vs. 1.17 respectively) indicates that the mechanisms operating in these systems are different.
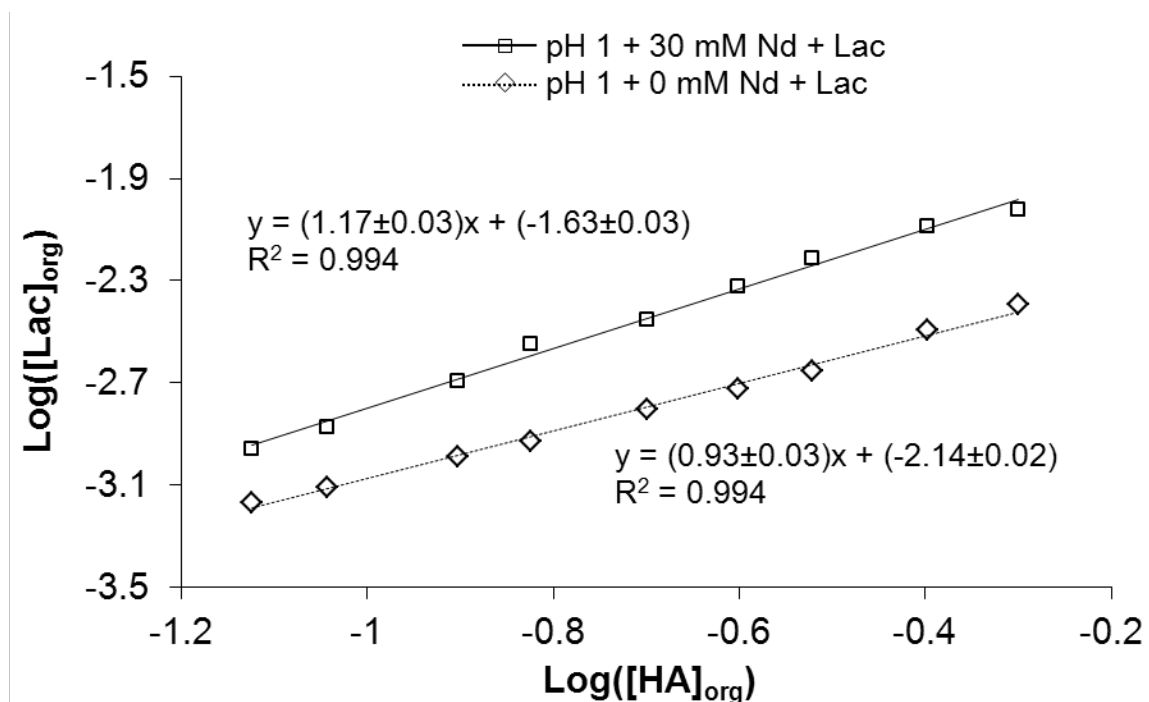
Figure 2.17- Log-slope analysis of Lac extraction vs. $[HA]_{org}$ for the pH 1 + (0, 30) mM Nd + Lac systems.

To observe the correlation between Nd^{3+} and Lac extraction, the $[Lac]_{org}$ values had to be adjusted to remove the $[Lac]_{org}$ that is present due to the reaction described by equation (2.29). This was performed by subtracting the $[Lac]_{org}$ observed in the pH 1 + 0 mM Nd + Lac system from the $[Lac]_{org}$ in the pH 1 + 30 mM Nd + Lac system for each $[HA]_{org}$. The adjusted Lac concentration is named '$[Lac]_{org,excess}$' signifying the Lac present in the organic phase 'in excess' of that observed in the corresponding non-Nd^{3+} system. The log-slope data for the Nd^{3+} vs. Lac

extraction is shown in Figure 2.18. The log-slope correlation between Nd^{3+} and Lac extraction

gives a slope of 1.18 ± 0.04, but this does yield a unique mechanism operating in this system.

More experiments must be run to determine the source of the enhancement of the lactate

extraction. It may be due to co-extraction with Nd^{3+}. Another option is that the electronic and

steric solvation environment of the organic phase due to highly aggregated $Nd(A)_3(HA)$ complex

species provides a more favorable solubility for lactic acid than HA dimers in the non-

neodymium system.
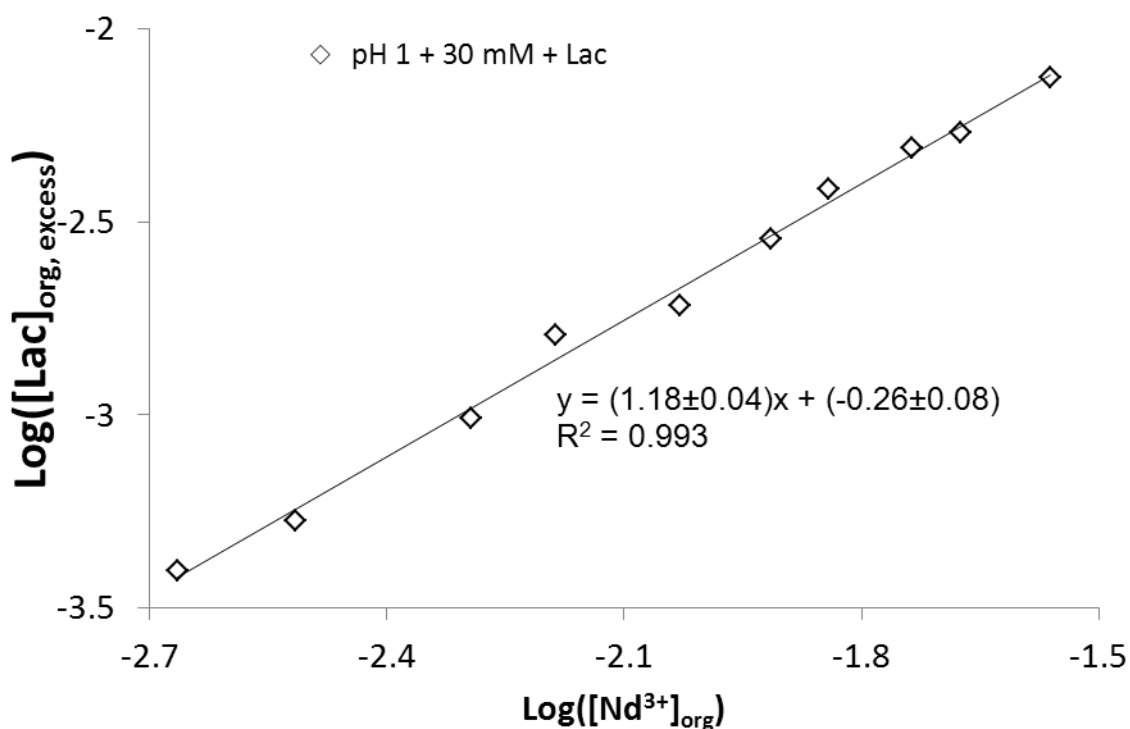
Figure 2.18- Log-slope plot for the Nd^{3+} vs. Lac dependence in the pH 1 + 30 mM Nd + Lac system.

In the pH 4 + 0 mM Nd + Lac system, a significantly higher concentration of Lac was extracted compared with pH 1 + (0, 30) mM Nd + Lac systems, presumably as sodium salt in accord with equation (2.28). The composition of the product species $(NaLac)(HA)_{2n}(org)$ was deduced based upon the assumption that in this system HA exists as two type of aggregates, namely a free or Na^+ salt dimer [as discussed above, our data demonstrated that conversion of HA into Na^+ salt, NaA(HA) does not change its aggregation of 2] and NaLac HA solvate. The analysis of the VPO data, total HA and Lac concentrations in the equilibrium organic phases indicated that the latter contained 5 (5.1 ± 0.3) extractant molecules so that 'n' in the equation (2.28) is equal to approximately 2.5 ± 0.2.

The distribution of Lac in the pH 4 + (30, 60) mM Nd + Lac systems is a complicated function with respect to the HA increase in HA concentrations. For $[Lac]_{org}$, there is an initial increase in $[Lac]_{org}$ from 0.025 through 0.075 M HA for the pH 4 + 30 mM Nd + Lac system, and from 0.025 through 0.125 M HA for the pH 4 + 60 mM Nd + Lac system (see Figure 2.19-A,B, respectively). Following this initial increase there was a decrease in $[Lac]_{org}$ from 0.09 to 0.25 M HA for the pH 4 + 30 mM Nd + Lac system and from 0.15 to 0.5 M HA for pH 4 + 60 mM Nd + Lac system. Finally there was an increase in $[Lac]_{org}$ with $[HA]_{org}$ from 0.3 to 1.0 M HA in the pH 4 + 30 mM Nd + Lac system and for 1 M HA in the pH 4 + 60 mM Nd + Lac system.

In systems with Na^+ extraction, the trend between Na^+ and lactate in the organic phase indicates the stoichiometry between these constituents. Some data near the transition between $NdLac^{2+}$ and NaLac extraction was disregarded because the contribution by the $NdLac^{2+}$ species to the overall lactate concentration moved the data points off the trend line. The data showing the correlation between Na^+ and lactate in the organic phase is shown in Figure 2.20. The slope obtained from this correlation (2.3 ± 0.1) is not indicative of a complex involving two or more Na^+ with one lactate in the organic phase. The stoichiometry between Na^+ and lactate cannot be

more than 1:1 due to the charge of these constituents. This slope merely indicates that since

sodium is 2.3 ± 0.1 more concentrated in the organic phase, and that there must be two

mechanisms and two complexes involved in Na⁺ extraction: NaLac and NaA.
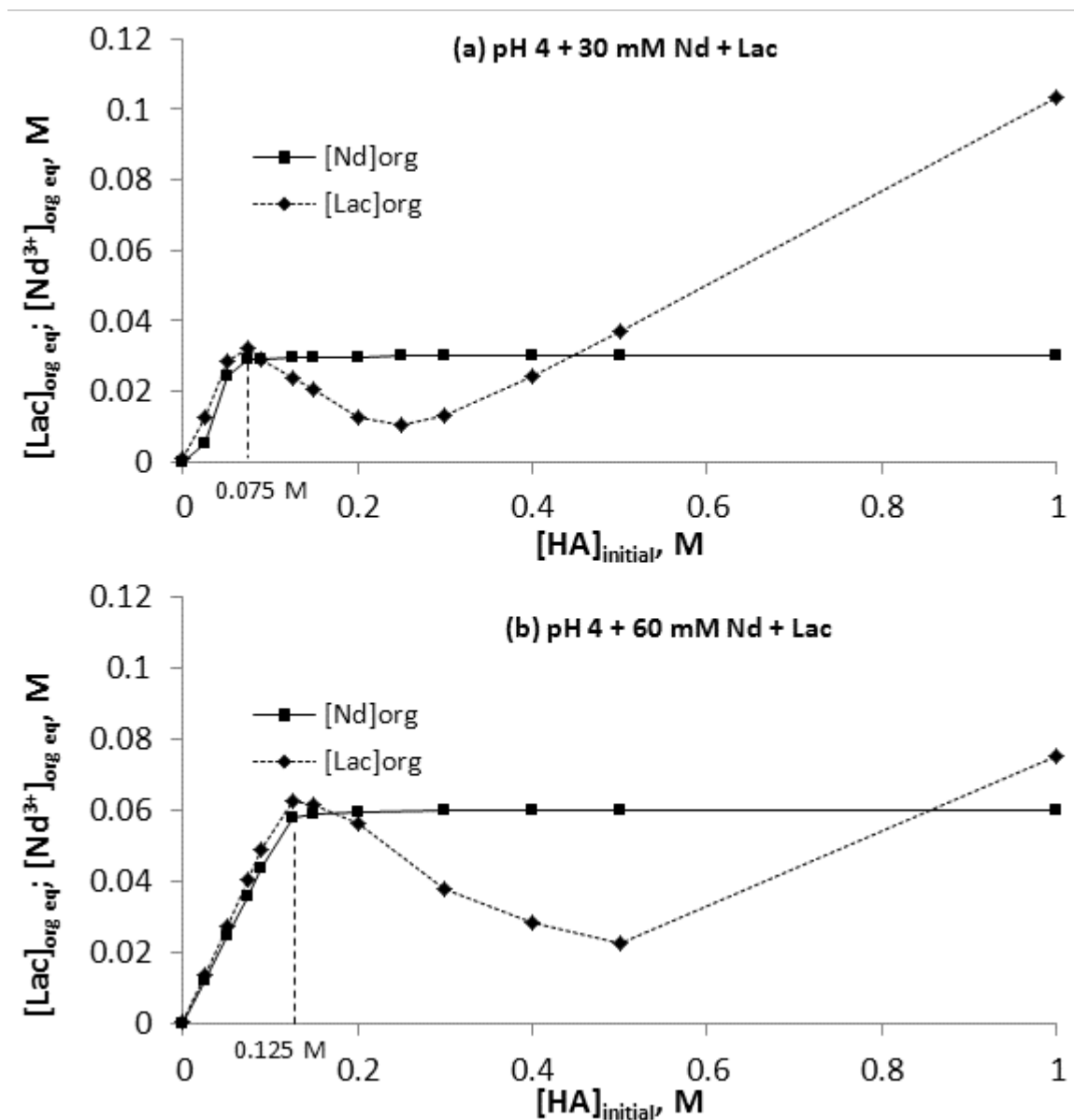
Figure 2.19- Dependence of organic Nd^{3+} and Lac concentrations on HA molarity in the pH 4 + 30 mM Nd + Lac systems.

The maximum in Lac extraction at low HA concentration was attributed to the high

extractant loading with Nd^{3+} promoting extraction of the $NdLac_b^{(3-b)+}$ (b = 1) complex and

formation of the mixed Nd/Lac/HA complex species in the organic phase. The initial increase in

organic Lac concentration correlated with organic Nd^{3+} concentration (see Figure 2.19-A,B). The

observed linear dependence of the organic Lac and Nd^{3+} concentrations had a slope of 1.09 ±

0.05 (R^2 = 0.998) and 1.08 ± 0.01 (R^2 = 0.9993) for pH 4 + (30, 60) mM Nd + Lac systems,

respectively (see Figure 2.21). Because Na^+ extraction was below detection, it was not necessary

to adjust the Lac concentration. The slope of 1 in both systems is consistent with extraction of

the aqueous $NdLac^{2+}$ (b=1) species in these systems under high extractant loading conditions as

described by equation (2.9). Moreover, Figure 2.19 (A and B) demonstrates that at high organic

loading, maximum organic Lac concentrations of 32 and 62 mM (ratio 1:2 with HA) are nearly

equal to the organic Nd^{3+} concentrations (30 and 60 mM) when Nd^{3+} extraction becomes

quantitative. As HA loading decreased, Nd^{3+} extraction described by equation (2.9) using a

$Nd(Lac)(HA)_2$ extraction complex, was gradually displaced by the extraction mechanism in

accord with equation (2.7) where NdA_3HA predominates as the Nd^{3+} extraction complex,

resulting in the decrease of the organic Lac concentration. Finally under the low organic loading

conditions (i.e. high HA concentration), organic Lac concentration increased due to the co-

extraction of Lac with Na^+ described by equation (2.28).
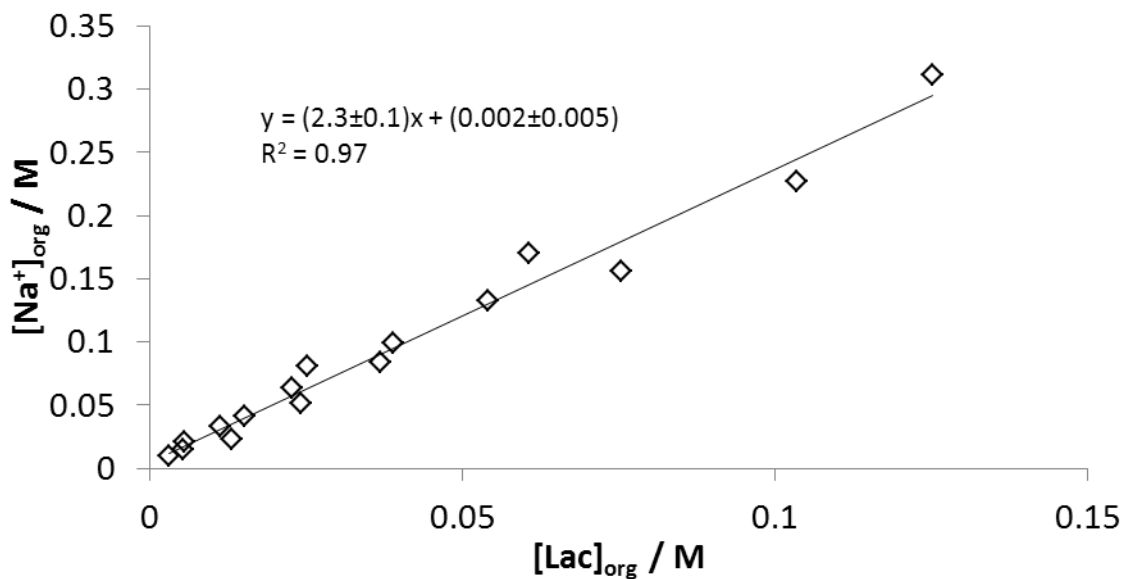
Figure 2.20- Correlation between organic phase Na^+ and lactate. This slope is not indicative of the stoichiometry between Na^+ and lactate in the organic phase, but indicates that Na+ must exist as both a lactate and HA salt.
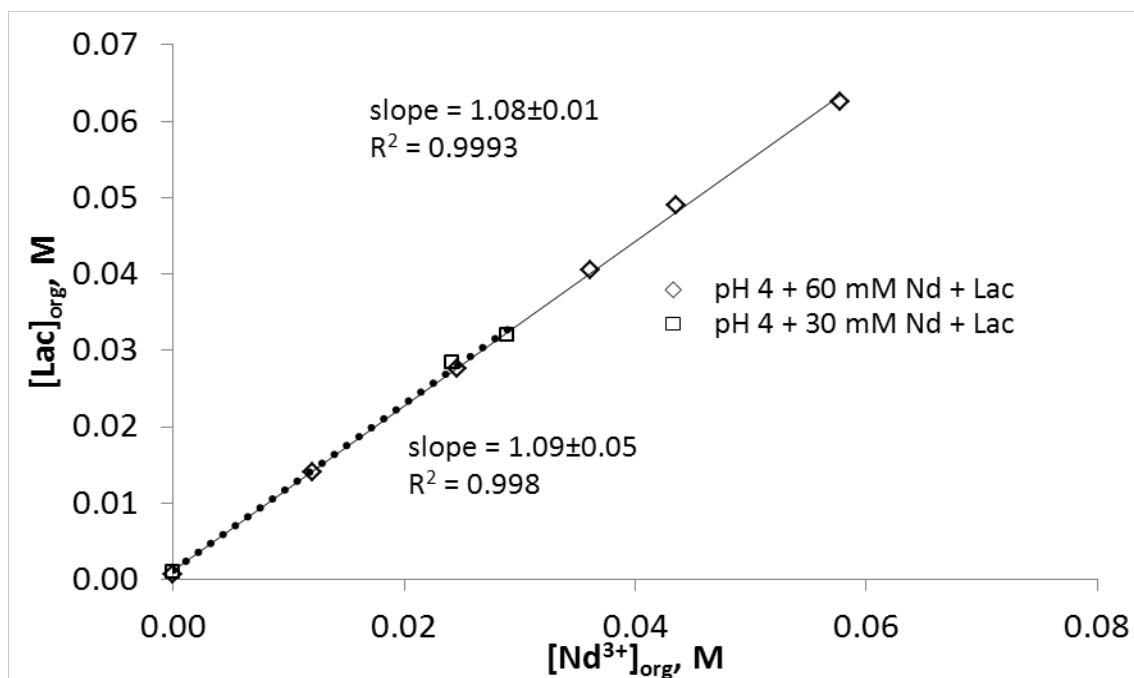
Figure 2.21- Linear scale dependence of the extraction of Lac and Nd^{3+} in the pH 4 + (30, 60) mM Nd + Lac systems. This data is limited to the data points where the $Nd(Lac)(HA)_2$ species was shown to be present.

Under the conditions of the high organic loading (i.e. low HA concentration) with $NdLac^{2+}$, the formation of the high-order aggregates was observed as suggested by VPO data (see section 2.5.1 and Figure 2.13 for details). The average aggregation number decreased from 19 ± 4 and 94 ± 42 at the highest loading to 2.75 ± 0.04 and 2.82 ± 0.06 at the intermediate loading for the pH 4 + (30, 60) mM Nd + Lac systems, respectively.

2.5.2.4 Water Distribution Results

To explore the hydration of organic phase species in the studied extraction systems, the water content of the post-contact organic extraction phases was measured by Karl Fischer titration. These results were compared with the water content of the corresponding pre-contact water-washed organic solutions. It was discovered that in all extraction systems except the pH 4 + (0, 30, 60) mM Nd + Lac systems, post-contact organic water concentration was within experimental error equal to the pre-contact organic water concentration in the water-washed HA/isooctane solutions due to the hydration of HA (see Table 2.17–18). The finding that organic water content did not increase upon Nd^{3+} extraction is consistent with the results in the HCl systems (see section 2.4.2.3 for details).

The result that no increase of the organic water was observed for the equilibrated organic phases in the pH 4 + 0 mM Nd + HCl system that exhibited Na^+ extraction suggests very little water co-extraction with the Na^+ ion. This is most likely due to the small Na^+ extraction and the limits of detection of water for that experiment. In the extraction systems pH 4 + (0, 30, 60) mM Nd + Lac that exhibited pronounced Lac transport into the solvent phase, equilibrium organic water concentration was significantly greater than in the corresponding washed solvent solutions (see Figure 2.22) where $[H_2O]_{org}$ is plotted as a function of HA concentration. The excess water in the organic phase is not associated with Nd^{3+} or Na^+ extraction. Due to the

similarity of the magnitude of excess water with the trends in lactate extraction, the correlation between water and lactate extraction was analysed. The trends showed a good correlation for the pH 4 + (0, 30) mM Nd + Lac systems when the conditions where Na^+ extraction was observed. The linear scale slope (see Figure 2.23) is indicative of the ratio of water-to-Lac in the organic phase and was observed at 7.1 ± 0.2, $R^2 = 0.993$ and 5.6 ± 0.1, $R^2 = 0.998$ for pH 4 + (0, 30) mM Nd + Lac systems, respectively. These slope results indicate a stoichiometry between water and lactate in the organic phase of between 5 and 7, which is dependent on the system; the 0 mM Nd system giving a slope of 7 and the 30 mM Nd system giving a slope of 5.

Table 2.17- Organic phase water concentration for the pH 1 + (0, 30) mM Nd + Lac systems.

| | | pH 1 + Lac | |
| | Washed Solvent | 0 mM Nd | 30 mM Nd |
$[HA]_{org}$ / M	$[H_2O]_{org}$ / M	$[H_2O]_{org}$ / M	$[H_2O]_{org}$ / M
0	0.000 ± 0.003	0.004 ± 0.003	0.003 ± 0.003
0.025	0.001 ± 0.003	0.004 ± 0.003	0.003 ± 0.003
0.05	0.003 ± 0.003	0.005 ± 0.003	0.005 ± 0.003
0.075	0.004 ± 0.003	0.007 ± 0.003	0.007 ± 0.003
0.09	0.007 ± 0.003	0.007 ± 0.003	0.008 ± 0.003
0.125	0.011 ± 0.003	0.010 ± 0.003	0.011 ± 0.000
0.15	0.014 ± 0.003	0.012 ± 0.003	0.016 ± 0.003
0.2	0.021 ± 0.003	0.019 ± 0.003	0.023 ± 0.003
0.25	0.023 ± 0.003	0.026 ± 0.003	0.030 ± 0.003
0.3	0.029 ± 0.005	0.042 ± 0.005	0.039 ± 0.006
0.4	0.053 ± 0.007	0.052 ± 0.007	0.062 ± 0.008
0.5	0.07 ± 0.01	0.08 ± 0.01	0.08 ± 0.01
1	0.21 ± 0.03	0.21 ± 0.03	0.23 ± 0.04

Table 2.18- Organic phase water concentration for the pH 4 + (0, 30, 60) mM Nd + Lac systems.

	pH 4 + Lac		
	0 mM Nd	30 mM Nd	60 mM Nd
$[HA]_{org}$ / M	$[H_2O]_{org}$ / M	$[H_2O]_{org}$ / M	$[H_2O]_{org}$ / M
0	0.002 ± 0.003	0.002 ± 0.003	0.003 ± 0.003
0.025	0.002 ± 0.003	0.007 ± 0.003	0.015 ± 0.003
0.05	0.009 ± 0.003	0.027 ± 0.003	0.028 ± 0.003
0.075	0.024 ± 0.003	0.031 ± 0.003	0.039 ± 0.003
0.09	0.034 ± 0.003	0.029 ± 0.003	0.047 ± 0.003
0.125	0.064 ± 0.003	0.027 ± 0.003	0.064 ± 0.003
0.15	0.095 ± 0.003	0.027 ± 0.003	0.062 ± 0.003
0.2	0.109 ± 0.003	0.027 ± 0.003	0.059 ± 0.003
0.25	0.172 ± 0.003	0.032 ± 0.003	0.059 ± 0.003
0.3	0.258 ± 0.006	0.055 ± 0.006	0.060 ± 0.004
0.4	0.373 ± 0.006	0.13 ± 0.01	0.070 ± 0.006
0.5	0.49 ± 0.01	0.21 ± 0.01	0.101 ± 0.008
1	1.07 ± 0.02	0.73 ± 0.01	0.48 ± 0.03

Trends between the water and Nd^{3+} and Na^+ are also of interest in understanding the hydration of metal ions in solution. The HCl systems showed no water extraction above the washed solvent hydration values as described in section 2.4.2.3. The presence of excess water in the organic phase in the low $[HA]_{org}$ values (see Figure 2.22) indicates that the Nd^{3+} organic phase species is hydrated. Due to the high loading of the HA by Nd^{3+} it was assumed that any hydration water associated with the HA dimers would be lost by complexation with Nd^{3+}, so the total organic phase water concentrations were used for this correlation. Linear scale correlations (Figure 2.24) between the organic Nd^{3+} and water concentrations showed that there was 1 water of hydration present in this species (slope = 1.01 ± 0.01, R^2 = 0.9999; 1.04 ± 0.02, R^2 = 0.998; for pH 4 + (30, 60) mM Nd + Lac systems, respectively; see Figure 2.24).
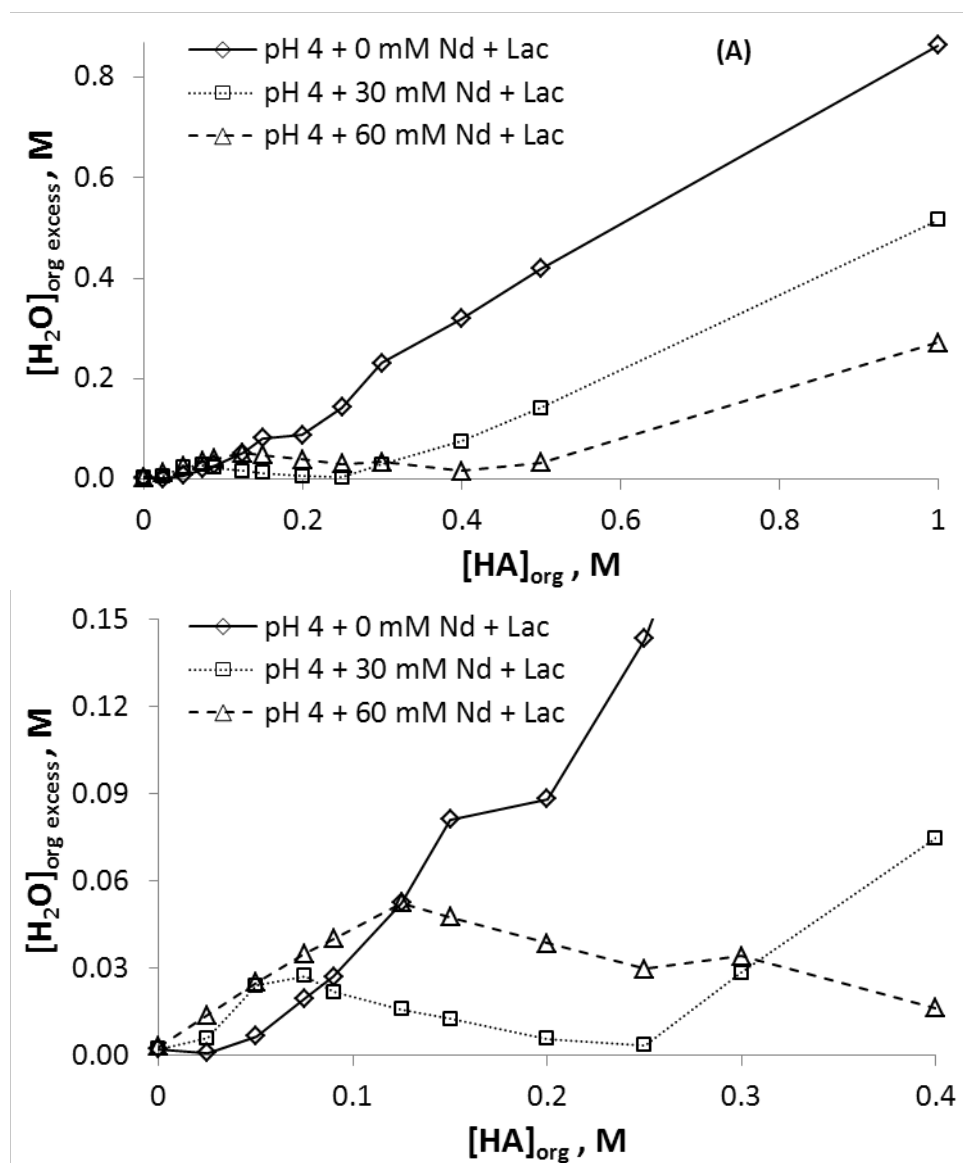
Figure 2.22- The extraction of water in excess of the HA hydration of the washed solvent for the pH 4 + (0, 30, 60) mM Nd + Lac systems.
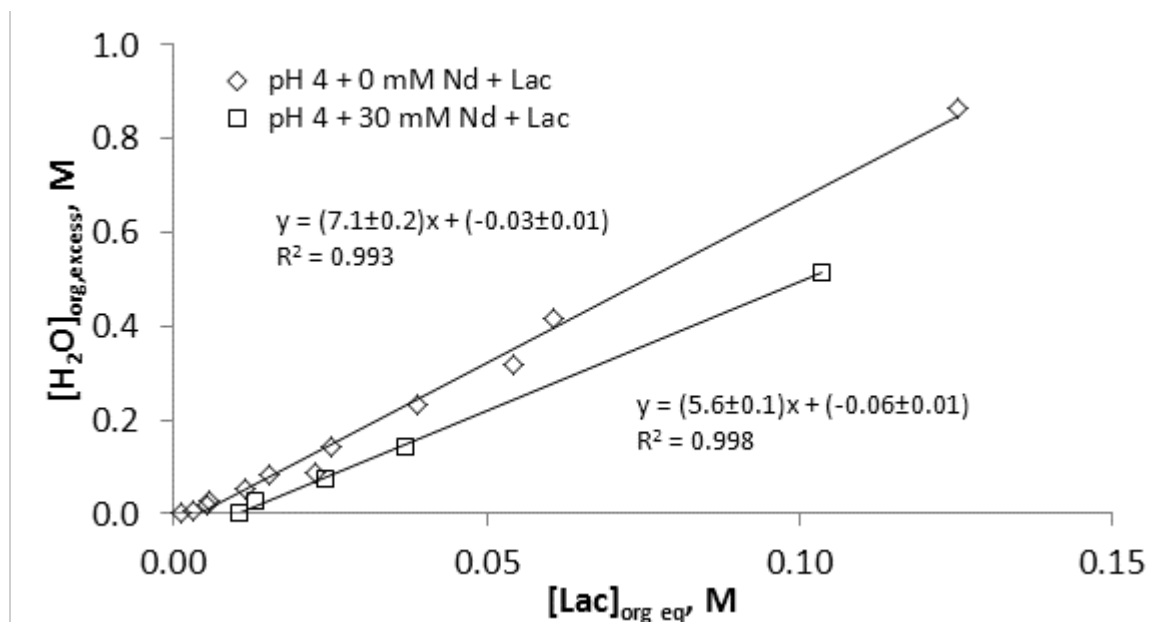
Figure 2.23- Dependence of organic H_2O concentration on the organic Lactate molarity. These data were selected from the entire pH 4 + (0, 30) mM Nd + Lac systems under conditions of NaLac extraction.
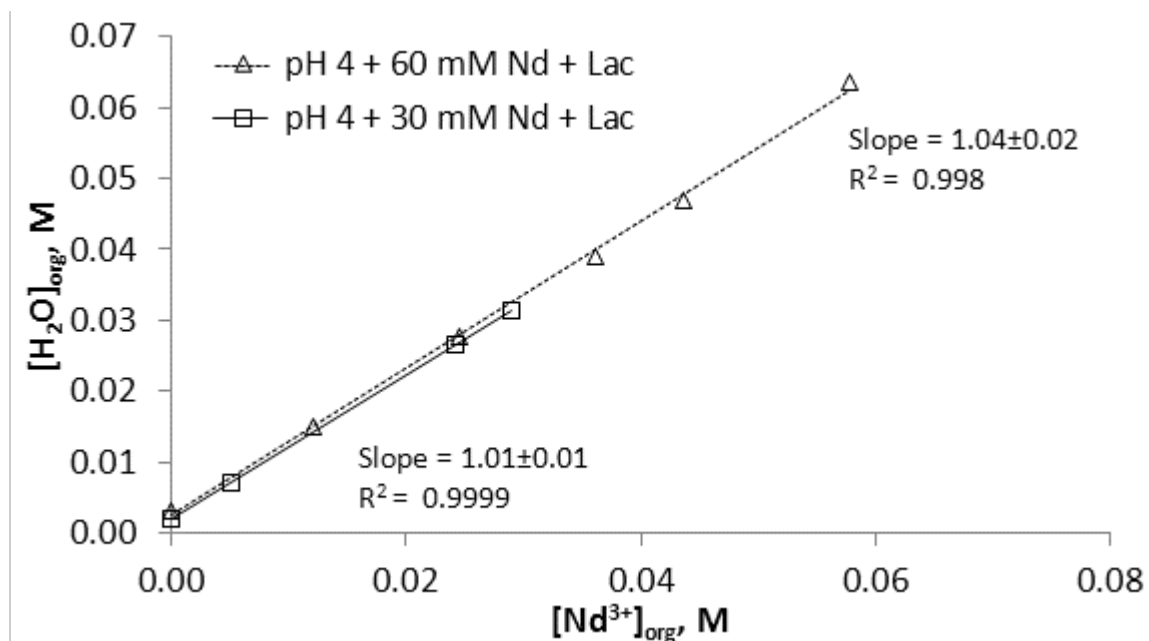
Figure 2.24- Linear scale correlation between organic phase Nd^{3+} and water concentration in the pH 4 + (30, 60) mM Nd + Lac systems. This data was selected from the pH 4 + (30, 60) mM Nd + Lac systems where $Nd(Lac)(HA)_2$ was shown to exist in the organic phase. Data points used were restricted to the $[HA]_{org}$ of 0–0.075 and 0–0.125 M HA respectively.

A correlation between the water and Na^+ extraction was prepared using the same assumption: high loading eliminates the HA hydration water eliminating the need to correct the extracted water concentration. The correlation showed that Na^+ extracted in the Lac systems has a hydration number of 3, with the slope being the ratio of water-to-Na^+ in the organic phase (slope = 3.3 ± 0.1, R^2 = 0.98; for pH 4 + (0, 30, 60) mM Nd + Lac systems, when fit as 1 data set; see Figure 2.25).
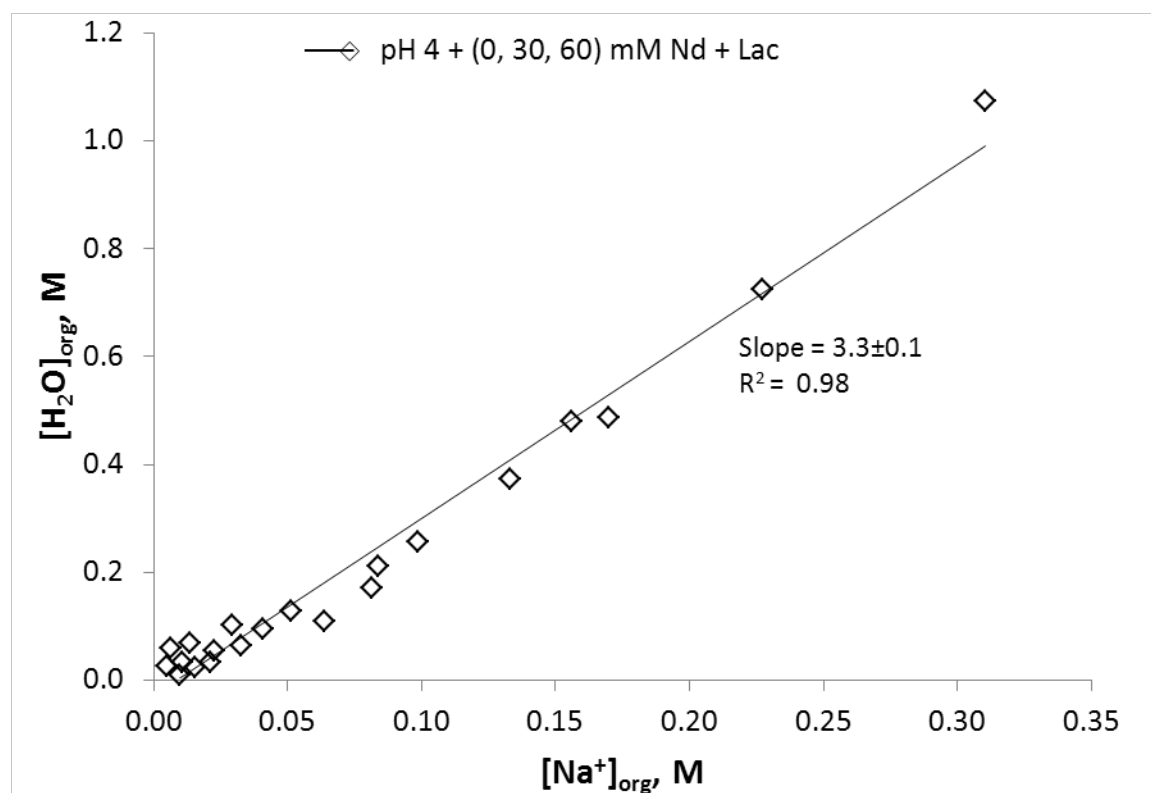
Figure 2.25- Linear scale correlation of organic phase water and Na^+ concentrations from the pH 4 + (0, 30, 60) mM Nd + Lac systems using only data where Na^+ extraction was observed. $[HA]_{org}$ utilized in this plot are: 0.025–1, 0.2–1 and 0.3–1 M HA respectively.

2.5.3 Visible Spectroscopy

2.5.3.1 <u>Aqueous Phase</u>

The absorbance bands observed for the aqueous phase Nd^{3+} ions in the pH 1 + 30 mM Nd + Lac

system (see Table 2.19) were the same as those observed for the pH (1,4) + 30 mM Nd + HCl

system (see Table 2.6 and Figure 2.9). In the pH 4 + (30, 60) mM Nd + Lac systems, where Nd^{3+}

complexation occurs in the aqueous phase, certain bands appear and others disappear in the

aqueous phase absorbance spectrum. All bands are unchanged from those observed for the pH

1 + 30 mM Nd + (Lac, HCl) systems except the following noted bands which shift in location

when free lactate in solution complexes the Nd^{3+} in the pH 4 + Lac systems: 575.28 nm →

580.42 nm (with a shoulder at 575 nm), 797.94 nm (with a shoulder at 794 nm) → 794.50 nm,

and 870.18 nm → 865.98 nm (with shoulder at 870 nm) (compare the two solid trace spectra in

Figure 2.26).

Table 2.19- Molar absorptivities observed for Nd^{3+} in the aqueous phase. R^2 ranged from 0.997–0.9999 for the listed molar absorptivities shown in this table.

| | pH 1 + 30 mM Nd + Lac | | pH 4 + Lac | |
| | | | 30 mM Nd | 60 mM Nd |
Wavelength (nm)	ε (L mol^{-1} cm^{-1})	Wavelength (nm)	ε (L mol^{-1} cm^{-1})	ε (L mol^{-1} cm^{-1})
511.83	2.05 ± 0.03	511.83	2.28 ± 0.01	2.207 ± 0.005
521.67	4.24 ± 0.02	523.37	5.39 ± 0.02	5.15 ± 0.01
575.28	7.65 ± 0.03	580.42	14.65 ± 0.02	14.04 ± 0.02
680.15	0.494 ± 0.007	678.54	0.53 ± 0.01	0.525 ± 0.005
732.31	3.96 ± 0.02	733.92	4.95 ± 0.01	4.88 ± 0.01
740.66	6.99 ± 0.02	741.63	7.64 ± 0.01	7.68 ± 0.02
794.5	9.94 ± 0.03	797.94	10.64 ± 0.01	10.407 ± 0.005
801.37	6.54 ± 0.02			
865.98	3.50 ± 0.03	870.18	3.02 ± 0.01	2.90 ± 0.01
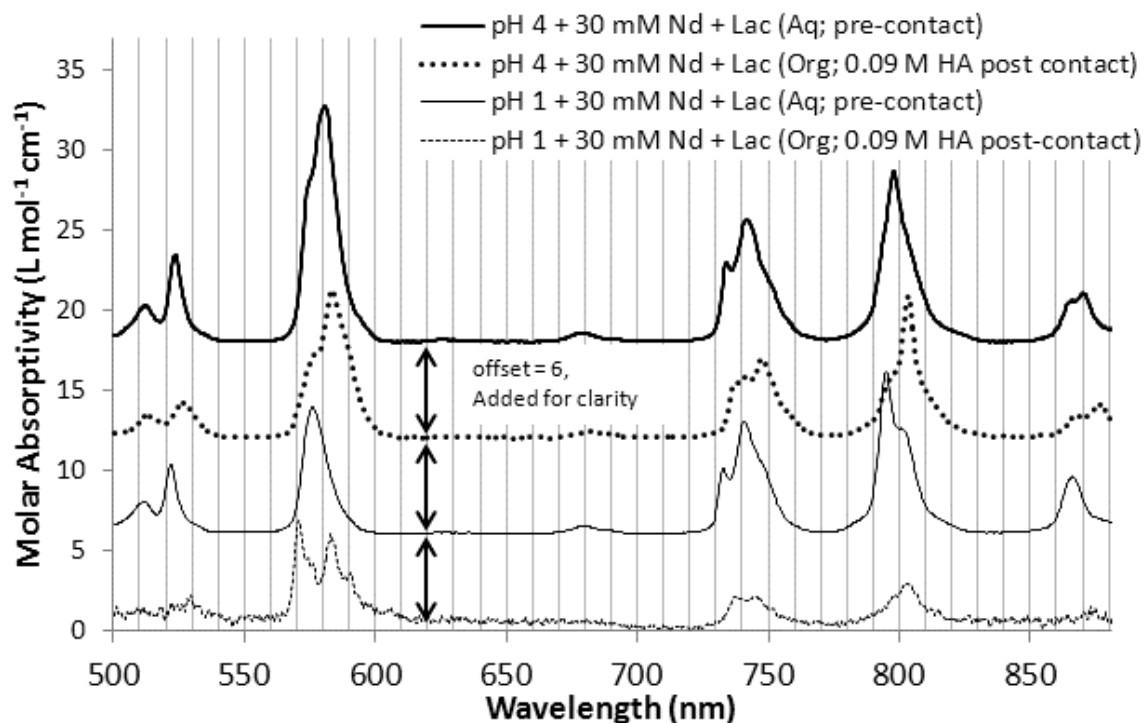
Figure 2.26- Comparison of the molar absorptivities that are representative of those observed for pH (1, 4) + (30, 60) mM Nd + Lac systems.

2.5.3.2   Organic Phase

The spectra obtained from the organic phase visible absorbance spectroscopy were converted to molar absorptivity scale using the $[Nd^{3+}]_{org}$ measured for each sample. In the pH 1 + 30 mM Nd + Lac system we observed the same spectral profile and shifts were observed as for the pH (1,4) 30 mM Nd + HCl systems, including the decrease of the absorptivity in the 570 nm band with the increase of ligand concentration that is discussed in section 0. In the pH 4 + (30, 60) mM Nd + Lac systems at low $[HA]_{org}$ the spectral profile was significantly different than previously observed systems. Instead of 5 bands in the 560–615 nm window, there were two, the strongest at 585, and a shoulder at 577 nm (see Figure 2.27). This spectral profile is consistent with a different coordination environment surrounding the Nd^{3+} metal

center. Based on the other analyses in this work (see sections 2.5.2.1 and 2.5.2.3), the species

present at 0.075 M HA portrayed in Figure 2.27 is $NdLac(A)_2$. This species contains three (one

Lactate plus two A) bidentate ligands surrounding the metal center. In papers that show

complexes with this coordination chemistry, a similar spectral profile is observed [for $Nd(A)_3$[69],

$Nd(Cyanex301)_3$,[64] and $Nd(Cyanex302)_3$[64]].
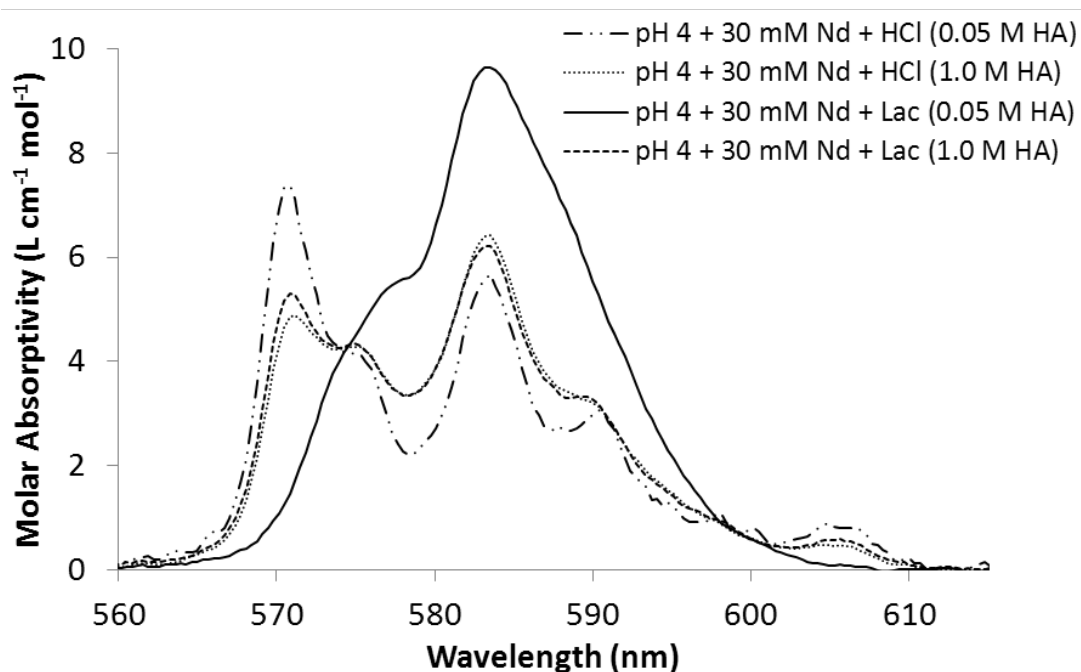
Figure 2.27- A comparison of the molar absorptivities for Nd^{3+} in the loaded organic phase
solutions in the HCl and Lac systems at pH 4 + 30 mM Nd systems.

2.5.4   Fourier Transform Infrared Spectrscopy of the Organic Phase

The FTIR of the organic phase contained previously observed bands in the pH 1 + Lac system

as the pH 1 + HCl systems, but showed new bands that appeared in the high loading regions of

the pH 4 + Lac system, just as in the visible absorbance of the organic phase. In order to focus on

the extracted complexes in the organic phase, the iso-octane solvent bands were subtracted from the loaded organic phase spectra. For comparison purposes, the spectral intensities were normalized (divided) by $[HA]_{org}$ resulting in the HA molar absorbance spectra. In all systems, the two peaks of highest interest for our study are the 1230 and 1035 cm^{-1} associated with P=O and P-O stretching, respectively (see Figure 2.28 for spectra).

The Nd^{3+} complexation by HA leads to a withdrawal of electron density in the P=O bond resulting in the decrease of the stretching mode frequency. This is supported by the shift in the 1230 band to 1200 cm^{-1} in all systems with Nd^{3+} extraction. A smaller shift is observed in systems that show Na^+ extraction with the maximum at 1222 cm^{-1}. This was supported by a shift from 1230 to broader 1222 cm^{-1} band in pH 4 + 0 mM Nd + Lac and the pH 4 + 30 mM Nd + Lac systems at high $[HA]_{org}$. Lactate co-extraction with Nd^{+3} as $NdLac^{2+}$ complex species in the pH 4 + 30 mM Nd + Lac systems at low $[HA]_{org}$ was confirmed by the appearance of FTIR band at 1565 cm^{-1} that is indicative of bi-dentate Lac complexation with Nd^{3+}.[106] The pH 4 + 30 mM Nd + Lac systems with high HA concentration exhibited a band at 1120 cm^{-1} indicative of the lactate secondary alcohol group.[106] This band appeared at 1116 cm^{-1} in the pH 4 + 0 mM Nd + Lac system associated with lactate co-extracted as NaLac. Formation of highly aggregated $(NdLacA_2)_x$ species leads to bridging –O–P–O– groups as evident from the appearance of the 1100 cm^{-1} band[71] in the pH 4 + 30 mM Nd + Lac systems and a 1097 cm^{-1} band for pH 4 + 30 mM Nd + HCl systems at low $[HA]_{org}$. Although the pH 4 + 60 mM Nd + Lac system was not featured in Figure 2.28, the same spectral shifts that were described in pH 4 + 30 mM Nd + Lac system were also observed in the pH 4 + 60 mM Nd + Lac system.
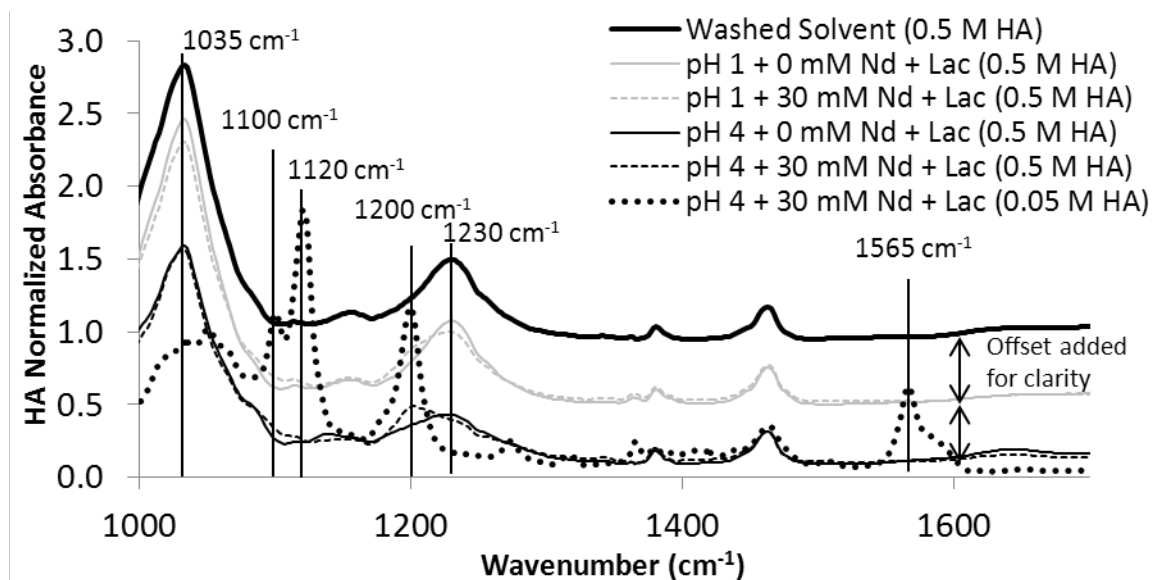
Figure 2.28- A comparison of the FTIR spectra for the pH (1, 4) + (0, 30) mM Nd + Lac systems and the washed solvent.

2.5.5 Nuclear Magnetic Resonance Spectroscopy of the Organic Phase

Organic phase samples prepared as described in section 2.2.15 were probed using ^{23}Na, ^{13}C and ^{31}P NMR. The initial results from the two samples were analysed to assess the feasibility of utilizing this technique to better understand the speciation of the organic phase. Most spectroscopic features are difficult to identify without running a sample set probing the variable loading of the system.

A background experiment was performed to verify that La^{3+} extraction causes the formation of the large aggregate species that Nd^{3+} did at high loading. Batch contact experiments were performed that were identical to the pH 4 + (30, 60) mM Nd + Lac systems, except La^{3+} was substituted for Nd^{3+}. The average aggregation of the organic phase solutions was determined by vapour pressure osmometry as described in section 2.2.13. The results obtained are shown in Figure 2.29. The aggregation results show that La^{3+} does form high-order aggregates just as Nd^{3+}

under high loading conditions (compare Figure 2.13 and Figure 2.29). It was assumed that all the other distribution trends with Na^+, Lac, H_2O, and La^{3+} were also the same between the two systems. Based on the aggregation results, two representative samples for the high loading/high aggregate condition, and the lower loading condition were selected: pH 4 + 60 mM La + Lac at 0.125 M $[HA]_{org}$ and pH 4 + 30 mM La + Lac at 1 M $[HA]_{org}$, respectively.
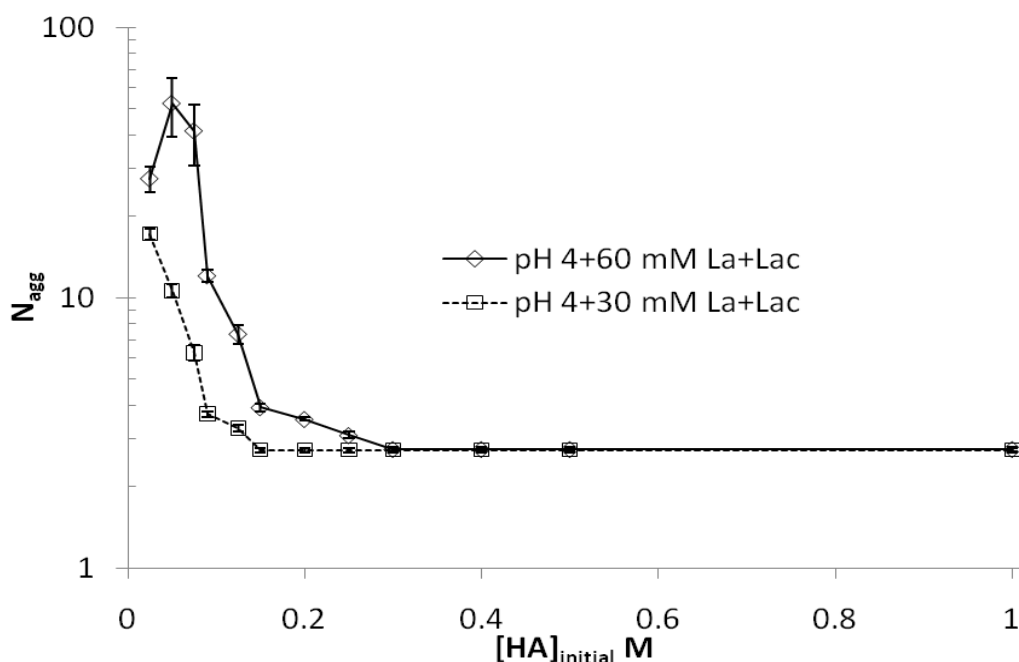
Figure 2.29- Aggregation results for the pH 4 + (30, 60) mM La + Lac systems.

The ^{23}Na scan of the pH 4 + 30 mM La + Lac (1 M $[HA]_{org}$) low-loading sample showed a single peak centered at 1.864 ppm. It was noted in the ^{22}Na distribution section (2.4.2.2) that Na^+ was most likely extracted by two mechanisms due to the presence of Lac in the same organic phases in a ratio of 2.7 ± 0.4 Na:Lac (see section 2.4.2.2 for details). One peak in the NMR spectrum may be indicative of one species, or there may be two present, provided that the

exchange rate between the species is more rapid than the NMR relaxation time, making it impossible to observe two peaks. With more effort in adjusting the relaxation time, two peaks may be resolved, but in the current experiment they were not. No ^{23}Na NMR was performed for the pH 4 + 60 mM La + Lac (0.125 M [HA]$_{org}$) sample because in the analogous Nd^{3+} system there was no ^{23}Na present.
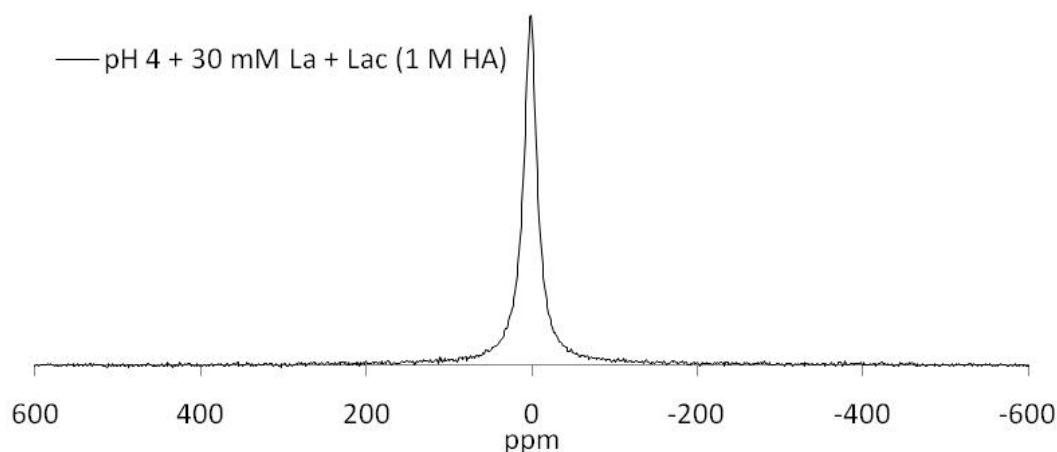
Figure 2.30- ^{23}Na NMR scan for pH 4 + 30 mM La + Lac (1.0 M HA) sample.

The ^{31}P NMR probed the environment of the ^{31}P in the HA molecule, and would thus offer understanding of what species the HA was involved in the organic phase. Both samples were analysed by this method and produced the spectra shown in Figure 2.31. The spectra obtained show peaks with different chemical shifts [0.477 ppm in the pH 4 + 30 mM La + Lac (1.0 M HA) sample and 1.456, –0.528, and –6.305 ppm in the pH 4 + 60 mM La + Lac (0.125 M HA) sample], which would be indicative of different speciation in each sample. This is the expected result, with the pH 4 + 60 mM La + Lac (0.125 M HA) sample showing the high aggregation speciation, and the pH 4 + 30 mM La + Lac (1.0 M HA) low aggregation speciation. It is difficult to analyze

82

these spectra without performing an array of NMR measurements over a dynamic range of loading, but it can be stated that these results show that the ^{31}P NMR spectra are sensitive to the speciation changes in the organic phase. These results definitely warrant further research with a larger sample array.
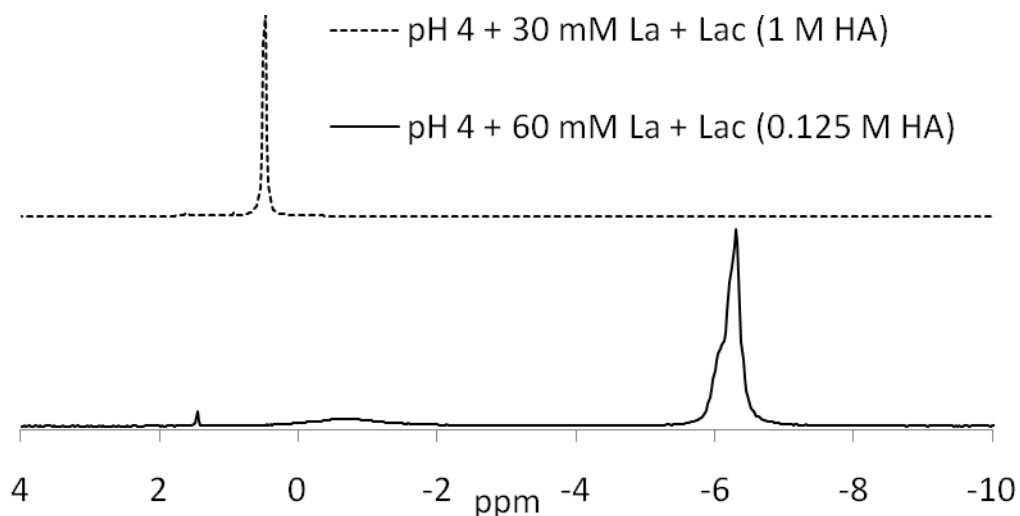
Figure 2.31- ^{31}P NMR spectra obtained from the pH 4 + 60 mM La + Lac (0.125 M HA) and pH 4 + 30 mM La + Lac (1.0 M HA) samples.

In the ^{13}C NMR, changes in the environment of carbon containing molecules offers some insight into the speciation of this system. Because of the natural abundance of ^{13}C (1.07%),[16] more peaks than those attributed to lactate appear in the spectrum that are associated with the isooctane diluent, and HA. In the pH 4 + 60 mM La + Lac (0.125 M HA) sample shown in Figure 2.32 most carbon species are too low in concentration for detection except the acid carbonyl at ~186 ppm, and the peaks associated with isooctane (see Table 2.20 for isooctane peak assignments). The weak multiplets observed in this spectrum are due to ^{13}C-^{2}H coupling in the deuterated isooctane. Peaks associated with HA were visible in pH 4 + 30 mM La + Lac (1 M HA)

due to its higher concentration in this sample. Doublets appearing at ~68, ~40, and ~25 ppm in

the pH 4 + 30 mM La + Lac (1 M HA) spectrum are not due to coupling between nuclei, but

rather due to a small change in the chemical shift of a fraction of HA. This change is likely due to

lanthanum bonding through the phosphate group which would lead to a slight increase in the

peak's chemical shift. A larger change in chemical shift observed for the acid carbonyl peak

between these spectra reflects the variation in the chemical environment that lactate

experiences when it complexes lanthanum vs. sodium. Because of the chemical shift data

obtained in these two scoping samples, more work using this technique is planned for other

experimental conditions.
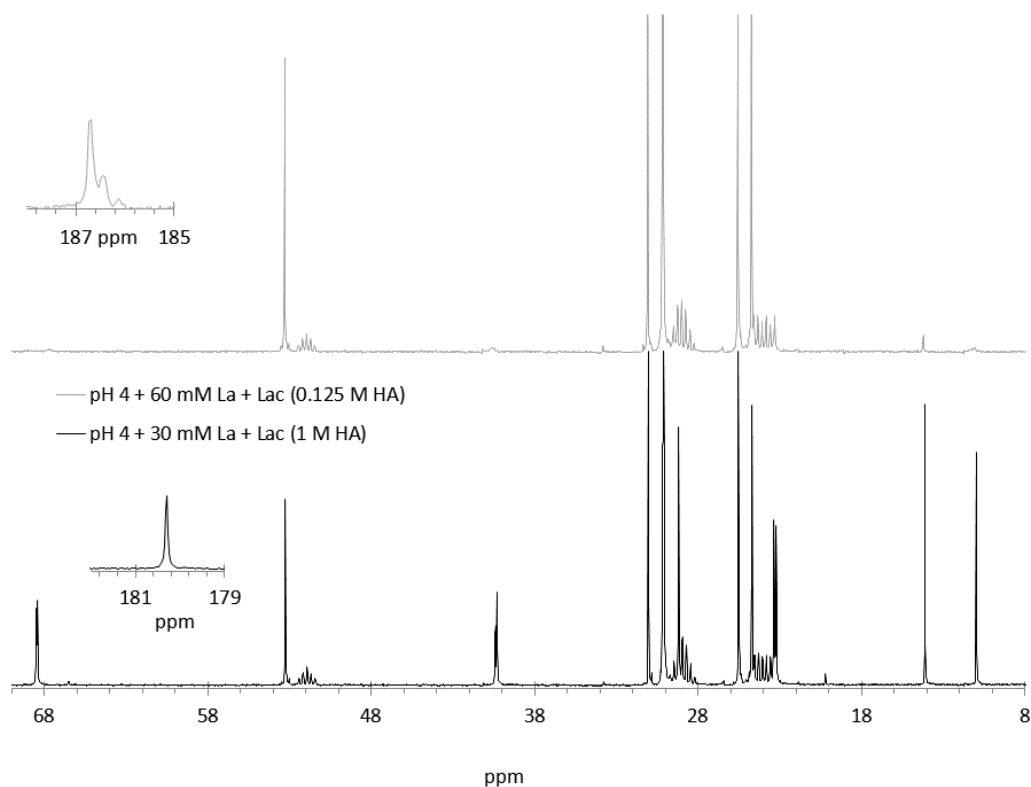
Figure 2.32- ^{13}C NMR scan spectra obtained from the pH 4 + 60 mM La + Lac (0.125 M HA) and
pH 4 + 30 mM La + Lac (1.0 M HA) samples.

Table 2.20- ^{13}C NMR Peak assignments for scoping experiment samples.

pH 4 + 60 mM La + Lac (0.125 M HA)		pH 4 + 30 mM La + Lac (1.0 M HA)		Peak Assignments
ppm	Integration	ppm	Integration	
186.697	1199			Lactate C=O (La complexed)
186.442	489.1	180.328	2796	Lactate C=O (Na complexed)
		68.524	1343	HA (La complexed)
		68.439	1471	HA (free)
53.268	7066	53.268	4556	Isooctane
52.439	213	52.439	160	Deuterated Isooctane splitting
52.192	411	52.192	355	
51.938	539	51.938	506	
51.711	392	51.683	320	
51.448	180	51.456	143	
		40.418	1308	HA (La complexed)
		40.333	1552	HA (free)
31.077	6691	31.077	4378	Isooctane
30.891	240	30.879	159	Deuterated Isooctane splitting
30.41	212	30.394	74	
30.325	405	30.313	244	
30.151	22719	30.143	18016	Isooctane

pH 4 + 60 mM La + Lac (0.125 M HA)		pH 4 + 30 mM La + Lac (1.0 M HA)		Peak Assignments
ppm	Integration	ppm	Integration	
29.852	283	29.844	123	Deuterated Isooctane splitting
29.759	360	29.751	343	
29.512	1013	29.496	755	
29.257	1602	29.213	4067*	HA
29.007	1430	28.995	1408	Deuterated Isooctane splitting
28.756	1167	28.744	1158	
28.505	601	28.493	629	
28.25	249	28.238	214	
25.562	14197	25.553	9296	isooctane
25.384	424	25.380	236	Deuterated Isooctane splitting
24.894	363	25.088	251	
		24.906	226	
24.729	7329	24.745	4940	isooctane
24.591	1117	24.583	863	Deuterated Isooctane splitting
24.34	1058	24.328	950	
24.086	891	24.074	775	
23.839	993	23.847	839	
23.584	762	23.596	677	
23.325	1392	23.398	3259*	HA (La complexed)
		23.257	3084*	HA (free)
		20.236	141	
14.207	360	14.151	2825	HA
		11.009	2690	HA

2.6   Conclusions

The conditional ionization constant (pK_a) of lactic acid at I = 2.0 M NaCl was quantified over the temperature range of 25–65°C. The results show very little change with temperature and a relatively small standard enthalpy of reaction. This work is of importance to the development of the TALSPEAK extraction model, specifically providing information that is useful for modeling the aqueous phase activity coefficients for lactate media solutions. Expanding this work to other ionic strengths will provide a more complete data set that will enable modeling of aqueous activity coefficients for lactate solutions in the TALSPEAK system.

The studies described in this chapter explored speciation of Nd^{3+} in the organic phase, including aggregation of HA under a range of condition (see Table 2.21). Extractions of Nd^{3+} by varied concentration HA (0–1 M) from HCl media at both pH 1 and 4 were compared with control samples without Nd^{3+} that were also at pH 1 and 4. A second set of samples measured the extraction of Nd^{3+} over the same HA concentrations from 1 M lactate media at pH 1 and 4. The initial concentration of Nd^{3+} was 30 mM for both HCl and lactate experiments; one additional experiment in lactate medium at 60 mM was also performed. The lactate series of extractions was also compared with non-Nd^{3+} control experiments at pH 1 and 4.

In the non-Nd^{3+} control samples for the HCl system [i.e. pH (1, 4) + 0 mM Nd + HCl], and the pH 1 lactate system [pH 1 + 0 mM Nd + Lac] an average aggregation number of 2 was observed, indicating that HA existed predominantly as a dimer. In the corresponding Nd^{3+} containing systems [i.e. pH (1, 4) + 30 mM Nd + HCl; pH 1 + 30 mM Nd + Lac] there was an increase in aggregation that was consistent with the mechanism for Nd^{3+} extraction by HA. Buffering in the pH 4 lactate systems led to high loading and the formation of large HA aggregates. In the pH 4 + 0 mM Nd + Lac system the average aggregation was 3.82 ± 0.05 which when modeled, showed the formation of NaA(HA) and NaLac(HA)$_Z$ with Z = 5.1 ± 0.3. The average aggregation in the pH

4 + (30, 60) mM Nd + Lac systems showed formation of high order aggregates at low $[HA]_{org}$ with an average aggregation as high as 100 observed. These high order aggregates diminished with increasing $[HA]_{org}$ until a constant aggregation was reached that corresponded with the low-loading extraction mechanism of Nd^{3+} by HA.

The Nd^{3+} distribution results were consistent with the extraction mechanism for Nd^{3+} by HA with the HA dimer stoichiometric coefficient (n) = 4 when Nd^{3+} loading of HA was moderate to low. Modeling of these systems by SXLSQI gave an equilibrium constant or Log K_{Nd} = −0.14 ± 0.06. In the pH 4 + (30, 60) mM Nd + Lac systems where Nd^{3+} loading of HA was high, Nd^{3+} saturated the organic phase at low $[HA]_{org}$, and was quantitatively extracted at higher $[HA]_{org}$.

The Na^+ extraction was suppressed in systems with pH of 1, with partial Nd^{3+} loading [pH (1, 4) + 30 mM Nd + HCl; pH 1 + 30 mM Nd + Lac systems], or where the HA was saturated with Nd^{3+} [pH 4 + (30, 60) mM Nd + Lac systems at HA concentrations < 4x total Nd^{3+}]. The Na^+ extraction occurred in systems where the pH was 4 and excess HA existed [pH 4 + 0 mM Nd + (HCl, Lac) system; pH 4 + (30, 60) mM Nd + Lac systems at HA concentrations > 4x total Nd^{3+}], in the Lac systems, Na^+ was extracted both as the HA sodium salt, and co-extracted with Lac. SXLSQI modeling of the pH 4 + 0 mM Nd + HCl system gave an equilibrium constant or Log K_{Na} = −0.989 ± 0.009.

Lactate was found to extract in all the Lac systems in various species. At pH 1, lactate was extracted as lactic acid, and possibly as $NdLac^{2+}$ salt in the presence of Nd^{3+}. In the pH 4 + 0 mM Nd + Lac system, and pH 4 + (30, 60) mM Nd + Lac systems at HA concentrations > 4x total Nd^{3+}, Lac was co-extracted with Na^+. In the pH 4 + (30, 60) mM Nd + Lac systems at HA concentrations < 4x total Nd^{3+} Lac was co-extracted with Nd^{3+} as $NdLac^{2+}$.

Water was found in the organic phase in all systems. In all systems but the pH 4 + (0, 30, 60) mM Nd + Lac systems the organic phase under low loading retained the levels of water found in

the washed solvent within experimental error. In the pH 4 + 0 mM Nd + HCl system where low

Na^+ loading was observed, a slight increase in the water concentration was observed. In the pH

4 + (0, 30, 60) mM Nd + Lac systems, water extraction was observed to increase with $NdLac^{2+}$

extraction, and increased even more with Na^+ extraction at higher HA organic phase

concentrations. Correlations of organic phase H_2O concentration with Nd^{3+} in the $NdLac^{2+}$

extraction regime indicates a 1:1 stoichiometry of water with Nd^{3+}. Correlations of organic phase

H_2O concentration with Na^+ when present in the pH 4 + (0, 30, 60) mM Nd + Lac systems

indicates a 3:1 stoichiometry of water with Na^+ or a hydration number of 3 for Na^+.

Organic phase visible spectroscopy in the pH (1, 4) + 30 mM Nd + HCl and pH 1 + 30 mM Nd

+ Lac systems indicate that the molar absorptivity of Nd^{3+} does not depend on pH or Nd^{3+}

loading of the organic phase, but rather on the organic phase HA concentration. The similar

spectra in the pH (1, 4) + 30 mM Nd + HCl systems indicate that the extraction mechanism is

unchanged from pH 1 to pH 4 in HCl media at $[HA]_{org} > 0.05$ M. Changes in the organic phase

visible spectra under the high loading conditions support the formation of $Nd(Lac)(HA)_2$. FTIR

results support the ion exchange mechanism at low to moderate Nd^{3+} loading, and the

extraction of $NdLac^{2+}$ and high HA loading, including the formation of high order aggregates with

HA participating in phosphate bridging in the organic phase.

The overall speciation results (see Table 2.21 for summary of species and conditions where

they were identified) indicate that at high Nd^{3+} loading in the pH 4 + Lac systems, Nd^{3+} exists as a

highly aggregated, $(NdLacA_2)_x$ species in the organic phase. As loading is decreased (i.e. HA

increased), the fraction of Nd^{3+} in the $(NdLacA_2)_x$ species decreases, while the fraction in the

mono-nuclear $NdA_3(HA)$ species increases until a complete conversion to $NdA_3(HA)$ is achieved.

Other species identified with the conditions where they were observed is shown in Table 2.21).

Table 2.21- Summary of species identified in the systems studied with the conditions where they were observed.

Species	System	Organic Phase Condition (M HA)
H(Lac)	pH 1 + 0 mM Nd + Lac	0.025–1.0
Na(A)	pH 4 + 0 mM Nd + HCl	0.05–1.0
Nd(A)$_3$(HA)	pH 1 + 30 mM Nd + HCl	0.05–1.0
	pH 4 + 30 mM Nd + HCl	0.05–1.0
	pH 4 + 30 mM Nd + Lac	0.15–1.0
	pH 4 + 60 mM Nd + Lac	0.3–1.0
[Nd(Lac)(A)$_2$]$_x$ (x = 2–50)	pH 4 + 30 mM Nd + Lac	0.025–0.15
	pH 4 + 60 mM Nd + Lac	0.025–0.3
Na(Lac) + Na(A)	pH 4 + 0 mM Nd + Lac	0.05–1.0
	pH 4 + 30 mM Nd + Lac	0.15–1.0
	pH 4 + 60 mM Nd + Lac	0.3–1.0

The initial NMR results obtained through the scoping experiment indicate that the ^{13}C and ^{31}P spectra obtained from the analogous pH 4 + (30, 60) mM La^{3+} + Lac systems are sensitive to the speciation changes in the system and more work with these methods is warranted. A complete interpretation of this system using NMR was not undertaken. However identified trends were consistent with the observed results from other methods.

CHAPTER 3

THE DETERMINATION OF BINDING CONSTANTS OF 8-HYDROXYQUINOLINE IN THE

TRITON X-114/WATER MIXED SOLVENT SYSTEM

3.1   Introduction

Cloud point extraction has been shown to separate lanthanum from gadolinium using the

surfactant Triton X-114 (see Figure 3.1) and the ligand 8-hydroxyquinoline (HQ) (see Figure

3.2).[5-7] The success of any extraction system to perform such a difficult separation led to

interest in applying this method to the separation of the trivalent actinides from the trivalent

lanthanides. Preliminary extraction experiments[107] using europium and curium have indicated

that there is some selectivity for curium over europium, but the data showed that the optimal

separation conditions occur over a very small pH range (Separation factor of ~10^3 at pH = 5.5).

The desire to model the system and the need for complexation constants under the conditions

of the cloud point extraction has motivated this research. The aim of this work is to design a

better separation technique through understanding the protonation and Eu^{3+} complexation

behavior of 8-hydroxyquinoline and the Eu^{3+} hydrolysis behavior in the Triton X-114/water

mixed solvent used in cloud point extraction.
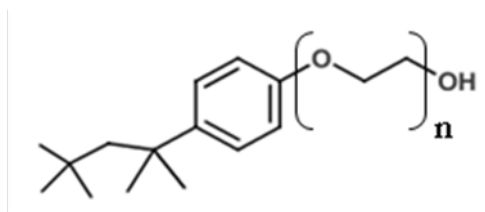
Figure 3.1- Chemical Structure of Triton X-114. This chemical is typically sold as a mixture with n
= 7–8 with the total mixture having an average molecular weight of 537 gm/mol.[108]
    Past research with 8-hydroxyquinoline extends back to 1881 when it was first synthesized by

Bedall and Fischer.[109-111] It was later discovered to form insoluble chelates with many metals[112-

[114] that proved useful for quantitative determination by gravimetric means. Solvent extraction with 8-hydroxyquinoline in chloroform has been explored,[115-123] but this is not a highly favored option for industrial application due to the toxicity and flammability of the solvent. Watanabe and Tanaka[9] introduced a new extraction technique in 1978 using cloud point extraction that relies on non-ionic surfactants and chelators that form water-insoluble complexes to extract metal ions from aqueous solutions. Cloud point extraction has experienced a large growth in research as witnessed by these reviews,[35-37, 40] but has generally been employed in laboratory analysis rather than industrial scale separations. Recent work on Continuous Rotating Disk Contactors[41-42, 124] is, perhaps, opening the door for industrial scale deployment of cloud point extraction, however this cited work deals with extraction of phenol from waste water rather than metal chelates which would seem to increase the complexity of the process. Industrial scale deployment for recycling of irradiated nuclear fuel is the ultimate goal of the continued research in trivalent actinide-trivalent lanthanide separation research.

The solubility of 8-hydroxyquinoline is the major issue that has driven the selection of experimental media for complexation constant determination. The solubility of 8-hydroxyquinoline is pH dependent due to its protonation states (see Figure 3.2). At pH extremes 8-hydroxyquinoline carries a charge but at intermediate pH values 8-hydroxyquinoline is uncharged, leading to increased solubility at pH extremes and low solubility at moderate pH values. Aqueous solubility of the neutral form of 8-hydroxyquinoline (as the species labeled 'B' in Figure 3.2) is approximately 3 mM (see Figure 3.3).[125-126] The speciation diagram included in Figure 3.3 was calculated from data by Ashton *et al.* ($pk_{a1} = 4.88$, $pK_{a2} = 10.05$).[127] Conditions that increase 8-hydroxyquinoline solubility are elevated temperature, and solvent modification such as mixed solvent conditions.[126] For this reason many of the reported values of the 8-hydroxyquinoline metal complexation constant data are given for mixed solvent systems such as

water/dioxane or water/ethanol. There was a reasonably complete determination of lanthanides complexation constants with 8-hydroxyquinoline in dioxane/water[128] which were used to model the Gd^{3+}/La^{3+} cloud point extraction results.[5] It was desired to use parameters for modeling the complexation behavior of Eu^{3+} and Cm^{3+} with 8-hydroxyquinoline, but Eu^{3+} was one of four lanthanides that were omitted from the dioxane/water study. There is very little data published for Eu^{3+} or Cm^{3+} complexation with 8-hydroxyquinoline. Constants from the literature[129] only showed 2 values for complexation between 8-hydroxyquinoline and Eu^{3+}: one[130] was a solubility study on $[Eu(Q)_3]$ and the other[131] was a study at 0.1 M $NaClO_4$ / 20 °C that lists only the 1st complexation constant. No complexation constants were listed in the IUPAC database for Cm^{3+} 8-hydroxyquinoline complexation.
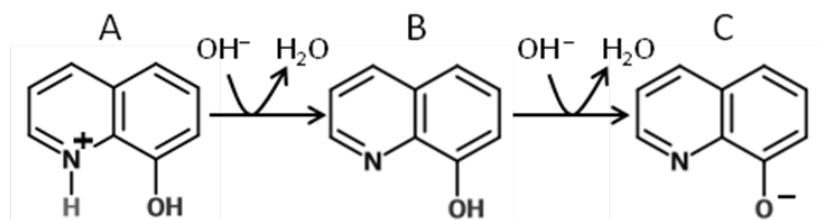
Figure 3.2- The protonation states of 8-hydroxyquinoline.

When modeling behavior under cloud point extraction conditions, the thermodynamic constants should ideally be determined in the experimental medium, which in this case is the Triton/water mixed solvent. One study determined the pK_{a1} and pK_{a2} of 8-hydroxyquinoline in Triton X-100[132][133]/water as a function of Triton X-100 concentration (0-10 wt%) at 0.1 M NaCl/20 °C[134] which in one paper represents the entire literature record on the stability constant modeling of 8-hydroxyquinoline in the water/triton mixed solvent system. This work aims to measure the protonation and Eu^{3+} complexation behavior of 8-hydroxyquinoline and the

Eu^{3+} hydrolysis behavior in the Triton X-114/water mixed solvent used in cloud point extraction to enable the design of a better separation technique.
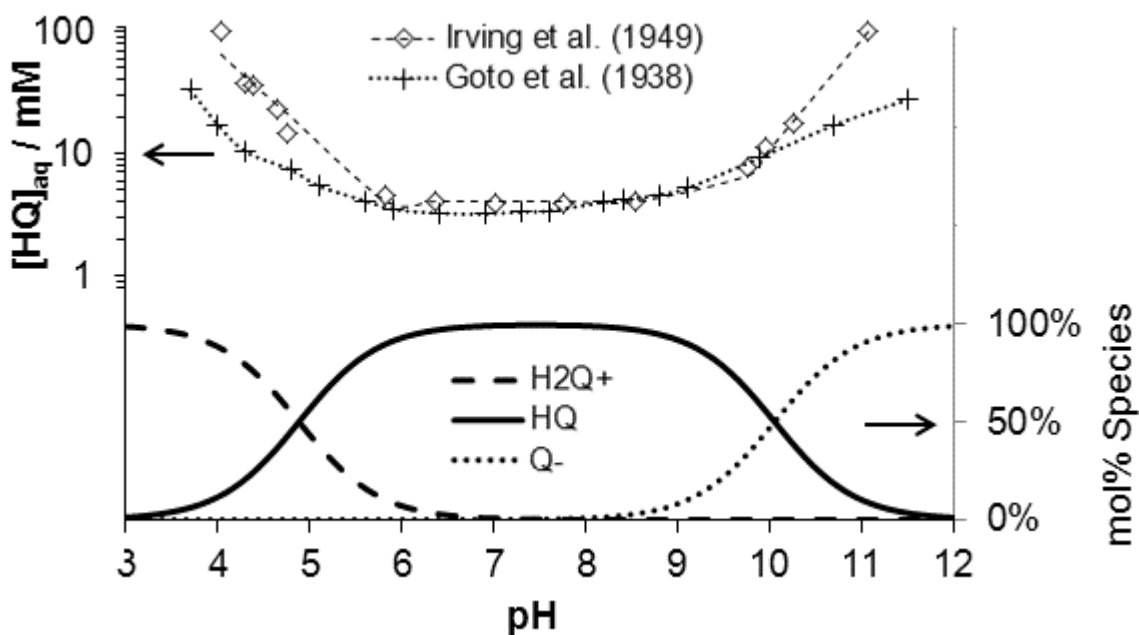
Figure 3.3- The aqueous solubility and speciation of 8-hydroxyquinoline as a function of pH.

The methods selected for the characterization of the protonation, hydrolysis and complexation behavior of 8-hydroxyquinoline and Eu^{3+} used in this study, are potentiometric and spectrophotometric titration techniques. Potentiometry will measure the pH buffering effects caused by the formation of different species in the solutions undergoing titration by a strong acid or base. The potentiometric titration curve can be analyzed by modeling software program such as Hyperquad,[135] to yield the conditional protonation, hydrolysis, and/or complexation constants. Hyperquad is a highly regarded program that has been utilized or cited within ~900[136] publications since its release in 1996. Similarly, recording the changing pH and

absorbance spectra of 8-hydroxyquinoline in a solution undergoing titration by a strong acid or base and analyzing the sequence of spectra using a spectrophotometric modeling program such as SQUAD,[137] will likewise provide the conditional protonation, hydrolysis, and/or complexation constants. "The Stability Quotients from Absorbance Data" (SQUAD) computer code, like hyperquad, has been widely used and was cited in 230[138] publications since its publication in 1975. Hyperquad can find the best fit for speciation parameters under investigation, and the overall system speciation from user-supplied pH titration data, chemical constituent concentrations, chemical equilibria expressions, and the known chemical equilibria constants. SQUAD utilizes the inputs listed above, but also requires the spectrophotometric titration data that correspond to the potentiometric titration data points. With this information, SQUAD can calculate the overall system speciation, the speciation parameters under investigation, and the spectrum of each absorbing species in solution.

Typically, cloud point extraction solutions are mixed below the surfactant cloud point temperature, which for Triton X-114 is 22 °C.[108] The phase separation in cloud point extraction is performed by heating the solution above the cloud point temperature and centrifuging and separating/disengagement of the phases. The thermal fluctuation of the system over the course of the separation makes it challenging to select a temperature that is representative of the conditions of the system at equilibrium. Further complications are introduced by the formation of two phases during separation, and the turbidity of the solution at temperatures above the cloud point. The use of spectrophotometry necessitates a non-turbid solution so that the solution absorbance spectrum is not obscured. Potentiometry is not affected by turbidity, but does require experiments to be conducted at a constant temperature. Therefore, the current study is carried out at a constant temperature maintained by ice slurry (T = ~1 °C) that will prevent turbidity due to cloud point separation.

The long-term goal to be achieved following the completion of this project is to develop a better trivalent actinide / trivalent lanthanide separation method using cloud point extraction. The modeling results described herein are an initial effort to understand preliminary cloud point extraction data involving Eu^{3+} and Cm^{3+} by 8-hydroxyquinoline using Triton X-114 that show at pH 5.5, a Cm^{3+}/Eu^{3+} separation factor of 10^3.[139] It is believed that when the Eu^{3+} system is fully characterized by the methods described above, that a comparative study of the relative complexation strength of Eu^{3+} and Cm^{3+} with 8-hydroxyquinoline by Time Resolved Laser Fluorescence Spectroscopy will provide clarity into the unpublished separation results while conserving Cm^{3+}. For the present time however, this work addresses the characterization of the protonation of 8-hydroxyquinoline, the hydrolysis of Eu^{3+}, and the complexation of 8-hydroxyquinoline and Eu^{3+} in the water/Triton X-114 mixed solvent system at about 1 °C.

3.2   Experimental

3.2.1   Chemicals

Europium chloride hexahydrate ($EuCl_3 \cdot 6H_2O$, 99.99%) was obtained from Alfa Aesar and used as received. Sodium Hydroxide (50 wt%) and NaCl were obtained from Aldrich and used as received. Triton X-114 was obtained from Fluka and used as received. 8-hydroxyquinoline was obtained from JT Baker and purified by sublimation prior to use.

3.2.2   Methods

Potentiometric data was recorded using a laptop controlled system running the Metrohm Tiamo 1-2 software. Potentiometric titrations were performed using the dynamic pH titration setting in the Tiamo software. The dosing unit (Metrohm Dosino 800), stir plate (Metrohm 801 Stirrer), and combination temperature/pH electrode (Metrohm 6.0258.010) were all connected to the laptop through a Metrohm Titrando 809. Temperature control at 1.7±0.3 °C was performed using a beaker (as the titration vessel) packed in ice chunks in a crystallizing dish and

a zippered plastic bag filled with ice chunks that was firmly wrapped around the combination temperature/pH electrode. Carbonate free NaOH was mixed from 50 wt% NaOH and boiled DI water, standardized, and stored in an Ascarite vented bottle.

Spectrophotometric titrations were performed by manual titration (using pipette) and pH was measured using Tiamo system in pH/Temperature measurement mode, the spectral data was saved electronically and the pH data was recorded by hand. Spectra were collected using an OceanOptics HR4000 spectrophotometer (190 – 1140 nm). Light was introduced to the sample using a fiber-optic dip probe from both deuterium and tungsten light sources. The tungsten light source's intensity was controlled using a 2.9 Optical Density glass filter. The spectra recorded were averages of 50 scans of 15 millisecond each with the boxcar averaging feature disabled. Resolution for the scans was 0.26 nm.

Calibration of pH probes was performed using standard pH 4, 7 and 10 buffers that were chilled to the temperature of the titration solutions. The system was recalibrated for each titration. Ionic strength was maintained at 0.1 mol/L using NaCl. The solution constituent concentrations for the potentiometric titrations are shown in Table 3.1 and Table 3.2. The solution constituent concentrations for the spectrophotometric titrations are shown in Table 3.3. Standardized NaOH was used for the potentiometric titrations with [NaOH] = 0.01024±0.00002 M, and [NaCl] = 0.09 M. Spectrophotometric titrations were performed with manual additions from solutions of NaOH of 0.1, 0.01, and 0.001 M depending on the needed pH change and solution buffering conditions on a point-by-point basis. These NaOH solutions were supplemented with NaCl to maintain a total ionic strength of 0.1 M.

Table 3.1- Solution constituent concentrations for the H_2O system potentiometric titrations.

Eu^{3+}:HQ Ratio	$pH_{initial}$	[HCl] M	[Eu^{3+}] M	[HQ] M	[NaCl] M	[Triton] wt%	T °C	
0:1	3.20	0.001	0	$3x10^{-4}$	0.1	0	1.5	±0.2
1:0	3.30	0.001	$3x10^{-4}$	0	0.1	0	1.7	±0.2
1:1	3.22	0.001	$3x10^{-4}$	$3x10^{-4}$	0.1	0	1.7	±0.2
1:2	3.21	0.001	$1.5x10^{-4}$	$3x10^{-4}$	0.1	0	1.9	±0.2
1:3	3.26	0.001	$1x10^{-4}$	$3x10^{-4}$	0.1	0	2.0	±0.2

Table 3.2- Solution constituent concentrations for the H_2O/Triton X-114 system potentiometric titrations.

Eu^{3+}:HQ Ratio	$pH_{initial}$	[HCl] M	[Eu^{3+}] M	[HQ] M	[NaCl] M	[Triton] wt%	T °C	
0:0	3.13	0.001	0	0	0.1	1	1.9	±0.2
0:1	3.25	0.001	0	$3x10^{-4}$	0.1	1	1.8	±0.2
1:0	3.05	0.001	$3x10^{-4}$	0	0.1	1	1.8	±0.2
1:1	3.21	0.001	$3x10^{-4}$	$3x10^{-4}$	0.1	1	1.8	±0.2
1:2	3.24	0.001	$1.5x10^{-4}$	$3x10^{-4}$	0.1	1	1.9	±0.1
1:3	3.22	0.001	$1x10^{-4}$	$3x10^{-4}$	0.1	1	1.9	±0.2

Table 3.3- Solution constituent concentrations for the H_2O and H_2O/Triton X-114 system spectrophotometric titrations.

Eu^{3+}:HQ Ratio	$pH_{initial}$	[HCl] M	[Eu^{3+}] M	[HQ] M	[NaCl] M	[Triton] wt%	T °C	
0:1	3.18	0.001	0	10^{-5}	0.1	0	1.9	±0.2
1:5	3.06	0.001	$2x10^{-6}$	10^{-5}	0.1	0	1.9	±0.2
0:1	3.19	0.001	0	10^{-5}	0.1	1	1.9	±0.2

To obtain the conditional stability constants, the potentiometric data was modeled using

Hyperquad software[135] and the spectrophotometric data were modeled using the SQUAD

computer code.[137] The pK_w for the water system was obtained using the Specific Interaction

Theorem[140] and Van't Hoff[141] equations to calculate the pK_w at T = 1.8 °C and I_μ = 0.1 M NaCl

from the pK_w for pure water at 25 °C of 14.0. Enthalpy data used in the Van't Hoff equation was

from Harned et al.[142] and calculations were performed using programs obtained from

IUPAC/Academic software.[143-144] The value calculated for the pKw at T = 1.8 °C and I_μ = 0.1 M

NaCl is 14.7.

The notation used in this work for the dissociation of acids is shown in the equations (3.1)

and (3.2)

$$HA \xleftrightarrow{\quad K_a \quad} H^+ + A^-$$ (3.1)
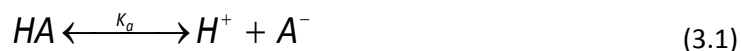
which is the same as writing

$$HA + OH^- \xleftrightarrow{\quad K_a \quad} H_2O + A^-$$ (3.2)

The equilibrium expression that describes both of these reactions is shown in equation (3.3).

$$K_a = \frac{[H^+][A^-]}{[HA]} = \frac{[A^-]}{[HA][OH^-]}$$ (3.3)

The shorthand for the negative logarithm of a value is shown in equation (3.4).

$$pK_a = -\log_{10}(K_a)$$ (3.4)

The notation used for the step-wise stability constants can be derived from the equilibrium

formation reactions outlined using the example of europium in equations (3.5), (3.6), and (3.7).

$$Eu^{3+} + H_2O \xleftrightarrow{\quad K_{1-10} \quad} [Eu(OH)]^{2+} + H^+$$ (3.5)

$$[Eu(OH)]^{2+} + H_2O \xleftrightarrow{\quad K_{1-20} \quad} [Eu(OH)_2]^+ + H^+$$ (3.6)

$$[Eu(OH)_2]^+ + H_2O \xleftrightarrow{\quad K_{1-30} \quad} [Eu(OH)_3] + H^+$$ (3.7)
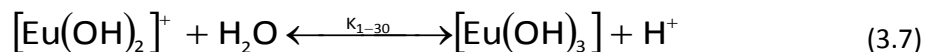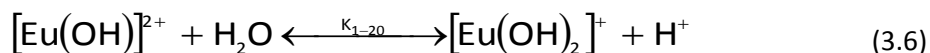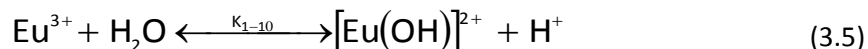
The first subscript of any K or β value will indicate the stoichiometry of europium. The second subscript refers to hydroxide (OH⁻) when negative or a proton (H⁺) when positive. Stepwise stability constants describing reactions adding Q⁻ utilize the third subscript to indicate which stepwise addition is taking place. The first addition of Q⁻ to europium is shown in equation (3.8).

$$Eu^{3+} + Q^- \xleftarrow{\quad K_{101} \quad} [Eu(Q)]^{2+} \tag{3.8}$$
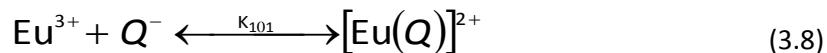
Overall stability constants will be used to describe equilibrium reactions as shown in equation (3.9)

$$Eu^{3+} + 3\,H_2O \xleftarrow{\quad \beta_{1-30} \quad} [Eu(OH)_3] + 3\,H^+ \tag{3.9}$$
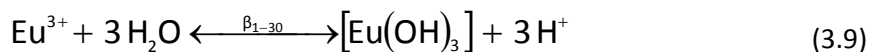
Overall stability constants are a product of the succession of stepwise stability constants that, when used in succession, result in the same reaction. An example is the overall stability constant shown for the formation of [Eu(OH)₃] shown in equation (3.10)

$$\beta_{1-30} = K_{1-10}K_{1-20}K_{1-30} \tag{3.10}$$

Mixed ligand reactions are a special case of the overall stability constant notation where europium hydrolyzes both waters and complexes Q⁻ in one step as shown in equation (3.11)

$$Eu^{3+} + 2\,H_2O + Q^- \xleftarrow{\quad \beta_{1-21} \quad} [Eu(OH)_2(Q)] + 2\,H^+ \tag{3.11}$$
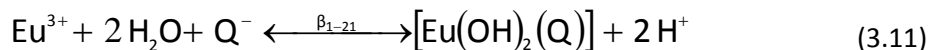
where the overall stability constant is a product of the successive stepwise reactions as shown in equation (3.12).

$$\beta_{1-21} = K_{101}K_{1-11}K_{1-21} = K_{1-10}K_{1-20}K_{1-21} \tag{3.12}$$

The K values presented in this text for mixed hydrolysis species are calculated by assuming that the order of addition of the mixed ligands is: first all Q⁻, then the successive hydroxides as is shown by the middle equivalence of equation (3.12). All results displayed in this text will

indicate parameters that are held constant by displaying no error (i.e. X.X), and parameters that were fit in the model by displaying error (i.e. X.X±X.X) in the tables.

3.3 Results: The H$_2$O System

The values of the pK$_a$'s of 8-hydroxyquinoline and europium hydrolysis constants were obtained prior to determining the europium 8-hydroxyquinoline stability constants. The europium 8-hydroxyquinoline systems of increasing complexity were created using solutions with Eu^{3+}:HQ ratio of 1:1, 1:2, and 1:3. This sequential progression provided the opportunity to fit (1) the [Eu(Q)]$^{2+}$, (2) [Eu(Q)$_2$]$^+$, with a fixed [Eu(Q)]$^{2+}$ formation parameter, and (3) [Eu(Q)$_3$], with fixed parameters for [Eu(Q)]$^{2+}$, [Eu(Q)$_2$]$^+$.

3.3.1 Determination of the pK$_a$'s of 8-Hydroxyquinoline by Potentiometric Titration

To obtain the protonation constants of 8-hydroxyquinoline, a solution of composition [HQ] = 3x10^{-4} M, [NaCl] = 0.1 M, [HCl] = 0.001 M was titrated with standardized NaOH ([NaOH = 0.01024±0.00002 M, and [NaCl] = 0.09 M). The temperature for this titration was 1.5±0.2 °C. The 1st derivative shown here and throughout this work was calculated by the TIAMO software using a modification of Fortuin's method for End Point Recognition.[145-146] Maxima in the 1st derivative curve show how many equivalence points were obtained during the titration and may provide an indication of the number of acid constants that may be fit to the titration curve. In this titration there are two maxima, indicating transitions between three species. This is expected given the protonation states of 8-hydroxyquinoline (see Figure 3.2). The equilibrium expressions shown in equations (3.13) and (3.14) were used to model the titration shown in Figure 3.4 using Hyperquad.

$$H_2Q^+ + OH^- \xleftarrow{\quad K_{a1} \quad} HQ + H_2O \tag{3.13}$$

$$HQ + OH^- \xleftarrow{\quad K_{a2} \quad} Q^- + H_2O \tag{3.14}$$
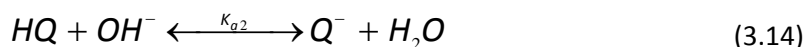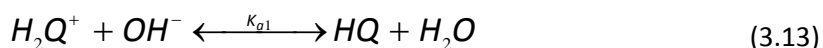
The water dissociation constant or pk_w was 14.7 for all modeling simulations in the H_2O system whose reaction is shown in equation (3.15)

$$H_2O \xleftrightarrow{K_w} H^+ + OH^-$$ (3.15)

The parameters that best fit the titration curve are shown in Table 3.4. The modeling results are shown in Figure 3.5.
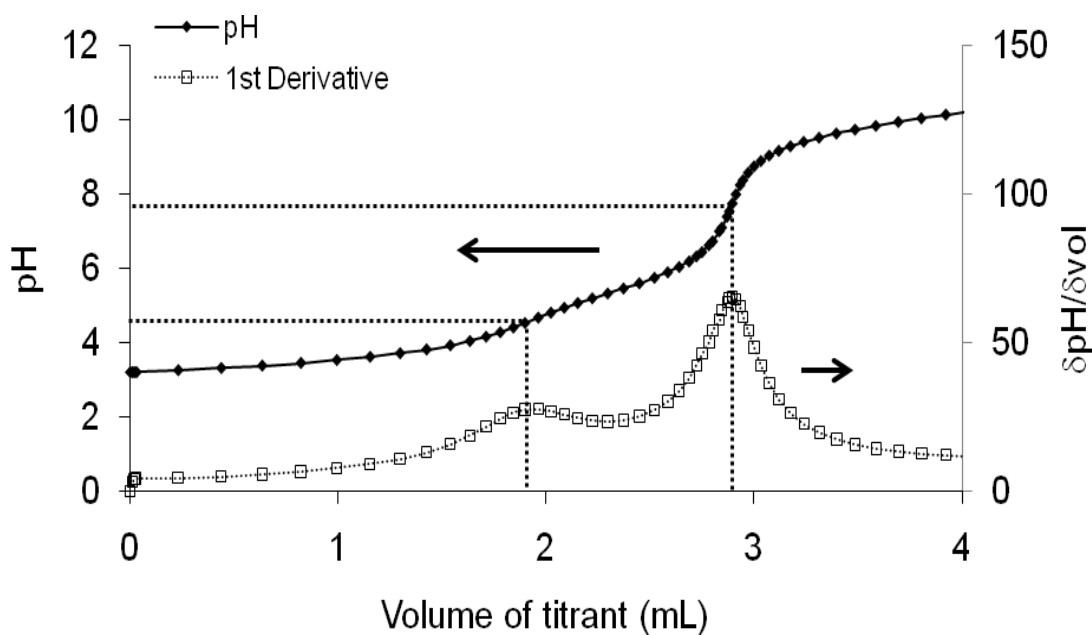
Figure 3.4- Titration of [HQ] = $3x10^{-4}$ M, [NaCl] = 0.1 M, [HCl] = 0.001 M by [NaOH] 0.01024±0.00002 M and [NaCl] = 0.09 M . T = 1.5±0.2 °C.

Table 3.4- Hyperquad fit parameters for 8-hydroxyquinoline deprotonation constants.

Equation	Formed Species	Parameter	Parameter Refined?	pβ	pK
(3.15)	OH^-	K_w	No	14.7	14.7
(3.13)	H(Q)	K_{a1}	Yes	5.6±0.1	5.6±0.1
(3.14)	Q^-	K_{a2}	Yes	15.2±0.1	9.5±0.1

101
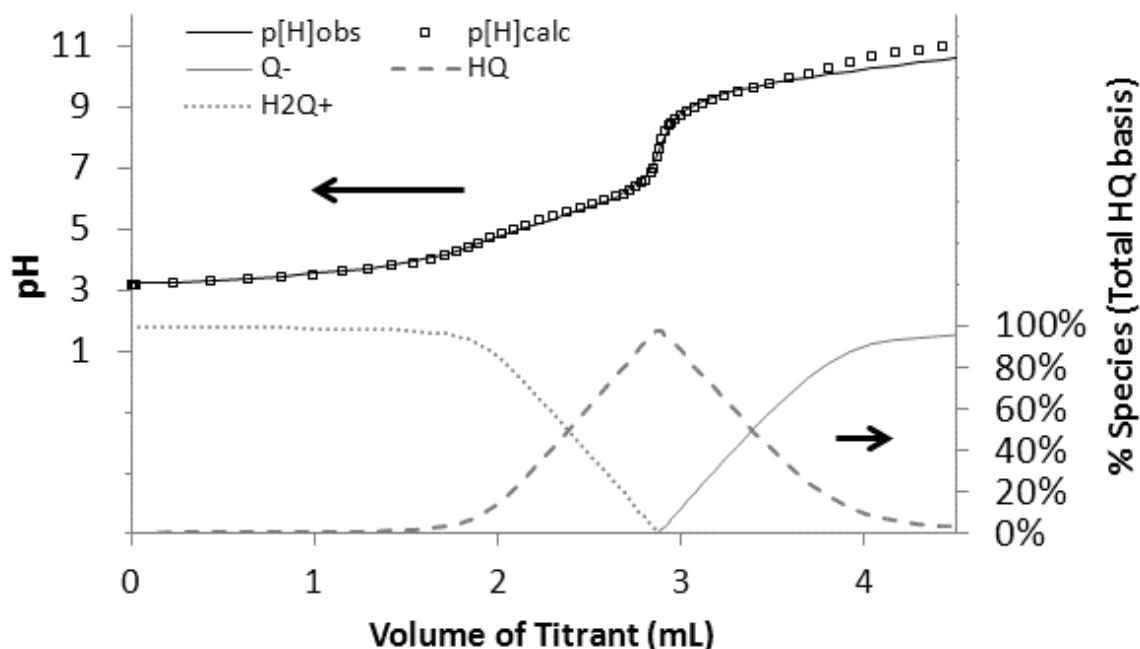
Figure 3.5-Hyperquad modeling results for the potentiometric titration of 8-hydroxyquinoline at T = 1.5±0.2 °C.

3.3.2   Determination of the pKₐ's of 8-Hydroxyquinoline by Spectrophotometric Titration

The absorbance spectrum of 8-hydroxyquinoline shows bands in the visible and UV regions.

This was immediately evident by the yellow color of the aqueous solution of 8-hydroxyquinoline.

The absorbance changes during a pH titration are shown in Figure 3.6 and Figure 3.7. The pH for

each spectrum is used as the label for each trace. The spectra in Figure 3.6 and Figure 3.7 show

an initial absorbance bands for the pH = 3.18 solution at 250.9, 306.9, 315.5, and 358.5 nm (see

Table 3.5). This is the absorbance spectrum attributed to H_2Q^+, the chemical structure of which

is shown in Figure 3.2-structure 'A'. As the pH increases the absorbance spectrum shifts to show

bands at 241.1, 270, and 306.5 nm (see Table 3.5). This absorbance spectrum shown in both

Figure 3.6 and Figure 3.7 at pH = 6.87 and is attributed to HQ, (Figure 3.2-structure 'B'). At the

highest pH shown in Figure 3.6 and Figure 3.7 there is a third spectrum shown for pH = 10.23

that is attributed to Q^- (Figure 3.2-structure 'C') and shows absorbance bands at 249.3, 331, and

352 nm (see Table 3.5). Isosbestic points for the transition between H_2Q^+ and HQ were observed

at 262 and 335 nm. Likewise, Isosbestic points for the transition between HQ and Q^- were

observed at 270 and 324 nm. It is notable that the spectrum associated with the species 'A' and

'C' show very similar absorbance bands whereas the spectrum of the species 'B' is much

different. This is due to the influence that the proton complexation has on the conjugated

aromatic bonds in the double ring structure. For instance, species 'A' and 'C' both share the 250

and 360 nm band and with similar bands at 319 in 'A' and 330 in 'C'. The 'B' species shows the

250 band shifted to 243, and the 360 band shifted to 307 nm.
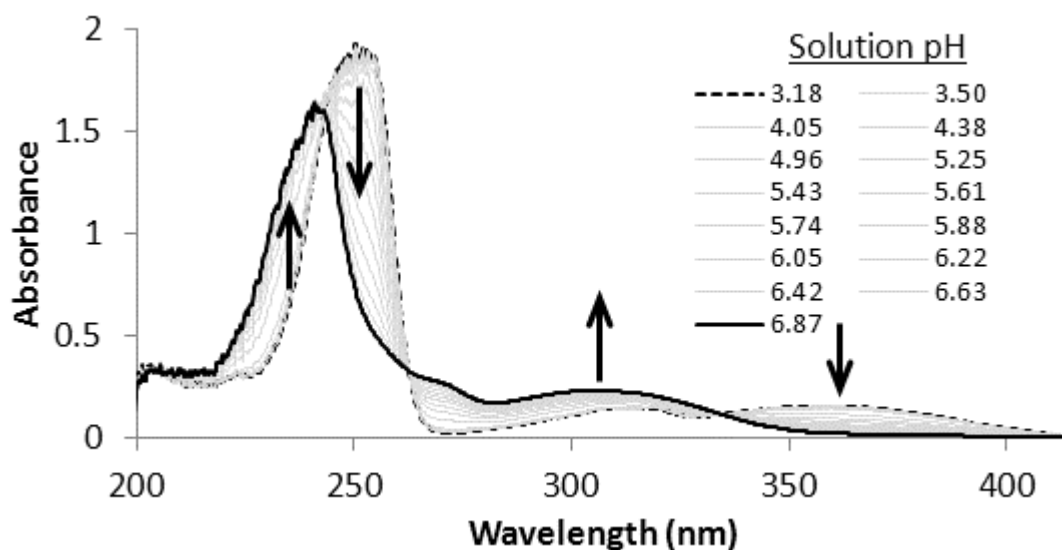
Figure 3.6-Spectral changes for [HQ] = 10^{-5} M, [NaCl] = 0.1 M, [HCl] = 0.001 M titrated by NaOH of varying concentration and volume at 1.8±0.2 °C. The solution pH for each spectrum is listed in the figure legend. Arrows indicate the direction of the spectral change as pH increases. These spectral changes represent the transition from 8-hydroxyquinoline protonation state A to B in Figure 3.2.
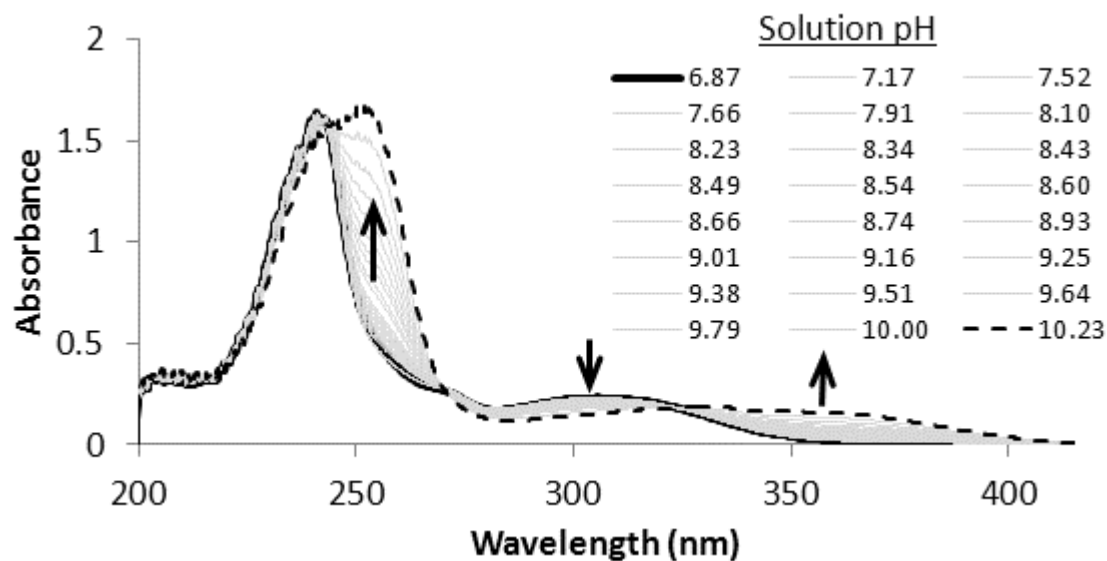
Figure 3.7- Spectral changes for [HQ] = 10^{-5} M, [NaCl] = 0.1 M, [HCl] = 0.001 M titrated by NaOH of varying concentration and volume at 1.8±0.2 °C. The solution pH for each spectrum is listed in the figure legend. Arrows indicate the direction of the spectral change as pH increases. These spectral changes represent the transition from 8-hydroxyquinoline protonation state B to C in Figure 3.2.

Table 3.5- The observed spectral maxima in the titration spectrum of 8-hydroxyquinoline. The wavelength of the peak in parenthesis is estimated, but does not have a clearly quantifiable maximum.

H_2Q^+	HQ	Q^-
Spectrum Maxima (nm)	Spectrum Maxima (nm)	Spectrum Maxima (nm)
	241.1	
250.9		249.3
	(270)	
306.9	306.5	
315.5		
		331
358.5		352
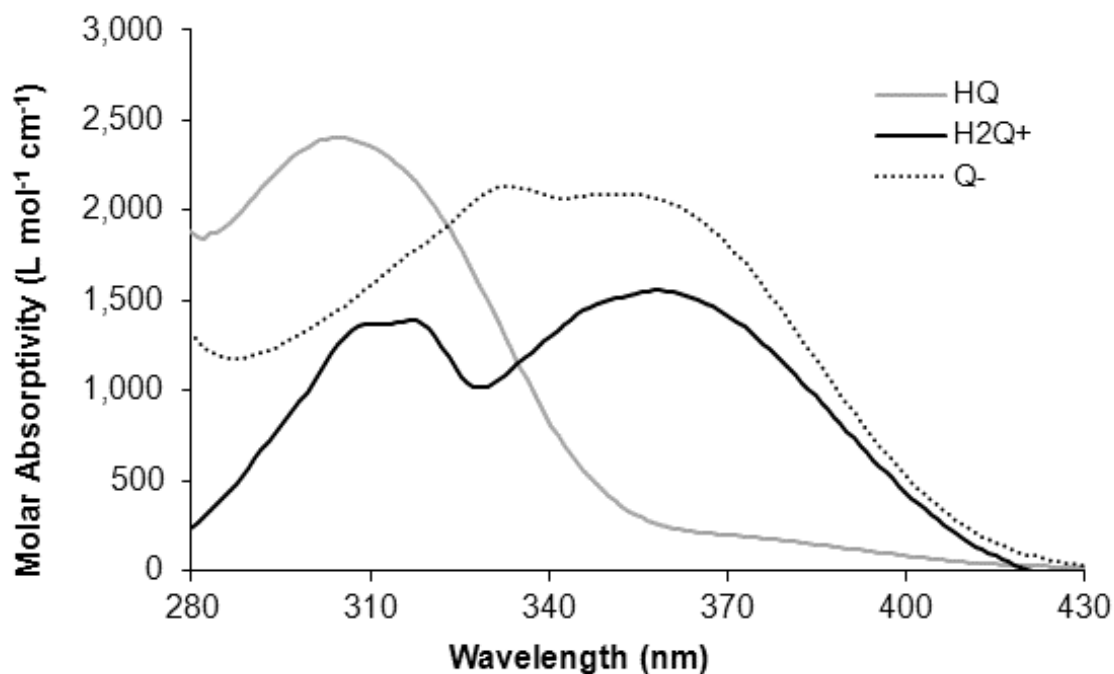
Figure 3.8-Molar absorptivity Spectra obtained from SQUAD modeling using the 280–430 nm spectral window called window B.
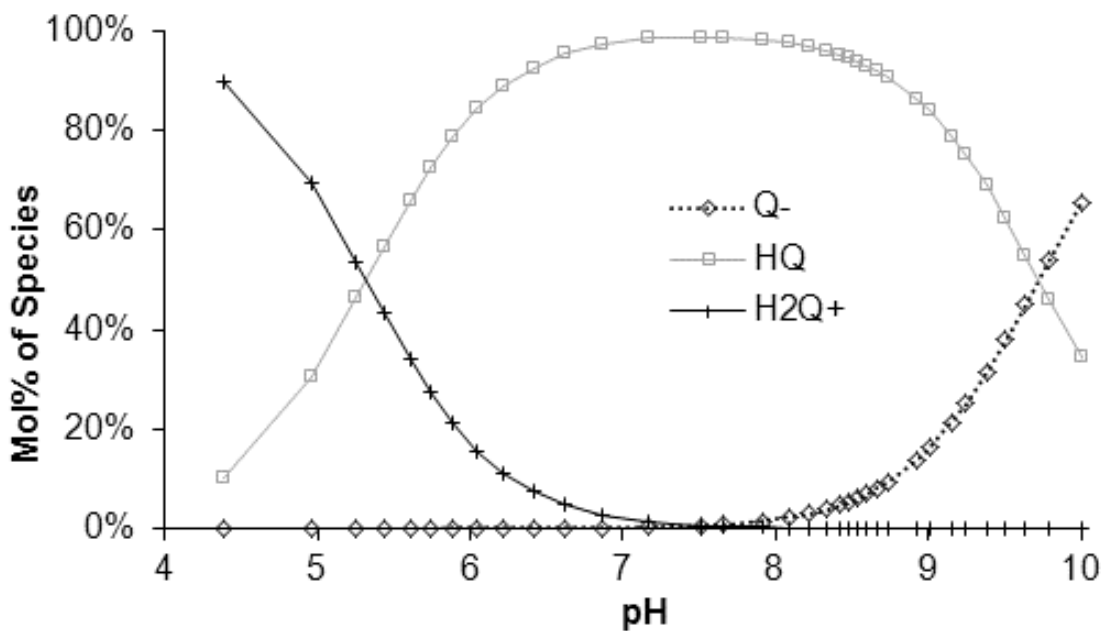
Figure 3.9- Calculated speciation curve obtained from SQUAD modeling using the 280–430 nm spectral window also called window B.

Equilibrium constants were calculated by SQUAD using different windows of the spectrophotometric data. The modeled windows are designated 'A' for the entire spectrum (220–445 nm), and two subsets: 'B' for the one that contained only the strongest absorbance bands in the UV (220–295 nm), and 'C' for the other that contained the weaker absorbance bands in the UV + Visible spectrum (280–430 nm) (see Table 3.6). Spectrophotometric data must be interpreted with caution when the absorbance is greater than ~1 because spectrophotometers can incorrectly record the absorbance of such samples.[54] It appears that this has happened with the spectra observed in window 'C' in Figure 3.6 and Figure 3.7 that shows absorbances in the range of 1.5–2.0. The only result that is unaffected by the extreme absorbance in the 220–270 nm region is window 'B' that excludes the high absorbing bands in the spectrum (i.e. 280–439 nm) (see Table 3.6). The values of pK_{a1} = 5.32 and pK_{a2} = 9.72 are those accepted in this work as most accurate from this technique and the others will be ignored in the future discussion. The molar absorbance spectra obtained for the H_2Q^+, HQ and Q^- species using window 'B' is shown in Figure 3.8. The speciation calculated using window 'B' obtained by SQUAD modeling is shown in Figure 3.9.

Table 3.6- SQUAD modeled parameters using varied spectral windows.

Modeling Window Designation	Window Limits		SQUAD Result	SQUAD Result
	Lower (nm)	Upper (nm)	pK_{a1}	pK_{a2}
A	220	446	5.71±0.01	9.58±0.01
B	280	430	5.32±0.01	9.72±0.01
C	220	296	5.72±0.01	9.58±0.01

3.3.3 Determination of the Europium Hydrolysis Constants by Potentiometric Titration

Lanthanides are known to hydrolyze,[147] just as other cations in solution,[148] under conditions of increasing pH. In the systems studied in this work europium hydrolysis is potentially a competitive process with the 8-hydroxyquinoline complexation reaction. Therefore, both processes must be quantitatively characterized so that the optimum separation can be designed for these systems.

A solution of $[Eu^{3+}]$ = 3×10^{-4} M, $[NaCl]$ = 0.1 M, and $[HCl]$ = 0.001 M was titrated with standardized 0.01 M NaOH (I = 0.1 M). The temperature for this titration was 1.7±0.2 °C. The titration curve is shown in Figure 3.10. Only two inflection points are indicated by the two maxima of the 1st derivative in Figure 3.10. The first endpoint is attributed to the neutralization of HCl in solution. The volume of added titrant between the first and second endpoints accounts for 3 equivalents of NaOH compared to 1 equivalent of europium. Literature data for the lanthanides[147] indicate that the first, second, and third stepwise hydrolysis formation constants are very similar in magnitude, within 0.04–0.66 logK units of each other. Because the second and third hydrolysis species form in such close succession to the first, it appears that the individual inflection points of the three hydrolysis species are impossible to observe in the titration curve and thus, the second endpoint is attributed to the complete hydrolysis of all Eu^{3+} in solution.
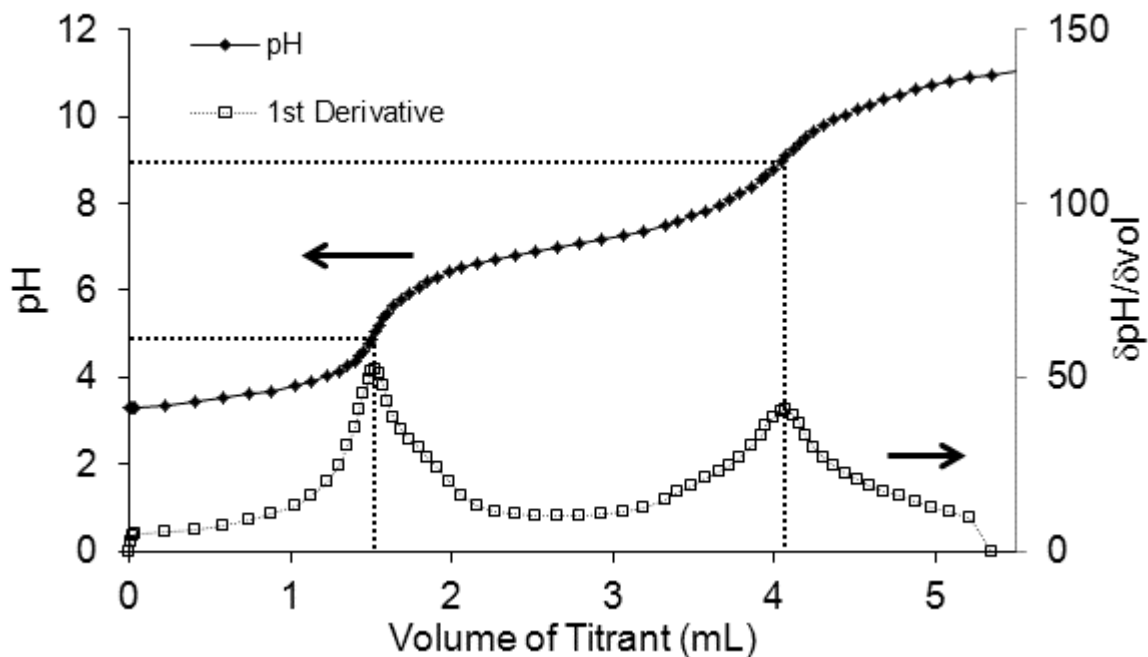
Figure 3.10- Titration of [Eu^{3+}] = 3x10^{-4} M, [NaCl] = 0.1 M, [HCl] = 0.001 M by [NaOH] 0.01024±0.00002 M and [NaCl] = 0.09 M. T = 1.7±0.2 °C.

Figure 3.11- Hyperquad modeling results for the titration of [Eu^{3+}] = 3x10^{-4} M, [NaCl] = 0.1 M, [HCl] = 0.001 M by [NaOH] 0.01024±0.00002 M and [NaCl] = 0.09 M. T = 1.7±0.2 °C.

The titration data was modeled in Hyperquad using 14.7 as the pK_w for the titration

conditions. The three hydrolysis reactions used in the model are shown in equations (3.16) –

(3.18).

$$Eu^{3+} + H_2O \xleftrightarrow{\quad \beta_{1-10} \quad} [Eu(OH)]^{2+} + H^+ \tag{3.16}$$

$$Eu^{3+} + 2\,H_2O \xleftrightarrow{\quad \beta_{1-20} \quad} [Eu(OH)_2]^+ + 2\,H^+ \tag{3.17}$$

$$Eu^{3+} + 3\,H_2O \xleftrightarrow{\quad \beta_{1-30} \quad} [Eu(OH)_3] + 3\,H^+ \tag{3.18}$$
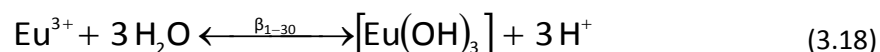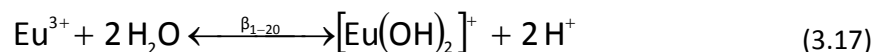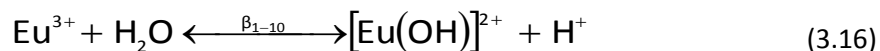
The fit parameters obtained from this model are shown in Table 3.7. These data are as expected

with the three hydrolysis constants in very close proximity on the pH scale. The data fitting

results are shown in Figure 3.11.

Table 3.7- Hyperquad fit parameters for the europium hydrolysis constants.

Equation	Formed Species	Parameter	Parameter Refined?	pβ	pK
(3.15)	OH^-	K_w	No	14.7	
(3.16)	$[Eu(OH)]^{2+}$	β_{1-10}	Yes	-8.0±0.2	-8.0±0.2
(3.17)	$[Eu(OH)_2]^+$	β_{1-20}	Yes	-15.8±0.1	-7.7±0.1
(3.18)	$[Eu(OH)_3]$	β_{1-30}	Yes	-22.5±0.2	-6.8±0.2

3.3.4 Determination of Europium 8-Hydroxyquinoline Stability Constants by Potentiometric Titration

The complexation constants from the modeling of Eu^{3+} hydrolysis reactions presented in

Section 3.3.3 were used in the fitting of the stability constants for complexes between europium

and 8-hydroxyquinoline. As described earlier, each of the subsequent titrations in the H_2O

system were designed to allow only the formation of certain species and preventing the

formation of others. In the first titration of a mixed Eu^{3+}/HQ solution, an equal concentration of

Eu^{3+} and HQ were used so that only the 1:1 complex $[Eu(Q)]^{2+}$ would be present. At higher pH

values it was anticipated that the mixed ligand/hydrolysis species will form, requiring the fit of 2

new species for this titration: $[Eu(OH)(Q)]^+$, and $[Eu(OH)_2(Q)]$. The titration curve obtained for

the 1:1 ligand to metal ratio is shown in Figure 3.12. The titration curve showed some very

minor maxima in the 1st derivative function shown in Figure 3.12. These results were fit using

previously obtained pK_a's of 8-hydroxyquinoline for the reactions in equations (3.13), and (3.14).

Stability constants for the Eu^{3+}-OH-HQ system were fit for the model according to equations

(3.19) – (3.21). The Hyperquad fit results show a gradual transition from one species to the next

as the pH increases with $[Eu(Q)]^{2+}$ forming first, $[Eu(OH)(Q)]^+$ forming next and $[Eu(OH)_2(Q)]$

forming last. The parameters that resulted from the Hyperquad modeling Fit are shown in Table

3.8.

$$Eu^{3+} + Q^- \xleftrightarrow{\beta_{101}} [Eu(Q)]^{2+} \qquad (3.19)$$

$$Eu^{3+} + H_2O + Q^- \xleftrightarrow{\beta_{1-11}} [Eu(OH)(Q)]^+ + H^+ \qquad (3.20)$$

$$Eu^{3+} + 2 H_2O + Q^- \xleftrightarrow{\beta_{1-21}} [Eu(OH)_2(Q)] + 2 H^+ \qquad (3.21)$$
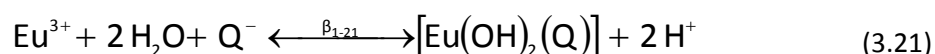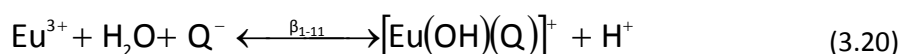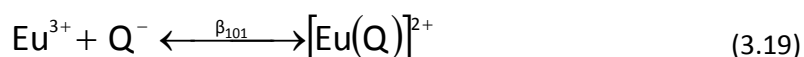
Table 3.8- Hyperquad fit parameters for the 1:1 ligand to metal ratio solutions.

Equation	Formed Species	Parameter	Parameter Refined?	pβ	pK
(3.15)	OH^-	K_w	No	14.7	
(3.13)	HQ	K_{a1}	No	5.6	5.6
(3.14)	Q^-	K_{a2}	No	15.2	9.5
(3.19)	$[Eu(Q)]^{2+}$	β_{101}	Yes	-6.9±0.1	-6.9±0.1
(3.20)	$[Eu(OH)(Q)]^+$	β_{1-11}	Yes	-13.3±0.1	-6.4±0.1
(3.21)	$[Eu(OH)(Q)_2]$	β_{1-21}	Yes	-18.8±0.1	-5.6±0.1
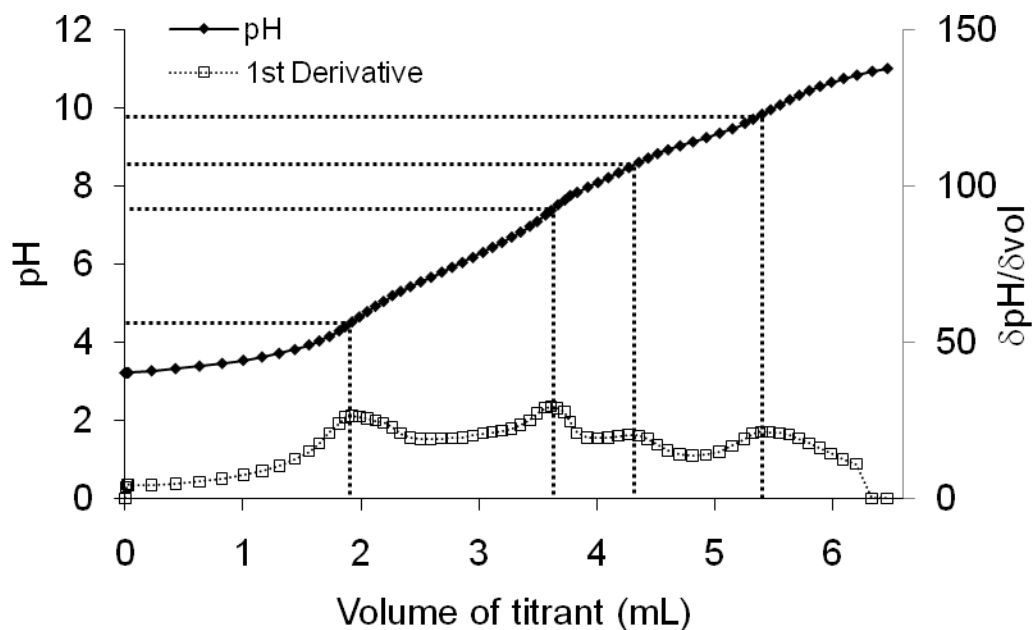
Figure 3.12- Titration of [HQ] = 3×10^{-4} M, [Eu^{3+}] = 3×10^{-4} M, [NaCl] = 0.1 M, [HCl] = 0.001 M by [NaOH] = 0.01024 ± 0.00002 M and [NaCl] = 0.09 M. T = 1.7±0.2 °C.
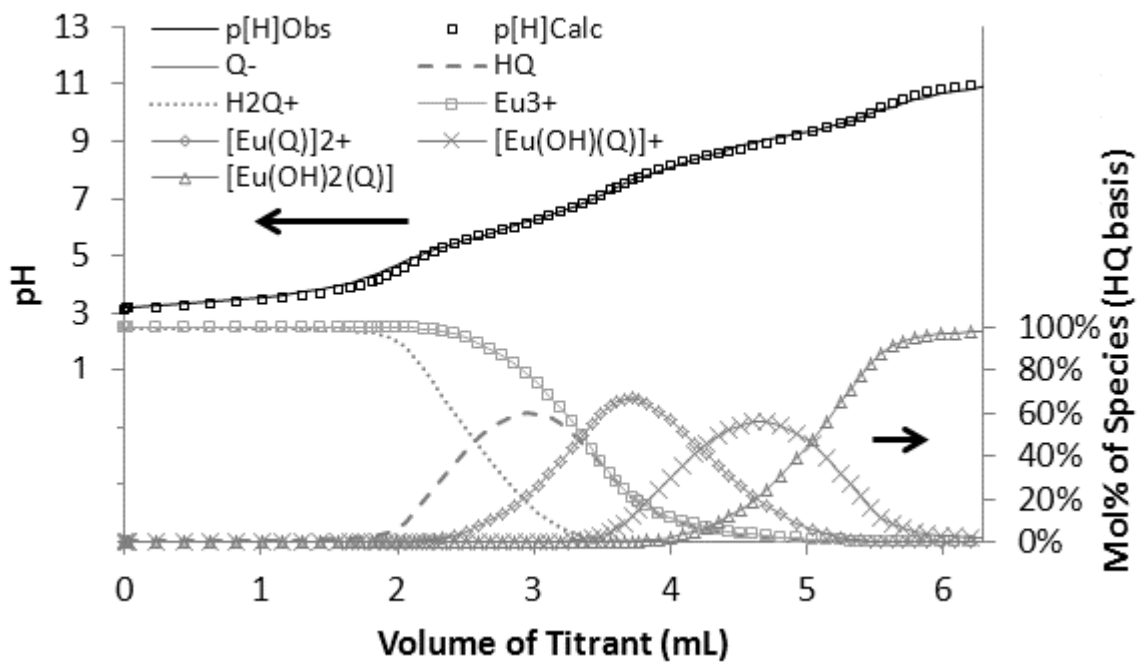
Figure 3.13- Hyperquad fit results for titration of [HQ] = 3×10^{-4} M, [Eu^{3+}] = 3×10^{-4} M, [NaCl] = 0.1 M, [HCl] = 0.001 M by [NaOH] = 0.01024 ± 0.00002 M and [NaCl] = 0.09 M. T = 1.7±0.2 °C.

The next titration was specifically designed to follow the formation of both $[Eu(Q)]^{2+}$ and $[Eu(Q)_2]^+$ but preventing the formation of $[Eu(Q)_3]$. The solution designed to achieve this was one with a 2:1 ligand to metal ratio. The titration curve obtained using this solution is shown in Figure 3.14. This titration curve appears very similar to that obtained for the 1:1 ligand to metal ratio solution. It was anticipated that this curve when fit would also yield a formation of 3 species just as in the 1:1 curve, but two previously unobserved species would be formed: $[Eu(Q)_2]^+$, and the mixed ligand/hydrolysis species $[Eu(OH)(Q)_2]$. This curve was fit using the previously obtained 8-hydroxyquinoline pK_a values [equations (3.13), (3.14)], the formation constant for $[Eu(Q)]^{2+}$ from the 1:1 ligand to metal solution modeling [equation (3.19)], and two new reactions that are shown in equations (3.22) – (3.23).

$$Eu^{3+} + 2\,Q^- \xleftrightarrow{\quad \beta_{102} \quad} \left[Eu(Q)_2\right]^+ \tag{3.22}$$

$$Eu^{3+} + H_2O + 2\,Q^- \xleftrightarrow{\quad \beta_{1-12} \quad} \left[Eu(OH)(Q)_2\right] + H^+ \tag{3.23}$$
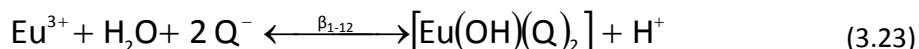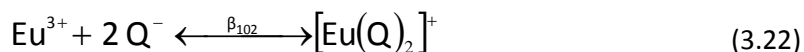
The Hyperquad fit results using the above described model are shown in Figure 3.15. The Hyperquad results show a smooth transition between three species as the pH increases. The order of the species formation is $Eu^{3+} \rightarrow [Eu(Q)]^{2+} \rightarrow [Eu(Q)_2]^+ \rightarrow [Eu(OH)(Q)_2]$. The parameters that define this system according to the model are shown in Table 3.9.

Table 3.9- Hyperquad fit Parameters for the 2:1 ligand to metal solution.

Equations	Formed Species	Parameter	Parameter Refined?	pβ	pK
(3.15)	OH^-	K_w	No	14.7	
(3.13)	HQ	K_{a1}	No	5.6	5.6
(3.14)	Q^-	K_{a2}	No	15.2	9.5
(3.19)	$[Eu(Q)]^{2+}$	β_{101}	No	-6.9	-6.9
(3.22)	$[Eu(Q)_2]^+$	β_{102}	Yes	-12.5±0.7	-5.6±0.7
(3.23)	$[Eu(OH)(Q)_2]$	β_{1-12}	Yes	-19.3±0.3	-6.7±0.3
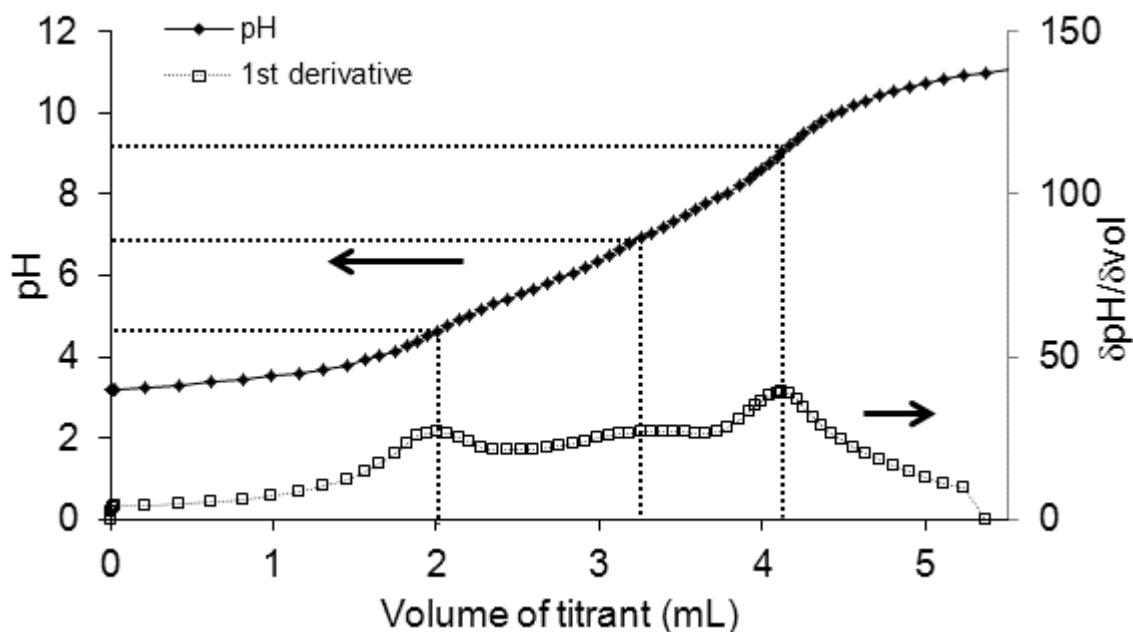
Figure 3.14- Titration of [HQ] = 3×10^{-4} M, [Eu^{3+}] = 1.5×10^{-4} M, [NaCl] = 0.1 M, [HCl] = 0.001 M by [NaOH] = 0.01024 ± 0.00002 M and [NaCl] = 0.09 M. T = 1.9±0.2 °C.
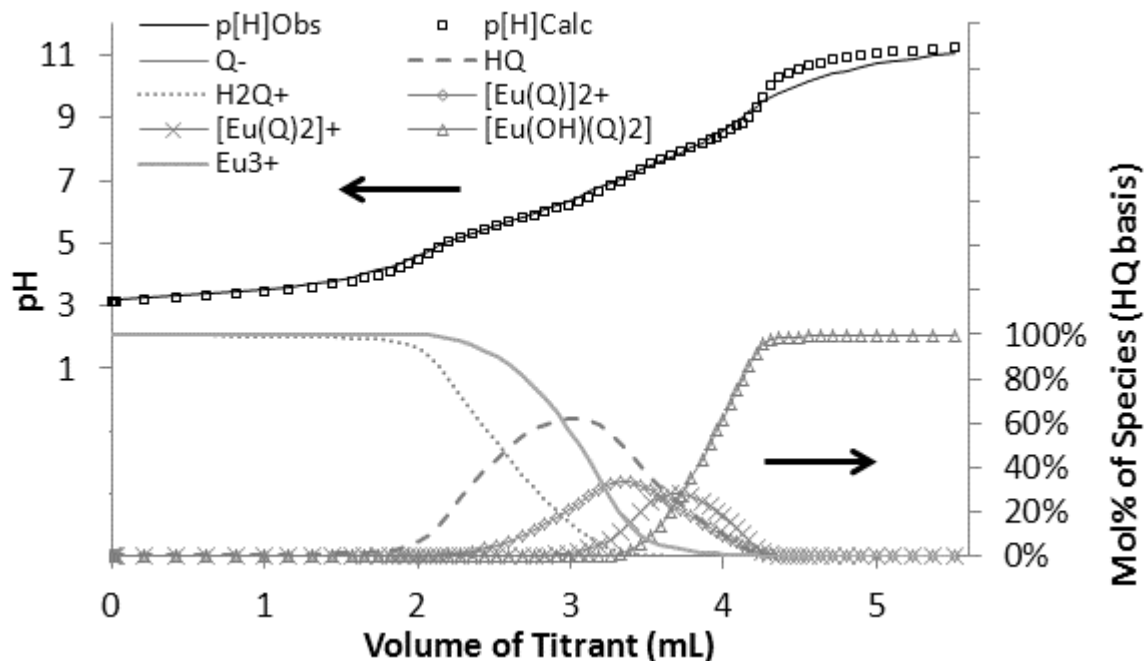
Figure 3.15- Hyperquad fit results for titration of [HQ] = 3×10^{-4} M, [Eu^{3+}] = 1.5×10^{-4} M, [NaCl] = 0.1 M, [HCl] = 0.001 M by [NaOH] = 0.01024 ± 0.00002 M and [NaCl] = 0.09 M. T = 1.7±0.2 °C.

The last titration was designed so that all three europium 8-hydroxyquinoline species could form: $[Eu(Q)]^{2+}$, $[Eu(Q)_2]^+$, $[Eu(Q)_3]$. This titration contained a 3:1 ligand to metal ratio, however a higher ratio would have also worked. The titration curve is shown in Figure 3.16. Using the previously obtained 8-hydroxyquinoline pK_a values [equations (3.13), and (3.14)], the complexation constants for the formation of $[Eu(Q)]^{2+}$, and $[Eu(Q)_2]^+$ [equation (3.19),], (3.22), the parameter for the formation of $[Eu(Q)_3]$ shown in reaction (3.24) was fit using Hyperquad.

$$Eu^{3+} + 3\,Q^- \xleftarrow{\quad \beta_{103} \quad} \left[Eu(Q)_3\right] \qquad\qquad (3.24)$$
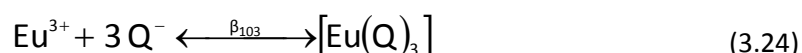
The only parameter that was allowed to vary in this fit was the $[Eu(Q)_3]$ formation parameter. Attempts to fit more parameters simultaneously led to larger standard deviations in the parameter error, which was interpreted as a poorer result and was thus rejected. The modeling speciation results are shown in Figure 3.17 with the stability constant results shown in Table 3.10.

Table 3.10- Parameters obtained from the Hyperquad fit of the 3:1 Ligand to metal solution titration.

Equation	Formed Species	Parameter	Parameter Refined?	pβ	pK
(3.15)	OH^-	K_w	No	14.7	
(3.13)	HQ	K_{a1}	No	5.6	5.6
(3.14)	Q^-	K_{a2}	No	15.2	9.5
(3.19)	$[Eu(Q)]^{2+}$	β_{101}	No	-6.9	-6.9
(3.22)	$[Eu(Q)_2]^+$	β_{102}	No	-12.5	-5.5
(3.24)	$[Eu(Q)_3]$	β_{103}	Yes	-18.7±0.5	-6.2±0.9

Figure 3.16- Titration of [HQ] = $3x10^{-4}$ M, [Eu^{3+}] = $1x10^{-4}$ M, [NaCl] = 0.1 M, [HCl] = 0.001 M by [NaOH] = 0.01024 ± 0.00002 M and [NaCl] = 0.09 M. T = 2.0±0.2 °C.
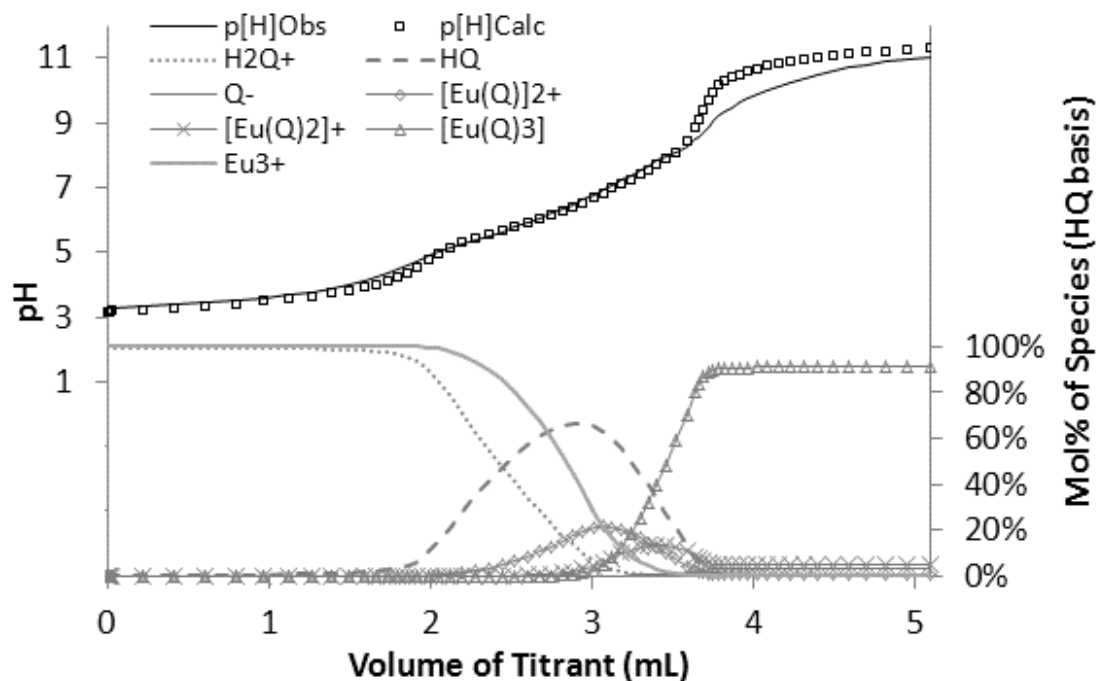
Figure 3.17- Hyperquad fit results for titration of [HQ] = $3x10^{-4}$ M, [Eu^{3+}] = $1x10^{-4}$ M, [NaCl] = 0.1 M, [HCl] = 0.001 M by [NaOH] = 0.01024 ± 0.00002 M and [NaCl] = 0.09 M. T = 2.0±0.2 °C.

115

3.3.5   Determination of Europium 8-Hydroxyquinoline Stability Constants by

Spectrophotometric Titration

The use of spectrophotometric titration to obtain the stability constants for europium 8-hydroxyquinoline complexation was tested. At the outset this technique poses some challenges due to the difference in molar absorptivity of the constituents involved. Europium absorbs very weakly, with multiple spectral bands in the range of 272 – 401 nm.[149] The largest absorbing band in this range is 394 nm with a molar absorptivity of 3.06 L mol^{-1} cm^{-1}.[149] By comparison, 8-hydroxyquinoline shows a molar absorptivity at 394 nm of 615, 105, and 738 L mol^{-1} cm^{-1} for H$_2$Q$^+$, HQ and Q$^-$, respectively (see section 3.3.2). The large absorbance of 8-hydroxyquinoline relative to europium makes it impossible to observe the spectral changes of europium directly.

A spectrophotometric titration of a solution containing both europium and 8-hydroxyquinoline was performed in an effort to obtain the stability constants for the europium 8-hydroxyquinoline complexes. The obtained spectra are shown below in Figure 3.18 – Figure 3.20. Attempts at modeling this spectral data using SQUAD were not successful. The spectral changes in the ligand absorbance upon complexation of europium were not sufficient for SQUAD to identify the separate metal:ligand species spectrum. Using a different metal ion with an absorbance band that is not obscured by the absorbance of 8-hydroxyquinoline would increase the likelihood of SQUAD being able to fit stability constant from spectrum. The absorbance of 8-hydroxyquinoline is zero above 430 nm, therefore, other lanthanides that are possible candidates are praseodymium (440 nm), neodymium (521, 720, or 794 nm), dysprosium (908 nm), holmium (537 nm), erbium (523 nm), thulim (683), or ytterbium (974 nm).[149]
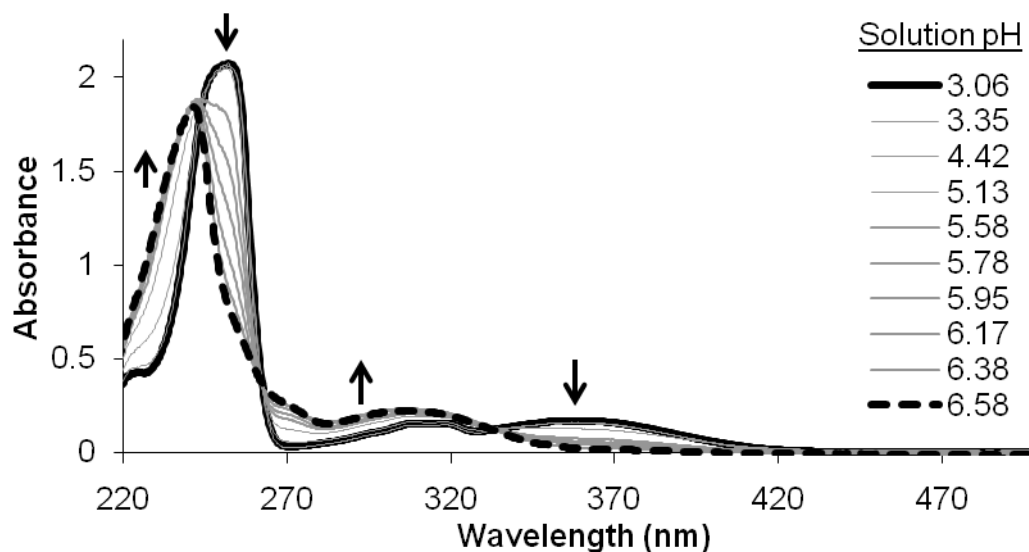
Figure 3.18- Spectral changes for [HQ] = 10^{-5} M, [Eu^{+3}] = 2x10^{-6} M, [NaCl] = 0.1 M, [HCl] = 0.001 M titrated by NaOH of varying concentration and volume at T = 1.8±0.2 °C. The solution pH for each spectrum is listed in the figure legend. Arrows indicate the direction of the spectral change as pH increases.

Figure 3.19- Spectral changes for [HQ] = 10^{-5} M, [Eu^{+3}] = 2x10^{-6} M, [NaCl] = 0.1 M, [HCl] = 0.001 M titrated by NaOH of varying concentration and volume at T = 1.8±0.2 °C. The solution pH for each spectrum is listed in the figure legend. Arrows indicate the direction of the spectral change as pH increases.

117

Figure 3.20- Spectral changes for $[HQ] = 10^{-5}$ M, $[Eu^{+3}] = 2 \times 10^{-6}$ M, $[NaCl] = 0.1$ M, $[HCl] = 0.001$ M titrated by NaOH of varying concentration and volume at T = 1.8±0.2 °C. The solution pH for each spectrum is listed in the figure legend. Arrows indicate the direction of the spectral change as pH increases.

3.4   Results: The Triton X-114/H$_2$O System

A similar approach was used in the Triton X-114/H$_2$O mixed solvent system as in the H$_2$O system for finding the complex stability constants for the europium 8-hydroxyquinoline complexes. No previous literature has reported the water dissociation constant (K_w) in the presence of Triton X-114. One paper measured the change in pK_w as a function of various organic/water mixed solvents with the change in wt% of the non-water constituent. The mixed solvent solutions included propane and butane diols, methyl/ethyl ethers, butanone, sulfolane, and triethylene glycol.[150] The data showed that the pK_w of water changed as the co-solvent concentration increased up to 65wt%, but changed very little at 1 wt% of any of the tested co-solvents. The co-solvent triethylene glycol, which is similar to Triton X-114, showed a change of 0.02 in the pK_w at a concentration of 3 wt%.[150] Because Triton X-114 is present at such a low concentration in this study (i.e. 1 wt%), it is assumed that Triton's effect on the pK_w is negligible.

Therefore, the pK_w of 14.7 that was used in the water system can also be used in the water/Trion X-114 system.

3.4.1 Characterization of Protolytic Behavior of Triton X-114 by Potentiometric Titration

Due to difficulties in modeling data in the Triton/water system and anomalies in the potentiometric titration data, a study of the protonation behavior of Triton X-114 was performed. The difficulties encountered while fitting the 8-hydroxyquinoline pK_a data are discussed in section 3.4.2. The anomaly noted in the potentiometric titration data is observed in the shape of the first inflection point of all titration data. In the water system data, the first derivative plots of the titrations curves for solutions containing 8-hydroxyquinoline have a peak (see Figure 3.4, Figure 3.12, Figure 3.14, and Figure 3.16), whereas in the Triton/water system data there is a rise to a plateau, but no peak (see Figure 3.23, Figure 3.34, Figure 3.36, and Figure 3.38). The combination of the modeling difficulties and the titration curve shape anomalies shared by the Triton/water data but not the water data led to the decision to explore potential protolytic impurities in the Triton X-114 stock. A titration of Triton X-114 that had been acidified by HCl is shown in Figure 3.21. There are two inflection points observed for this titration. The distance between the two inflection points is small and correlates to 0.24 mL of titrant or 2.4×10^{-6} moles of NaOH. With only HCl, NaCl and Triton X-114 present, it seemed obvious that this small species was some protolytic impurity in the system. The data was modeled by Hyperquad fitting the deprotonation of an unknown mono-protic acid H(XX) shown in equation (3.25).

$$H(XX) + OH^- \xleftarrow{\quad K_{XX} \quad} XX^- + H_2O \qquad (3.25)$$
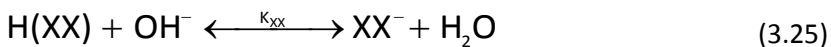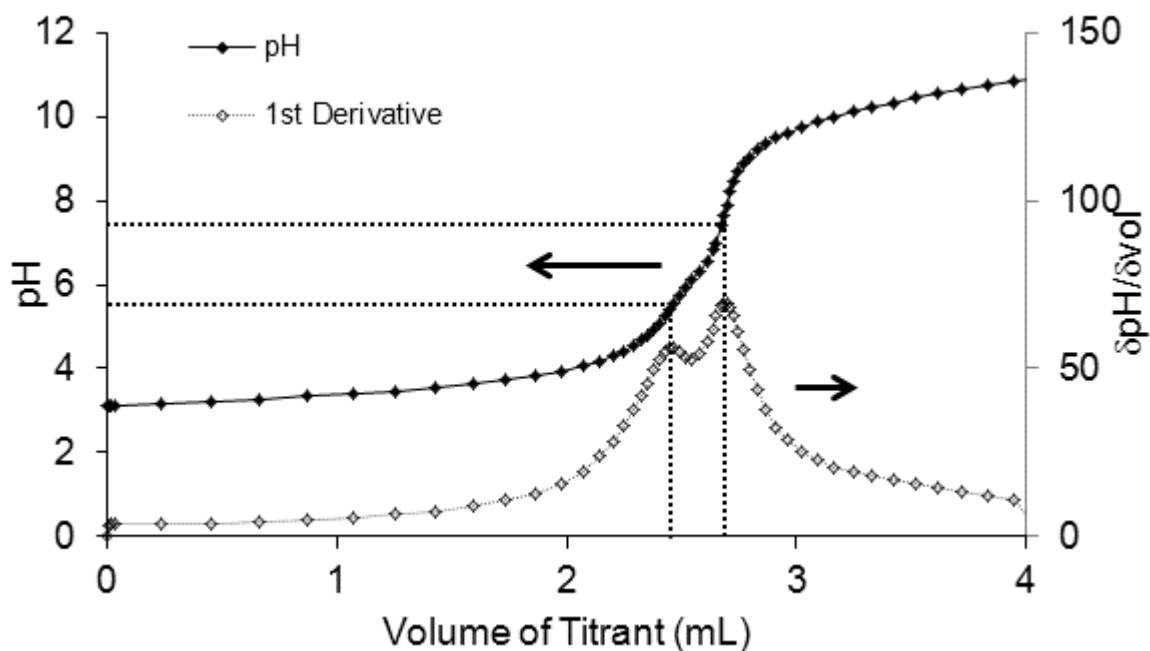
Figure 3.21-Titration of [HCl] = 0.001 M, [Triton X-114] = 1 wt% (~0.02 mol/L) by
[NaOH] = 0.01024 ± 0.00002 M and [NaCl] = 0.09 M. T = 1.9±0.2 °C.
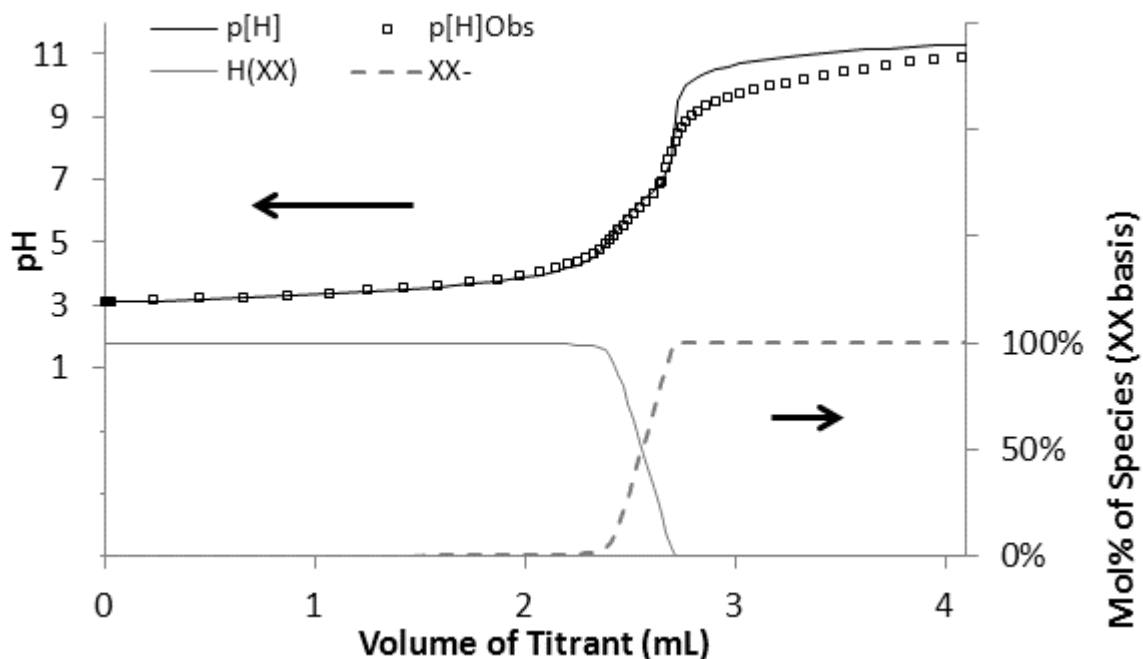
Figure 3.22- Hyperquad fit for the titration of [HCl] = 0.001 M, [Triton X-114] = 1 wt% (~0.02
mol/L) by [NaOH] = 0.01024 ± 0.00002 M and [NaCl] = 0.09 M. T = 1.9±0.2 °C.

Because the quantity of the impurity present is unknown, the concentration was fit together with the protonation constant and the pK_w. The Hyperquad modeling results are shown in Figure 3.22. The estimated concentration of XX is 0.0001 ± 0.0015, indicating that the concentration of impurity is statistically insignificant (see Table 3.12). The percent impurity on a total Triton X-114 basis is $0.5 \pm 8.1\%$. Although statistically insignificant, the inclusion of this impurity in the Hyperquad models of the Triton/water system leads to more reliable data when compared to literature sources (see section 3.4.2). The source of this impurity is assumed for now to be the Triton X-114, but more experiments are needed to identify the source and eliminate its presence from these solutions.

Table 3.11- Fit parameters for the deprotonation of the protolytic impurity.

Equation	Formed Species	Parameter	Parameter Refined?	pβ, pK
(3.15)	OH^-	K_w	No	14.7
(3.25)	XX^-	K_{XX}	Yes	6.3 ± 0.1

Table 3.12- Concentration of unknown protolytic species obtained from Hyperquad simulation for the 1 wt% Triton solution titration.

	Concentration (mol/L)
[XX]	0.0001 ± 0.0015

3.4.2   Determination of the pK_a's of 8-Hydroxyquinoline by Potentiometric Titration

The pK_a's of 8-hydroxyquinline were obtained for the Triton X-114/water system by titrating a solution that was identical to that used in the H_2O system except there was 1 wt%

(approximately 0.02 mol/L) of Triton X-114 present (see Figure 3.23). Inspection of the 1st

derivative in Figure 3.23 will reveal that there was only one discernible maxima. This result was

completely unexpected and is attributed to the presence of the surfactant, or protolytic

impurity (see section 3.4.1). When the titration curve in Figure 3.23 was fit using the same

reactions (3.13), and (3.14) as were used for the H_2O system the resulting fit was not

satisfactory (see Figure 3.24). The model used to fit this data imposed an inflection point where

there is not one in the observed titration curve leading to a poor fit. The parameters from this

model are shown in Table 3.13.
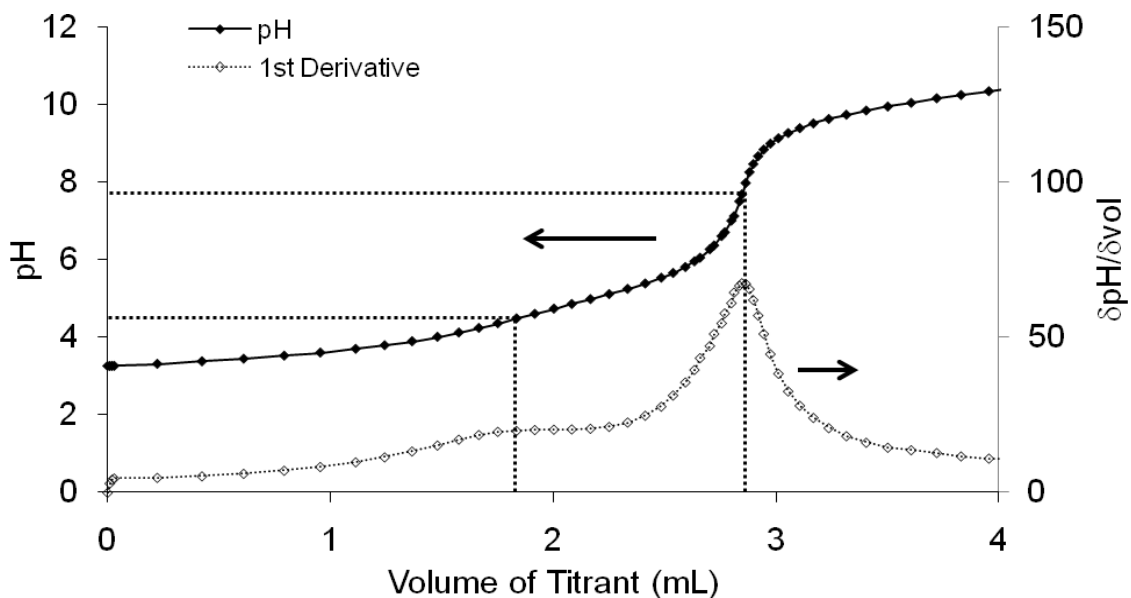
Figure 3.23- Titration of [HQ] = $3x10^{-4}$ M, [NaCl] = 0.1 M, [HCl] = 0.001 M, [Triton X-114] = 1 wt% (~0.02 M) by [NaOH] = 0.01024 ± 0.00002 M and [NaCl] = 0.09 M. T = 1.8±0.2 °C.

Figure 3.24- Hyperquad fit for the titration of [HQ] = 3×10^{-4} M, [NaCl] = 0.1 M, [HCl] = 0.001 M, [Triton X-114] = 1 wt% (~0.02 M) by [NaOH] = 0.01024 ± 0.00002 M and [NaCl] = 0.09 M. T = 1.8±0.2 °C.

Table 3.13- Hyperquad parameters obtained for the protonation of 8-hydroxyquinoline in the H_2O/Triton X-114 system when the pK_{XX} parameter is excluded from the model.

Equation	Formed Species	Parameter	Parameter Refined?	pβ	pK
(3.15)	OH⁻	K_w	No	14.7	
(3.13)	HQ	K_{a1}	Yes	6.0±0.1	6.0±0.1
(3.14)	Q⁻	K_{a2}	Yes	16.0±0.1	10.0±0.1

The results from this model led to speculation that the Triton X-114 was playing a larger role

in the system than merely mix-solvent or solvent modifier. With the protolytic impurity

characterized, this species was included in the fit of all the subsequent titration data, including

the fit of the 8-hydroxyquinoline titration shown in Figure 3.23. Reactions (3.13) and (3.14),

(3.25) were fit simultaneously. Results from this modeling experiment are shown in Figure 3.25.

The modeling program still introduces a slight inflection point where there is none, but it more

closely matches the actual titration data than the model without the inclusion of the protolytic

impurity reaction. Fit parameters for this fit are shown in Figure 3.14.

Table 3.14- Hyperquad parameters obtained for the protonation of 8-hydroxyquinoline in the H_2O/Triton X-114 system when the pK_{XX} parameter is included in the model.

Equation	Formed Species	Parameter	Parameter Refined?	pβ	pK
(3.15)	OH⁻	K_w	No	14.7	
(3.25)	XX⁻	K_{XX}	No	6.3	
(3.13)	HQ	K_{a1}	Yes	5.2±0.2	5.2±0.2
(3.14)	Q⁻	K_{a2}	Yes	15.2±0.1	10.0±0.1
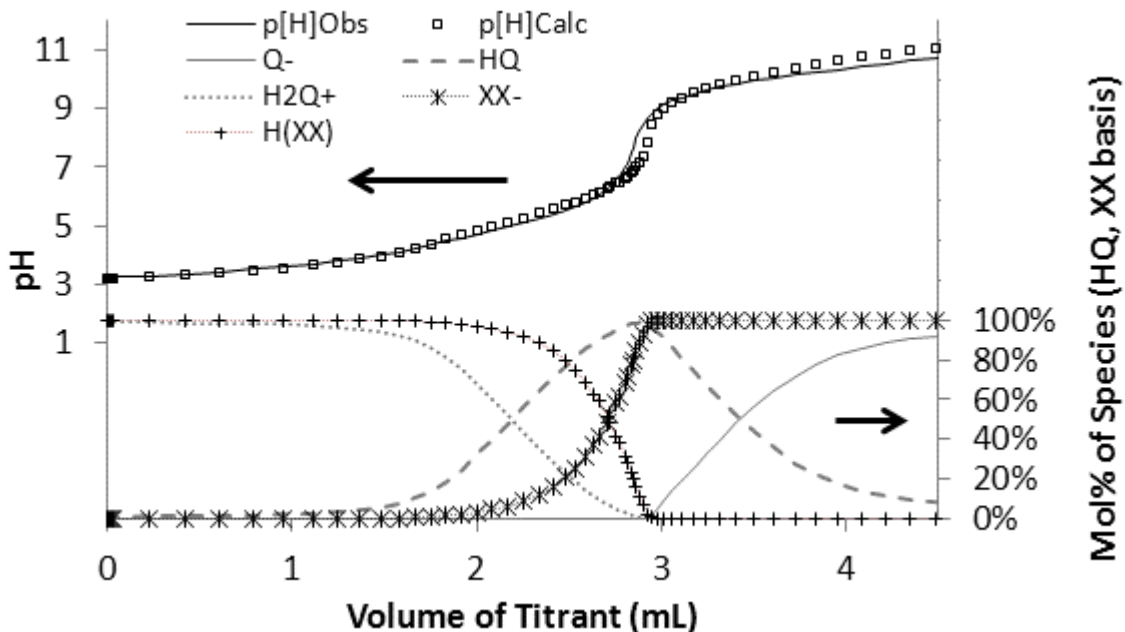
Figure 3.25- Hyperquad fit for the Hyperquad fit for the titration of [HQ] = 3x10⁻⁴ M, [NaCl] = 0.1 M, [HCl] = 0.001 M, [Triton X-114] = 1 wt% (~0.02 M), by [NaOH] = 0.01024 ± 0.00002 M and [NaCl] = 0.09 M. T = 1.8±0.2 °C.

Although the use of the pK_{XX} parameter in the model would appear to act as an extraneous term for obtaining a better fit of the titration curve, the use of the pK_{XX} term in the model was supported by several independent sources as will now be explained. First, the pK_a's of 8-hydroxyquinoline in the Triton X-114/water system obtained by spectrophotometry returned a similar value (4.94±0.01; see Section 3.4.3) as is obtained when including the pK_{XX} parameter in the Hyperquad model of the potentiometric data (5.2±0.2; see Table 3.14). The value obtained by Hyperquad modeling when excluding the pK_{XX} parameter is significantly higher (6.0±0.1; see Table 3.13). Second, a comparison of the literature data trend in the pK_a values of 8-hydroxyquinoline show a decrease in pK_{a1} with an increase in surfactant concentration[134] (see Figure 3.42). The pK_{a1} obtained when the pK_{XX} is excluded from the model gives a pK_{a1} that creates a trend opposite as the one shown in previous literature, whereas the result from the potentiometric method when the pK_{XX} is used gives a trend that is consistent with previously published literature. Thus, inclusion of the pK_{XX} parameter in the Hyperquad model gives data that was confirmed by an independent technique, and supported by literature data, and will therefore be included in all models in the Triton X-114/water system.

3.4.3   Determination of the pK_a's of 8-Hydroxyquinoline by Spectrophotometric Titration

An effort to quantify the deprotonation behavior of 8-hydroxyquinoline in the Triton/water mixed solvent by spectrophotometric titration was performed. The series of spectra obtained are shown in Figure 3.26 through Figure 3.29 with Figure 3.27, and Figure 3.29 showing a smaller, higher detail view of the spectral changes. As is observed in Figure 3.26 and Figure 3.28, the solution absorbance in the 220-300 nm window is large and constant, unlike the changes observed in the H_2O system spectrophotometric titration. The 8-hydroxyquinoline absorbance bands in this region appear to be obscured by the UV absorption by Triton X-114. The only

usable portion of the spectra is limited to the spectral window above 300 nm. The spectral data

using the 300-412 nm spectral window were modeled using SQUAD. The modeling parameters

obtained are shown in Table 3.15.

Table 3.15- SQUAD modeling parameters for the pK$_a$'s of 8-hydroxyquinoline in 1 wt% Triton, T=0 °C.

Window Limits			
Lower	Upper		
(nm)	(nm)	pK$_{a1}$	pK$_{a2}$
300	412	4.94±0.01	9.69±0.01
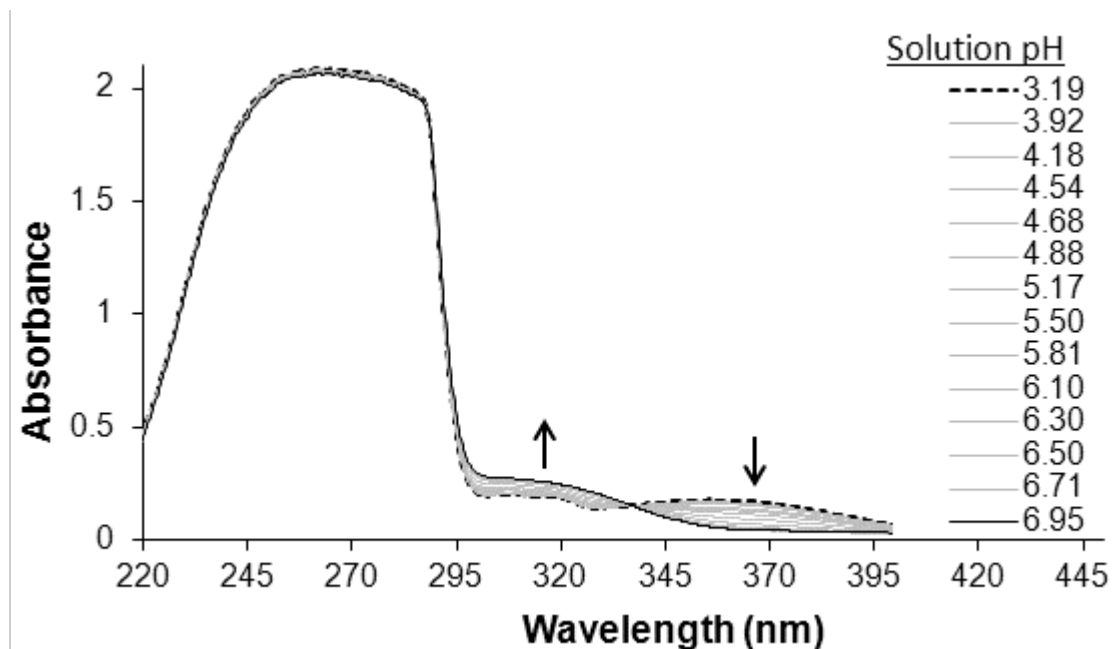
Figure 3.26-Spectra obtained while titrating a solution containing: [HQ] = 0.0001 M, [NaCl] = 0.1 M, [Triton X-114] = 1 wt%. Spectra shown are of pH 3.19–6.95. The arrows indicate the spectral change as pH increases.
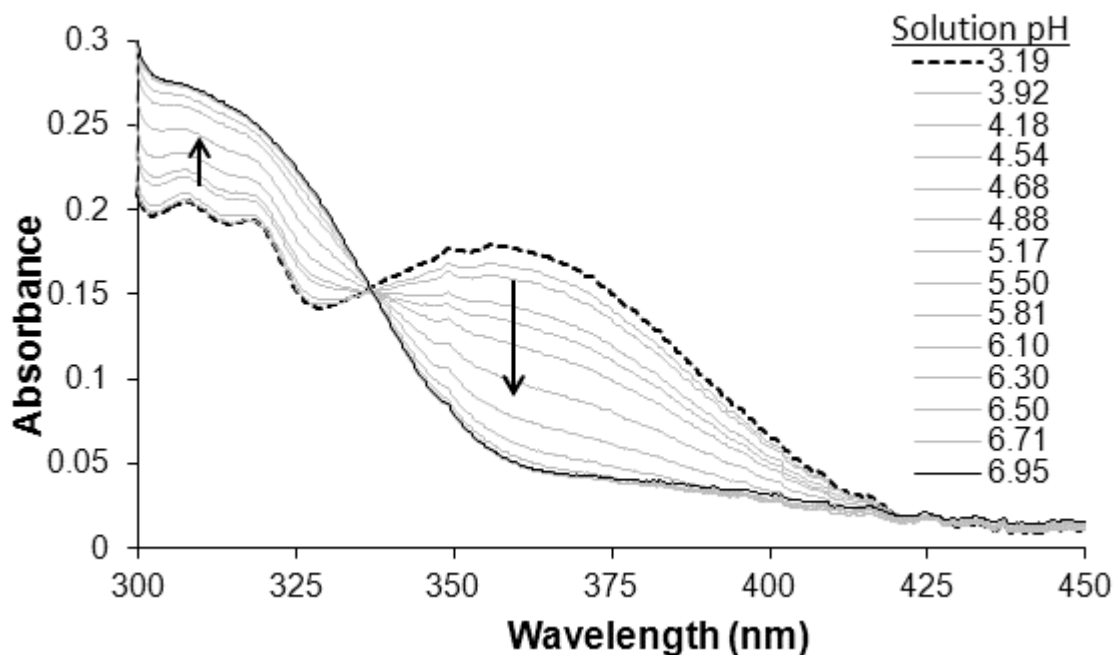
Figure 3.27- A select window of the spectra obtained while titrating a solution containing: [HQ] = 0.0001 M, [NaCl] = 0.1 M, [Triton X-114] = 1 wt%. Spectra shown are of pH 3.19–6.95. The arrows indicate the spectral change as pH increases.
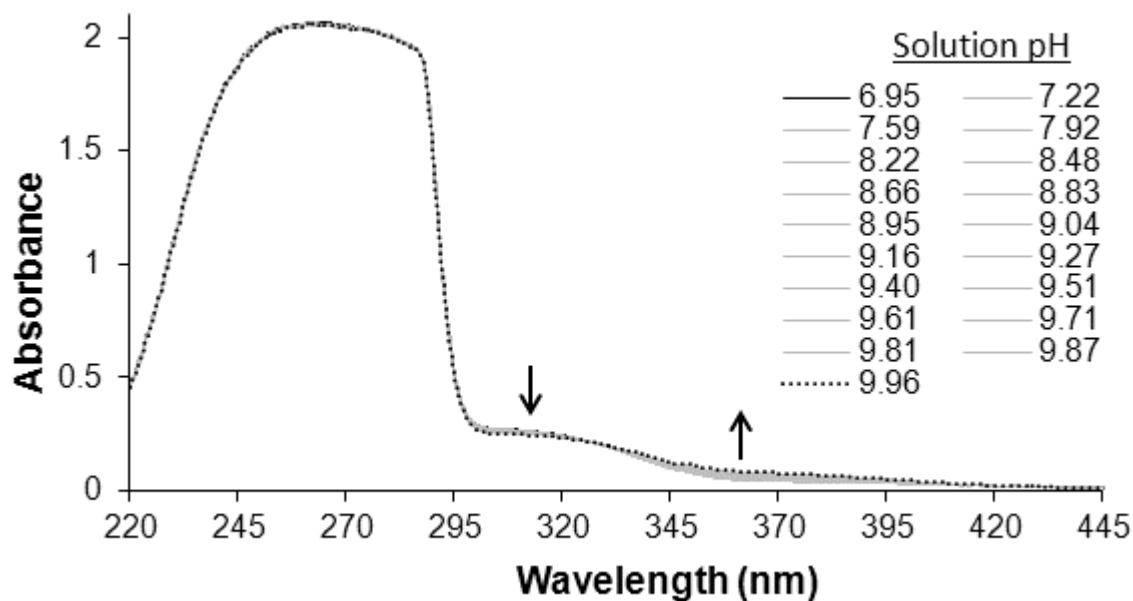
Figure 3.28- Spectra obtained while titrating a solution containing: [HQ] = 0.0001 M, [NaCl] = 0.1 M, [Triton X-114] = 1 wt%. Spectra shown are of pH 6.95–9.96. The arrows indicate the spectral change as pH increases.
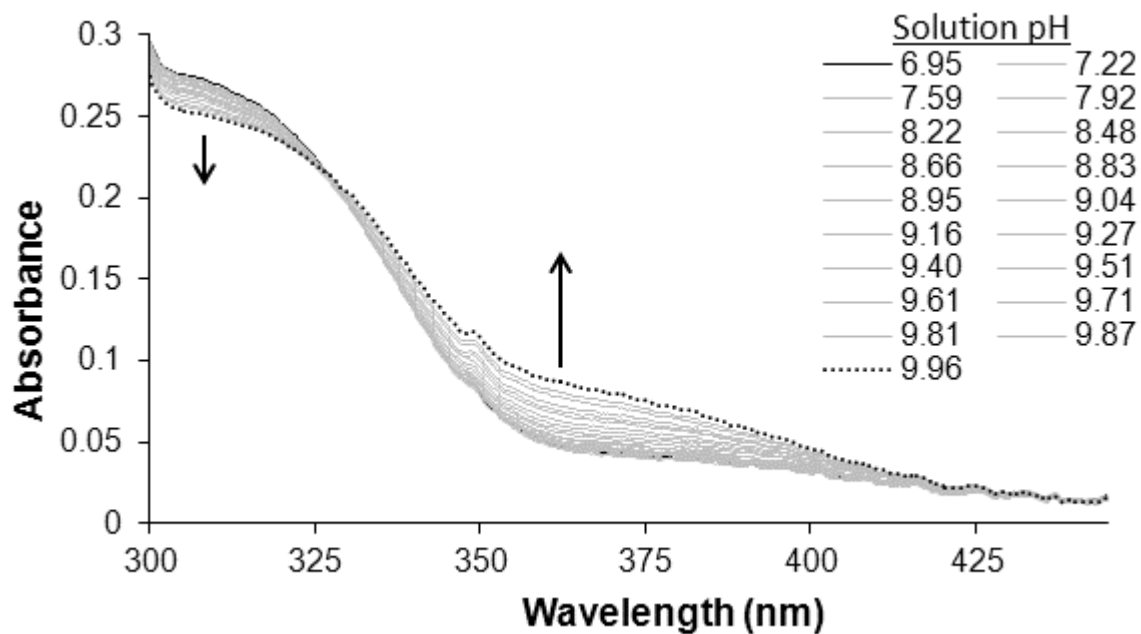
Figure 3.29- A select window of the spectra obtained while titrating a solution containing: [HQ] = 0.0001 M, [NaCl] = 0.1 M, [Triton X-114] = 1 wt%. Spectra shown are of pH 6.95–9.96. The arrows indicate the spectral change as pH increases.
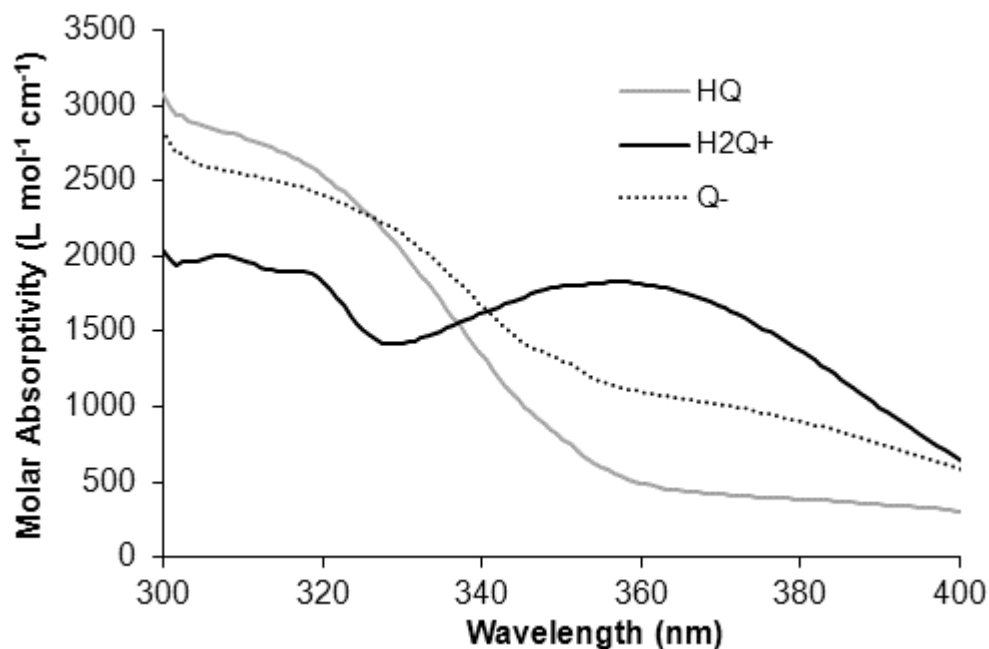
Figure 3.30- Molar absorptivity Spectra obtained from SQUAD modeling using the 300–412 nm spectral window.
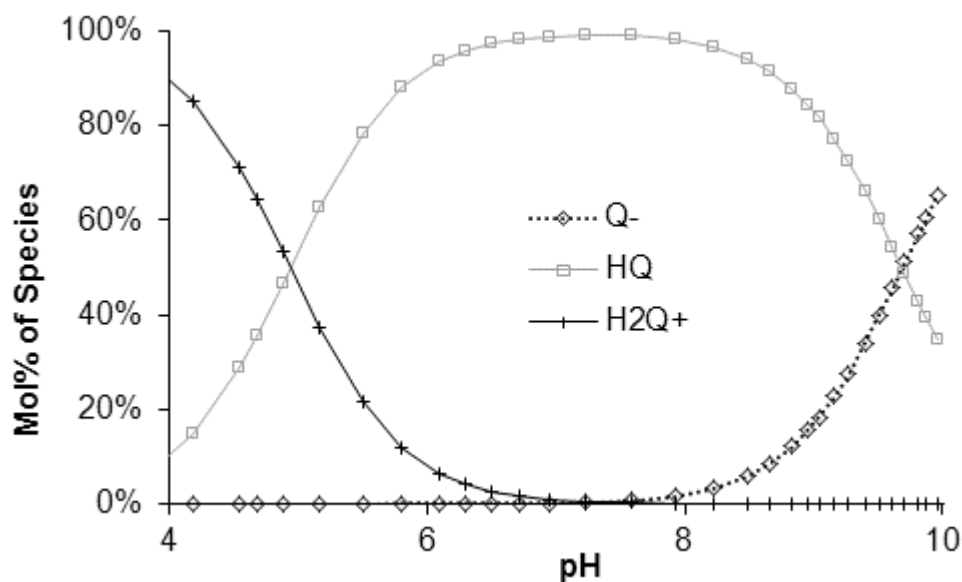
Figure 3.31- Calculated speciation curves obtained from SQUAD modeling using the 300–412 nm window.

3.4.4 Determination of the Europium Hydrolysis Constants by Potentiometric Titration

Modeling using the protolytic impurity was used in the fitting of the europium hydrolysis constants for Eu^{3+} in 1 wt% Triton. The titration data obtained for Eu^{3+} in 1 wt% Triton is shown in Figure 3.32. The reactions used to fit this system were the europium hydrolysis reactions [equations (3.16) – (3.18)], along with the parameter for the protolytic impurity (pK_{XX}) [equation (3.25)]. The fit results are shown in Figure 3.33. The fit parameters obtained are shown in Table 3.16.
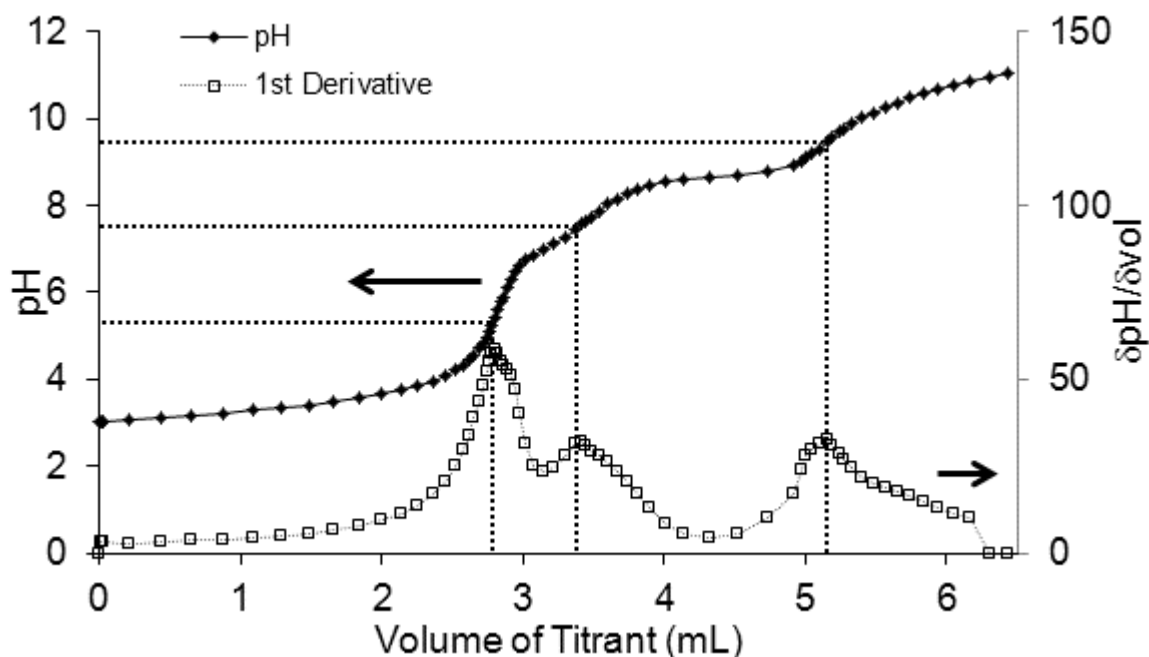
Figure 3.32- Titration of $[Eu^{3+}]$ = 3x10^{-4} M, [NaCl] = 0.1 M, [HCl] = 0.001 M, [Triton X-114] = 1 wt% (~0.02 M), by [NaOH] = 0.01024 ± 0.00002 M and [NaCl] = 0.09 M. T = 1.8±0.2 °C.
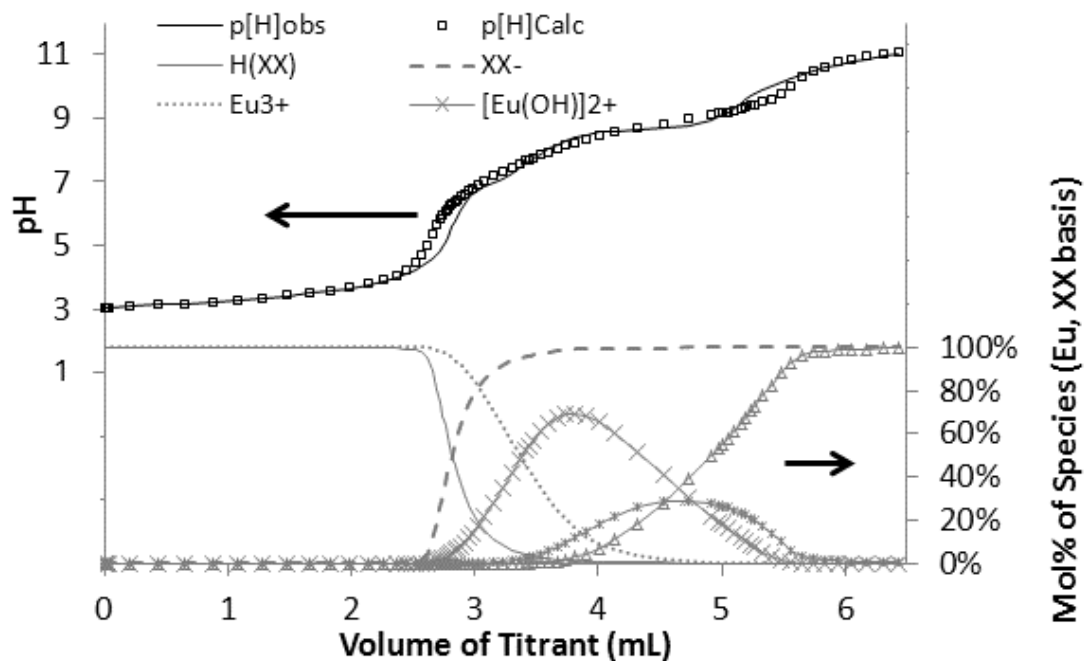
Figure 3.33- Hyperquad fit for the titration of $[Eu^{3+}]$ = 3x10^{-4} M, [NaCl] = 0.1 M, [HCl] = 0.001 M, [Triton X-114] = 1 wt% (~0.02 M), by [NaOH] = 0.01024 ± 0.00002 M and [NaCl] = 0.09 M. T = 1.8±0.2 °C.

Table 3.16- Hyperquad fit parameters for the titration data from the Eu^{3+} in 1 wt% Triton.

Equation	Formed Species	Parameter	Parameter Refined?	pβ	pK
(3.15)	OH$^-$	K$_w$	No	14.7	
(3.25)	XX$^-$	K$_{XX}$	No	6.3	
(3.16)	[Eu(OH)]$^{2+}$	$\beta_{1\text{-}10}$	Yes	-7.1±0.1	-7.1±0.1
(3.17)	[Eu(OH)$_2$]$^+$	$\beta_{1\text{-}20}$	Yes	-12.8±0.1	-5.7±0.1
(3.18)	[Eu(OH)$_3$]	$\beta_{1\text{-}30}$	Yes	-18.7±0.1	-5.9±0.2

3.4.5 Determination of Europium 8-Hydroxyquinoline Complex Stability Constants by Potentiometric Titration

The stability constants were obtained using the same progression of 1:1, 2:1 and 3:1 ligand to metal ratio solutions used in the H$_2$O system. The titration of the 1:1 ligand to metal ratio solution is shown in Figure 3.34. The reactions used to fit this titration curve are shown in Table 3.17, including the reaction for the formation of [Eu(HQ)]$^{3+}$ shown in equation (3.26) that was added to improve the fit shown in Figure 3.35. The 2:1 ligand to metal solution titration was the performed next (see Figure 3.36). The fit obtained using the reactions shown in Table 3.18 is shown in Figure 3.37.

$$\text{Eu}^{+3} + \text{H}^+ + \text{Q}^- \xleftrightarrow{\ \beta_{111}\ } \left[\text{Eu}(H\,\text{Q})\right]^{3+} \tag{3.26}$$
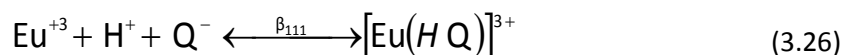
Table 3.17- Hyperquad fit parameters for the 1:1 ligand to metal solution titration in 1 wt% Triton

Equation	Formed Species	Parameter	Parameter Refined?	pβ	pK
(3.15)	OH$^-$	K$_w$	No	14.7	
(3.25)	XX$^-$	K$_{XX}$	No	6.3	
(3.13)	HQ	K$_{a1}$	No	5.2	
(3.14)	Q$^-$	K$_{a2}$	No	15.2	
(3.19)	[Eu(Q)]$^{2+}$	β_{101}	Yes	-7.78±0.04	-7.78±0.04
(3.20)	[Eu(OH)(Q)]$^+$	$\beta_{1\text{-}11}$	Yes	-14.4±0.1	-6.6±0.1
(3.21)	[Eu(OH)(Q)$_2$]	$\beta_{1\text{-}21}$	Yes	-19.8±0.1	-5.4±0.1
(3.26)	[Eu(HQ)]$^{3+}$	β_{111}	Yes	-14.07±0.06	-6.28±0.06
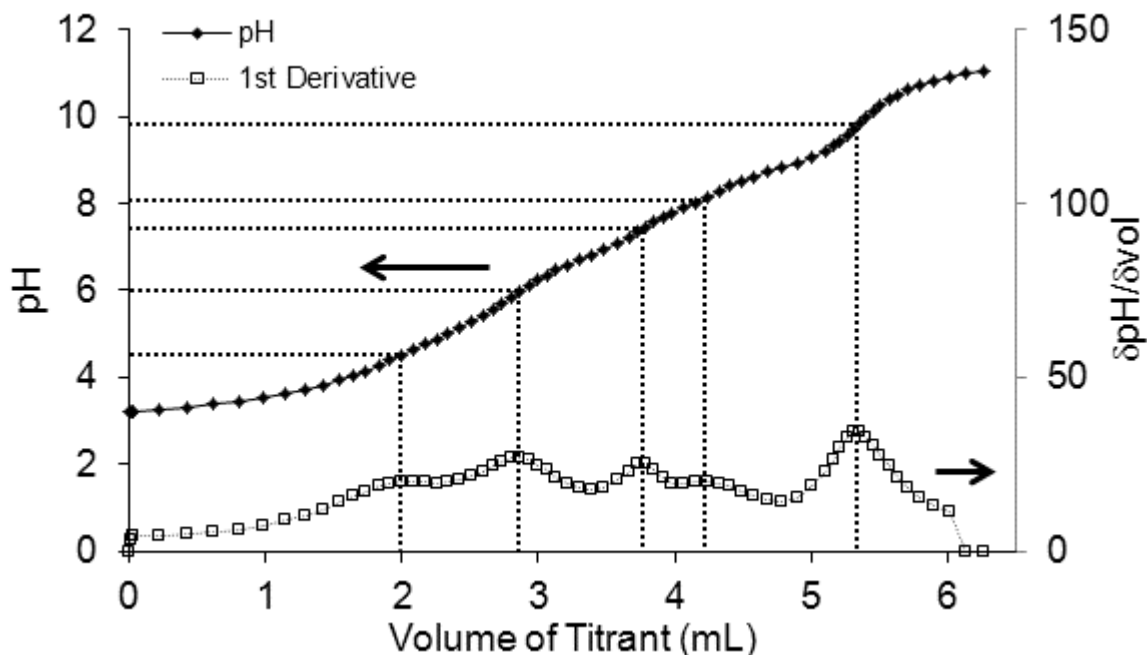
Figure 3.34- Titration of [HQ] = 3x10^{-4} M, [Eu^{3+}] = 3x10^{-4} M, [NaCl] = 0.1 M, [HCl] = 0.001 M, [Triton X-114] = 1 wt% (~0.02 M), by [NaOH] = 0.01024 ± 0.00002 M and [NaCl] = 0.09 M. T = 1.8±0.2 °C.
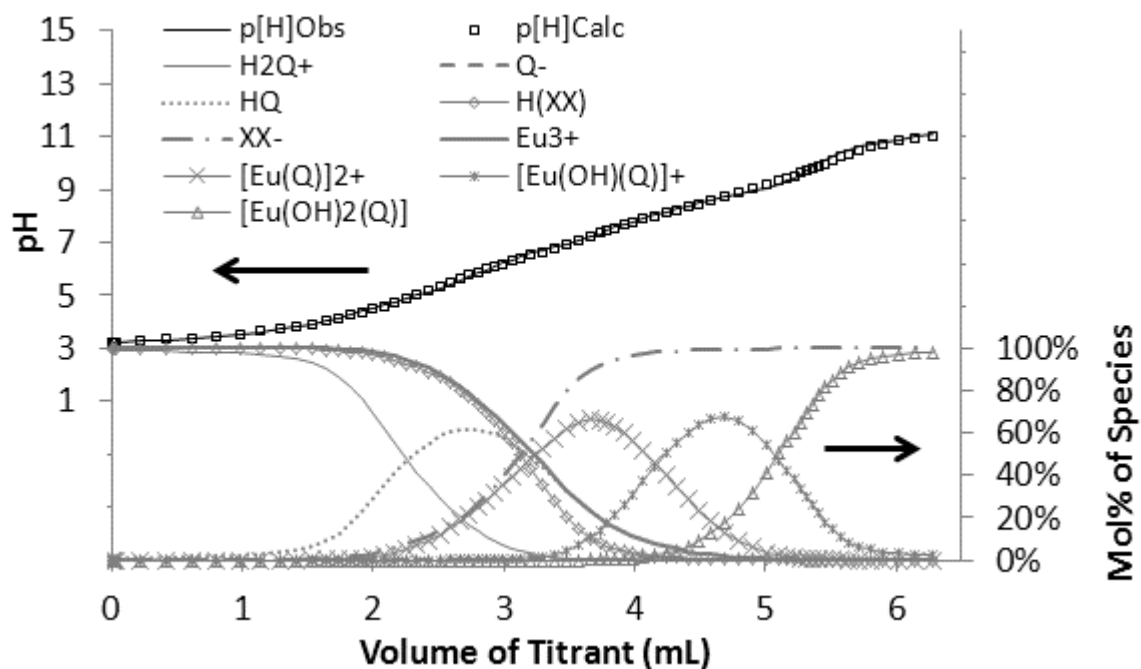
Figure 3.35- Hyperquad fit for the titration of [HQ] = 3x10^{-4} M, [Eu^{3+}] = 3x10^{-4} M, [NaCl] = 0.1 M, [HCl] = 0.001 M, [Triton X-114] = 1 wt% (~0.02 M), by [NaOH] = 0.01024 ± 0.00002 M and [NaCl] = 0.09 M. T = 1.8±0.2 °C.
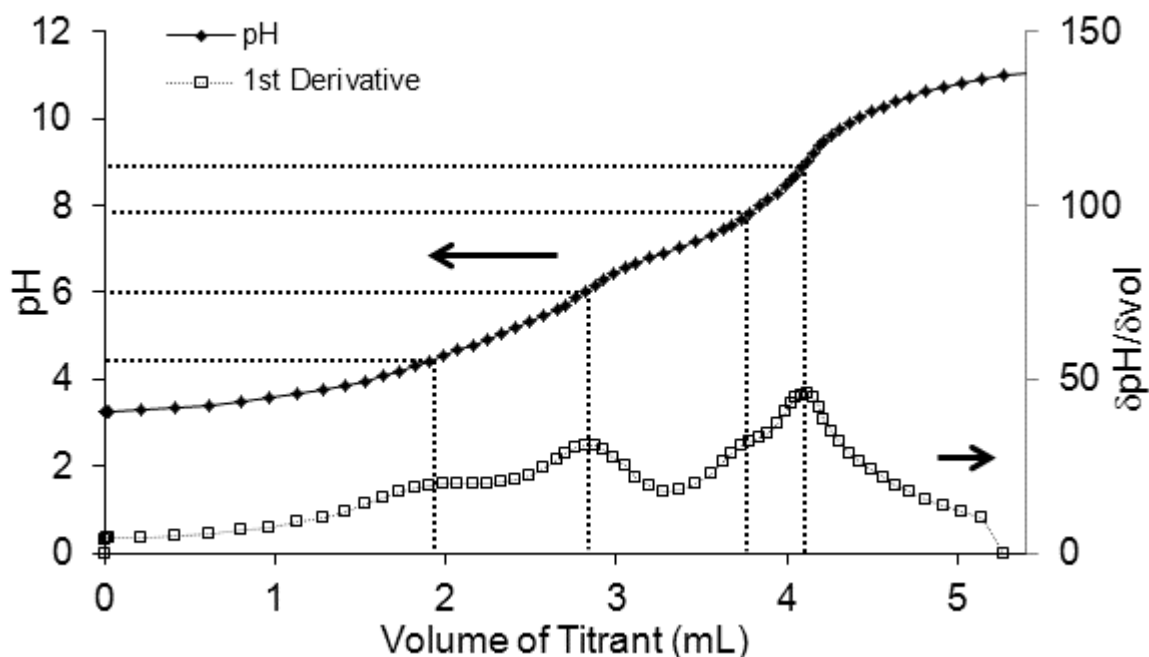
Figure 3.36- Titration of [HQ] = 3×10^{-4} M, [Eu^{3+}] = 1.5×10^{-4} M, [NaCl] = 0.1 M, [HCl] = 0.001 M, [Triton X-114] = 1 wt% (~0.02 M), by [NaOH] = 0.01024 ± 0.00002 M and [NaCl] = 0.09 M. T = 1.9±0.1 °C.
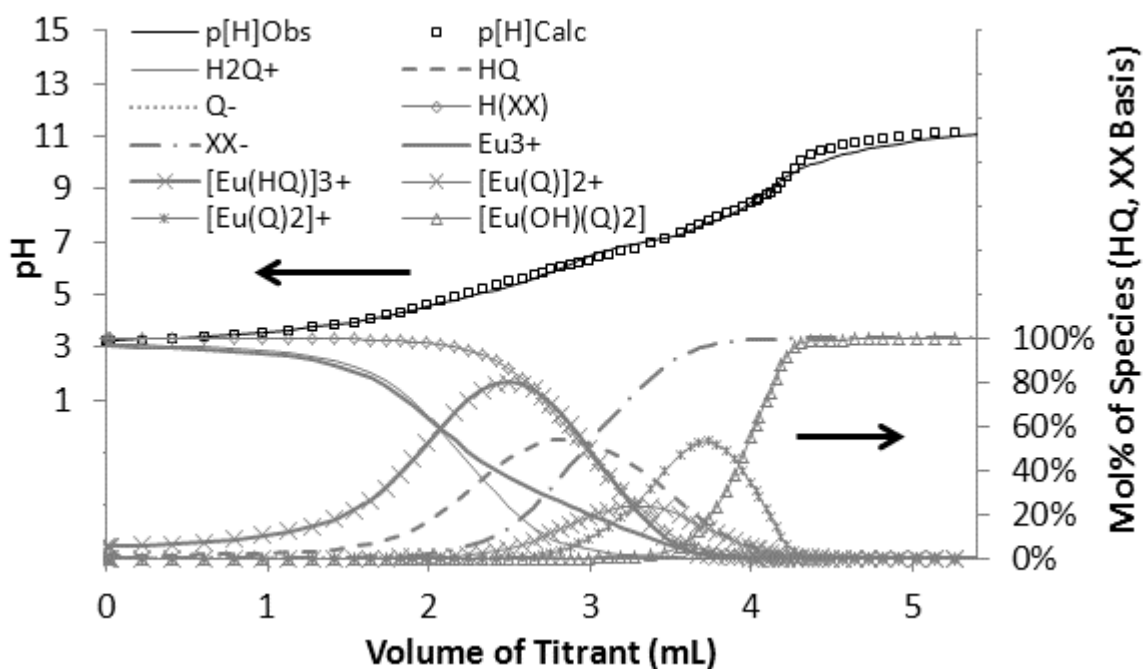
Figure 3.37- Hyperquad fit for the titration of [HQ] = 3×10^{-4} M, [Eu^{3+}] = 1.5×10^{-4} M, [NaCl] = 0.1 M, [HCl] = 0.001 M, [Triton X-114] = 1 wt% (~0.02 M), by [NaOH] = 0.01024 ± 0.00002 M and [NaCl] = 0.09 M. T = 1.9±0.1 °C.

Table 3.18- Hyperquad fit parameters for the 2:1 ligand to metal solution titration in 1 wt% Triton.

Equation	Formed Species	Parameter	Parameter Refined?	pβ	pK
(3.15)	OH^-	K_w	No	14.7	
(3.25)	XX^-	K_{XX}	No	6.3	
(3.13)	HQ	K_{a1}	No	5.2	
(3.14)	Q^-	K_{a2}	No	15.2	
(3.19)	$[Eu(Q)]^{2+}$	β_{101}	No	-7.78	
(3.22)	$[Eu(Q)_2]^+$	β_{102}	Yes	-14.7±0.2	-6.9±0.2
(3.23)	$[Eu(OH)(Q)_2]$	β_{1-12}	Yes	-21.1±0.2	-6.4±0.2
(3.26)	$[Eu(HQ)]^{3+}$	β_{111}	No	-14.1	-6.3

Four different models were used in an effort to find the best fit for the 3:1 ligand to metal ratio titration data with differing results. The models all relied on equations (3.13), (3.14), (3.19), (3.22), (3.24), and (3.25), which were all used for fitting the 3:1 titration in the H_2O system. Equation (4.20) associated with the H(XX) species was added to all models to be consistent with the Triton/water system evaluation. The equation (3.26) that relates to the formation of $[Eu(HQ)]^{3+}$ was used in Models C and D to test its effect on curve fit and parameter values. A new reaction between europium and the protolytic impurity shown in equation (3.27) was included in Model A and D to see if it would improve the modeling results.

$$Eu^{+3} + XX^- \xleftarrow{\quad \beta_{1001} \quad} [Eu(XX)]^{2+} \tag{3.27}$$
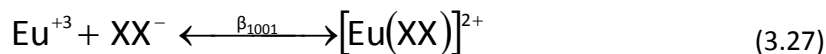
The fits from the parameters obtained in Table 3.19 are shown in Figure 3.39 and show that all modeling attempts give a reasonable fit for the data with the best fit shown for the model with the most parameters (Model D). Despite a slightly superior fit, the inclusion of the formation of the $[Eu(XX)]^{2+}$ species leads to larger error in the $[Eu(Q)_3]$ formation constant. Given that the parameter for the formation of $[Eu(Q)_3]$ from all modeling attempts are all statistically the same, the model using the most parameters that give a largest errors (Model D) must be rejected for

the simpler model providing less error (Model C). Model C was chosen over the simplest (A) because $[Eu(HQ)]^{3+}$ included in the other Triton/water system parameter calculations.
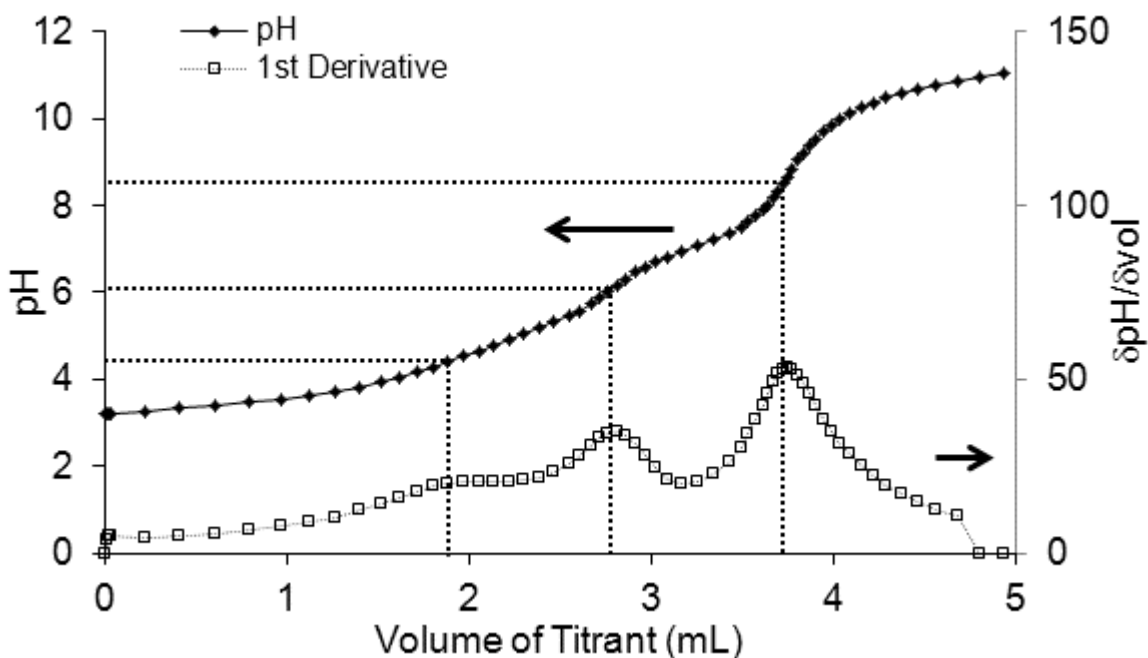
Figure 3.38- Titration of [HQ] = $3x10^{-4}$ M, $[Eu^{3+}]$ = $1x10^{-4}$ M, [NaCl] = 0.1 M, [HCl] = 0.001 M, [Triton X-114] = 1 wt% (~0.02 M), by [NaOH] = 0.01024 ± 0.00002 M and [NaCl] = 0.09 M. T = 1.9±0.2 °C.

Table 3.19-Parameters from the four models used to fit the 3:1 ligand to metal ratio solution titration.

Equation	Formed Species	Parameter		Model A	Model B	Model C	Model D
(3.15)	OH^-	K_w		14.7	14.7	14.7	14.7
(3.25)	XX^-	K_{XX}		6.3	6.3	6.3	6.3
(3.13)	HQ	K_{a1}		5.2	5.2	5.2	5.2
(3.14)	Q^-	K_{a2}	pβ	15.2	15.2	15.2	15.2
			pK	10.0	10.0	10.0	10.0
(3.27)	$[Eu(XX)]^{2+}$	β_{1001}		(not used)	-6.4±0.5	(not used)	-6.2±0.5
(3.19)	$[Eu(Q)]^{2+}$	β_{101}		-7.78	-7.78	-7.78	-7.78
(3.22)	$[Eu(Q)_2]^+$	β_{102}	pβ	-14.7	-14.7	-14.7	-14.7
			pK	-6.9	-6.9	-6.9	-6.9
(3.24)	$[Eu(Q)_3]$	β_{103}	pβ	-21.3±0.2	-22.1±0.5	-21.4±0.2	-22.0±0.4
			pK	-6.6±0.2	-7.4±0.5	-6.7±0.2	-7.3±0.4
(3.26)	$[Eu(HQ)]^{3+}$	β_{111}	pβ	(not used)	(not used)	-14.1	-14.3
			pK			-6.5	-6.5
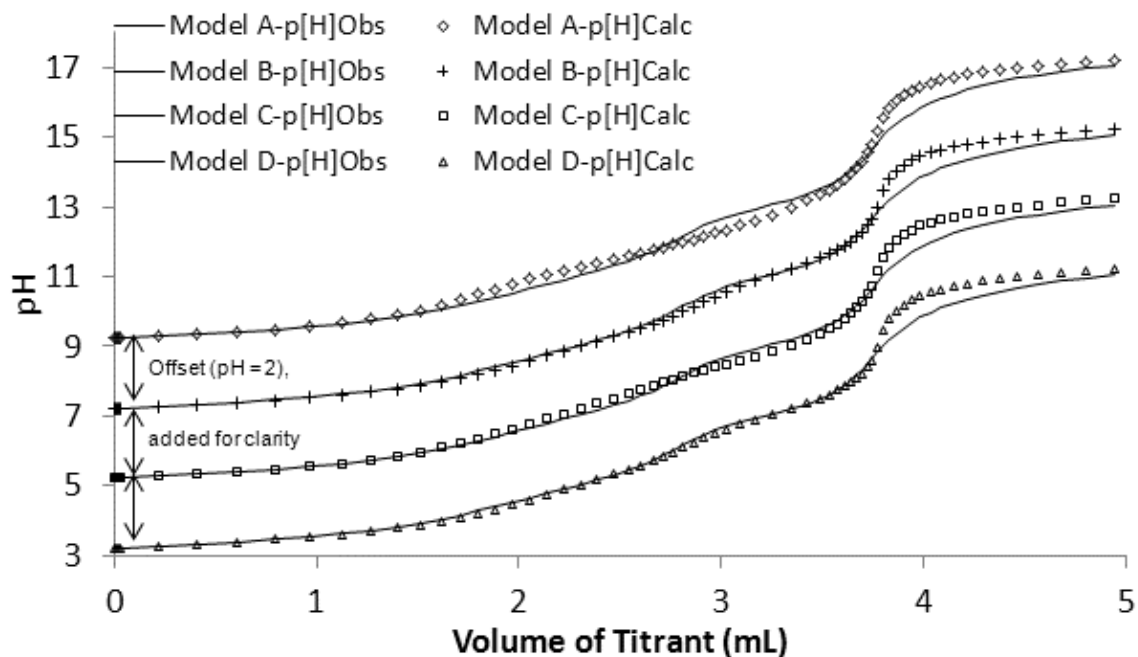
Figure 3.39- Results from four attempts at fitting the 3:1 ligand to metal titration curve.
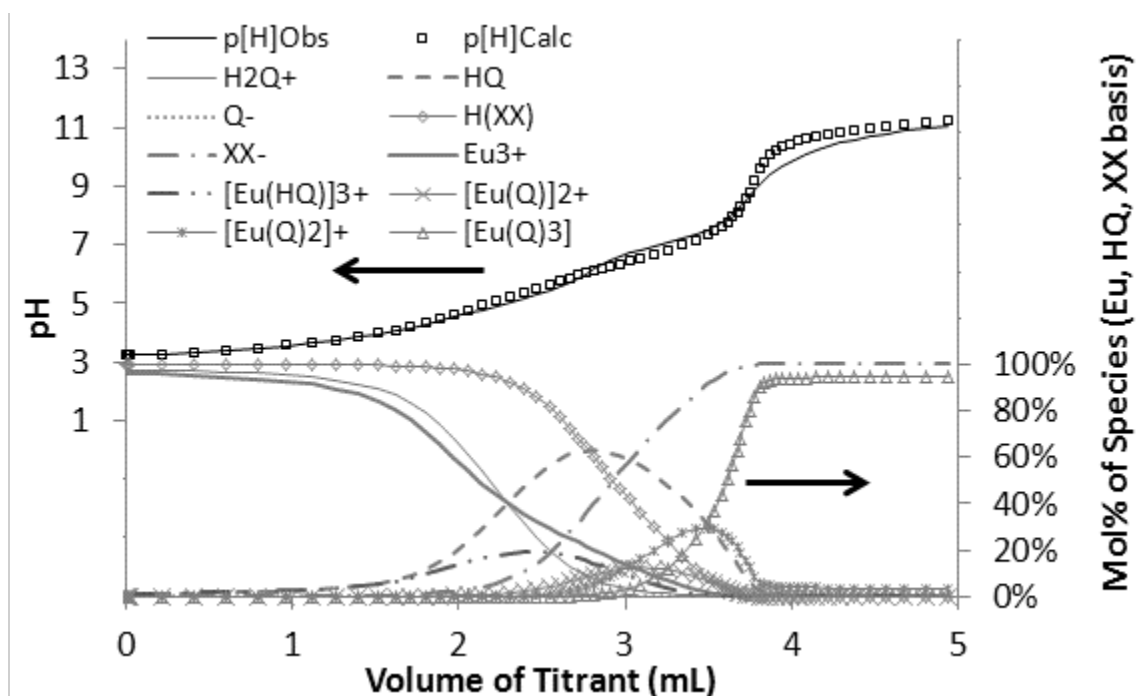
Figure 3.40- Hyperquad fit using Model C for the titration of [HQ] = $3x10^{-4}$ M, [Eu^{3+}] = $1x10^{-4}$ M, [NaCl] = 0.1 M, [HCl] = 0.001 M, [Triton X-114] = 1 wt% (~0.02 M), by NaOH] = 0.01024 ± 0.00002 M and [NaCl] = 0.09 M. T = 1.9±0.1 °C.

Table 3.20- Hyperquad fit parameters for the 3:1 ligand to metal solution titration in 1 wt% Triton.

Equation	Formed Species	Parameter	Parameter Refined?	pβ	pK
(3.15)	OH⁻	K_w	No	14.7	
(3.25)	XX⁻	K_{XX}	No	6.3	
(3.13)	HQ	K_{a1}	No	5.2	
(3.14)	Q⁻	K_{a2}	No	15.2	
(3.19)	$[Eu(Q)]^{2+}$	β_{101}	No	-7.78	
(3.22)	$[Eu(Q)_2]^+$	β_{102}	No	-14.7	-6.9
(3.24)	$[Eu(Q)_3]$	β_{103}	Yes	-21.4±0.2	-6.7±0.2
(3.26)	$[Eu(HQ)]^{3+}$	β_{111}	No	-14.1	-6.3

3.5   Discussion

3.5.1   The pK_a's of 8-Hydroxyquinoline

Literature data for the 8-hydroxyquinoline protonation constants measured at 1°C in 0.1 M NaCl are not available for comparison. However, using the Van't Hoff equation, these results can be compared with data measured under the same ionic strength, but at different temperatures. Previously published pK_a data for 8-hydroxyquinoline measured in 0.1 M NaCl at T = 25 and 60 °C are available.[151-152] These data as presented are shown in a modified Van't Hoff plot, which shows the data in $\log_{10}$ instead of ln (see Figure 3.41). The linearity of data with 1/T is still preserved as presented. The comparison of pK_a values measured in this work with the literature shows very good consistency with previously published data. Using the Van't Hoff equation, the standard enthalpy of reaction was calculated using the data from the literature and results of this work (see Table 3.21).

Comparing the pK_a results of the water system with the Triton X-114/water system gives insight into the effect of the Triton on the deprotonation of 8-hydroxyquinoline. Literature values measured in Triton X-100 at 20°C[134] show the same trend (see Figure 3.42) as the

observed results measured in this work (see Table 3.23, the pK_a average of both techniques).

When comparing the average values it is notable that the pK_a's were changed in opposite

directions with the pK_{a1} lowered by 0.4±0.2 and the pK_{a2} increased by 0.3±0.1 (see Table 3.23).

In this work, the pK_{a1} refers to the deprotonation of the aromatic nitrogen, and the pK_{a2} refers

to the deprotonation of the phenolic oxygen. The divergent trend in the pK_a values of 8-

hydroxyquinoline is consistent with data presented by Irving *et al.*[153] which indicate that ligands

with –OH functional groups experience an increase in pK_a with increasing organic content of a

mixed solvent, whereas ligands with –NH functional groups show a decrease. Irving et al.[153]

interprets the data to mean that increasing the organic content of the mixed solvent will

decrease the dielectric constant of the medium. This leads to increased ionic interaction

between the proton and negatively charged oxygen in –OH functional groups [see equation

(3.28)].[153] In the –NH functional groups there is a smaller change in the ion-dipole forces

between the nitrogen and proton than in the ion-dipole forces between the proton and the

more electronegative oxygen donors of the solvent.[153] In the case of –OH functional groups,

electrostatic effects can explain the change in pK_a with increased organic content of a mixed

solvent, but with –NH functional groups the reaction is charge neutral [see equation (3.29)].

Because the change in pK_a for –NH functional groups cannot be described by electrostatic

effect, it has been linked to such variables as basicity of solvent,[154-155] solvation effects, [154-155]

stabilization of the free base, [154] and interaction of ionic solutes with solvent species.[153-154]

When dealing with the medium effects caused by mixed solvents, the thermodynamic

treatment of the system involves the inclusion of the Gibbs free energy of transfer of the solute

species from water to the mixed solvent solution (ΔG_t).[153, 156] These factors when taken

together offer an explanation for the divergent trends observed in this work for the pK_a's of 8-

hydroxyquinoline as the surfactant concentration increases.

$$[R - OH] \leftrightarrow H^+ + [R - O]^-$$ (3.28)

$$[R - NH]^+ \leftrightarrow H^+ + [R - N]$$ (3.29)
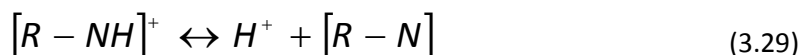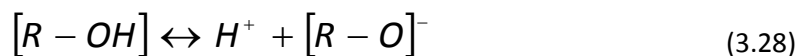
Table 3.21- Calculated Standard Enthalpy of reaction for the deprotonation of 8-hydroxyquinoline. Data utilized for this calculation are shown in Table 3.22.

	K_{a1}	K_{a2}
Van't Hoff Slope	-2700±300	-760±620
ΔH ° (kJ/mol)	22±3	6±5

Table 3.22- Data used in the Van't Hoff Analysis of the pK_a's of 8-hydroxyquinoline in the water system.

Medium	Temp (°C)	pK_{a1}	pK_{a1}	Source
0.1 M NaCl	1	5.6±0.1	9.52±0.06	This Work (Potentiometry)
0.1 M NaCl	1	5.32±0.01	9.72±0.01	This work (Spectrophotometry)
0.1 M KCl	25	5.02	9.68	Matrosovich et al.[151]
0.1 M KCl	60	4.63	9.38	Lobanov et al.[152]

Table 3.23-Summary of pK_a results from potentiometric (Potent.) and spectrophotometric (Spect.) titration methods. The results from these methods were averaged for a final result from this study.

Parameter	H_2O			Triton X-114/H_2O		
	Potent.	Spect.	Avg.	Potent.	Spect.	Avg.
pK_{a1}	5.6±0.1	5.32±0.01	5.5±0.1	5.2±0.2	4.94±0.01	5.1±0.2
pK_{a2}	9.5±0.1	9.72±0.01	9.6±0.1	10.0±0.1	9.69±0.01	9.9±0.1
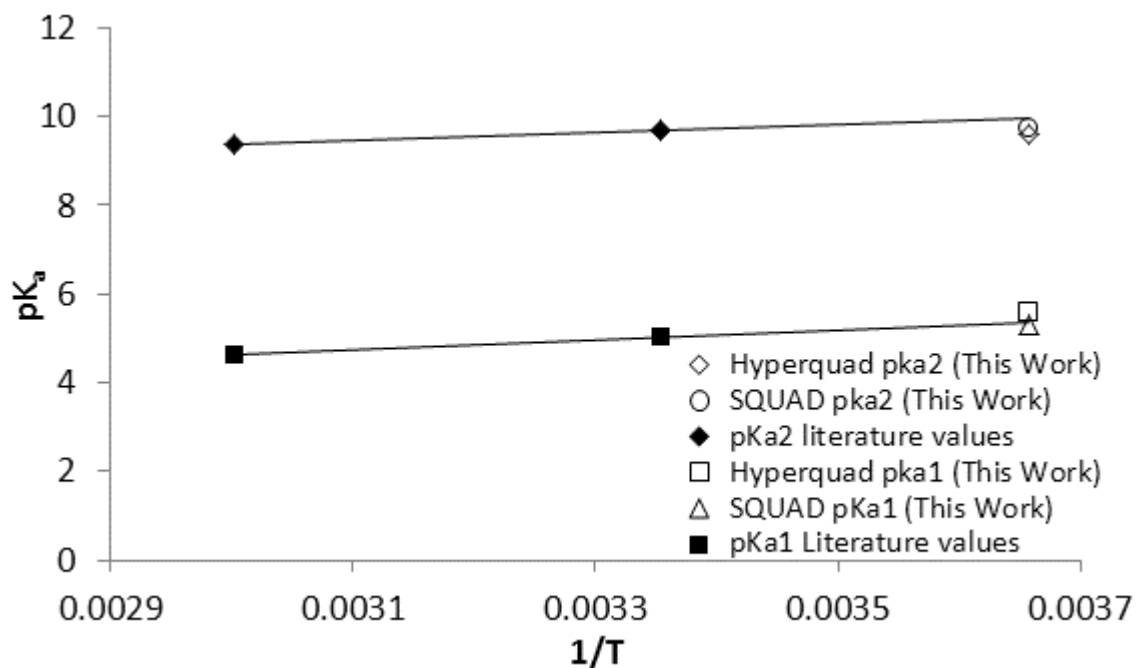
Figure 3.41- Comparison of measured pK_a values for 8-hydroxyquinoline with literature data from Lobanov *et al.*[151-152] utilizing the Van't Hoff relation. Data used in this plot are shown in Table 3.22.
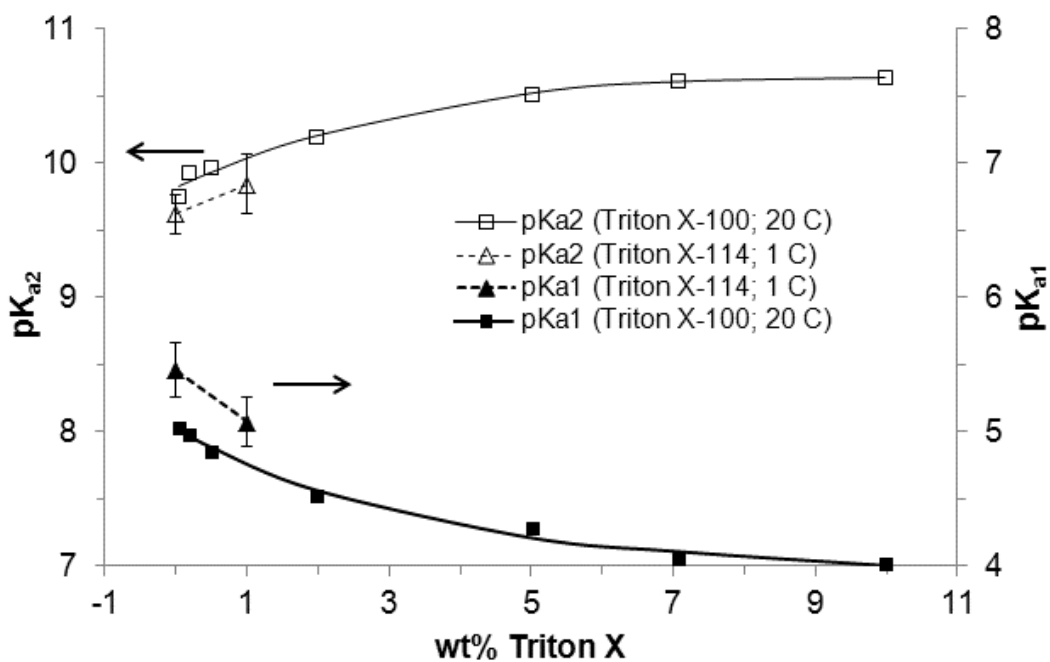
Figure 3.42- Comparison of the pK_a of 8-hydroxyquinoline in Triton X-100/water with the pK_a of 8-hydroxyquinoline in Triton X-114/water measured in this work. The literature values are from Hoshino *et al.*[134]

140

3.5.2 Europium Hydrolysis Behavior

Europium hydrolysis constants have not been measured previously at 1 °C, however, there exists a rather complete set of data for the first hydrolysis constant at 25 °C over a range of ionic strength presented in the literature.[157] This data compares reasonably well with the data measured in this work at 1 °C and 0.1 M NaCl as shown in Figure 3.43and Table 3.7. Because there is not a great deal of europium hydrolysis data that is comparable with the values measured in this work, it is reasonable to compare with hydrolysis data from the entire lanthanide series. Lanthanides, as trivalent ions, share a similar chemistry that is altered very slightly by the lanthanide contraction, giving fairly predictable data trends. Any holes in series of data are reasonably easy to interpolate. The lanthanide series data presented here will be shown as a function of inverse ionic radius (Table 3.24). Figure 3.44 shows a comparison of observed data with literature is that of the first, second and third hydrolysis constants of select lanthanides with the observed values for europium measured at 1 °C in 0.1 M NaCl. Literature data in Figure 3.44 were calculated from the data in Baes[147] at 25 °C and infinite dilution using an accompanying equation to adjust the data to 0.1 M $NaClO_4$ conditions. The data observed in this work agrees with the general trend of the literature data, but as the values progress from 1st to 2nd to 3rd, the agreement is poorer.
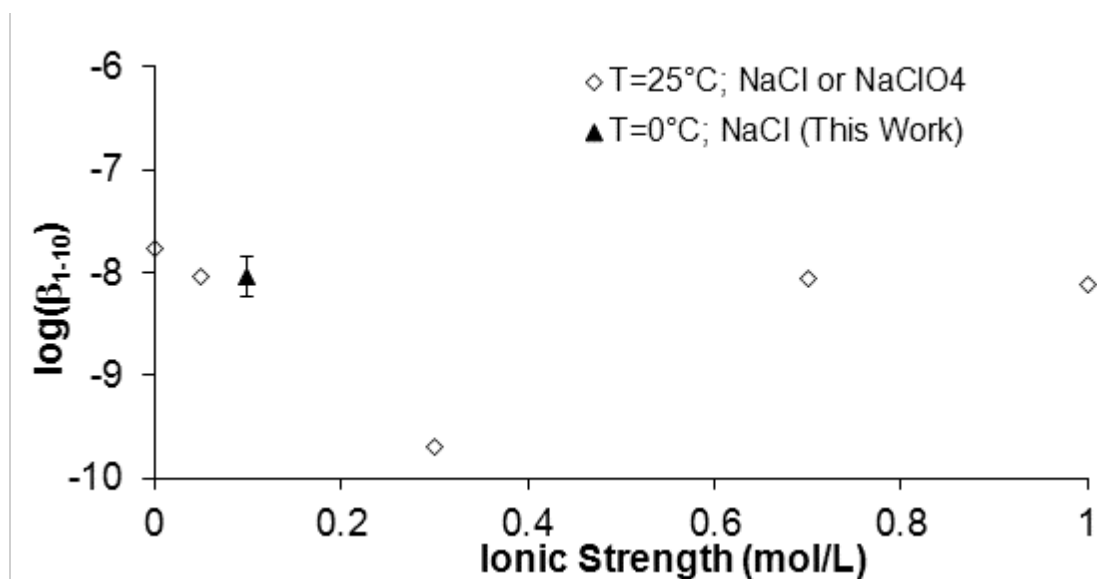
Figure 3.43- Comparison of the first hydrolysis constant (Log β_{1-10}) obtained in this work at 1 °C with literature data at 25 °C.

Table 3.24- Values used for the inverse ionic radius of the trivalent lanthanides.[14]

Ion	1/r (Å^{-1})
La^{3+}	0.969
Ce^{3+}	0.990
Pr^{3+}	1.010
Nd^{3+}	1.017
Pm^{3+}	1.031
Sm^{3+}	1.044
Eu^{3+}	1.056
Gd^{3+}	1.066
Tb^{3+}	1.083
Dy^{3+}	1.096
Ho^{3+}	1.110
Er^{3+}	1.124
Tm^{3+}	1.136
Yb^{3+}	1.152
Lu^{3+}	1.161
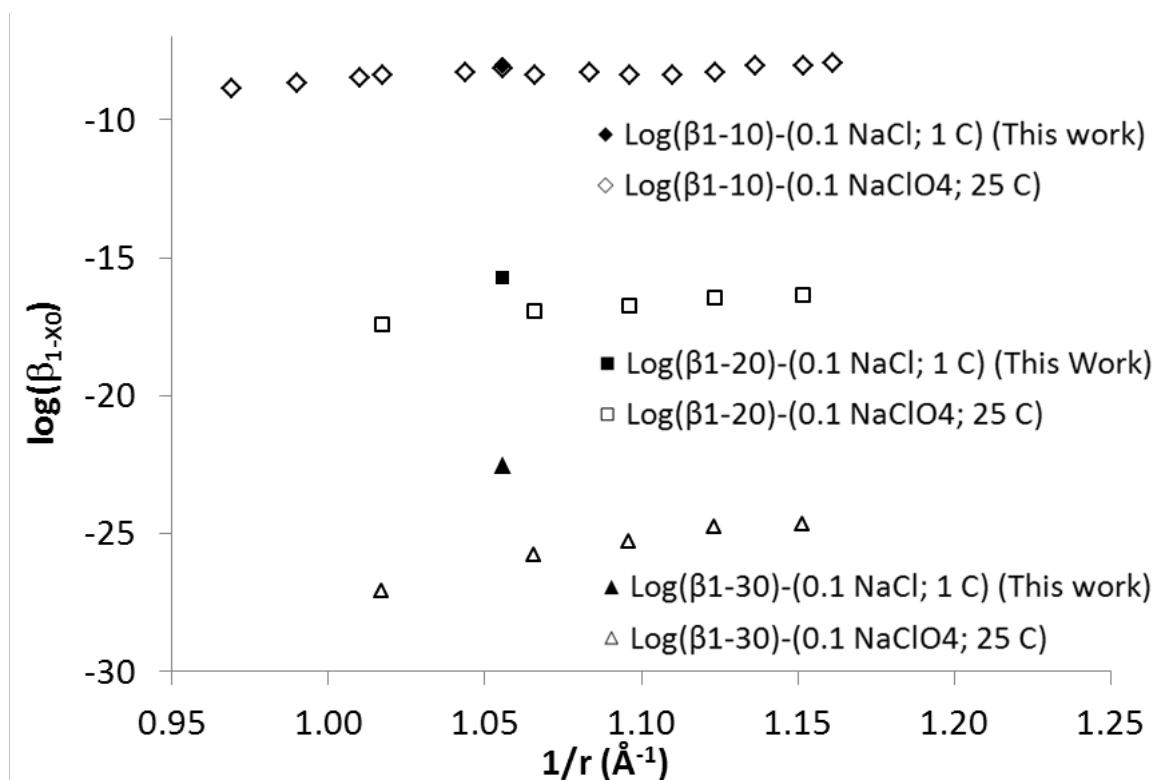
Figure 3.44- Comparison of observed and literature data values for the first hydrolysis constant as a function of inverse ionic radius.

The comparison of hydrolysis constants between the water and the Triton X-114/water system offers insight as to the role that Triton X-114 plays in the hydrolysis of lanthanides in this system. There is a significant change in the hydrolysis constants when Triton X-114 is added to the system with higher stability in the complexes (as indicated by higher log β values) (see Table 3.25). These results are consistent with the description by Irving et al.[153] of ligands, or in the case of europium hydrolysis, hydrated metal centers with –OH functional groups. In the hydrolysis reaction, the ligand with –OH functional group is the hydroxide, the proton is the Eu^{3+} ion, and the europium hydrolysis species are analogous to the protonated oxygen group. Adapting the description of the system in Irving *et al.*[153] to the hydrolysis system, the increase in organic character of the mixed solvent leads to increased ionic interaction between the

europium and negatively charged oxygen in the hydroxide causing the formation of hydrolysis species.

The system can also be described in terms of ΔG_t. Based on tabulated ΔG_t data in Kalidas *et al.*[158] the only data available involving lanthanides is for the methanol/water mixed solvent. These data show an approximately 8–10 fold increase in ΔG_t as methanol content is increased from 10–30%. An increase in Gibbs free energy indicates lower stability of a species. Therefore, the increase in ΔG_t for Eu^{3+} in the mixed solvent favors its elimination from the system, including the formation of other species, leading to higher stability of $[Eu(OH)]^{2+}$, $[Eu(OH)_2]^+$, and $[Eu(OH)_3]$.

When considering the case of the mixed hydrolysis species (those involving europium with both Q^- and OH^- simultaneously) the comparison between the systems shows that no significant change was observed (see Table 3.26). This result indicates that the mixed solvent has no effect on the formation of these species. This is an unexpected result considering the description of the hydrolysis species above, and the europium 8-hydroxyquinoline complexation data discussed in section 3.5.3.

Table 3.25- Comparison of the H_2O/Triton X-114 vs. H_2O system europium hydrolysis constants.

Species Formed	Parameter	H_2O	H_2O/Triton X-114
		pK	pK
$[Eu(OH)]^{2+}$	β_{1-10}	-8.0±0.2	-7.1±0.1
$[Eu(OH)_2]^+$	β_{1-20}	-7.7±0.1	-5.7±0.1
$[Eu(OH)_3]$	β_{1-30}	-6.8±0.2	-5.9±0.2

Table 3.26- Comparison of the mixed ligand hydrolysis species parameters.

Species Formed	Parameter	H$_2$O	H$_2$O/Triton X-114
		pK	pK
[Eu(OH)(Q)]$^+$	$\beta_{1\text{-}11}$	-6.4±0.1	-6.6±0.1
[Eu(OH)$_2$(Q)]	$\beta_{1\text{-}21}$	-5.6±0.1	-5.4±0.1
[Eu(OH)(Q)$_2$]	$\beta_{1\text{-}12}$	-6.6±0.4	-6.4±0.2

3.5.3 The Europium 8-Hydroxyquinline Stability Constants

Previous measurements of the formation constant for [Eu(Q)]$^{2+}$ (i.e. log β_{101}) have been performed at 20-25 °C in 0.1 M of various ionic media.[131, 159] These results are shown compared with the value measured in this work at 1 °C and 0.1 M NaCl in Figure 3.45. The data are reasonably close given the fact that most the literature data is at 20–25 °C and the value measured in this work is at 1 °C. The one value in the literature for [Eu(Q)]$^{2+}$ formation at 20 °C was 7.2 compared with this work's value of 6.9±0.1 at 1 °C.

The effect of the presence of Triton X-114 on the [Eu(Q)]$^{2+}$ formation constant has not been reported in the literature. However, one work[160] measured this formation constant in 50% dioxane, which would cause a similar effect as Triton X-114. The 50% dioxane data are shown with the data from this work using 1 wt% Triton X-114, and the data measured without any co-solvent present[131] for comparison. These data are shown in Figure 3.46. The data show that increasing the organic component of the mixed-solvent causes an increase in the stability of the formation of [Eu(Q)]$^{2+}$ that is consistent between the 50% dioxane data and the 1 wt% Triton data. A similar comparison can be made for the data concerning the formation of [Eu(Q)$_2$]$^+$ also using data from the previously cited 50% dioxane paper[160], and one with no dioxin.[159] These data are shown for comparison with the data observed in this work at 0 and 1 wt% Triton X-114 in Figure 3.47. Just as with the formation of [Eu(Q)]$^{2+}$, the formation of [Eu(Q)$_2$]$^+$ also appears to be more favored (forming a stronger complex) by increasing the organic component of the

mixed solvent. This is consistent between the 0 and 50% dioxane as it is with the 0 and 1wt% Triton X-114 data.
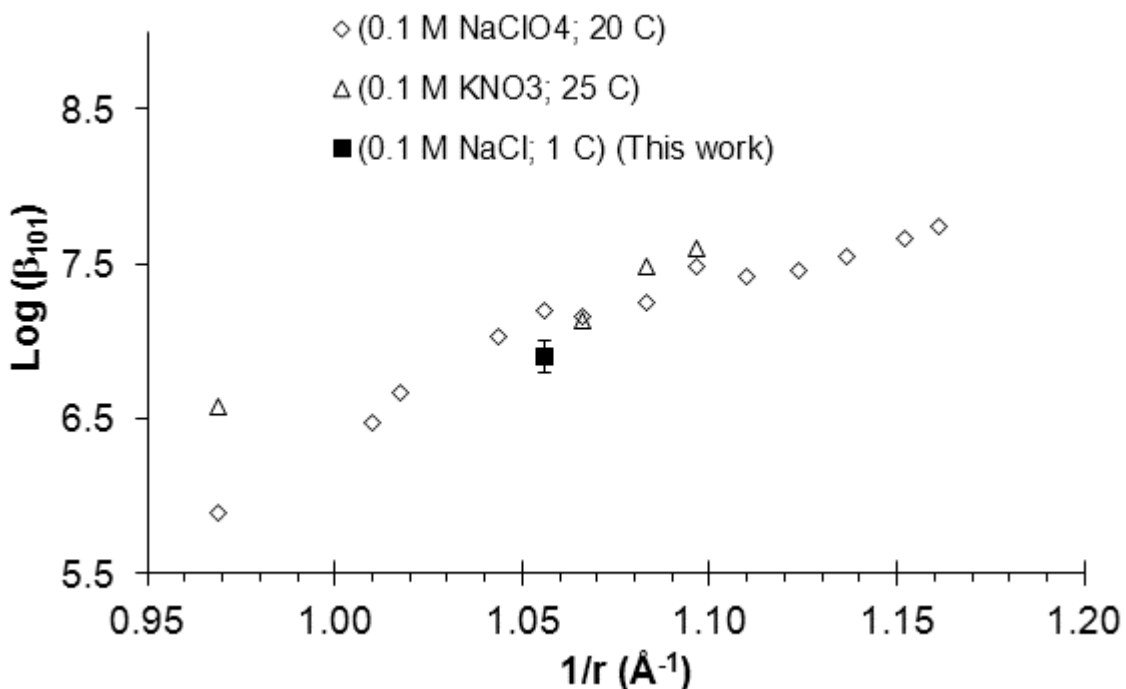
Figure 3.45- A Comparison of the formation constants for $[Eu(Q)]^{2+}$ (Log β_{101}) in 0.1 M Ionic media at various temperatures, to various lanthanides' $[Ln(Q)]^{2+}$ formation constants represented as a function of ionic radius.

When comparing only the data observed in this work, it is clear that the stability of the complexes between europium and 8-hydroxyquinoline were affected by the presence of Triton X-114. There is a significant increase in the strength of the strength of the 1st and 2nd europium 8-hydroxyquinoline complexation constants in the Triton/water mixed solvent with an increase of 0.9±0.1 and 1.3±0.6 respectively (see Table 3.27). A statistically insignificant increase was also noted for the 3rd complexation constant of 0.5±0.9. These results are also consistent with the

description by Irving *et al.*[153] of ligands with –OH functional groups. In the europium 8-hydroxyquinoline complexation reaction, the ligand with –OH functional group is the deprotonated 8-hydroxyquinoline, the proton is the Eu^{3+} ion, and the europium 8-hydroxyquinoline complex is analogous to the protonated oxygen group. Adapting the description of the system in Irving *et al.*[153] to the 8-hydroxyquinoline complexation, the increase in organic character of the mixed solvent leads to increased ionic interaction between the europium and negatively charged oxygen in the deprotonated 8-hydroxyquinoline causing the formation of hydrolysis species. The discussion involving ΔG_t in the hydrolysis reactions also apply to the formation of europium 8-hydroxyquinoline complexes. The increase of ΔG_t for free europium in the system still favors its elimination from the system through 8-hydroxyquinoline complexation.
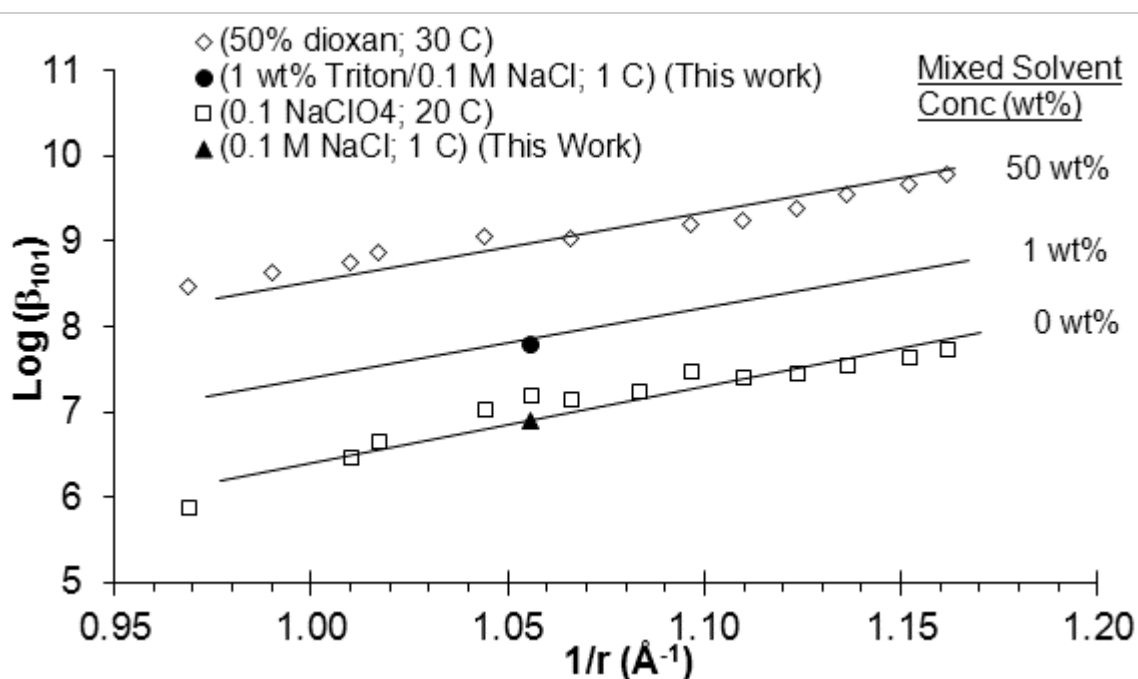
Figure 3.46- Comparison of Literature data for the formation of $[Eu(Q)]^{2+}$ in 50% dioxane (at T=30 °C), and 0% dioxane (at T = 20 °C) with the observed values at 1 wt% Triton X-114 (at 1 °C) and 0 wt% Triton X-114 (at 1 °C).
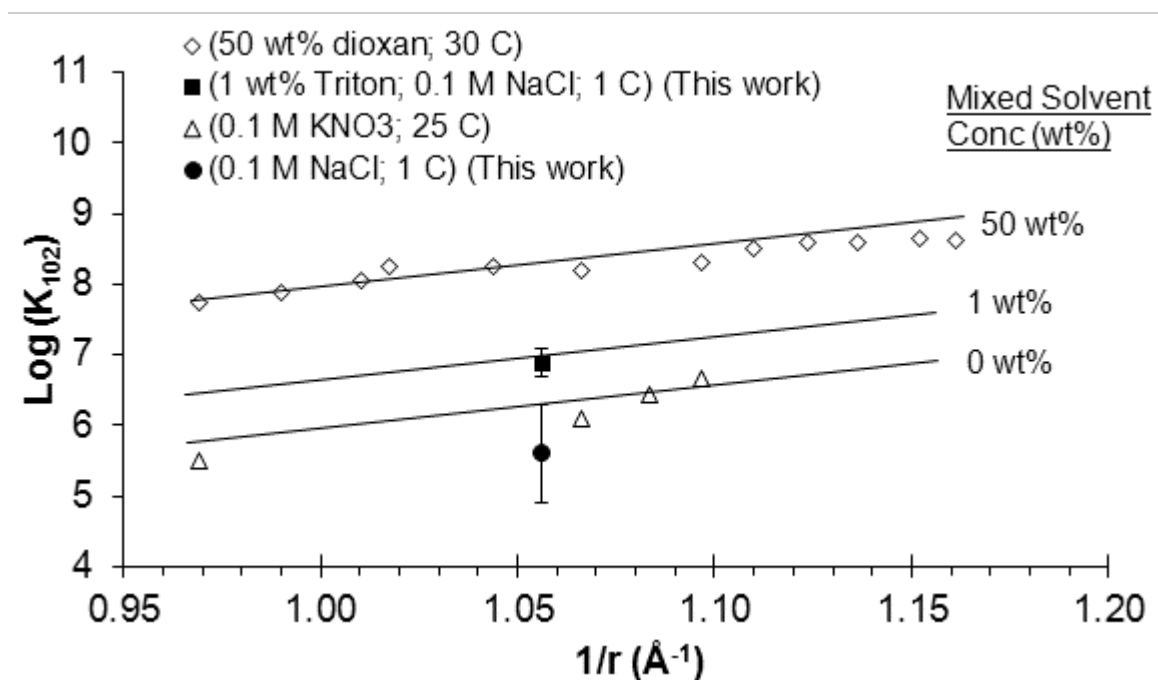
Figure 3.47-- Comparison of Literature data for the formation of $[Eu(Q)_2]^+$ in 50% dioxane (at T=30 °C), and 0% dioxane (at T = 25 °C) with the observed values at 1 wt% Triton X-114 (at 1 °C) and 0 wt% Triton X-114 (at 1 °C).

Table 3.27- A comparison of the stability constants obtained from the H_2O and the H_2O/Triton X-114 systems.

Species Formed	Parameter	H_2O	H_2O/Triton X-114
		pK	pK
$[Eu(Q)]^{2+}$	β_{101}	-6.9±0.1	-7.78±0.04
$[Eu(Q)_2]^+$	β_{102}	-5.6±0.7	-6.9±0.2
$[Eu(Q)_3]$	β_{103}	-6.2±0.9	-6.7±0.2

3.6   Conclusions

The speciation of 8-hydroxyquinoline and europium in both water and the Triton X-114/water mixed solvent at 1°C and 0.1 M NaCl has been quantified. The results are summarized in Table 3.28. The complex stability constants in the Triton X-114/Water system are all affected by the presence of Triton X-114. In the case of europium hydrolysis and europium 8-

hydroxyquinoline complexation, the formation of these species is favored in the presence of Triton. The formation of mixed 8-hydroxyquinoline/hydrolysis species defied this trend showing no change between the water and the Triton/water mixed solvent. 8-Hydroxyquinoline protonation behavior showed divergent trends in its pK_a values. The aromatic nitrogen group and the phenolic oxygen group showing a decrease and increase in pK_a in the Triton/water system, respectively.

Table 3.28- Summary of parameters measured in this work. All parameters were measured at 0.1 M NaCl and T = 1°C. The H_2O/Triton X-114 system also contained 1 wt% Triton X-114.

Reaction	H₂O System		Triton X-114/H₂O System		Technique
	pβ	pK	pβ	pK	
$H_2O \xrightarrow{K_w} H^+ + OH^-$	14.7	14.7	14.7	14.7	
$H_2Q^+ + OH^- \xrightarrow{K_{a1}} HQ + H_2O$	5.6±0.1	5.6±0.1	5.2±0.2	5.2±0.2	Pot.
	5.32±0.01	5.32±0.01	4.94±0.01	4.94±0.01	Spec.
$HQ + OH^- \xrightarrow{K_{a2}} Q^- + H_2O$	15.2±0.1	9.5±0.1	15.2±0.1	10.0±0.1	Pot.
	15.04±0.01	9.72±0.01	14.63±0.01	9.69±0.01	Spec.
$Eu^{3+} + H_2O \xrightarrow{\beta_{1-10}} [Eu(OH)]^{2+} + H^+$	-8.0±0.2	-8.0±0.2	-7.1±0.1	-7.1±0.1	Pot.
$Eu^{3+} + 2H_2O \xrightarrow{\beta_{1-20}} [Eu(OH)_2]^+ + 2H^+$	-15.8±0.1	-7.7±0.1	-12.8±0.1	-5.7±0.1	Pot.
$Eu^{3+} + 3H_2O \xrightarrow{\beta_{1-30}} [Eu(OH)_3] + 3H^+$	-22.5±0.2	-6.8±0.2	-18.7±0.1	-5.9±0.2	Pot.
$Eu^{3+} + Q^- \xrightarrow{\beta_{101}} [Eu(Q)]^{2+}$	-6.9±0.1	-6.9±0.1	-7.78±0.04	-7.78±0.04	Pot.
$Eu^{3+} + 2Q^- \xrightarrow{\beta_{102}} [Eu(Q)_2]^+$	-12.5±0.7	-5.6±0.7	-14.7±0.2	-6.9±0.2	Pot.
$Eu^{3+} + 3Q^- \xrightarrow{\beta_{103}} [Eu(Q)_3]$	-18.7±0.5	-6.2±0.9	-21.4±0.2	-6.7±0.2	Pot.
$Eu^{3+} + H_2O + Q^- \xrightarrow{\beta_{1-11}} [Eu(OH)(Q)]^+ + H^+$	-13.3±0.1	-6.4±0.1	-14.4±0.1	-6.6±0.1	Pot.
$Eu^{3+} + 2H_2O + Q^- \xrightarrow{\beta_{1-21}} [Eu(OH)_2(Q)] + 2H^+$	-18.8±0.1	-5.6±0.1	-19.8±0.1	-5.4±0.1	Pot.
$Eu^{3+} + H_2O + 2Q^- \xrightarrow{\beta_{1-12}} [Eu(OH)(Q)_2]^- + H^+$	-19.3±0.3	-6.7±0.3	-21.1±0.2	-6.4±0.2	Pot.
$Eu^{+3} + H^+ + Q^- \xrightarrow{\beta_{111}} [Eu(HQ)]^{3+}$	N/A	N/A	-14.07±0.06	-6.28±0.06	Pot.
$H(XX) + OH^- \xrightarrow{K_{XX}} XX^- + H_2O$	N/A	N/A	6.3±0.1	6.3±0.1	Pot.

CHAPTER 4

CONSLUSIONS

4.1 <u>Conclusions Concerning the TALSPEAK Study</u>

The conditional ionization constant (pK_a) of lactic acid at I = 2.0 M NaCl was quantified over

the temperature range of 25–65°C. The results show very little change with temperature and a

relatively small standard enthalpy of reaction. This work is of importance to the development of

the TALSPEAK extraction model, specifically providing information that is useful for modeling the

aqueous phase activity coefficients for lactate media solutions. Expanding this work to other

ionic strengths will provide a more complete data set that will enable modeling of aqueous

activity coefficients for lactate solutions in the TALSPEAK system.

Additional studies described in this work explored speciation of Nd^{3+} in the organic phase,

including aggregation of HA under a range of conditions. Extractions of Nd^{3+} by varied

concentration HA (0–1 M) from HCl media at both pH 1 and 4 were compared with control

samples without Nd^{3+} that were also at pH 1 and 4. A second set of samples measured the

extraction of Nd^{3+} over the same HA concentrations from 1 M lactate media at pH 1 and 4. The

initial concentration of Nd^{3+} was 30 mM for both HCl and lactate experiments; one additional

experiment in lactate medium at 60 mM was also performed. The lactate series of extractions

was also compared with non-Nd^{3+} control experiments at pH 1 and 4.

In the non-Nd^{3+} control samples for the HCl system [i.e. pH (1, 4) + 0 mM Nd + HCl], and the

pH 1 lactate system [pH 1 + 0 mM Nd + Lac] an average aggregation number of 2 was observed,

indicating that HA existed predominantly as a dimer. In the corresponding Nd^{3+} containing

systems [i.e. pH (1, 4) + 30 mM Nd + HCl; pH 1 + 30 mM Nd + Lac] there was an increase in

aggregation that was consistent with the mechanism for Nd^{3+} extraction by HA. Buffering in the

pH 4 lactate systems led to high loading and the formation of large HA aggregates. In the pH 4 +

0 mM Nd + Lac system the average aggregation was 3.82 ± 0.05 which when modeled, showed

the formation of NaA(HA) and NaLac(HA)$_Z$ with Z = 5.1 ± 0.3. The average aggregation in the pH

4 + (30, 60) mM Nd + Lac systems showed formation of high order aggregates at low [HA]$_{org}$ with

an average aggregation as high as 100 observed. These high order aggregates diminished with

increasing [HA]$_{org}$ until a constant aggregation was reached that corresponded with the low-

loading extraction mechanism of Nd^{3+} by HA.

The Nd^{3+} distribution results were consistent with the extraction mechanism for Nd^{3+} by HA

with the HA dimer stoichiometric coefficient (n) = 4 when Nd^{3+} loading of HA was moderate to

low. Modeling of these systems by SXLSQI gave an equilibrium constant or Log K$_{Nd}$ = −0.14 ±

0.06. In the pH 4 + (30, 60) mM Nd + Lac systems where Nd^{3+} loading of HA was high, Nd^{3+}

saturated the organic phase at low [HA]$_{org}$, and was quantitatively extracted at higher [HA]$_{org}$.

The Na$^+$ extraction was suppressed in systems with pH of 1, with partial Nd^{3+} loading [pH (1,

4) + 30 mM Nd + HCl; pH 1 + 30 mM Nd + Lac systems], or where the HA was saturated with Nd^{3+}

[pH 4 + (30, 60) mM Nd + Lac systems at HA concentrations < 4x total Nd^{3+}]. Na$^+$ extraction

occurred in systems where the pH was 4 and excess HA existed [pH 4 + 0 mM Nd + (HCl, Lac)

system; pH 4 + (30, 60) mM Nd + Lac systems at HA concentrations > 4x total Nd^{3+}], in the Lac

systems, Na$^+$ was extracted both as the HA sodium salt, and co-extracted with Lac. SXLSQI

modeling of the pH 4 + 0 mM Nd + HCl system gave an equilibrium constant or Log K$_{Na}$ = −0.989

± 0.009.

Lactate was found to extract in all the Lac systems in various species. At pH 1, lactate was

extracted as lactic acid, and possibly as NdLac^{2+} salt in the presence of Nd^{3+}. In the pH 4 + 0 mM

Nd + Lac system, and pH 4 + (30, 60) mM Nd + Lac systems at HA concentrations > 4x total Nd^{3+},

Lac was co-extracted with Na$^+$. In the pH 4 + (30, 60) mM Nd + Lac systems at HA concentrations

< 4x total Nd^{3+} Lac was co-extracted with Nd^{3+} as NdLac^{2+}.

Water was found in the organic phase in all systems. In all systems but the pH 4 + (0, 30, 60) mM Nd + Lac systems the organic phase under low loading retained the levels of water found in the washed solvent within experimental error. In the pH 4 + 0 mM Nd + HCl system where low Na^+ loading was observed, a slight increase in the water concentration was observed. In the pH 4 + (0, 30, 60) mM Nd + Lac systems, water extraction was observed to increase with $NdLac^{2+}$ extraction, and increased even more with Na^+ extraction at higher HA organic phase concentrations. Correlations of organic phase H_2O concentration with Nd^{3+} in the $NdLac^{2+}$ extraction regime indicates a 1:1 stoichiometry of water with Nd^{3+}. Correlations of organic phase H_2O concentration with Na^+ when present in the pH 4 + (0, 30, 60) mM Nd + Lac systems indicates a 3:1 stoichiometry of water with Na^+ or a hydration number of 3 for Na^+.

Organic phase visible spectroscopy in the pH (1, 4) + 30 mM Nd + HCl and pH 1 + 30 mM Nd + Lac systems indicate that the molar absorptivity of Nd^{3+} does not depend on pH or Nd^{3+} loading of the organic phase, but rather on the organic phase HA concentration. The similar spectra in the pH (1, 4) + 30 mM Nd + HCl systems indicate that the extraction mechanism is unchanged from pH 1 to pH 4 in HCl media at $[HA]_{org} > 0.05$ M. Changes in the organic phase visible spectra under the high loading conditions support the formation of $Nd(Lac)(HA)_2$. FTIR results support the ion exchange mechanism at low to moderate Nd^{3+} loading, and the extraction of $NdLac^{2+}$ and high HA loading, including the formation of high order aggregates with HA participating in phosphate bridging in the organic phase.

The overall speciation results (see Table 2.21 for summary of species and conditions where they were identified) indicate that at high Nd^{3+} loading in the pH 4 + Lac systems, Nd^{3+} exists as a highly aggregated, $(NdLacA_2)_x$ species in the organic phase. As loading is decreased (i.e. HA increased), the fraction of Nd^{3+} in the $(NdLacA_2)_x$ species decreases, while the fraction in the mono-nuclear $NdA_3(HA)$ species increases until a complete conversion to $NdA_3(HA)$ is achieved.

Other species identified with the conditions where they were observed is shown in Table 2.21).

Table 4.1- Summary of species identified in the systems studied with the conditions where they were observed.

Species	System	Organic Phase Condition (M HA)
H(Lac)	pH 1 + 0 mM Nd + Lac	0.025–1.0
Na(A)	pH 4 + 0 mM Nd + HCl	0.05–1.0
$Nd(A)_3(HA)$	pH 1 + 30 mM Nd + HCl	0.05–1.0
	pH 4 + 30 mM Nd + HCl	0.05–1.0
	pH 4 + 30 mM Nd + Lac	0.15–1.0
	pH 4 + 60 mM Nd + Lac	0.3–1.0
$[Nd(Lac)(A)_2]_x$ (x = 2–50)	pH 4 + 30 mM Nd + Lac	0.025–0.15
	pH 4 + 60 mM Nd + Lac	0.025–0.3
Na(Lac) + Na(A)	pH 4 + 0 mM Nd + Lac	0.05–1.0
	pH 4 + 30 mM Nd + Lac	0.15–1.0
	pH 4 + 60 mM Nd + Lac	0.3–1.0

The initial NMR results obtained through the scoping experiment indicate that the ^{13}C and ^{31}P spectra obtained from the analogous pH 4 + (30, 60) mM La^{3+} + Lac systems are sensitive to the speciation changes in the system and more work with these methods is warranted. A complete interpretation of this system was not undertaken.

4.2   Recommendations for Future Research: TALSPEAK

A full characterization of the TALSPEAK extraction behavior was not quite realized in this work. A characterization of the chloride extraction is necessary to resolve whether chloride co-extraction is occurring. This can be done using a ^{36}Cl radioactive tracer study using liquid scintillation counting. The full set of NMR data must be collected and interpreted to understand HA, lactate, Ln^{3+} and Na^+ speciation at high and low loading as well as through the transition. The method for this experiment was shown to work in the previous studies for ^{13}C, ^{31}P, and ^{23}Na

nuclei but must be extended to ^{139}La. The inclusion of DTPA is not anticipated to change the organic phase speciation of the system, but this assumption must be rigorously tested before accepted. This can be done by adding 0.05 M DTPA to the previously studied lactate system contact experiments and characterizing by VPO. If VPO measurements in the presence and absence of DTPA are consistent, then the influence of DTPA can be assumed to be negligible. The formation of DTPA neodymium complexes in the aqueous phase will need to be accounted for in the results, because DTPA is known to complex lanthanides strongly at pH greater than 2.5.

Characterization of the TALSPEAK system generated some unanswered questions that could be investigated. In the lactate distribution experiments, there was an increase in lactate distributions at pH 1 when neodymium was present than when it was absent. The lactate extraction exactly doubled under the conditions of the experiments in this work. It was not possible to conclude if the extra lactate extracted in the presence of neodymium was due to co-extraction with Nd as $[Nd(Lac)]^{2+}$ as it was at pH 4, or if the extra lactate was lactic acid that was extracted due to a more favorable solvation environment in the organic phase. This could be tested by performing other extractions at pH 1 in lactate, but with other concentrations of neodymium such as 15 and 45 mM. It is anticipated that the pattern in the excess lactate extraction would reveal more about the species present.

Another question in the TALSPEAK characterization experiments was in the water distribution results. In the HCl media experiments, and the lactate media at pH 1 there was no excess water extracted with neodymium in the organic phase. This was consistent with literature results for europium extraction under similar conditions. However, at high loading, one water per neodymium and per lactate was observed in the organic phase. It was never clear if the water in the organic phase was present in the inner coordination sphere of neodymium or

if it was associated with the lactate only. This question could be answered by performing Time Resolved Laser Fluorescence Spectroscopy (TRLFS) experiments using europium or terbium in place of neodymium at a single high loading condition. By increasing the percent of deuterated water in the aqueous phase through a series of extractions at the same loading condition, the change in the fluorescence lifetime of the europium would indicate if the water was in the inner coordination sphere of the extracted lanthanide. If there was no change in fluorescence lifetime of europium as a function of percent deuterated water in the aqueous phase, then the extracted under the high loading conditions is associated with lactate and is not in the inner coordination sphere of the metal.

Once the TALSPEAK systems are fully characterized, extraction modeling is needed to understand the equilibrium constants that describe the system. This modeling has already been performed for the systems involving extraction from the HCl media because pitzer parameters were available to model the activities of the species in the aqueous phase. There are no pitzer parameters available for solutions containing mixtures of lanthanides, lactate and sodium. These parameters must be quantified before the extraction modeling in the lactate media can be performed. The characterization of the pK_a of lactate at various ionic strengths and temperatures is a good beginning. The technique described in this work is effective for a quantitative analysis.

In addition to the pK_a of lactate, the activity of water, lactate and neodymium must be quantified. This can be done through the measurement of the water activity of solutions of these constituents alone and mixed together in a systematic series. By modeling the change in water activity as a function of the concentrations of each constituent, the thermodynamic parameters used to predict the activity of the constituents can be obtained.

4.3   <u>Conclusions Concerning the Europium 8-Hydroxyquinoline Work</u>

The speciation of 8-hydroxyquinoline and europium in both water and the Triton X-114/water mixed solvent at 1°C and 0.1 M NaCl has been quantified. The complex stability constants in the Triton X-114/Water system are all affected by the presence of Triton X-114. In the case of europium hydrolysis and europium 8-hydroxyquinoline complexation, the formation of these species is favored in the presence of Triton. The formation of mixed 8-hydroxyquinoline/hydrolysis species defied this trend showing no change between the water and the Triton/water mixed solvent. The 8-hydroxyquinoline protonation behavior showed divergent trends in its pK_a values. The aromatic nitrogen group and the phenolic oxygen group showing a decrease and increase in pK_a in the Triton/water system, respectively.

4.4   <u>Recommendations for Future Research: Europium 8-Hydroxyquinoline</u>

The work involving europium 8-hydroxyquinoline complexation is promising, but needs additional effort to be complete. Because cloud point extraction relies on a separation technique involving a temperature change, the complexation parameters of the system must be measured under different conditions so the system behavior is understood. A similar study of the behavior of europium and 8-hydroxyquinoline as was present in this work should be repeated using the Triton X-100 surfactant that is very similar to Triton X-114 but has a higher cloud point temperature of 60°C. This will allow potentiometric determination of system behavior at higher temperatures. The issue of the protolytic impurity must also be resolved. Efforts to eliminate carbon dioxide absorption during titration, such as utilizing an argon gas purge, may resolve this issue if the impurity is carbonate absorbed from the atmosphere. If efforts to eliminate carbon dioxide prove unsuccessful, then performing a purification of the Triton, or obtaining a higher purity material may solve the problem.

Measuring the stability constants for actinides in this system by the potentiometric technique employed in this study is problematic due to the high specific activity of the trivalent actinides. An alternative would be to use TRLFS to measure the stability constants of curium. Curium has been shown to fluoresce, allowing for its study by TRLFS at very low concentrations.

Cloud point extraction data comparing the separation of the lanthanides and the actinides must be collected if the trivalent actinide trivalent lanthanide separation potential is to be understood. This can be done by tracer study using europium, americium or curium and measuring the distribution in cloud point extraction experiments. By keeping the concentration of the metal much less than the ligand (less than 10% of theoretical loading), log-slope data can be analyzed for mechanistic information. Separation factors can also be calculated from the distribution ratios.

With the complexation constants and the extraction data, the separation of the trivalent lanthanides from the trivalent actinides can be modeled. Modeled data would be compared with extraction data to ensure a good fit. Modeling of the system can show if the optimum separation condition was observed during experimental separations, or if a different condition should be re-tested for optimum separation.

One unanswered question in the europium 8-hydroquinoline complexation work is why the mixed hydrolysis 8-hydroxyquinoline species formation constants were not changed in the presence of Triton. An initial effort to study this question would be to try and crystallize the mixed hydrolysis 8-hydroxyquinoline species from the water system and perform powder or single crystal X-ray diffraction measurements to work out the complex's coordination chemistry. While crystallized compounds are not always the same as the species in solution, they may offer clues as to why the surfactant did not affect their formation in solution.

APPENDIX 1

Instructions and Description of the Use of SQUAD

A1.1 General Description

Stability **QU**otients from **A**bsorbance **D**ata, or SQUAD, is a FORTAN compiled program that

uses user-supplied absorbance spectra, metal and ligand concentrations, and pH to calculate

complexation stability constants. The program limitations depend on the compiled program and

differ slightly for different compilations. In the current manual, the compilation used is entitled

"sqd5.exe" and has the following limits: spectra are limited to 140 data points, up to 35 spectra

per run, 10 modeled complexes, with 6 varied complexation constants allowed. It is expected

that much of the information provided herein will apply to other SQUAD compilations that have

different limitations. The limitations are described in accompanying "Readme" type files, or can

be discovered by the user through trial and error.

A1.2 Data Preparation

Before SQUAD can model absorbance data an appropriate input file must be created. Most

spectrometers today have a resolution of less than 1 nm, which means that, given the 140 data

points per spectrum limitation, only a small window of the spectrum can be fit. An alternative is

to use a wider window of the spectrum by only using every 2nd, 3rd or nth data point. A

spreadsheet program such as Excel can be programmed to provide these truncated spectra. To

provide an example, the titration of 8-hydroxyquinoline (HQ) by NaOH will be used to

demonstrate the data preparation process. The following spectra were obtained at 0°C (see

Figure A1.1 and Figure A1.2).
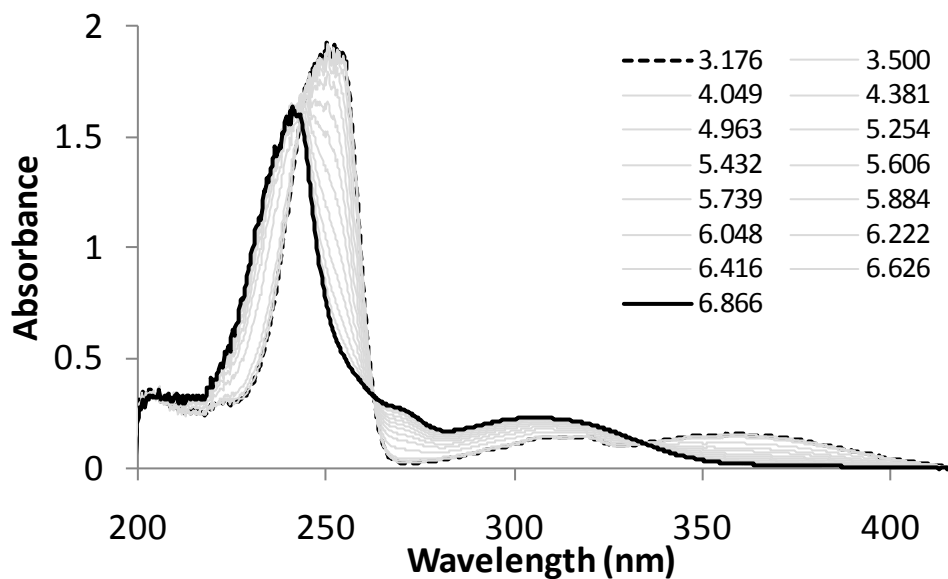
Figure A1.1- pH titration of HQ from pH 3.18 to 6.87 at T = 0°C.
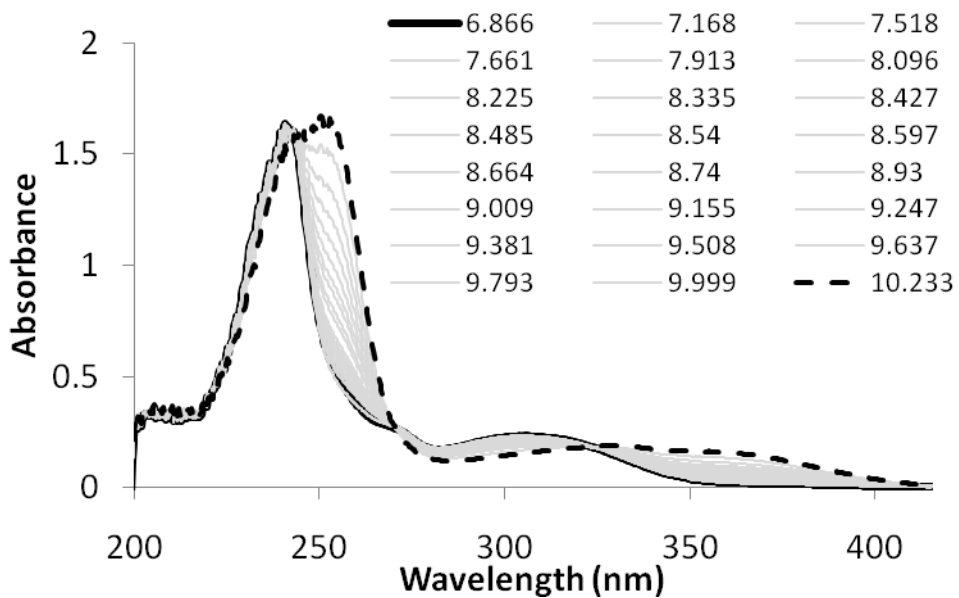
Figure A1.2- pH titration of HQ from pH 6.87 to 10.23 at T = 0°C.

The HQ titration spectrum is from 220-445 nm. The average resolution for these spectra is 0.27 nm for a total of 883 data points. Since this exceeds the data limit for SQUAD, a

spreadsheet was programmed to use only a 1 out of every n spectra for a total of 140 data

points. A screen shot shows the spreadsheet parameters used in preparing the data.

	A	B	C	D	E	F	G	H	
1		Start λ	Avg Step	Spec jump			0	0	
2		220	1.625	6			3.176	3.5	
3		Start λ	Final λ	total pts			0	0.0	
4		219.77	445.69	140	0	0.0	0.00000000	0.00000000	0.0(
5					[8-HQ]	0.0	0.00009942	0.00009889	0.0(
6		2		3	4	5	6	7	
7	#	Spec #	Sep (nm)	WL (nm)		1.8163	1.8163	1.8076	
8							0.0069	0.0075	
9									
10	1	92		219.77	92	0	0.2652	0.2619	
11	2	98	1.64	221.41	98	0	0.2935	0.2911	
12	3	104	1.64	223.05	104	0	0.3167	0.3143	
13	4	110	1.65	224.7	110	0	0.3077	0.3079	
14	5	116	1.64	226.34	116	0	0.3300	0.3316	
15	6	122	1.64	227.98	122	0	0.3591	0.3622	
16	7	128	1.64	229.62	128	0	0.4007	0.4052	
17	8	134	1.64	231.26	134	0	0.4644	0.4703	

Figure A1.3- Spectrum preparation spreadsheet screenshot.

As is shown in Figure A1.3, the nominal starting wavelength (λ) was 220, with the

spreadsheet function used returning the actual value of 219.77 nm. The "spec jump" parameter,

which is the 'n' in the "1 out of every n spectra" shows that every 6th point was used. The final λ

is 445.69 nm if all 140 data points are used. The spreadsheet creates a truncated spectrum

where only every 6th data point is used, and from this truncated spectrum calculates the average

step between data points which is a necessary parameter to know that will be input into the

SQUAD program.

The truncated spectra now need to be saved into individual files that can be accessed by the

GWBASIC.EXE program. The GWBASIC.EXE program changes the orientation of a spectral file

from a vertical column of numbers to a horizontal row with text-wrapping so that it will become

a block of numbers as shown in Figure A1.4.
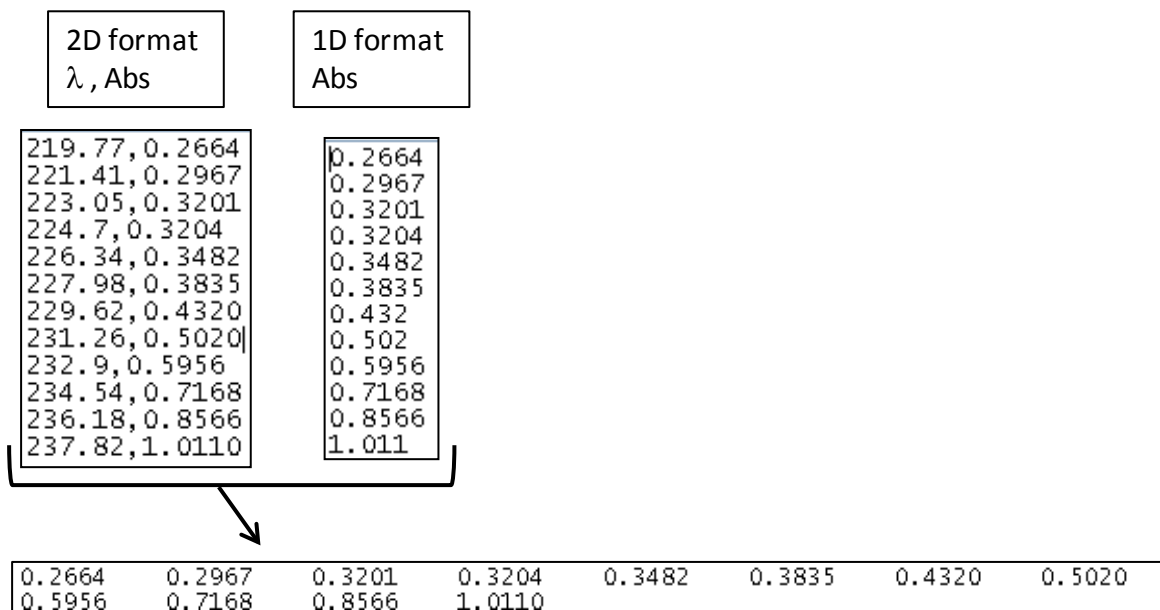
Figure A1.4- Format manipulation by "GWBASIC.EXE" on each Spectum file.

GWBASIC.EXE accepts the "comma separated values" file format or .CSV. This format can be

created if the data are copied and pasted one spectrum at a time into a blank Excel spreadsheet

and each file is saved as a .CSV file.

The user can create either a 1D or 2D absorbance files (see Figure A1.4). The 1D consists of

one column of absorbance values only. The 2D file format contains the wavelength values in the

first column and the absorbance values in the second column. The GWBASIC.EXE program will

discard the wavelength column of data in the 2D file format. While the GWBASIC.EXE program

does not make use of these values, the user may find this format useful if they return to these

data files at a later date. After saving the spectral data files in the .CSV file format, the user must

remove the .CSV file extension manually prior to manipulating or reading these files into the

GWBASIC.EXE program. Once this is done the user can move on to making a header file

described in the next section.

A1.3 Creating a SQUAD Header File

Once individual spectra are in the ".CSV" file format it is time to create the SQUAD input file.

GWBASIC.EXE and the SQUAD-IN-BAS must be moved to the same folder as the spectral data

files. In addition, a header file must be moved to this folder. Generally a header file is created by

the user, or the user can alter a previously existing header file. There is no program that will

generate the header file, but the "Notepad" program can be used to create or alter header and

input files.[1] An example header file that will be explained in detail is shown below.

A1.3.1 Example of the SQUAD Header File

```
* * * * * * * * * * * * * * * * * * * * * * * * * * * * * * * *
 _ _ _ _ _ _ _ _ _ _ _ _ _ _ _ _ _ _ _ _ _ _ _ _ _ _ _ _ _ _ 

1      8-hydroxyquinoline pka fitting experiment. Wavelength range: 219...445.0nm
2      System 0.1M NaCl; April 2, 2009 experiment, Dip-probe with normal pathlength (10mm)

3      DICTIONARY:
4      MTL1=Nd;LIG1=Q;PROT=H;HYDX=OH:
5      END:
6      SPECIES:
7      Nd(1)Q(1);5.81;FB;FE:
8      H(1)Q(1);9.02;VB;VE:
9      H(2)Q(1);15.02;VB;VE:
10     END:
11     OTHER:
```

---

[1] Column spacing can be verified in "Notepad" by activating the status bar in the "View" dropdown menu. The status bar will display the cursor position in the lower right corner. To check the correct column spacing, place the cursor at the immediate left of the character of interest.

```
12   Q;FE:
13   END:
14   DATA:
15   219.77      445.69      +1.625
16   LOGB
17   PRIN
18   CARD
19   MR
20   NOPL
21   CRT
22   50
23   1.0
24   MOL.ABS.:
25   Q:
26   END:
27   1.65974
28   1.51247
29   1.38166
30   1.26868
31   1.16853
32   1.08550
33   0.11676
...
(lines 34-143 omitted for brevity)
...
144  0.11121
145  0.10984
146  0.11090
147  0.11015
148  BASELINE:
149  -.0101700 -.0098500 -.0096500 -.0092000 -.0097000 -.0094300 -.0094700 -.0095200
150  -.0092300 -.0087800 -.0084800 -.0080700 -.0075500 -.0072900 -.0074200 -.0078200
151  -.0075400 -.0069900 -.0074900 -.0075800 -.0072500 -.0067000 -.0061900 -.0062200
152  -.0062500 -.0059100 -.0064700 -.0063100 -.0069600 -.0065600 -.0067500 -.0060000
153  -.0054900 -.0056600 -.0053900 -.0048200 -.0048200 -.0056600 -.0056400 -.0057600
154  -.0061900 -.0060000 -.0058000 -.0049100 -.0044300 -.0038300 -.0036600 -.0044300
155  -.0048300 -.0059100 -.0051400 -.0057300 -.0054300 -.0051300 -.0055300 -.0046400
156  -.0047600 -.0041700 -.0034300 -.0042500 -.0045200 -.0046900 -.0047400 -.0049600
157  -.0053800 -.0053000 -.0047900 -.0044800 -.0037000 -.0041800 -.0034500 -.0037200
158  -.0037400 -.0037400 -.0049700 -.0046400 -.0042200 -.0043600 -.0043700 -.0043800
159  -.0041900 -.0042600 -.0042300 -.0038600 -.0034400 -.0027700 -.0035100 -.0042600
160  -.0044200 -.0042000 -.0045100 -.0044400 -.0047500 -.0043400 -.0035200  .0045600
161  .0049400  .0055000  .0055300  .0051400  .0054000  .0047500  .0055800  .0044700
162  .0040000  .0039100  .0049200  .0053600  .0036100  .0040600  .0041200  .0039800
163  .0033000  .0035900  .0034800  .0030400  .0034400  .0031900  .0038800  .0036100
164  .0032900  .0023100
165  SPECTRA:
```

* *
‾ ‾

The left hand column of numbers was not a part of the original file but is included to increase

the ease of referencing specific lines of the header file while describing their function.

A1.3.2 Description of the SQUAD Header File Line-by-line

A) <u>Lines 1 and 2</u>: Descriptive text

    a) <u>Function</u>: To provide a description of the current experiment. It does not have any effect on the SQUAD program's operation

    b) <u>Commands and Syntax</u>: Regular text, numbers and punctuation are used here. This section is always limited to the first two lines. No COLON is required to finish these lines.

B) <u>Line 3</u>: Initiation of the "Dictionary section

    a) <u>Function</u>: This begins the dictionary section where all metal and ligands used in the model are defined by user supplied names.

    b) <u>Commands and Syntax</u>: "DICTIONARY" followed by a COLON to finish the line.

C) <u>Line 4</u>: Declaration of metal and ligands used in the model

    a) <u>Function</u>: This section assigns specific names to the metals (up to 2), ligands (up to 2), and proton and hydroxide ions that will be used in the model.

    b) <u>Commands and Syntax</u>: SQUAD programs are CASE SENSITVE, so all commands are in capitol letters. Names supplied by user can be mixtures of upper and lower case, however. SQUAD recognizes up to 2 metals ("MTL1", "MTL2"), 2 ligands ("LIG1", "LIG2"), proton "PROT", and hydroxide "HYDX". Even if a chemical system does not contain a metal, a metal must be included in the program or SQUAD will crash. If there is no metal present in the actual system, simply set the metal concentration to an extremely low number. A concentration of 1E-19 M has worked in this author's experience.

D) <u>Line 5</u>: End of "Dictionary" section

    a) <u>Function</u>: This ends the dictionary section.

    b) <u>Commands and Syntax</u>: "END" followed by a COLON to finish the line.

E) <u>Line 6</u>: Beginning of "Species" declarations

    a) <u>Function</u>: This begins the species declaration section where the species are defined by stoichiometry, and formation constants are entered.

    b) <u>Commands and Syntax</u>: "SPECIES" followed by a COLON to finish the line.

F) <u>Line 7</u>: Species declarations

   a) <u>Function</u>: All formation constants are mathematically defined by the user.

   b) <u>Commands and Syntax</u>:

      i) <u>Species Formed</u>: Using the user-defined names from the "Dictionary" section (see line 4) the species stoichiometry is defined. The stoichiometric coefficient is enclosed in parentheses (such as 'H(2)Q(1)' for the species $[H_2Q]^+$). An example of the type of expression for the species formation by SQUAD is shown in equation (1). Up to 10 species can be included in this section with 1 species per line. The species definition is followed by a semi-colon.

$$M + 2L \xrightarrow{\beta_{12}} M(1)L(2) \tag{1}$$
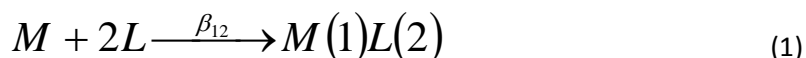
      ii) <u>Stability constant Value or initial guess</u>: This value is the log β for the expression defined in the previous step. *This number is followed by a semi-colon.*

      iii) <u>Fixed or Variable log β</u>: The two commands allowed here are "VB" for "variable log β" or "FB" for "fixed log β". "Variable" refers to an unknown value that SQUAD will solve for using the user-supplied guess, whereas fixed is a known value supplied by the user. SQUAD will only allow a total of 6 species to have a variable log β. If the guessed value is outside the program's test criteria, SQUAD will usually replace it with a better one at the initiation of the calculations. All caps must be used here or SQUAD will return an error. *This command is followed by a semi-colon.*

      iv) <u>Fixed or Variable Molar Absorptivity, ε</u>: SQUAD can solve for the molar absorptivity of different complexes in the system. The two commands allowed here are "FE" for Fixed Molar Absorptivity or "VE" for Variable Molar Absorptivity. If "FE" is declared here and no molar absorptivity spectrum is supplied to the program later in the header, SQUAD assumes that the species has a constant, zero molar absorptivity. All caps must be used here or SQUAD will return an error. *This command is followed by a **COLON** because it is the end of the line.*

G) <u>Line 10</u>: End of Species declaration section

   a) <u>Function</u>: Ends the section where species can be declared

H) <u>Line 11</u>: Begins "OTHER" species instructions section **<u><<<Optional>>>: Omit lines 11–13 together if the "OTHER" section is not used.</u>**

   a) <u>Function</u>: Introduces the section that allows the user to specify any free species that contain a molar absorbance.

   b) <u>Commands and Syntax</u>: "OTHER" followed by a **COLON** *to finish the line*.

I) <u>Line 12</u>: Other species declaration **<u><<<Optional>>>: Omit lines 11–13 together if the "OTHER" section is not used.</u>**

a) Function: Allows the user to specify which free species have a molar absorbance.

b) Commands and Syntax: As many lines can be used as there are free species that have a molar absorbance; one species per line.

   i) Free Species name: Use the free species as it was defined by the user in the dictionary. *This is followed by a semi-colon*.

   ii) Fixed or Variable Molar Absorptivity or ε: The two commands allowed here are "FE" for Fixed Molar Absorptivity or "VE" for Variable Molar Absorptivity. If "FE" is declared here and no molar absorptivity spectrum is supplied to the program later in the header, SQUAD assumes that the species has a constant, zero molar absorptivity (this declaration would be useless since SQUAD assumes this if no declaration is made in the "OTHER" section. So if using the "FE" command here, make sure the spectrum is supplied later). *All caps must be used here or SQUAD will return an error. This command is followed by a **COLON** because it is the end of the line*.

J) Line 13: End of "OTHER" section" **<<<Optional>>>: Omit lines 11–13 together if the "OTHER" section is not used.**

   a) Function: Signals to SQUAD that there are no other free species with a molar absorbance to be declared.

   b) Commands and Syntax: "END" followed by a **COLON** *to finish the line*.

K) Line 14: Beginning of the "DATA" section

   a) Function: Gives instruction and clarification for modeling the data.

   b) Commands and Syntax: "DATA" followed by a **COLON** *to end the line*.

L) Line 15: Wavelength declaration

   a) Function: This line defines the wavelength range of the spectrum. It is not mathematically important in modeling, but is necessary for accurately displaying the SQUAD-calculated molar absorptivities. The program will refuse to run if the correct information is not supplied here. No error is displayed in the output file to indicate that the wavelength range or increment is incorrect, so this line must be checked manually.

   b) Commands and Syntax:

   i) Column 1= Starting wavelength: The lower bound of the spectrum wavelength. This number is in decimal format. There is **NO SEMI-COLON** *after this number*. Add spaces until column 13 is reached and then enter the next value (described below) in this line.

   ii) Column 13=Ending wavelength: The lower bound of the spectrum wavelength. This number is in decimal format. Because no semi-colon is used after the previous

number, it is important that this number's first digit be placed in column 13 by adding spaces after the previous number in this line. The column number can be checked by placing the cursor immediately to the left of the character in question and checking the status bar in the lower right-hand corner of window when using the "Notepad" program. It is not recommended to use "Word" or other word processing software for editing SQUAD input files. There is **NO SEMI-COLON** *after this number*. Add spaces until column 23 is reached and then enter the next value (described below) in this line.

  iii) <u>Column 23=Wavelength Increment Value</u>: Because wavelengths of the absorbance values are not explicitly provided to the program, SQUAD calculates the wavelengths for each absorbance value using an increment value. The increment between each wavelength in the spectrum is written with a '+' leading the decimal number. The '+' must be positioned in the 23 column by spaces or SQUAD will not acquire the value correctly. If the (starting wavelength) + [(the number of points in a spectrum) × (Wavelength Increment Value)] is not equal to the final Ending Wavelength, then SQUAD will crash, generating an incomplete output file that has no error message, so it is necessary to manually check this input line.

M) <u>Line 16</u>: Stability constant format options

 a) <u>Function</u>: Instructs SQUAD what form the stability constants are supplied in the "SPECIES" section and determines the format for the calculated/refined stability constants.

 b) <u>Commands and Syntax</u>: Allowed values here are "LOGB" or "EXPB", *in all caps*. These signify that the stability constants will be refined as $\log(\beta)$, or β (i.e. $10\char`^(\log \beta)$).

N) <u>Line 17</u>: Full or abbreviated display of input data in the output file

 a) <u>Function</u>: Instructs SQUAD whether to display the full set of input data or an abbreviated version in the output file

 b) <u>Commands and Syntax</u>: Allowed values here are "PRIN" for full input data display, or "NOPR" for the abbreviated input data display. *These commands must be in all caps*.

O) <u>Line 18</u>: Option to check initial guess values prior to calculation

 a) <u>Function</u>: Instructs SQUAD whether to test the initial guesses provided by the user prior to calculation. This test is called a "GRID SEARCH" in the output file.

 b) <u>Commands and Syntax</u>: Allowed values here are "CARD" if the test of the initial estimate is desired, or "NOCD" for no test of the initial estimated values. *These commands must be in all caps*. The "NOCD" command would only be used if the user were adamant that the program start calculations with the user supplied values. It is the experience of the author that using the "CARD" option is generally preferred.

P) <u>Line 19</u>: Algorithm used to calculate the molar absorbance of the variable absorbance species.

a) Function: This instructs SQUAD whether to use a multiple regression or non-negative least squares fitting algorithm.

b) Commands and Syntax: "MR" is used for multiple regression and "NNLS" is used for non-negative least squares. Based on the author's experiences, the algorithm has little effect on the data outcome. If the spectra, pH and concentrations are correct, then either algorithm is appropriate.

Q) Line 20: Instructs SQUAD whether to plot or not to plot

a) Function: This command line has no perceived function in the SQUAD program when run on modern computers. It is believed to be an artifact from an older type of system and maybe instructed a printer whether to plot the results or not. The only important thing is that one of the allowed commands must be used or the program will crash.

b) Commands and Syntax: "PLOT" or "NOPL". If omitted there will be an error and SQUAD will not run.

R) Line 21: Another artifact that must be included, but does not appear to affect the function of SQUAD

a) Function: Must be present or the program will prematurely stop and provide an error message.

b) Commands and Syntax: "PAGE" or "CRT"

S) Line 22: Maximum number of iterations

a) Function: Tells SQUAD how many interations are allowed before SQUAD assumes that no solution was reached.

b) Commands and Syntax: Positive integer value. "50" is the default.

T) Line 23: Activity coefficient for H^+ ions.

a) Function: Informs SQUAD of the activity of the H^+ ions in solution.

b) Commands and Syntax: This value can be *any decimal value*. "1.0" is the default value. When the unreasonable value of "50.0" was used, SQUAD did perform calculations, so this input line must be checked manually.

U) Line 24: Begins the declaration of species with a declared molar absorbance in the header file. **<<<Optional>>>: Omit lines 24–147 together if the "MOL.ABS." section is not used.**

a) Function: Begins the section where species with a fixed and non-zero molar absorbance are declared.

b) Commands and Syntax: The command for this line is "MOL.ABS." and *the line ends with a **COLON***.

V) Line 25: Declaration of species with a fixed and non-zero molar absorbance. **<<<Optional>>>: Omit lines 24–147 together if the "MOL.ABS." section is not used.**

   a) Function: This line tells SQUAD the column order in which the species with molar absorbances will be specified by the user.

   b) Commands and Syntax: All species with a fixed and non-zero absorbance are *listed separated by a semi-colon. A **COLON** ends the line after the last species*. Any type of species, whether a free species, or one that forms a complex can be declared in this section. Species that form a complex are listed in the same syntax as in the "SPECIES" section e.g.: "Q" (for free hq) or "H(1)Q(1)" [for the species H(1)hq(1)]. All species that are listed on this line must be declared either in the "OTHER:" or the "SPECIES" sections as having a fixed molar absorbance or "FE". Any species listed as "FE" in the "OTHER" or the "SPECIES" sections that are not listed in the "MOL.ABS." section will be assumed by SQUAD to have zero molar absorbance.

W) Line 26: End of the "MOL.ABS." section. **<<<Optional>>>: Omit lines 24–147 together if the "MOL.ABS." section is not used.**

   a) Function: This tells SQUAD that this section is complete

X) Lines 27-147: This is the fixed molar absorbance for the species declared in line 25 in this example. **<<<Optional>>>: Omit lines 24–147 together if the "MOL.ABS." section is not used.**

   a) Function: These are the actual values read in for the species listed in line 25.

   b) Commands and Syntax: In the event that more than one species is listed in the "MOL.ABS." section the molar absorbance for the listed species should be added as columns in the order that they are declared, left to right. Data columns must be aligned with the following text columns: 1, 11, 21, 31, 41, 51, etc. for as many columns are needed. *No semi-colon or colons are needed to separate the values. They need only be aligned in the proper text columns to be read in properly*.

Y) Line 148: Begins the declared baseline correction. **<<<Optional>>>: Omit lines 148–164 together if the "BASELINE" section is not used.**

   a) Function: If all spectra are in need of a baseline correction, this instructs SQUAD that a baseline will be provided.

   b) Commands and Syntax: "BASELINE" followed by **COLON** *to end the line*.

Z) Lines 149-164: Values provided as the baseline to be applied to all the spectra. **<<<Optional>>>: Omit lines 148–164 together if the "BASELINE" section is not used.**

   a) Function: These are the values that represent the baseline occurring in all the spectra.

   b) Commands and Syntax: This block of text is a horizontal row of absorbance data that is wrapped just as the GWBASIC.EXE program will do to the spectra files. It is

recommended that the baseline be prepared in the same manner as the spectra files are in the GWBASIC.EXE program and pasted into either the header, or the input file. If GWBASIC.EXE is used to prepare this block of numbers, the spacing for proper read-in to the SQUAD program will be already done.

AA) <u>Line 166</u>: Beginning of the "SPECTRA" section

    a) <u>Function</u>: Informs SQUAD that all necessary information has been provided, except the solution absorbance data.

    b) <u>Commands and Syntax</u>: "SPECTRA:" followed by a **COLON** *to end the line*.

This concludes the description of the header file. It is noted that the line numbers cited in this description are not absolute values of the lines where these commands should appear, but are merely references to the header file example presented. The order of the lines is important, but the optional sections, when not needed, will change the actual line numbers where these different commands appear. NOTE: *Before the header file can be used by the GWBASIC.EXE program, the file extension .TXT must be manually removed by the user*.

A1.4 <u>Creating the SQUAD input file using GWBASIC.EXE while running the SQUAD-IN.BAS instruction file</u>

It is important to verify that all files needed by the GWBASIC.EXE program are in the same folder. The files required for the operations described in this section are: 1) all the absorbance data files saved individually in the .CSV file format, *but with the .CSV file extension removed*, 2) the user created header file described in the previous section saved in the .TXT file format, *but with the .TXT file extension removed*, 3) the GWBASIC.EXE program, and 4) the SQUAD-IN.BAS data file. Once all of this is done, the following instructions can be followed to prepare the SQUAD input file.

A1.4.1 Step-by-step instructions for using GWBASIC.EXE and SQUAD-IN.BAS to

create a SQUAD Input File

1. Run the "GWBASIC.EXE" program by double clicking. The following screen will appear (See Figure A1.5):
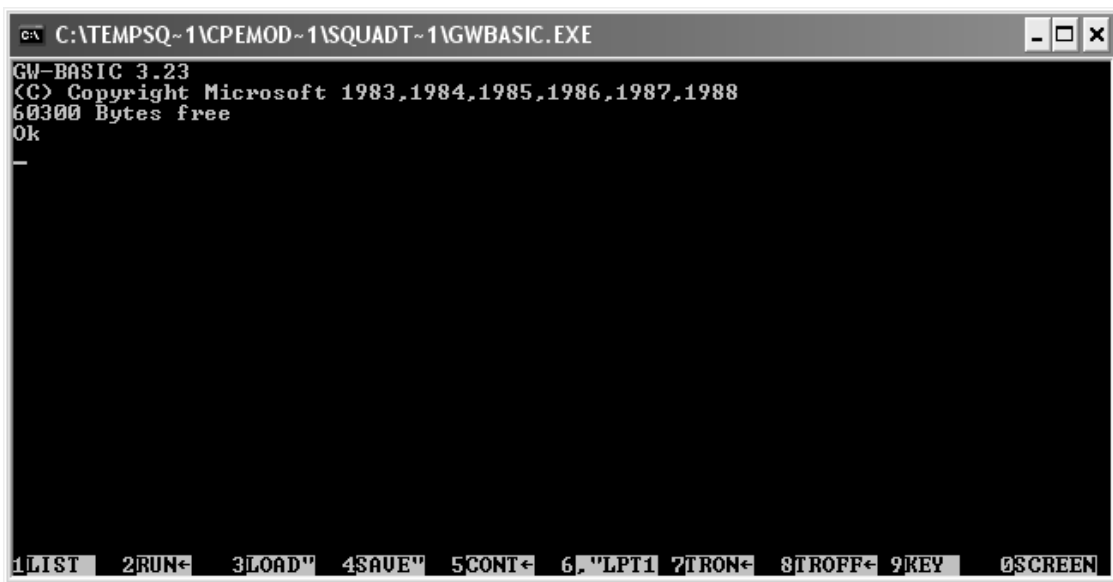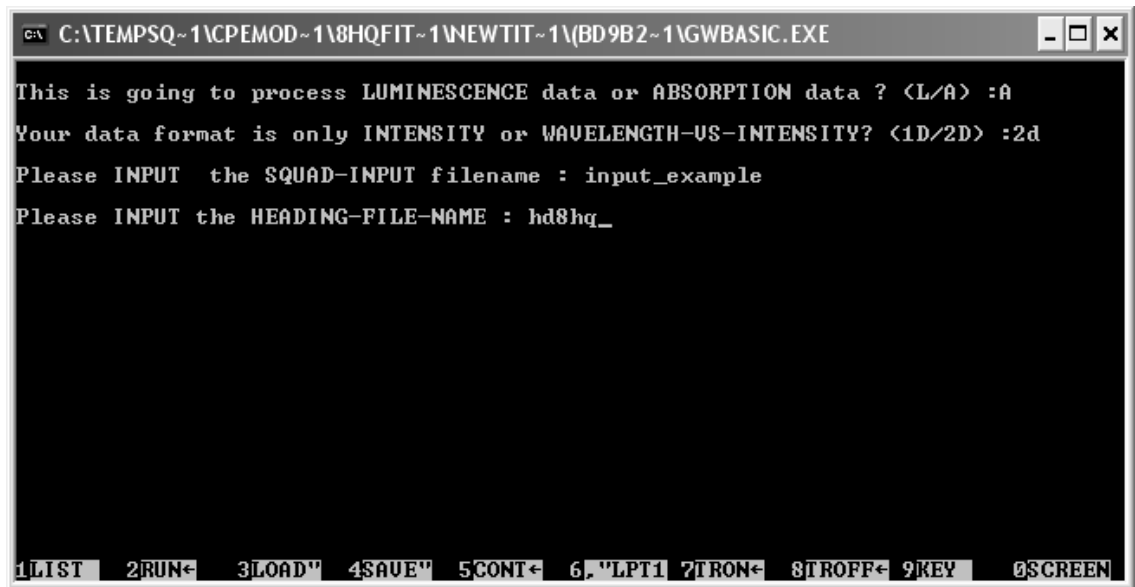
Figure A1.5-Screen shot showing the start-up of the "GWBASIC.EXE" program.

2. Press the "F3" function key which will cause the string "LOAD" to appear.

3. Next type "squad-in.bas" and press enter. "OK" will appear.

4. Press the "F2" function key to run the "squad-in.bas" program.

5. A new window will appear, prompting the user for the following information:

a. "This is going to process LUMINESCENCE data or ABSORPTION data ? (L/A) :" to which the user responds with either "L" or "A" depending on data type.

b. "Your data format is only INTENSITY or WAVELENGTH-VS-INTENSITY? (1D/2D) :" to which the user responds either "1D" or "2D" depending on if the user's spectrum files have 1 or 2 columns. An example and description of the 1D and 2D data formats are shown in Figure A1.4 and the accompanying text.

172

c. "Please INPUT the SQUAD-INPUT filename:" to which the user types the name you want the newly generated input file to be named. *If you enter the name of a file that currently exists, it will be overwritten* so care must be taken with naming the SQUAD-INPUT file.

d. "Please INPUT the HEADING-FILE-NAME:" to which the user types the name of the user created header file. (See screen shot in Figure A1.6)


```
C:\TEMPSQ~1\CPEMOD~1\8HQFIT~1\NEWTIT~1\(BD9B2~1\GWBASIC.EXE          _ □ ×

This is going to process LUMINESCENCE data or ABSORPTION data ? <L/A> :A

Your data format is only INTENSITY or WAVELENGTH-VS-INTENSITY? <1D/2D> :2d

Please INPUT  the SQUAD-INPUT filename : input_example

Please INPUT the HEADING-FILE-NAME : hd8hq_




1LIST    2RUN←   3LOAD"   4SAVE"   5CONT←  6."LPT1 7TRON←  8TROFF← 9KEY     0SCREEN
```

Figure A1.6- Screen shot showing the first user prompts upon starting the "SQUAD-IN.BAS" program.

a. If a HEADING-FILE-NAME is entered that does not exist in the same file folder with the GWBASIC.EXE or SQUAD-IN.BAS programs that are running then the following error will result (see Figure A1.7):
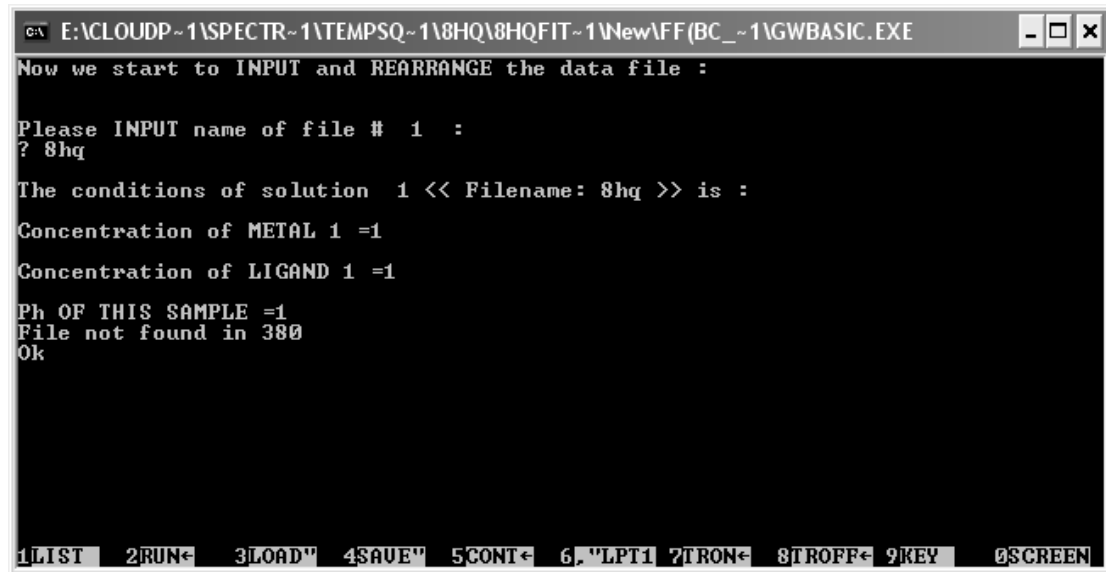
Figure A1.7- Screen shot showing the error result from entering a header file name that does not exist in the folder that contains the "SQUAD-IN.BAS" program that is running.

If this happens, the program can be restarted by pressing the 'F2' function key and the user will be returned to step 5. Otherwise, the program will continue to the next step.

6. Following this, a new window will display: "Now we start to INPUT and REARRANGE the data file:" and it asks the user for the following information:

   a. "Please INPUT name of file #1 :" where the user inputs the 1st spectral data file name.

      i. Note: These files must be saved in the comma delimited format or ".csv", but prior to importing these spectrum files, the file name must be altered to remove the ".csv" suffix.

   b. "The conditions of solution 1 << Filename: "XXXX >> is:" where "XXXX" is the file name that was previously entered, and on the next line is "Concentration of METAL 1 =" where the user enters it in and pushes enter.

      i. Note: In solutions were the METAL concentration is zero, it is important to the program that there is not exactly zero concentration present so input instead a small number such as 1e19 for zero.

   c. "Concentration of LIGAND 1 =" where the user enters the ligand concentration and pushes enter.

   d. "Ph OF THIS SAMPLE =" where the user enters the pH and pushes enter.

174

i. If the user entered the name of a spectral file (in step 6a) that does not appear in the file folder with the GWBASIC.EXE or SQUAD-IN.BAS programs that are running then the following error will result (see Figure A1.8):

Figure A1.8- Screen shot showing the result of entering an input file name that does not exist in the folder that contains the "SQUAD-IN.BAS" program that is running.

If this happens, the program can be restarted by pressing the 'F2' function key and the user will be returned to step 5. Otherwise, the program will continue to the next step.

e. This is followed by "file XXXX has been input. Do you want to INPUT one more data file ?" you answer either "Y" or "N". (Screen shot shown in Figure A1.9):

Figure A1.9- Screen shot showing the user prompt displayed upon supplying the "SQUAD-IN.BAS" program with the correct information for 1 spectrum file.

    f.   If 'YES', then steps 6(a-e) are repeated.

        i. It has been observed that the SQUAD-IN.BAS can only be used to compile 25 spectral files. If a 26th file is input in step 6(a) following error appears (see Figure A1.10):
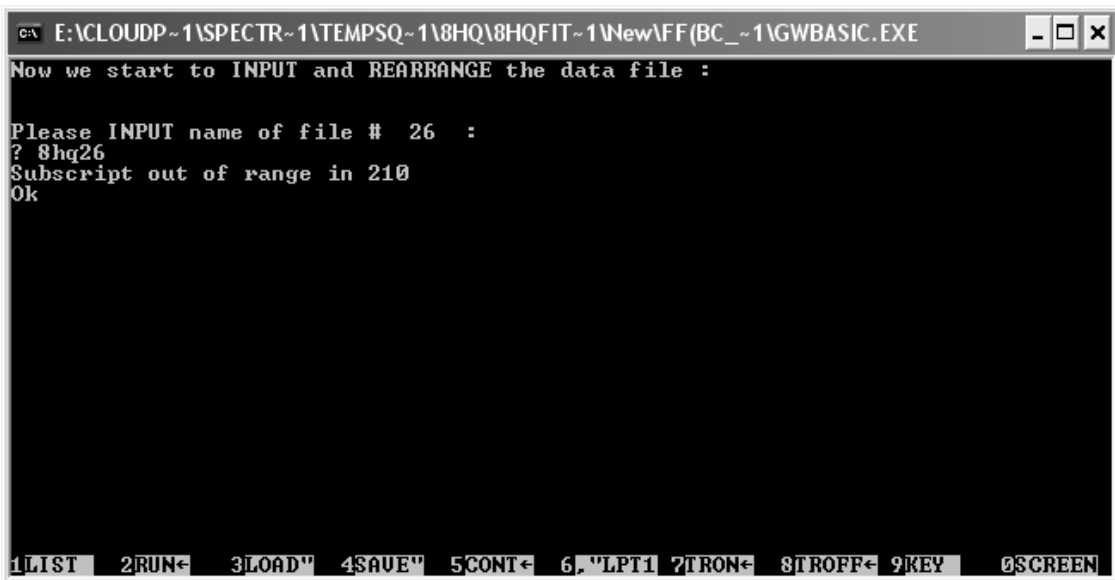
Figure A1.10- Screen shot showing the error that results following the input of the 26th consecutive spectrum file.

The SQUAD-IN.BAS program will have quit, but can be restarted by simply pressing the 'F2' function key. A second input file can be created with spectra 26 and greater by following the steps 5-a. The two files can then be opened in "Notepad" and the spectral files from the second input file can be pasted at the bottom of the first input file.

g. If 'NO', then the following will appear: "All of the data files have been put into the << [your input file name here] >>. Do you want to print out :" with the options:

<1> nothing.

<2> The headings only.

<3> The solution conditions only.

<4> The headings and solution conditions only.

<5> The Whole [your input file name here].

Please make your choice <1/2/3/4/5/> :" to which the user enters a number.

h. If selecting "<1> Nothing" then the polite program responds with: "WE FINISHED, SIR." And "OK"

7. This sequence has created an input file, but the SQUAD program is very particular about spacing. Correct spacing must be verified, and corrected if necessary.

The following is an example of a GWBASIC.EXE generated input file with the required spacing. The file was shortened by deleting all of the spectral data except for two spectra. A column of numbers was added to aid in referencing each line clearly in the accompanying description of the correct spacing.

A1.4.2 Example of a SQUAD Input File

-*-

```
1   8-hydroxyquinoline pka fitting experiment. Wavelength range: 226..272.0nm
2   System 0.1M NaCl; April 2, 2009 experiment, Dip-probe with normal pathlength (10mm)

3   DICTIONARY:
4   MTL1=Nd;LIG1=Q;PROT=H;HYDX=OH:
5   END:
6   SPECIES:
7   Nd(1)Q(1);5.81;FB;FE:
8   H(1)Q(1);9.02;VB;VE:
9   H(2)Q(1);15.02;VB;VE:
10  END:
11  OTHER:
12  Q;VE:
13  END:
14  DATA:
15  219.77      295.61      +0.546
16  LOGB
17  PRIN
18  CARD
19  MR
20  NOPL
21  CRT
22  50
23  1.0
24  SPECTRA:
25  1.00000e-19    0.0000E-00    0.00009842    0.0000E-00    4.381    1.0
26  0.2687   0.2961   0.2896   0.3023   0.3106   0.3146   0.3215   0.3271
27  0.3299   0.3350   0.3387   0.3447   0.3516   0.3591   0.3687   0.3819
28  0.3985   0.4158   0.4366   0.4604   0.4862   0.5140   0.5455   0.5786
29  0.6136   0.6506   0.6912   0.7353   0.7812   0.8279   0.8775   0.9320
30  0.9876   1.0475   1.1050   1.1626   1.2232   1.2842   1.3399   1.3962
```

```
31  1.4520  1.5060  1.5607  1.6068  1.6416  1.6754  1.7082  1.7342
32  1.7544  1.7698  1.7862  1.8017  1.8164  1.8345  1.8398  1.8458
33  1.8571  1.8554  1.8610  1.8629  1.8512  1.8492  1.8454  1.8189
34  1.7900  1.7399  1.6729  1.5872  1.4802  1.3572  1.2310  1.1004
35  0.9721  0.8475  0.7324  0.6269  0.5314  0.4462  0.3717  0.3071
36  0.2522  0.2061  0.1681  0.1375  0.1132  0.0943  0.0799  0.0690
37  0.0610  0.0553  0.0512  0.0483  0.0464  0.0450  0.0441  0.0436
38  0.0432  0.0431  0.0430  0.0431  0.0432  0.0434  0.0437  0.0440
39  0.0445  0.0450  0.0456  0.0464  0.0472  0.0481  0.0491  0.0502
40  0.0514  0.0526  0.0538  0.0552  0.0565  0.0580  0.0595  0.0611
41  0.0627  0.0644  0.0662  0.0681  0.0699  0.0719  0.0740  0.0761
42  0.0782  0.0805  0.0828  0.0852  0.0876  0.0898  0.0920  0.0942
43  0.0963  0.0973  0.0982  0.0991
44  1.00000e-19   0.0000E-00   0.00009837   0.0000E-00   4.963   1.0
45  0.3005  0.3319  0.3250  0.3441  0.3563  0.3643  0.3765  0.3877
46  0.3963  0.4082  0.4191  0.4335  0.4482  0.4641  0.4826  0.5057
47  0.5335  0.5612  0.5934  0.6294  0.6669  0.7056  0.7488  0.7923
48  0.8362  0.8804  0.9274  0.9773  1.0265  1.0728  1.1200  1.1716
49  1.2209  1.2738  1.3180  1.3602  1.4044  1.4471  1.4817  1.5174
50  1.5511  1.5853  1.6232  1.6530  1.6737  1.6958  1.7188  1.7369
51  1.7522  1.7636  1.7781  1.7924  1.8066  1.8253  1.8321  1.8390
52  1.8501  1.8478  1.8523  1.8520  1.8352  1.8245  1.8094  1.7708
53  1.7274  1.6630  1.5833  1.4888  1.3776  1.2556  1.1344  1.0128
54  0.8958  0.7841  0.6816  0.5884  0.5045  0.4300  0.3652  0.3095
55  0.2624  0.2232  0.1912  0.1656  0.1455  0.1299  0.1181  0.1093
56  0.1027  0.0979  0.0944  0.0917  0.0897  0.0881  0.0868  0.0856
57  0.0845  0.0834  0.0822  0.0810  0.0799  0.0787  0.0776  0.0766
58  0.0757  0.0749  0.0743  0.0740  0.0738  0.0739  0.0742  0.0746
59  0.0752  0.0760  0.0769  0.0779  0.0790  0.0804  0.0818  0.0834
60  0.0851  0.0868  0.0886  0.0905  0.0924  0.0944  0.0965  0.0987
61  0.1009  0.1032  0.1056  0.1080  0.1104  0.1128  0.1151  0.1173
62  0.1193  0.1204  0.1214  0.1224
63  -1
```

_-*-

A1.4.3 Line-by-line Description of the SQUAD Input File

A) <u>Lines 1-24</u>: These lines make up the header and were described in section A1.3.2.

B) <u>Line 25</u>: This line contains the first solution's concentration make-up. The spacing of the numbers on this line is important. If the spacing provided by the GWBASIC.EXE program is not correct, the user must correct the column spacing by inserting or deleting spaces until the values are in the columns specified. Column spacing can be verified in the "notepad" program when the "status bar" is activated in the "View" drop down menu. When the cursor is placed to the immediate left of the character in question, the column number will be shown in the status bar at the lower right corner.

a)   Column 1: This number is the value representing the MTL1 concentration. It is critical that this number be something other than zero, otherwise SQUAD will crash. If there is no metal present in the solution, then a small number such as 1E-19 can be substituted (see section A1.3.2).

b)   Column 17: This number is the value representing the MTL2 concentration. It can be left at zero.

c)   Column 32: This number is the value representing the LIG1 concentration.

d)   Column 47: This number is the value representing the LIG2 concentration. It can be left at zero.

e)   Column 61: This number is the value representing the solution pH.

f)   Column 72: This number is the value representing the optical pathlength for the solution measured.

C)   Lines 26-43: These values represent the solution absorbance values that were read-in by the GWBASIC.EXE program. These values are transposed from the column format that was saved in the .CSV format and are now a horizontal row of absorbance values that are text-wrapped to fit in the width of the "notepad" file. Their spacing should be perfectly aligned; however, the user can verify that they are correct. The columns that the first digit of the numbers should be in are: 3, 13, 23, 33, …73.

D)   Line 44: Same spacing and description as line 25 except this is for second solution in the series.

E)   Lines 45-62: These are the same as lines 26-43 above, except this is for the second solution in the series.

F)   Line 63: "-1" marks the end of the input file and instructs SQUAD that there is no more data to be read-in. This "-1" sometimes appears as "-1.0" but it doesn't matter to the program which is used.

     It is necessary to save the spacing changes to the input file before it can be run by SQUAD.

To do this the user can press "Save" and the file will be ready to use. If the user desires to use

the "Saved As" option, the input file will be saved as a .TXT file format. If this is done, the .TXT

file extension will need to be removed prior to reading the input file into the SQUAD program. If

desired, after removing any file extensions from the input file, the user may leave the input file

open on their computer while the SQUAD program reads the file in and creates the output file

with the modeling results.

A1.5 Using SQUAD to Read-in Data from the Input File and Create an Output File

Once the input file is properly formatted with all the correct commands included, the

SQUAD program can be run. Running the SQUAD program is probably the simplest part of the

entire SQUAD modeling process

A1.5.1 Step-by-step Instructions for Using SQUAD to create an Output File

1) Before running the program it must be copied into the file folder that contains the input file.

2) Once the SQUAD program of choice has been moved to the file folder containing your input file, run the SQUAD program by double clicking on the program

3) A new command prompt window will appear with the following instruction:

   "INPUT file name for SQUAD run ="

4) The user then types the input file name and presses 'ENTER'. If a file name is entered that is not in the file folder where the SQUAD program is located then a brief error message is flashed in the window concerning a run-time error and the window automatically closes. If this happens, simply restart the program by returning to Step 2) in this section.

5) If the input file name is correct then the following instruction will appear next:

   "OUTPUT file name for SQUAD run ="

6) The user then types the desired output file name and presses 'ENTER'. If a file name is entered that already exists in the file folder where the SQUAD program is located then a brief error message is flashed in the window concerning a run-time error and the window automatically closes. If this happens, simply restart the program by returning to Step 2) in this section.

7) If the input and output file names are correct then SQUAD begins to calculate and brief messages concerning iterations will be flashed up in the window. SQUAD will automatically close the window that is running the program and the user will notice a newly created output file in the file folder where the SQUAD program is located.

The data obtained from the SQUAD calculations for the data shown in Figure A1.1 and

Figure A1.2 will be used as the example to explain the output file.

A1.5.2 Example of a SQUAD Output File

_-*-

Lines 1-9 are the following ASCII art picture:

```
 SS    QQQQ   U   U   AAA    DDDD
S   S  Q    Q  U   U  A   A   D    D
S      Q    Q  U   U  A   A   D    D
 SS    Q    Q  U   U  AAAAA   D    D
    S  Q    Q  U   U  A   A   D    D
    S  Q    Q  U   U  A   A   D    D
S   S  Q  Q Q  U   U  A   A   D    D
 SS    QQQQ    UUU    A   A   DDDD
          Q
```

10 8-hydroxyquinoline pka fitting experiment. Wavelength range: 226..272.0nm

11 System 0.1M NaCl; April 2, 2009 experiment, Dip-probe with normal pathlength (10

12 DICTIONARY...

13 METAL1 METAL2 LIGAND1 LIGAND2 PROTON HYDROXO

14 ****** ****** ******* ******* ****** *******

15 Nd   ABSENT   Q   ABSENT   H   OH

16 SPECIES   FORMULA   LOG BETA   F OR V   MOL.ABS.

17 1   Nd(1)Q(1)................... 5.8100   FIXED   FIXED

18 2   H(1)Q(1)................... 11.0200   VARY   VARY

19 3   H(2)Q(1)................... 16.0200   VARY   VARY

20 NUMBER OF METALS = 1   NUMBER OF LIGANDS = 1   NUMBER OF COMPLEXES = 3

21 NUMBER OF CONSTANTS TO BE VARIED = 2

22 NUMBER OF SETS OF MOLAR ABSORPTIVITIES TO BE FOUND = 3

23 THE FOLLOWING MOL. ABS. OF THE COMPONENT(S) WILL BE VARIED.

24 I.E... Q

25 THE MOL. ABS. OF ALL OTHER COMPONENTS WILL BE FIXED

26 THE FOLLOWING SPECIES AND/OR COMPLEXES HAVE FIXED (ZERO OR READ IN) MOL. ABS.

27 Nd

28 Nd(1)Q(1)

29 THE FOLLOWING PRINT-OUT AND CALCULATION OPTIONS ARE IN EFFECT:-

30 LOGARITHMIC STABILITY CONSTANTS WILL BE REFINED

31 FULL INPUT DATA WILL BE PRINTED OUT

32 GRID SEARCH WILL BE EXECUTED

33 MOLAR ABSORPTIVITIES WILL BE CALCULATED USING A MULTIPLE REGRESSION
    ALGORITHM
34 NO PRINTER PLOTS WILL BE PRODUCED

35 GAMMA FOR H+ = 1.0000

36 NUMBER OF CYCLES DESIRED = 50

37 TEMPERATURE IS 25.0 DEGREE C

38 SPECTRAL REGION COVERED IS   219.7700 TO   445.6900 AT   1.6250 INTERVALS

39 KNOWN AND FIXED MOLAR ABSORPTIVITIES

40 HEADING 1 REFERS TO THE SPECIES Nd
41 HEADING 2 REFERS TO THE SPECIES MTL2 IS ABSENT
42 HEADING 4 REFERS TO THE SPECIES LIG2 IS ABSENT
43 HEADING 5 REFERS TO THE SPECIES Nd(1)Q(1)

44 1   2   4   5
45 219.77 0.0000D+00 0.0000D+00 0.0000D+00 0.0000D+00
46 221.40 0.0000D+00 0.0000D+00 0.0000D+00 0.0000D+00
47 223.02 0.0000D+00 0.0000D+00 0.0000D+00 0.0000D+00
48 224.65 0.0000D+00 0.0000D+00 0.0000D+00 0.0000D+00
49 226.27 0.0000D+00 0.0000D+00 0.0000D+00 0.0000D+00
50 227.90 0.0000D+00 0.0000D+00 0.0000D+00 0.0000D+00
…
Lines 51-181 were omitted for brevity
…
182 442.39 0.0000D+00 0.0000D+00 0.0000D+00 0.0000D+00
183 444.02 0.0000D+00 0.0000D+00 0.0000D+00 0.0000D+00
184 445.64 0.0000D+00 0.0000D+00 0.0000D+00 0.0000D+00

185 COMPOSITION OF SOLUTIONS USED TO OBTAIN SPECTRA
186 SPECTRUM   METAL 1   METAL 2   LIGAND 1   LIGAND 2   PH   PATHLENGTH
187 NUMBER   --------------- MOLES PER LITER --------------   (CMS.)
188 1   1.0000D-19 0.0000D+00 9.8420D-05 0.0000D+00 4.3810 1.000
189 2   1.0000D-19 0.0000D+00 9.8370D-05 0.0000D+00 4.9630 1.000
190 3   1.0000D-19 0.0000D+00 9.8170D-05 0.0000D+00 5.2540 1.000
191 4   1.0000D-19 0.0000D+00 9.8040D-05 0.0000D+00 5.4320 1.000
192 5   1.0000D-19 0.0000D+00 9.7920D-05 0.0000D+00 5.6060 1.000
193 6   1.0000D-19 0.0000D+00 9.7820D-05 0.0000D+00 5.7390 1.000
194 7   1.0000D-19 0.0000D+00 9.7720D-05 0.0000D+00 5.8840 1.000
195 8   1.0000D-19 0.0000D+00 9.7630D-05 0.0000D+00 6.0480 1.000
196 9   1.0000D-19 0.0000D+00 9.7530D-05 0.0000D+00 6.2220 1.000

```
197 10    1.0000D-19 0.0000D+00 9.7440D-05 0.0000D+00 6.4160  1.000
198 11    1.0000D-19 0.0000D+00 9.7340D-05 0.0000D+00 6.6260  1.000
199 12    1.0000D-19 0.0000D+00 9.7250D-05 0.0000D+00 6.8660  1.000
200 13    1.0000D-19 0.0000D+00 9.7150D-05 0.0000D+00 7.1680  1.000
201 14    1.0000D-19 0.0000D+00 9.7060D-05 0.0000D+00 7.5180  1.000
202 15    1.0000D-19 0.0000D+00 9.6960D-05 0.0000D+00 7.6610  1.000
203 16    1.0000D-19 0.0000D+00 9.6870D-05 0.0000D+00 7.9130  1.000
204 17    1.0000D-19 0.0000D+00 9.6770D-05 0.0000D+00 8.0960  1.000
205 18    1.0000D-19 0.0000D+00 9.6680D-05 0.0000D+00 8.2250  1.000
206 19    1.0000D-19 0.0000D+00 9.6580D-05 0.0000D+00 8.3350  1.000
207 20    1.0000D-19 0.0000D+00 9.6490D-05 0.0000D+00 8.4270  1.000
208 21    1.0000D-19 0.0000D+00 9.6400D-05 0.0000D+00 8.4850  1.000
209 22    1.0000D-19 0.0000D+00 9.6300D-05 0.0000D+00 8.5400  1.000
210 23    1.0000D-19 0.0000D+00 9.6210D-05 0.0000D+00 8.5970  1.000
211 24    1.0000D-19 0.0000D+00 9.6090D-05 0.0000D+00 8.6640  1.000
212 25    1.0000D-19 0.0000D+00 9.5930D-05 0.0000D+00 8.7400  1.000
213 26    1.0000D-19 0.0000D+00 9.5440D-05 0.0000D+00 8.9300  1.000
214 27    1.0000D-19 0.0000D+00 9.5170D-05 0.0000D+00 9.0090  1.000
215 28    1.0000D-19 0.0000D+00 9.5110D-05 0.0000D+00 9.1550  1.000
216 29    1.0000D-19 0.0000D+00 9.5060D-05 0.0000D+00 9.2470  1.000
217 30    1.0000D-19 0.0000D+00 9.4980D-05 0.0000D+00 9.3810  1.000
218 31    1.0000D-19 0.0000D+00 9.4890D-05 0.0000D+00 9.5080  1.000
219 32    1.0000D-19 0.0000D+00 9.4770D-05 0.0000D+00 9.6370  1.000
220 33    1.0000D-19 0.0000D+00 9.4620D-05 0.0000D+00 9.7930  1.000
221 34    1.0000D-19 0.0000D+00 9.4380D-05 0.0000D+00 9.9990  1.000
222 35    1.0000D-19 0.0000D+00 9.4090D-05 0.0000D+00 ******  1.000
```

223 BASELINE CORRECTION NOT APPLIED

224 * * * * INTERMEDIATE CALCULATIONS * * * * *

225 USER-SUPPLIED INITIAL ESTIMATES HAVE BEEN REPLACED

226 HESSIAN MATRIX APPROXIMATION
227 6.868194D+00 -6.847144D+00
228 -6.847144D+00   6.950316D+00
229 ELEMENTS OF CONSTANT VECTOR
230 -4.197037D+00
231 3.828173D+00
232 HESSIAN (INVERTED)
233 8.150616D+00   8.029627D+00
234 8.029627D+00   8.054312D+00

235 EXTREME OVERSHIFT, VARIABLE CONSTANT NO. 1 X(I)=-3.470E+00

236 EXTREME OVERSHIFT, VARIABLE CONSTANT NO. 2 X(I)=-2.867E+00

237 CORRELATION MATRIX
238 .100000D+01
239 .991028D+00   .100000D+01

240 THE STANDARD DEVIATION IN THE ABSORBANCE DATA WITH THE INPUT CONSTANTS IS
    3.7108D-02

241 THE STANDARD DEVIATION IN THE ABSORBANCE DATA IS 3.3470D-02
242 10.040000   .0956   SHIFT= -.9800 FOR H(1)Q(1)
243 15.040000   .0950   SHIFT= -.9800 FOR H(2)Q(1)

244 1 CYCLE(S) CALCULATED

245 HESSIAN MATRIX APPROXIMATION
246 8.405028D+00 -6.926368D+00
247 -6.926368D+00   7.539305D+00
248 ELEMENTS OF CONSTANT VECTOR
249 -4.795847D+00
250 4.391715D+00
251 HESSIAN (INVERTED)
252 4.897721D-01   4.499541D-01
253 4.499541D-01   5.460116D-01

254 CORRELATION MATRIX
255 .100000D+01
256 .870102D+00   .100000D+01

257 THE STANDARD DEVIATION IN THE ABSORBANCE DATA IS 1.7179D-02
258 9.667199   .0120   SHIFT= -.3728 FOR H(1)Q(1)
259 15.280017   .0127   SHIFT=   .2400 FOR H(2)Q(1)

260 CYCLE(S) CALCULATED

261 HESSIAN MATRIX APPROXIMATION
262 9.368666D+00 -6.811129D+00
263 -6.811129D+00   8.065930D+00
264 ELEMENTS OF CONSTANT VECTOR
265 -8.699003D-01
266 6.998994D-01
267 HESSIAN (INVERTED)
268 2.764622D-01   2.334535D-01
269 2.334535D-01   3.211139D-01

270 CORRELATION MATRIX
271 .100000D+01
272 .783525D+00   .100000D+01

273 THE STANDARD DEVIATION IN THE ABSORBANCE DATA IS 1.6639D-02
274 9.590098   .0087   SHIFT= -.0771 FOR H(1)Q(1)
275 15.301683   .0094   SHIFT=   .0217 FOR H(2)Q(1)

276 CYCLE(S) CALCULATED

277 HESSIAN MATRIX APPROXIMATION
278 9.223845D+00 -6.498355D+00
279 -6.498355D+00   7.879332D+00
280 ELEMENTS OF CONSTANT VECTOR
281 -6.300704D-03
282 -3.888409D-02
283 HESSIAN (INVERTED)
284 2.587704D-01   2.134168D-01
285 2.134168D-01   3.029264D-01

286 CORRELATION MATRIX
287 .100000D+01
288 .762259D+00   .100000D+01

289 THE STANDARD DEVIATION IN THE ABSORBANCE DATA IS 1.6635D-02
290 9.580169   .0085   SHIFT= -.0099 FOR H(1)Q(1)
291 15.288559   .0092   SHIFT= -.0131 FOR H(2)Q(1)

292 CYCLE(S) CALCULATED

293 HESSIAN MATRIX APPROXIMATION
294 9.245685D+00 -6.512480D+00
295 -6.512480D+00   7.907041D+00
296 ELEMENTS OF CONSTANT VECTOR
297 -8.051318D-03
298 2.563333D-03
299 HESSIAN (INVERTED)
300 2.576119D-01   2.121770D-01
301 2.121770D-01   3.012250D-01

302 CORRELATION MATRIX
303 .100000D+01
304 .761675D+00   .100000D+01

305 THE STANDARD DEVIATION IN THE ABSORBANCE DATA IS 1.6635D-02

306 9.578639   .0084   SHIFT= -.0015 FOR H(1)Q(1)
307 15.287623   .0091   SHIFT= -.0009 FOR H(2)Q(1)

308 CYCLE(S) CALCULATED

309 HESSIAN MATRIX APPROXIMATION
310 9.246031D+00 -6.510857D+00
311 -6.510857D+00   7.907711D+00
312 ELEMENTS OF CONSTANT VECTOR
313 -6.388213D-04
314 -2.746067D-04
315 HESSIAN (INVERTED)
316 2.573816D-01   2.119165D-01
317 2.119165D-01   3.009414D-01

318 CORRELATION MATRIX
319 .100000D+01
320 .761439D+00   .100000D+01

321 THE STANDARD DEVIATION IN THE ABSORBANCE DATA IS 1.6635D-02
322 9.578416   .0084   SHIFT= -.0002 FOR H(1)Q(1)
323 15.287405   .0091   SHIFT= -.0002 FOR H(2)Q(1)

324 CYCLE(S) CALCULATED

325 *** CONVERGENCE ACHIEVED IN 6 CYCLES ***

326 STAND. DEV. OF FIT FOR SPECTRUM NUMBER 1 = 5.9624E-02
327 STAND. DEV. OF FIT FOR SPECTRUM NUMBER 2 = 1.3362E-02
328 STAND. DEV. OF FIT FOR SPECTRUM NUMBER 3 = 1.5027E-02
329 STAND. DEV. OF FIT FOR SPECTRUM NUMBER 4 = 2.5973E-02
330 STAND. DEV. OF FIT FOR SPECTRUM NUMBER 5 = 2.8568E-02
331 STAND. DEV. OF FIT FOR SPECTRUM NUMBER 6 = 2.6721E-02
332 STAND. DEV. OF FIT FOR SPECTRUM NUMBER 7 = 2.2282E-02
333 STAND. DEV. OF FIT FOR SPECTRUM NUMBER 8 = 1.6887E-02
334 STAND. DEV. OF FIT FOR SPECTRUM NUMBER 9 = 1.2959E-02
335 STAND. DEV. OF FIT FOR SPECTRUM NUMBER 10 = 1.1980E-02
336 STAND. DEV. OF FIT FOR SPECTRUM NUMBER 11 = 1.1874E-02
337 STAND. DEV. OF FIT FOR SPECTRUM NUMBER 12 = 1.3943E-02
338 STAND. DEV. OF FIT FOR SPECTRUM NUMBER 13 = 1.4091E-02
339 STAND. DEV. OF FIT FOR SPECTRUM NUMBER 14 = 1.2175E-02
340 STAND. DEV. OF FIT FOR SPECTRUM NUMBER 15 = 8.3334E-03
341 STAND. DEV. OF FIT FOR SPECTRUM NUMBER 16 = 8.0491E-03
342 STAND. DEV. OF FIT FOR SPECTRUM NUMBER 17 = 7.4988E-03

343 STAND. DEV. OF FIT FOR SPECTRUM NUMBER 18 = 7.0119E-03
344 STAND. DEV. OF FIT FOR SPECTRUM NUMBER 19 = 6.5921E-03
345 STAND. DEV. OF FIT FOR SPECTRUM NUMBER 20 = 6.7444E-03
346 STAND. DEV. OF FIT FOR SPECTRUM NUMBER 21 = 7.2449E-03
347 STAND. DEV. OF FIT FOR SPECTRUM NUMBER 22 = 7.1423E-03
348 STAND. DEV. OF FIT FOR SPECTRUM NUMBER 23 = 6.6514E-03
349 STAND. DEV. OF FIT FOR SPECTRUM NUMBER 24 = 6.6122E-03
350 STAND. DEV. OF FIT FOR SPECTRUM NUMBER 25 = 5.9381E-03
351 STAND. DEV. OF FIT FOR SPECTRUM NUMBER 26 = 4.9635E-03
352 STAND. DEV. OF FIT FOR SPECTRUM NUMBER 27 = 5.4146E-03
353 STAND. DEV. OF FIT FOR SPECTRUM NUMBER 28 = 4.1101E-03
354 STAND. DEV. OF FIT FOR SPECTRUM NUMBER 29 = 3.9495E-03
355 STAND. DEV. OF FIT FOR SPECTRUM NUMBER 30 = 6.9922E-03
356 STAND. DEV. OF FIT FOR SPECTRUM NUMBER 31 = 8.8144E-03
357 STAND. DEV. OF FIT FOR SPECTRUM NUMBER 32 = 8.1250E-03
358 STAND. DEV. OF FIT FOR SPECTRUM NUMBER 33 = 6.6455E-03
359 STAND. DEV. OF FIT FOR SPECTRUM NUMBER 34 = 1.7384E-03
360 STAND. DEV. OF FIT FOR SPECTRUM NUMBER 35 = 1.2596E-02

361 SUM OF SQUARES OF (OBSVD. - CALC.) =   1.2392D+00

362 CONCENTRATION MATRIX Q(NUMPH,NSPECIES)

363 FREE Nd   FREE MTL2   FREE Q   FREE LIG2
364 SOLN. 1 9.9998E-20 0.0000E+00 2.8037E-11 0.0000E+00
365 SOLN. 2 9.9977E-20 0.0000E+00 3.6288E-10 0.0000E+00
366 SOLN. 3 9.9922E-20 0.0000E+00 1.2078E-09 0.0000E+00
367 SOLN. 4 9.9844E-20 0.0000E+00 2.4195E-09 0.0000E+00
368 SOLN. 5 9.9704E-20 0.0000E+00 4.6011E-09 0.0000E+00
369 SOLN. 6 9.9529E-20 0.0000E+00 7.3231E-09 0.0000E+00
370 SOLN. 7 9.9242E-20 0.0000E+00 1.1837E-08 0.0000E+00
371 SOLN. 8 9.8742E-20 0.0000E+00 1.9737E-08 0.0000E+00
372 SOLN. 9 9.7924E-20 0.0000E+00 3.2835E-08 0.0000E+00
373 SOLN. 10 9.6510E-20 0.0000E+00 5.6004E-08 0.0000E+00
374 SOLN. 11 9.4118E-20 0.0000E+00 9.6787E-08 0.0000E+00
375 SOLN. 12 8.9798E-20 0.0000E+00 1.7597E-07 0.0000E+00
376 SOLN. 13 8.0990E-20 0.0000E+00 3.6355E-07 0.0000E+00
377 SOLN. 14 6.5258E-20 0.0000E+00 8.2457E-07 0.0000E+00
378 SOLN. 15 5.7474E-20 0.0000E+00 1.1460E-06 0.0000E+00
379 SOLN. 16 4.3201E-20 0.0000E+00 2.0363E-06 0.0000E+00
380 SOLN. 17 3.3513E-20 0.0000E+00 3.0728E-06 0.0000E+00
381 SOLN. 18 2.7463E-20 0.0000E+00 4.0909E-06 0.0000E+00
382 SOLN. 19 2.2934E-20 0.0000E+00 5.2046E-06 0.0000E+00
383 SOLN. 20 1.9612E-20 0.0000E+00 6.3486E-06 0.0000E+00
384 SOLN. 21 1.7738E-20 0.0000E+00 7.1830E-06 0.0000E+00
385 SOLN. 22 1.6111E-20 0.0000E+00 8.0647E-06 0.0000E+00
386 SOLN. 23 1.4569E-20 0.0000E+00 9.0820E-06 0.0000E+00
387 SOLN. 24 1.2939E-20 0.0000E+00 1.0421E-05 0.0000E+00

```
388 SOLN. 25  1.1311E-20  0.0000E+00  1.2144E-05  0.0000E+00
389 SOLN. 26  8.1301E-21  0.0000E+00  1.7501E-05  0.0000E+00
390 SOLN. 27  7.1226E-21  0.0000E+00  2.0196E-05  0.0000E+00
391 SOLN. 28  5.6132E-21  0.0000E+00  2.6043E-05  0.0000E+00
392 SOLN. 29  4.8752E-21  0.0000E+00  3.0220E-05  0.0000E+00
393 SOLN. 30  4.0310E-21  0.0000E+00  3.6874E-05  0.0000E+00
394 SOLN. 31  3.4302E-21  0.0000E+00  4.3603E-05  0.0000E+00
395 SOLN. 32  2.9715E-21  0.0000E+00  5.0573E-05  0.0000E+00
396 SOLN. 33  2.5680E-21  0.0000E+00  5.8764E-05  0.0000E+00
397 SOLN. 34  2.2140E-21  0.0000E+00  6.8406E-05  0.0000E+00
398 SOLN. 35  1.9711E-21  0.0000E+00  7.7026E-05  0.0000E+00

399 NSPECIES     1         2         3
400 SOLN.  1  1.8102E-24  4.4172E-06  9.4003E-05
401 SOLN.  2  2.3424E-23  1.4969E-05  8.3401E-05
402 SOLN.  3  7.7920E-23  2.5492E-05  7.2677E-05
403 SOLN.  4  1.5598E-22  3.3896E-05  6.4141E-05
404 SOLN.  5  2.9619E-22  4.3180E-05  5.4736E-05
405 SOLN.  6  4.7059E-22  5.0595E-05  4.7217E-05
406 SOLN.  7  7.5845E-22  5.8567E-05  3.9142E-05
407 SOLN.  8  1.2583E-21  6.6942E-05  3.0668E-05
408 SOLN.  9  2.0760E-21  7.4602E-05  2.2895E-05
409 SOLN. 10  3.4897E-21  8.1402E-05  1.5982E-05
410 SOLN. 11  5.8815E-21  8.6742E-05  1.0501E-05
411 SOLN. 12  1.0202E-20  9.0752E-05  6.3219E-06
412 SOLN. 13  1.9010E-20  9.3536E-05  3.2506E-06
413 SOLN. 14  3.4742E-20  9.4764E-05  1.4711E-06
414 SOLN. 15  4.2526E-20  9.4756E-05  1.0583E-06
415 SOLN. 16  5.6799E-20  9.4245E-05  5.8918E-07
416 SOLN. 17  6.6487E-20  9.3314E-05  3.8277E-07
417 SOLN. 18  7.2537E-20  9.2308E-05  2.8134E-07
418 SOLN. 19  7.7066E-20  9.1160E-05  2.1567E-07
419 SOLN. 20  8.0388E-20  8.9969E-05  1.7222E-07
420 SOLN. 21  8.2262E-20  8.9068E-05  1.4918E-07
421 SOLN. 22  8.3889E-20  8.8105E-05  1.3001E-07
422 SOLN. 23  8.5431E-20  8.7015E-05  1.1261E-07
423 SOLN. 24  8.7061E-20  8.5574E-05  9.4914E-08
424 SOLN. 25  8.8689E-20  8.3708E-05  7.7939E-08
425 SOLN. 26  9.1870E-20  7.7892E-05  4.6825E-08
426 SOLN. 27  9.2877E-20  7.4936E-05  3.7556E-08
427 SOLN. 28  9.4387E-20  6.9042E-05  2.4723E-08
428 SOLN. 29  9.5125E-20  6.4821E-05  1.8780E-08
429 SOLN. 30  9.5969E-20  5.8094E-05  1.2363E-08
430 SOLN. 31  9.6570E-20  5.1279E-05  8.1456E-09
431 SOLN. 32  9.7028E-20  4.4191E-05  5.2159E-09
432 SOLN. 33  9.7432E-20  3.5853E-05  2.9547E-09
433 SOLN. 34  9.7786E-20  2.5972E-05  1.3320E-09
434 SOLN. 35  9.8029E-20  1.7063E-05  5.1056E-10
```

435 MOLAR ABSORPTIVITIES OF INDIVIDUAL SPECIES CALCULATED BY PROGRAM
436 USING MULTIPLE REGRESSION ALGORITHM.

437 HEADING 1 REFERS TO THE SPECIES H(1)Q(1)
438 HEADING 2 REFERS TO THE SPECIES H(2)Q(1)
439 HEADING 3 REFERS TO THE SPECIES Q

440 WAVELENGTH   1   2   3
441 219.77   3.8477E+03   2.9827E+03   3.9572E+03
442 221.40   4.6363E+03   3.4218E+03   4.6347E+03
443 223.02   5.6608E+03   3.8614E+03   5.4501E+03
444 224.65   6.4788E+03   4.1640E+03   5.9961E+03
445 226.27   7.5971E+03   4.7461E+03   6.8618E+03
446 227.90   8.7195E+03   5.4318E+03   7.7667E+03
447 229.52   9.8757E+03   6.2679E+03   8.7584E+03

...

Lines 448-577 were omitted for brevity

...

578 442.39   1.0416E+01   -7.4789E+01   -2.1898E+00
579 444.02   1.0359E+01   -7.5821E+01   -3.5862E+00
580 445.64   1.0393E+01   -7.5956E+01   -3.3932E+00

581 STANDARD DEVN. OF CALCULATED MOLAR ABSORPTIVITIES

582 WAVELENGTH   1   2   3
583 219.77   2.1639E+01   4.6063E+01   5.8835E+01
584 221.40   2.9588E+01   6.2983E+01   8.0447E+01
585 223.02   3.9691E+01   8.4489E+01   1.0792E+02
586 224.65   5.6437E+01   1.2014E+02   1.5345E+02

...

Lines 587-716 were omitted for brevity

...

717 437.52   2.5558E+00   5.4405E+00   6.9490E+00
718 439.14   2.5343E+00   5.3947E+00   6.8905E+00
719 440.77   2.5691E+00   5.4687E+00   6.9850E+00
720 442.39   2.5545E+00   5.4377E+00   6.9454E+00
721 444.02   2.5481E+00   5.4240E+00   6.9279E+00
722 445.64   2.5283E+00   5.3820E+00   6.8742E+00

        _-*-

A1.5.3 Description of the SQUAD Output File Line-by-line

A) Lines 1-9: ASCII art spelling out the word SQUAD.

B) Lines 10-11: This is a reproduction of the text description of this experiment taken from the first two lines of the header/input (H/I) file.

C) Lines 12-15: These lines display the user-defined components as they were provided in the header file "DICTIONARY" section. Note: In a text file the columns align much better than in MS Word.

D) Lines 16-19: These lines display the formed species, log beta values, and the user-provided instructions on whether the log beta or molar absorptivity should be varied or not.

E) Line 20: This line summarizes the number of metals, ligands and complexes.

F) Line 21: This line displays the number of constants to be varied.

G) Line 22: This line displays the number of molar absorptivities to be found.

H) Line 23-24: These lines display the components whose molar absorptivities will be calculated. The species listed are those identified in the "OTHER" section with instructions to SQUAD to "VE" or "vary the molar absorptivity".

I) Line 25-28: These lines display the components or complexes that possess fixed molar absorptivities that will be assumed to be zero, or explicitly read-in.

J) Line 29: Beginning of the explanation of the user requested calculation instructions.

K) Line 30: Messages correspond to the instructions entered in (H/I) file Line 16 that is described in Section A1.3 of this manual. When the instruction "LOGB" is used on line 16 of the (H/I) file, the message: "LOGARITHMIC STABILITY CONSTANTS WILL BE REFINED" appears on this line. When the instruction "EXPB" is used on line 16 of the (H/I) file, the message: "ANTILOGARITHM OF LOG(BETA) WILL BE REFINED" appears instead.

L) Line 31: Messages correspond to the instructions entered in Line 17 of the (H/I) file that is described in Section A1.3 of this manual. When the instruction "PRIN" is used on line 17 of the (H/I) file, the message: "FULL INPUT DATA WILL BE PRINTED OUT" appears on this line. When the instruction "NOPR" is used on line 16 of the (H/I) file, the message: "ABBREVIATED INPUT DATA WILL PRINTED OUT" appears instead.

   a) The abbreviated version of the input data omits lines 39-222 that are displayed in the example output file shown.

M) Line 32: Messages correspond to the instructions entered in Line 18 of the header file that is described in Section A1.3 of this manual. When the instruction "CARD" is used on line 18 of the header, the message: "GRID SEARCH WILL BE EXECUTED" appears on this line. When the instruction "NOCD" is used on line 16 of the (H/I) file, the message: "GRID SEARCH WILL NOT BE EXECUTED" appears instead.

   a) When the Grid search is performed, the SQUAD program judges the user supplied values to see if they are good. If so, then the message "USER-SUPPLIED INITIAL ESTIMATES ARE GOOD" appears on line 225. If they user-supplied values are not good, then the message: "USER-SUPPLIED INITIAL ESTIMATES HAVE BEEN REPLACED" appears on line 225. SQUAD does not explicitly indicate what values are used in the place of the user-supplied are replaced.

b) If no grid search is performed, then the message on line 225 is omitted.

N) <u>Line 33</u>: Messages correspond to the instructions entered in Line 19 of the header file that is described in section A1.3 of this manual. When the instruction "MR" is used on line 19 of the header, the message: "MOLAR ABSORPTIVITIES WILL BE CALCULATED USING A MULTIPLE REGRESSION ALGORITHM" appears on this line. When the instruction "NNLS" is used on line 16 of the (H/I) file, the message: "MOLAR ABSORPTIVITIES WILL BE CALCULATED USING A NON-NEGATIVE LLSQ ALGORITHM" appears instead.

O) <u>Line 34</u>: Messages correspond to the instructions entered in Line 20 of the header file that is described in section A1.3 of this manual. When the instruction "PLOT" is used on line 20 of the header, the message: "NO PRINTER PLOTS WILL BE PRODUCED" appears on this line. When the instruction "NNLS" is used on line 16 of the (H/I) file, the message: "NO PRINTER PLOTS WILL BE PRODUCED" appears instead.

   a) It would seem that this feature was disabled by the programmer prior to the compilation of this version of SQUAD. It is not known what this feature does in a version of SQUAD where this option is activated.

P) <u>Line 35</u>: This indicates what the user-supplied value for the H^+ activity coefficients is for this modeling calculation. This value is specified in line 23 of the (H/I) file.

Q) <u>Line 36</u>: This indicates the user-supplied maximum number of iterations allowed by SQUAD. This value is defined in line 22 of the (H/I) file.

R) <u>Line 37</u>: This indicates the assumed temperature for the experiment is 25.0 degrees. The author has tried, but failed to find a way to change the assumed temperature for the experiment. It is assumed that temperature is not used in the computations performed by SQUAD.

S) <u>Line 38</u>: This indicates what the lower and upper bounds of the wavelengths and the interval between wavelengths for the absorbance data that were supplied by the user in line 15 of the (H/I) file.

T) <u>Lines 39-44</u>: These lines offer clarification of the Fixed Molar Absorptivities being displayed in lines 45-184, specifying which column pertains to which component or species.

U) <u>Lines 45-184</u>: These lines show the "Fixed Molar Absorptivities" for the components that were identified as having fixed molar absorptivities.

V) <u>Lines 185-187</u>: These lines act as column headings for the data table showing the "Composition of Solutions used to Obtain Spectra" indicating units for concentration and optical pathlength.

W) <u>Lines 188-222</u>: These lines contain the data values that SQUAD imported from the (H/I) file concerning the solution concentrations. The lines in the (H/I) file these data come from are lines 25 and 44 shown in the example (H/I) file in Section A1.3.

X) <u>Line 223</u>: This line indicates whether there was a baseline spectrum read in to the SQUAD program. If a baseline spectrum was read in then "BASELINE CORRECTION APPLIED" will appear in this line. If no baseline spectrum was read in then "BASELINE CORRECTION NOT APPLIED" will appear in this line.

Y) <u>Line 224</u>: This shows the beginning of the actual iterations that SQUAD performed while fitting the data.

Z) <u>Line 225</u>: This indicates whether the "GRID SEARCH" or check of the "goodness" of the guess values was performed based on the user-supplied information. If no "GRID SEARCH" was performed then no notification will appear here. If the "GRID SEARCH" determines that estimates are good then the message appears: "USER-SUPPLIED INITIAL ESTIMATES ARE GOOD". If the "GRID SEARCH" determines that estimates are not good then the message, "USER-SUPPLIED INITIAL ESTIMATES HAVE BEEN REPLACED" appears on line 225. SQUAD never indicates what numbers are used if the user estimates are replaced.

AA) <u>Lines 226-244</u>: These lines contain the data obtained from the first iteration of calculations.

    a) <u>Lines 226-234</u>: These lines contain the Hessian matrix, the constant vector and the inverted Hessian matrix.

    b) <u>Lines 235-236</u>: These lines contain information concerning the "EXTREME OVERSHIFT, VARIABLE CONSTANT". This message and reported values disappear as SQUAD approaches a solution.

    c) <u>Lines 237-239</u>: These lines contain information concerning the "CORRELATION MATRIX". The documentation supplied with SQUAD did not provide the significance of these values.

    d) <u>Line 240</u>: This line shows "THE STANDARD DEVIATION IN THE ABSORBANCE DATA WITH THE INPUT CONSTANTS". The documentation supplied with SQUAD did not provide the significance of this value.

    e) <u>Line 241</u>: This line shows "THE STANDARD DEVIATION IN THE ABSORBANCE DATA"; The documentation supplied with SQUAD did not provide the significance of this value, nor the difference between this value and that shown on line 240.

    f) <u>Line 242-243</u>: These lines show the log β values calculated by the program:

        i) <u>First number</u>: Log β resulting from the first iteration.

        ii) <u>Second number</u>: Standard Deviation of the log β resulting from the first iteration.

        iii) "SHIFT="

        iv) <u>Third number</u>: The shift that SQUAD made in the log β value from the previous iteration value.

> v) <u>Species identification</u>: "FOR XXXXX" the XXX identifies the species to which the log β corresponds.

    g) <u>Line 244</u>: This line indicates the end of the presentation of data relating to the 1st iteration with the message: "1 CYCLE(S) CALCULATED"

BB) <u>Lines 245-324</u>: These lines show the other 5 iterations and are identical in nature to those explained above in lines 226-244.

CC) <u>Line 325</u>: This line indicates that a solution has been achieved and the number of iterations that were performed.

DD) <u>Lines 326-360</u>: These lines show the "Standard Deviation of the Fit" for each spectrum. These data would help a user to identify particular spectra that have a poor fit that might be excluded for a better solution.

EE) <u>Line 361</u>: This shows the sum of squares for the calculations performed.

FF) <u>Lines 362-363</u>: These lines introduce and clarify the columns of data as they relate to the final free concentrations of the components that were obtained from the calculations.

GG) <u>Lines 364-398</u>: The data for the final free concentrations of the components that were obtained from the calculations.

HH) <u>Lines 299-434</u>: These are the concentrations of the species that were obtained from the calculations. <u>The column numbers shown here correspond to the numbers shown in lines 17-19 of the output file. These column numbers should not be equated or confused with the upcoming column numbers shown in lines 437-439</u> for the "Molar Absorptivity" calculations that appear almost directly under this data table. Note: SQUAD renumbers the species in the "Molar Absorptivities" section which could lead to some confusion.

II) <u>Lines 435-440</u>: These lines clarify the "Molar Absorptivity" data presented in lines 441-722.

    a) <u>Lines 435-436</u>: These lines restate the algorithm used to fit the molar absorptivities: Multiple Regression or Non-Negative Least Squares methods.

    b) <u>Lines 437-439</u>: These lines establish a new numbering for the presentation of molar absorptivities of the species and components with varied molar absorptivities. These heading numbers are different, and should not be confused with the heading numbers used in line 399 of this example output file.

    c) <u>Line 440</u>: Displays the column headings for the molar absorptivities.

JJ) <u>Lines 441-580</u>: Displays the molar absorptivities of the species and components with varied molar absorptivities.

KK) <u>Line 581</u>: This line divides the molar absorptivities from the standard deviations of the molar absorptivities.

LL) <u>Line 582</u>: Displays the column headings for the table of standard deviations for the calculated molar absorptivities of the species and components with varied molar absorptivities.

MM)   <u>Lines 583-722</u>: This table gives the standard deviations for the calculated molar absorptivities of the species and components with varied molar absorptivities.

BIBLIOGRAPHY

1.   Weaver, B.; Kappelmann, F. A., TALSPEAK: A New Method of Separating Americium and Curium from the Lanthanides by Extraction from an Aqueous Solution of an Aminopolyacetic Acid Complex with a Monoacidic Organophosphate or Phosphonate; ORNL-3559; Oak Ridge National Laboratory: Oak Ridge, TN, **1964**.

2.   Gelis, A. V.; Vandegrift, G. F.; Bakel, A.; Bowers, D. L.; Hebden, A. S.; Pereira, C.; Regalbuto, M., *Radiochim. Acta* **2009**, *97*, 231–232.

3.   Nilsson, M.; Nash, K., *Solvent Extr. Ion Exch.* **2007**, *25*, 665–701.

4.   Leggett, C. J.; Liu, G.; Jensen, M. P., *Solvent Extr. Ion Exch.* **2010**, *28*, 313–334.

5.   De Jong, N.; Draye, M.; Favre-Reguillon, A.; LeBuzit, G.; Cote, G.; Foos, J., *J. Colloid Interface Sci.* **2005**, *291*, 303–306.

6.   Draye, M.; Thomas, S.; Cote, G.; Favre-Reguillon, A.; LeBuzit, G.; Guy, A.; Foos, J., *Sep. Sci. Technol.* **2005**, *40*, 611–622.

7.   Favre-Reguillon, A.; Draye, M.; Lebuzit, G.; Thomas, S.; Foos, J.; Cote, G.; Guy, A., *Talanta* **2004**, *63*, 803–806.

8.   Miura, J.; Ishii, H.; Watanabe, H., *Bunseki Kagaku* **1976**, *25*, 808–809.

9.   Watanabe, H.; Tanaka, H., *Talanta* **1978**, *25*, 585–589.

10. Madic, C.; Boullis, B.; Baron, P.; Testard, F.; Hudson, M. J.; Liljenzin, J. O.; Christiansen, B.; Ferrando, M.; Facchini, A.; Geist, A.; Modolo, G.; Espartero, A. G.; De Mendoza, J., *J. Alloys Compd.* **2007**, *444-445*, 23–27.

11. Seaborg, G. T., Extraction Method for Separating Uranium, Plutonium, and Fission Products from Compositions Containing Same. U.S. Patent 2,811,415,**1957**.

12. Mathur, J. N.; Murali, M. S.; Krishna, M. V. B.; Iyer, R. H.; Chitnis, R. R.; Wattal, P. K.; Theyyunni, T. K.; Ramanujam, A.; Dhami, P. S.; Gopalakrishnan, V., *Sep. Sci. Technol.* **1996**, *31*, 2045–2063.

13. Mathur, J.; Murali, M.; Balarama Krishna, M.; Iyer, R.; Chitnis, R.; Wattal, P.; Bauri, A.; Banerji, A., *J. Radioanal. Nucl. Chem.* **1996**, *213*, 419–429.

14. Shannon, R. D., *Acta Crystallogr. Sect. A* **1976**, *32*, 751-767.

15. Nilsson, M.; Nash, K. L., *Solvent Extraction and Ion Exchange* **2007**, *25*, 665 - 701.

16. Baum, E. M.; Knox, H. D.; Miller, T. R. *Nuclides and Isotopes,* 16th ed., Knolls Atomic Power Laboratory, Niskayuna, NY, **2002**.

17. Croff, A. G., ORIGEN2 - A Revised and Updated Version of the Oak Ridge Isotope Generation and Depletion Code; ORNL-5621; Oak Ridge National Laboratory: **1980**.

18. Guenther, R. J.; Blahnik, D. E.; Campbell, T. K.; Jenquin, U. P.; Mendel, J. E.; Thomas, L. E.; Thornhill, C. K., Characterization of Spent Fuel Approved Testing Material - ATM-105; PNL-5109-105; Pacific Northwest Laboratory: Richland, WA, **1989**.

19. Irish, E. R.; Reas, W. H., The PUREX Process- A Solvent Extraction Reprocessing Method for Irradiated Uranium; HW-49483A; Hanford Atomic Products Operation: Richland, WA, **1957**.

20. Musikas, C., *Miner. Process. Extr. Metall. Rev.* **1997**, *17*, 109–142.

21. Law, J. D.; Herbst, R. S.; Peterman, D. R.; Tillotson, R. D.; Todd, T. A., *J. Am. Chem. Soc.* **2004**, *147*, 284–290.

22. Stoyanov, E. S.; Smirnov, I. V.; Babain, V. A.; Antonov, N. G.; Peterman, D.; Herbst, R. S.; Todd, T. A.; Luther, T. A., *Radiochem.* **2004**, *46*, 540–545.

23. Leonard, R. A.; Aase, S. B.; Arafat, H. A.; Conner, C.; Chamberlain, D. B.; Falkenberg, J. R.; Regalbuto, M. C.; Vandegrift, G. F., *Solvent Extr. Ion Exch.* **2003**, *21*, 505–526.

24. Delmau, L. H.; Bonnesen, P. V.; Engle, N. L.; Haverlock, T. J.; Sloop, F. V.; Moyer, B. A., *Solvent Extr. Ion Exch.* **2006**, *24*, 197–217.

25. Law, J. D.; Garn, T. G.; Meikrantz, D. H.; Warburton, J., *Sep. Sci. Technol.* **2010**, *45*, 1769–1775.

26. Street, K.; Seaborg, G. T., *J. Am. Chem. Soc.* **1950**, *72*, 2790–2792.

27. Madic, C.; Hudson, M. J.; Liljenzin, J.-O.; GLatz, J.-P.; Nannicini, R.; Facchini, A.; Kolarik, Z.; Odoj, R., *Prog. Nucl. Energy* **2002**, *40*, 523–526.

28. Mehdoui, T.; Berthet, J.-C.; Thuéry, P.; Ephritikhine, M., *J. Chem. Soc., Dalton Trans.* **2004**, 579–590.

29. Vandegrift, G. F.; Regalbuto, M. C.; Aase, S. B.; Arafat, H. A.; Bakel, A. J.; Bowers, D. L.; Byrnes, J. P.; Clark, M. A.; Emergy, J. W.; Falkenberg, J. R.; Gelis, A. V.; Hafenrichter, L. D.; Leonard, R. A.; Pereira, C.; Quigley, K. J.; Tsai, Y.; Vander Pol, M. H.; Laidler, J. J., Lab-Scale Demonstration of the UREX+ Process. Proceedings of Waste Management 2004 International Symposium, Tucson, AZ, February 29-March 4, 2004.

30. Vandegrift, G. F.; Regalbuto, M. C.; Aase, S.; Bakel, A.; Battisti, T. J.; Bowers, D. L.; Byrnes, J. P.; Clark, M. A.; Cummings, D. G.; Emery, J. W.; Falkenberg, J. R.; Gelis, A. V.; Pereira, C.; Hafenrichter, L.; Tsai, Y.; Quigley, K. J.; Vander Pol, M. H., Designing and Demonstration of the UREX+ Process Using Spent Nuclear Fuel. Proceedings of ATALANTE 2004 - Advances for Future Nuclear Fuel Cycles, Nimes, France, June 21-24, 2004.

31. Romanovskiy, V. N.; Smirnov, I. V.; Babain, V. A.; Todd, T. A.; Herbst, R. S.; Law, J. D.; Brewer, K. N., *Solvent Extr. Ion Exch.* **2001**, *19*, 1–21.

32. Law, J. D.; Herbst, R. S.; Todd, T. A.; Romanovskiy, V. N.; Babain, V. A.; Esimantovskiy, V. M.; Smirnov, I. V.; Zaitsev, B. N., *Solvent Extr. Ion Exch.* **2001**, *19*, 23–36.

33. Lumetta, G. L.; Sinkov, S.; Neiner, D.; Levitskaia, T.; Braley, J. C.; Carter, J. C.; Warner, M. G.; Pittman, J. W.; Rapko, B. M., Sigma Team for Minor Actinide Separation: PNNL FY 2010 Status Report; Pacific Northwest National Laboratory: **2010**.

34. Lumetta, G. J.; Carter, J. C.; Gelis, A. V.; Vandegrift, G. F., *Nucl. Energy Environ., Vol. 1046*, American Chemical Society, **2010**, pp. 107–118.

35. Stalikas, C. D., *Trends Anal. Chem.* **2002**, *21*, 343–355.

36. Paleologos, E. K.; Giokas, D. L.; Karayannis, M. I., *Trends Anal. Chem.* **2005**, *24*, 426–436.

37. Bezerra, M. d. A.; Arruda, M. A. Z.; Ferreira, S. L. C., *Appl. Spectrosc. Rev.* **2005**, *40*, 269–299.

38. Tani, H.; Kamidate, T.; Watanabe, H., *J. Chromatogr., A* **1997**, *780*, 229–241.

39. Pires, M. J.; Aires-Barros, M. R.; Cabral, J. M. S., *Biotechnol. Prog.* **1996**, *12*, 290–301.

40. Hinze, W. L.; Pramauro, E., *Crit. Rev. Anal. Chem.* **1993**, *24*, 133–177.

41. Trakultamupatam, P.; Scamehorn, J. F.; Osuwan, S., *Sep. Sci. Technol.* **2002**, *37*, 1291–1305.

42. Trakultamupatam, P.; Scamehorn, J. F.; Osuwan, S., *Sep. Sci. Technol.* **2005**, *39*, 479–499.

43. Choppin, G. R.; Silva, R. J., *J. Inorg. Nucl. Chem.* **1956**, *3*, 153–154.

44. Smith, H. L.; Hoffman, D. C., *J. Inorg. Nucl. Chem.* **1956**, *3*, 243–247.

45. Wheelwright, E. J.; Spedding, F. H.; Schwarzenbach, G., *J. Am. Chem. Soc.* **1953**, *75*, 4196–4201.

46. Wheelwright, E. J.; Spedding, F. H., *J. Am. Chem. Soc.* **1953**, *75*, 2529–2530.

47. Pearson, R. G., *J. Am. Chem. Soc.* **1963**, *85*, 3533–3539.

48. Nash, K. L., *Solvent Extr. Ion Exch.* **1993**, *11*, 729–768.

49. Choppin, G. R., *J. Alloys Compd.* **2002**, *344*, 55–59.

50. Kolarik, Z., *Miner. Process. Extr. Metall. Rev.* **2000**, *21*, 89–141.

51. Cotton, F. A.; Wilkinson, G., *Advanced Inorganic Chemistry*, 5th ed., Wiley Interscience: New York, **1988**, pp. 1–1455.
52. Nilsson, M.; Nash, K. L., *Solvent Extr. Ion Exch.* **2007**, *25*, 665-701.
53. Weaver, B.; Kappelmann, F. A., *J. Inorg. Nucl. Chem.* **1968**, *30*, 263–272.
54. Harris, D. C., *Quantitative Chemical Analysis*, 4th ed., W. H. Freeman and Company: New York, **1995**, p. 186.
55. Portanova, R.; Lajunen, L. H. J.; Piispanen, J., *Pure Appl. Chem.* **2003**, *75*, 495–540.
56. Peppard, D. F.; Mason, G. W.; Maier, J. L.; Driscoll, W. J., *J. Inorg. Nucl. Chem.* **1957**, *4*, 334–343.
57. Lundqvist, R.; Lu, J.; Svantesson, I., *Acta Chem. Scand.* **1983**, *A37*, 743–753.
58. Dubuquoy, C.; Guillaumont, R.; Bouissières, G., *Radiochimica Acta* **1967**, *8*, 49–57.
59. Thomas, N. E.; Burkhart, L. E., *J. Inorg. Nucl. Chem.* **1974**, *36*, 1369–1376.
60. Mel'nik, M. I.; Filimonov, V. T.; Karelin, E. A., *Radiochem.* **1999**, *41*, 70–73.
61. Sato, T.; Ueda, M., *J. Inorg. Nucl. Chem.* **1973**, *35*, 1003–1010.
62. Mikhailichenko, A. I.; Pimenova, R. M., *Sov. Radiochem.* **1969**, *11*, 6–10.
63. Svantesson, I.; Persson, G.; Hagström, I.; Liljenzin, J. O., *J. Inorg. Nucl. Chem.* **1980**, *42*, 1037–1043.
64. Jensen, M. P.; Chiarizia, R.; Urban, V., *Solvent Extr. Ion Exch.* **2001**, *19*, 865–884.
65. Yurtov, E.; Murashova, N.; Datsenko, A., *Russ. J. Inorg. Chem.* **2006**, *51*, 670–675.
66. Anticó, E.; Masana, A.; Hidalgo, M.; Salvadó, V.; Iglesias, M.; Valiente, M., *Anal. Chim. Acta* **1996**, *327*, 267–276.
67. Kizim, N. F.; Lar'kov, A. P., *Sov. Radiochem.* **1988**, *30*, 177-181.
68. Trifonov, Y. I.; Legin, E. K.; Suglobov, D. N., *Sov. Radiochem.* **1992**, *34*, 373–377.
69. Trifonov, Y. I.; Legin, E. K.; Suglobov, D. N., *Sov. Radiochem.* **1985**, *27*, 387–393.
70. Spiryakov, V. I.; Krutikov, P. G.; Barinov, V. M.; Solovkin, A. S.; Yakovlev, G. N., *Sov. Radiochem.* **1972**, *14*, 589–591.
71. Mel'nik, M. I.; Spiryakov, V. I.; Filimonov, V. T.; Karelin, E. A., *Radiochem.* **1997**, *39*, 432–437.
72. Trifonov, Y. I.; Legin, E. K.; Suglobov, D. N., *Sov. Radiochem.* **1992**, *34*, 369–372.
73. Myers, A. L.; McDowell, W. J.; Coleman, C. F., *J. Inorg. Nucl. Chem.* **1964**, *26*, 2005–2011.
74. Wang, D.; Li, Y.; Wu, J.; Xu, G., *Solvent Extr. Ion Exch.* **1996**, *14*, 585–601.
75. Blake, C. A.; Crouse, D. J.; Coleman, C. F.; Brown, K. B.; Kelmers, A. D., Progress Report: Further Studies of the Dialkylphosphoric Acid Extraction (DAPEX) Process for Uranium; ORNL-2172; Oak Ridge National Laboratory: Oak Ridge, TN, **1956**.
76. Blake, C. A.; Brown, K. B.; Coleman, C. F., The Extraction and Recovery of Uranium (and Vanadium) From Acidic Liquors with Di(2-ethylhexyl) Phosphoric Acid and some other Organophosphorus Acids; ORNL-1903; Oak Ridge Naional Laboratory: Oak Ridge, TN, **1955**.
77. Jensen, M. P.; Bond, A. H., *Radiochimica Acta* **2002**, *90*, 205–209.
78. Sokolov, E. I.; Melkaya, R. F.; Tevelev, L. G.; Nikolaev, V. M., *Russ. J. Inorg. Chem.* **1975**, *20*, 1399–1402.
79. Peppard, D. F.; Ferraro, J. R., *J. Inorg. Nucl. Chem.* **1959**, *10*, 275–288.
80. Nakamoto, K.; Ferraro, J. R.; Mason, G. W., *Appl. Spectrosc.* **1969**, *23*, 521–527.
81. Li, Q.; Weng, S. F.; Wu, J. G.; Zhou, N. F., *J. Phys. Chem. B* **1998**, *102*, 3168–3174.
82. Beitz, J. V.; Sullivan, J. C., *J. Less-Common Met.* **1989**, *148*, 159–166.
83. Lis, S.; Mathur, J. N.; Choppin, G. R., *Solvent Extr. Ion Exch.* **1991**, *9*, 637–647.
84. McDowell, W. J.; Coleman, C. F., *J. Inorg. Nucl. Chem.* **1965**, *27*, 1117–1139.

85. Unknown, *VAPRO Vapor Pressure Osmometer Model 5520 User's Manual*, M2468-4 rev B ed., Wescor, Inc., **2004**, pp. 29–42.

86. Boiani, J. A., *J. Chem. Educ.* **1986**, *63*, 724–726.

87. Gran, G., *Analyst (Cambridge, U.K.)* **1952**, *77*, 661–671.

88. Rossotti, F. J.; Rossotti, H., *J. Chem. Educ.* **1965**, *42*, 375–378.

89. Partanen, J. I.; Juusola, P. M.; Minkkinen, P. O., *Fluid Phase Equilib.* **2003**, *204*, 245–266.

90. Bukietynska, K.; Mondry, A.; Osmeda, E., *J. Inorg. Nucl. Chem.* **1981**, *43*, 1321–1330.

91. Nilsson, M. University of California, Irvine, Irvine, CA. Personal communication, 2010.

92. Ryabchikov, D. I.; Ryabukhin, V. A., *Analytical Chemistry of Yttrium and the Lanthanide Elements* (Ed.: A. P. Vinogradov), Ann Arbor-Humphrey Science Publisher, Ann Arbor, MI, **1970**, pp. 159–177.

93. Moeller, T.; Brantley, J. C., *Anal. Chem.* **1950**, *22*, 433–441.

94. Baes, J. C. F., SXLSQI, A Program for Modeling Solvent Extraction System; ORNL-TM-13604; Oak Ridge, TN, **1998**.

95. Kolarik, Z., *Solvent Extr. Ion Exch.* **2010**, *28*, 707–763.

96. Pitzer, K. S., *Activity Coefficients in Electrolyte Solutions* (Ed.: K. S. Pitzer), CRC Press, Boca Raton, Florida, **1991**, pp. 75–153.

97. Barton, A. F. M., *CRC Handbook of Solubility Parameters and Other Cohesion Parameters*, CRC Press: Boca Raton, Florida, **1991**.

98. Baes, C. F.; Moyer, B. A., *J. Phys. Chem. B* **1997**, *101*, 6566–6574.

99. Harris, R. K.; Becker, E. D.; De Menezes, S. M. C.; Goodfellow, R.; Granger, P., *Pure Appl. Chem.* **2001**, *73*, 1795–1818.

100. Adamson, A. W., *A Textbook of Physical Chemistry*, 3rd ed., Academic Press, Inc.: Orlando, FL, **1986**, pp. 1–972.

101. De Stefano, C.; Foti, C.; Giuffrè, O.; Sammartano, S., *J. Chem. Eng. Data* **2001**, *46*, 1417–1424.

102. The reported reaction in De Stefano et al. (protonation) is the reverse of what is reported in this work (deprotonation). When comparing enthalpy of reaction, reversing the direction of the reaction merely changes the sign of the enthalpy. De Stefano et al. show a decrease in the enthalpy for the reverse reaction, which equates to an increase in the enthalpy for the reaction presented in this paper.

103. Miralles, N.; Sastre, A.; Martinez, M.; Aguilar, M., *Anal. Sci.* **1992**, *8*, 773–777.

104. Jensen, M.; Chiarizia, R.; Urban, V., *Solvent Extr. Ion Exch.* **2001**, *19*, 865 - 884.

105. Colthrup, N. B.; Daly, L. H.; Wiberly, S. E., *Introduction to Infrared and Raman Spectroscopy*, 3rd ed., Academic Press, Inc., **1990**, pp. 355–386.

106. Socrates, G., *Infrared and Raman Characteristic Group Frequencies*, 3rd ed., Wiley and Sons, Inc., New York, **2001**, pp. 96, 128.

107. Czerwinski, K.; Draye, M.; Favre-Reguillon, A., in *232nd ACS National Meeting*, San Francisco, CA, **2006**.

108. Sigma-Aldrich, "Triton X-114 Product Description", http://www.sigmaaldrich.com/catalog/ProductDetail.do?lang=en&N4=X114|SIAL&N5=SEARCH_CONCAT_PNO|BRAND_KEY&F=SPEC, accessed April 22, 2011.

109. Bedall, K.; Fischer, O., *Ber. Dtsch. Chem. Ges.* **1881**, *14*, 442.

110. Bedall, K.; Fischer, O., *Ber. Dtsch. Chem. Ges.* **1881**, *14*, 1366.

111. Bedall, K.; Fischer, O., *Ber. Dtsch. Chem. Ges.* **1882**, *15*, 683.

112. Berg, R., *Fresenius J. Anal. Chem.* **1927**, *71*, 23–36.

113. Hahn, F., *Angew. Chem.* **1926**, *39*, 1198.

114. Hollingshead, R. G. W., *Oxine and its Derivatives, Vol. 1*, Butterworths Scientific Publications: London, **1954**.
115. Czakissulikowska, D.; Kuznik, B.; Malinowska, A.; Kijanowicz, U., *Chem. Anal. (Warsaw)* **1993**, *38*, 53–62.
116. Czakis-Sulikowska, D.; Pustelnik, N.; Kuznik, B.; Malinowska, A., *J. Alloys Compd.* **2000**, *300-301*, 234–237.
117. Starý, J., *Anal. Chim. Acta* **1963**, *28*, 132–149.
118. Dyrssen, D.; Dahlberg, V., *Acta Chem. Scand.* **1953**, *7*, 1186–1196.
119. Schweitzer, G. K.; Bramlitt, E. T., *Anal. Chim. Acta* **1960**, *23*, 419–422.
120. Schweitzer, G. K.; Coe, G. R., *Anal. Chim. Acta* **1961**, *24*, 311–315.
121. Oosting, M., *Anal. Chim. Acta* **1959**, *21*, 301–308.
122. Oosting, M., *Anal. Chim. Acta* **1959**, *21*, 397–406.
123. Oosting, M., *Anal. Chim. Acta* **1959**, *21*, 505–510.
124. Taechangam, P.; Scamehorn, J. F.; Osuwan, S.; Rirksomboon, T., *Sep. Sci. Technol.* **2008**, *43*, 3601–3623.
125. Irving, H.; Ewart, J. A. D.; Wilson, J. T., *J. Chem. Soc.* **1949**, 2672–2674.
126. Goto, H., *Scientific Reports of the Tohoku Imperial University, First Series* **1938**, 418–428.
127. Ashton, L. A.; Bullock, J. I.; Simpson, P. W. G., *J. Chem. Soc., Faraday Trans. 1* **1982**, *78*, 1961-1970.
128. Gupta, R. D.; Manku, G. S.; Bhat, A. N.; Jain, B. D., *J. Less-Common Met.* **1970**, *20*, 345–352.
129. Powell, K. J.; Solov'ev, V., *The IUPAC Stability Constants Database*, ScQuery Vn. 5.7 ed., Academic Software: Timble, Otley, UK, **2001**.
130. Firsching, F. H.; Cuca, R. C., *J. Chem. Eng. Data* **1981**, *26*, 116–118.
131. Skorik, N. A., *Zh. Neorg. Khim.* **1977**, *22*, 1425–1427.
132. Triton X-100 is identical to Triton X-114 except the n = 9–10 with an average molecular weight of 625.
133. Sigma-Aldrich, "Triton X-100 Product Description", http://www.sigmaaldrich.com/catalog/ProductDetail.do?lang=en&N4=T9284|SIAL&N5= SEARCH_CONCAT_PNO|BRAND_KEY&F=SPECi, accessed May 2, 2011.
134. Hoshino, H.; Saitoh, T.; Taketomi, H.; Yotsuyanagi, T.; Watanabe, H.; Tachikawa, K., *Anal. Chim. Acta* **1983**, *147*, 339–345.
135. Gans, P.; Sabatini, A.; Vacca, A., *Talanta* **1996**, *43*, 1739–1753.
136. 899 papers citing the Hyperquad publication on Web of Science on the access date 5/3/2011.
137. Leggett, D. J.; McBryde, W. A. E., *Anal. Chem.* **1975**, *47*, 1065–1070.
138. 230 papers citing the SQUAD publication on Web of Science on the access date 5/3/2011.
139. Robinson, T. A. University of Nevada, Las Vegas, Las Vegas, NV, Unpublished work, 2007.
140. Harned, H. S.; Owen, B. B., *The Physical Chemistry of Electrolytic Solutions*, 2nd ed., Reinhold Publishing Corp: New York, **1950**, pp. 1–645.
141. Levine, I. N., *Physical Chemistry*, 2nd ed., McGraw-Hill Book Company, New York, **1983**, pp. 170–173.
142. Harned, H. S.; Hamer, W. J., *J. Am. Chem. Soc.* **1933**, *55*, 2194–2206.
143. Pettit, L. D.; Puigdomenech, I.; Wanner, H.; Sukhno, I.; Buzko, V., *Ionic Strength Corrections for Stability Constants*, 2.0 ed., IUPAC, **2004**.
144. Buzko, V.; Polushin, A.; Sukhno, I.; Pettit, L. D., *Temp Effects*, 1.2 ed., IUPAC, **2004**.
145. Unknown, Metrohm AG, Switzerland, **2006**, p. 372.

146. Fortuin, J. M. H., *Anal. Chim. Acta* **1961**, *24*, 175–191.
147. Baes, J. C. F.; Mesmer, R. E., *The Hydrolysis of Cations*, John Wiley and Sons: New York, NW, **1986**, pp. 137.
148. Baes, J. C. F.; Mesmer, R. E., *The Hydrolysis of Cations*, John Wiley and Sons: New York, NY, **1976**, pp. 1–489.
149. Ryabchikov, D. I.; Ryabukhin, V. A., *Analytical Chemistry of Yttrium and the Lanthanide Elements*, Ann Arbor-Humphrey Science Publisher: Ann Arbor, MI, **1970**, pp. 292.
150. Woolley, E. M.; George, R., *J. Solution Chem.* **1974**, *3*, 119–126.
151. Matrosovich, T. Y.; Lobanov, F. I.; Makarov, N. V., *Zh. Neorg. Khim.* **1986**, *31*, 1441–1446.
152. Lobanov, F. I.; Matrosovich, T. Y., *Zh. Neorg. Khim.* **1981**, *26*, 3001–3006.
153. Irving, H.; Rossotti, H., *Acta Chem. Scand.* **1956**, *10*, 72–93.
154. Bates, R. G., *J. Electroanal. Chem. Interfacial Electrochem.* **1971**, *29*, 1–19.
155. Demirelli, H.; Köseoğlu, F., *J. Solution Chem.* **2004**, *33*, 1501–1515.
156. Kılıç, E.; Köseoğlu, F.; Başgut, Ö., *Anal. Chim. Acta* **1994**, *294*, 215–220.
157. Ramírez-García, J. J.; Solache-Ríos, M.; Jiménez-Reyes, M.; Rojas-Hernández, A., *J. Solution Chem.* **2003**, *32*, 879–896.
158. Kalidas, C.; Hefter, G.; Yizhak, M., *Chem. Rev.* **2000**, *100*, 819–852.
159. Narayana, V. G.; Swamy, S. J.; Lingaiah, P., *Indian J. Chem., Sect A* **1986**, *25*, 491–493.
160. Gupta, R. D.; Manku, G. S.; Bhat, A. N.; Jain, B. D., *Aust. J. Chem.* **1970**, *23*, 1387–1395.

VITA

Graudate College
University of Nevada, Las Vegas

Troy A Robinson

Degrees:
    Bachelor of Science, Chemical Engineering, 2005
    Brigham Young University

Special Honors and Awards:
    US DOE Office of Civilian Radioactive Waste Management Graduate Fellow,
    2006-2010

Publications:
    Herbst, R.S.; Peterman, D.R.; Robinson, T.A. "PEG-400 Partitioning in the
    HCCD/PEG Process for Cs and Sr Recovery" Separation Science and Technology
    (2008), 43(9), 2557-2571.

Dissertation Title: Equilibrium Speciation of Select Lanthanides in the Presence of Acidic
    Ligands in Homo- and Heterogeneous Solutions

Dissertation Examination Committee:
    Chairperson, Kenneth R. Czerwinski, Ph.D.
    Committee Member, Tatiana G. Levitskaia, Ph.D.
    Committee Member, Sam A. Bryan, Ph.D.
    Committee Member, Patricia Paviet-Hartmann, Ph.D.
    Graduate Faculty Representative, Ralf Sudowe, Ph.D.